AUSTRALIA

BMR JOURNAL

OF AUSTRALIAN GEOLOGY & GEOPHYSICS

VOLUME 12 NUMBER 1

BMR JOURNAL

OF AUSTRALIAN GEOLOGY & GEOPHYSICS

VOLUME 12 NUMBER 1

CONTENTS

Front cover: BMR field party sampling water bases on Nauru Island, central Pacific Ocean, with local assistance. Much of the surface of the island has been removed by open-cut phosphate mining, and rehabilitation works are proposed by the Nauru government. BMR's groundwater investigation has led to the definition of water resources for rehabilitation works and the island's future supply. The chemistry of Nauru's groundwater system is described in a paper by Jankowski & Jacobson in this issue.

[Photo by Gerry Jacobson]

Cover design by Saimonne Bissett.

Figures prepared by BMR Cartographic Services Unit unless otherwise indicated.

AUSTRALIAN GOVERNMENT PUBLISHING SERVICE CANBERRA 1991

ISSN 0312–9608

Month of issue: February

Subscriptions to the BMR Journal are available through the BMR (GPO Box 378, Canberra, ACT 2601; tel. (06) 249 9642, fax (06) 257 6466) or the Australian Government Publishing Service (Mail Order Sales, GPO Box 84, Canberra, ACT 2601; telephone (06) 295 4485).

Other matters concerning the Journal should be sent to the Director, marked for the attention of the Editor, BMR Journal.

Department of Primary Industries and Energy

Minister for Resources: The Hon. Alan Griffiths, MP

Secretary: Geoff Miller

Bureau of Mineral Resources, Geology and Geophysics

Director: R.W.R. Rutland, A.O.

Editor, BMR Journal: Bernadette Hince

Printed in Australia by R. D. RUBIE, Commonwealth Government Printer, Canberra

BMR Journal of Australian Geology & Geophysics, 12, 1–4

Hypocentre locations from a microearthquake survey, Cadoux, Western Australia, 1983

V.F. Dent[1]

A microearthquake survey around the fault scarp caused by the 1979 Cadoux, Western Australia, earthquake located 36 earthquakes (ML 0–2.4) over 7 weeks from October to December 1983. The earthquakes show a NNE–SSW trend on the westward side of the fault complex, consistent with a westward dipping fault plane. The earthquakes are evenly distributed along the length of the fault. The more accurately located earthquakes are 0–6 km deep.

Introduction

The Mundaring Geophysical Observatory (MGO) has been monitoring and locating Western Australian earthquakes since 1959 (Gregson & others, 1985). The seismicity of Western Australia to June 1965 has been described by Everingham (1968). Southwestern Western Australia is a zone of special significance (Jaeger & Browne, 1958). Between 1968 and 1979, three earthquakes with coseismic faulting occurred in this area. These were at Meckering on October 14, 1968, MS 6.8 (Gordon & Lewis, 1980), Calingiri on March 10, 1970, MS 5.1 (Gordon & Lewis, 1980), and Cadoux on June 2, 1979, MS 6.1 (Gregson & Paull, 1979).

The earthquakes occurred in a Precambrian shield area, the Yilgarn Block, and are of special interest because they are intra-cratonic events. The area was classified as an international site for research on earthquake prediction by the International Association of Seismology and Physics of the Earth's Interior (IASPEI) in 1983 (International Union of Geology & Geophysics, 1984). The first study of the crustal structure of the region was conducted in 1969 (Mathur, 1974), and a more extensive survey was conducted by the Explosion Seismology Section of the BMR in 1983.

In contrast to the Meckering and Calingiri regions, seismic activity at Cadoux has continued at a relatively high (although declining) level until now (1990). A network of seismograph stations around Cadoux at Ballidu (BAL), Kellerberrin (KLB) and Mundaring (MUN) (Fig. 1) is used to locate earthquakes of magnitude ML >2 near Cadoux, to accuracies of ± 5 km. Plots of earthquake epicentres have shown a broad NNE–SSW trend. Depths have not been precisely determined, because of poor station distribution, and they have normally been assigned a nominal value of 10 km.

The Cadoux fracture zone (Fig. 2) extends over a length of about 15 km (Lewis & others, 1981). North of Cadoux, there is a complicated set of faults, with a general northwest–southeast trend. South of Cadoux, there is a continuous fracture, the Robb Fault, which is a thrust fault dipping to the west.

At the completion of the 1983 crustal survey, 20 field seismographs were made available to the Mundaring Geophysical Observatory for one week, and four of these were retained for a further six weeks. Data from these seismographs allowed earthquake locations to be determined far more precisely than was previously possible. Before this survey, the only temporary seismograph to operate in the Cadoux area was one positioned 20 km north of the township, at Burakin, three weeks after the earthquake of 2 June 1979. Results from the station have been presented by Dent (1990).

[1] BMR Mundaring Geophysical Observatory, Mundaring, WA 6073.

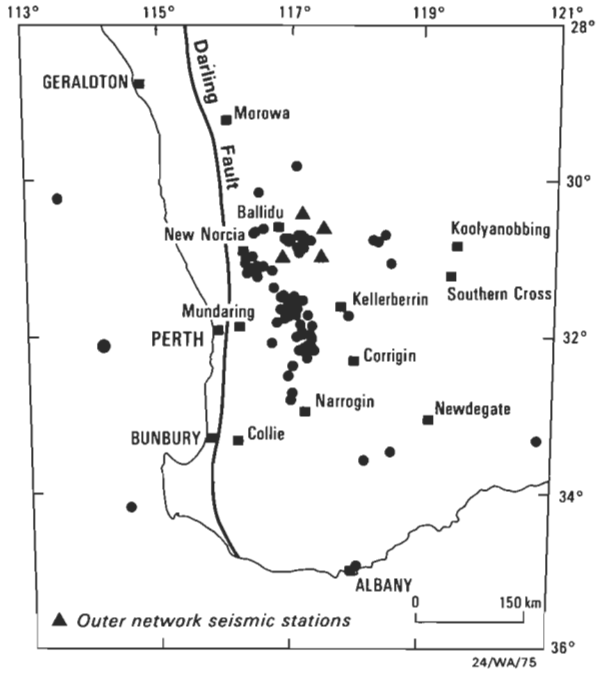

Figure 1. Locality map and seismicity (magnitude ML>4.0) in southwestern Australia, 1960–1984.

Survey structure

As many events have occurred north of Cadoux, it was decided to deploy sixteen of the seismographs on a 10 km^2 grid immediately north of the township. This gave spacings between the seismographs of 3 to 4 km. These seismographs operated for one week (26 October to 2 November 1983), and are referred to as the 'inner network' in this paper. An additional four seismographs were placed around Cadoux at a greater distance (~40 km) and operated for seven weeks (26 October to 15 December 1983); these are referred to as the 'outer network' (Fig. 1). Station coordinates are listed in Dent & Gregson (1986) and Dent (1988).

The field seismographs recorded data on magnetic tape, and these data were not available until replayed on a play-back unit. A visual recorder was therefore required to determine the approximate onset times and magnitudes of the earthquakes which occurred during the survey. A Teledyne-Geotech MEQ-800 seismograph was put near the centre of the inner network for the first week of the survey, and from this recorder over 200 local events, mostly magnitude ML <1, were detected (Dent & Gregson, 1986). After the removal of this seismograph, local events were identified from Ballidu (BAL) records (which came from the permanent seismograph network).

Earthquakes which occurred in the first week within the inner network were accurately located by latitude and longitude (± 1

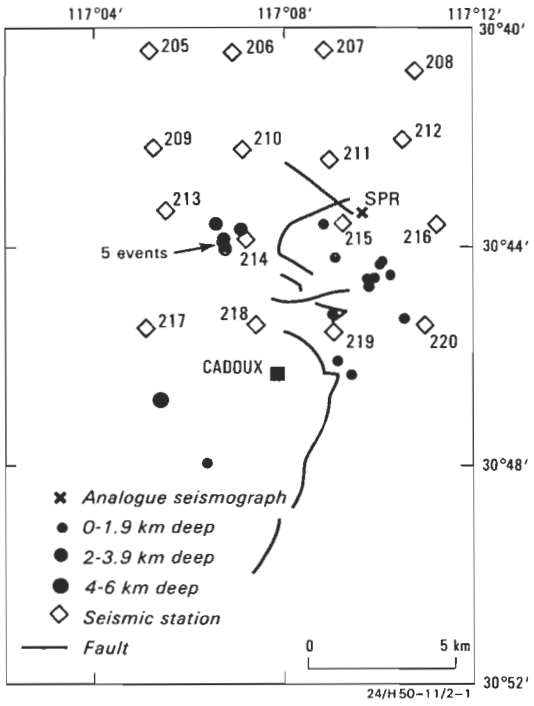

Figure 2. Earthquakes located in the first week of the survey. Surface fractures associated with the 1979 Cadoux earthquake are indicated.

km) and depth (±2 km) within the 95% confidence limit. However, accuracy decreases with distance out from this survey area. Earthquakes located using only the outer network (and regional stations when possible) were not located as accurately, but the hypocentres were still more accurate than those obtained routinely using the permanent seismograph network.

Because of the small distances involved, more accurate arrival times were required than for normal observatory recordings. Playback of data at high speed (generally 25 mm/s) allowed scaling to ±0.02 s (compared with ±0.2 s for normal seismographs).

Time control on most seismographs was good, with clock rates generally less than 10 milliseconds per day, though some were of the order of 100 milliseconds per day.

Earthquake hypocentre solutions

Using the inner network, earthquakes down to about magnitude ML 0.0 could be located. Using the outer network only, the minimum magnitude for earthquakes which could be located was about ML 1.0.

The crustal model WA2 (Dent, 1989) was used in this study (Table 1). This model is derived from the inversion of earthquake phase arrival data. The earthquakes used in this inversion originated in southwestern Western Australia. The model was used in preference to a model presented in Collins (1988), which was for P waves only and did not use shear wave travel times. For its routine epicentral determinations, the Mundaring Geophysical Observatory has been using a different crustal model (Table 1) based on earlier studies (Mathur, 1974). The model used by the Observatory has a significantly higher upper crustal velocity than that found in the WA2 or Collins models.

Table 1. Crustal models used by the Mundaring Observatory (MGO) and this study (WA2).

WA2 crustal model			*MGO*		
Depth (km)	*P velocity (km/s)*	*S velocity (km/s)*	*Depth (km)*	*P velocity (km/s)*	*S velocity (km/s)*
0–<19	6.13	3.62	0–<19	6.5	3.69
19–<36	7.14	3.96	19–<37	7.17	4.07
>36	8.27	4.75	>37	8.11	4.61

Five earthquakes of ML >1.0, and 19 smaller events, were located during the first week of the survey. Approximately 200 smaller events were also detected, but not located. Another 54 earthquakes were detected by the outer network in the following 6 weeks, and 12 of them have been located.

The earthquakes which were located are listed in Table 2 and plotted on Figures 2 and 3. They were located using the EQLOCL earthquake location program, written by staff at the Seismology Research Centre of the Phillip Institute of Technology, Victoria.

The computed solutions indicate that the epicentre coordinates are accurate to ±0.5 km and focal depth to ±1.0 km in most cases. However, because of accuracy limitations in timing and scaling (of the order of 30 milliseconds), the errors are probably about twice this figure. For those earthquakes with only a small number of arrivals, or for those which occurred outside the recording network, uncertainties in coordinates are in reality larger. Events have been graded by degree of accuracy (A, B, or C) within a 95% confidence limit (Table 2).

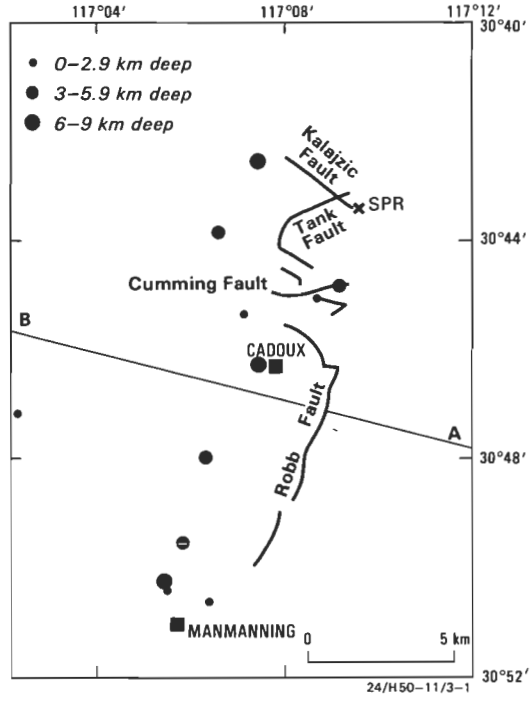

Figure 3. Earthquakes located 2 November–15 December 1983, after the first week of the survey.

Comparison with location by standard methods

Three earthquakes of magnitude greater than ML 2.0 occurred during the survey (on 26 and 28 October and 14 December 1983), and were located by the observatory using arrival times

Table 2. Earthquakes in the Cadoux region, Western Australia, located using survey data.

Date 1983	*Time*[1]	*Latitude (°S)*	*Longitude (°E)*	*Depth (km)*	*Magnitude (ML)*	*Accuracy*[2]	*Remarks*
Oct 26	0706 01.4	30.730	117.112	3.9	2.4	A	MGO also located
	2234 22.9	30.767	117.152	1C		C	
Oct 27	0720 28.9	30.731	117.111	3.8		A	
	2009 58.0	30.736	117.151	0.9	0.9	B	
	2129 26.8	30.884	117.140	5.7		B	13 km S of Cadoux
Oct 28	0256 21.0	30.738	117.167	1.6	2.1	A	MGO also located
	0256 56.6	30.741	117.171	1.4		B	
	0533 47.7	30.726	117.109	3.8		B	
	0550 00.4	30.742	117.165	1.3		A	
	1357 16.8	30.745	117.163	0.5		B	
	1946 00.6	30.799	117.090	4.1	0.6	A	4 km W of Cadoux
	2311 55.0	30.737	117.168	1C		A	
Oct 29	0210 47.1	30.726	117.147	1.7		A	
	0505 30.6	30.733	117.112	3.6	1.5	A	
	1909 04.7	30.733	117.113	3.5		A	
Oct 30	0035 18.2	30.733	117.112	3.6		A	
	0300 32.9	30.771	117.157	1.6		A	
	1448 42.6	30.734	117.111	3.3	1.2	A	Near ML 2.4 event
	1935 54.4	30.733	117.113	3.6		A	Near ML 2.4 event
	2035 41.0	30.728	117.118	3.1		A	Near ML 2.4 event
Oct 31	0155 05.6	30.753	117.150	1.2		A	
	0342 07.8	30.798	117.106	0.7	1.1	B	5 km SW of Cadoux
	1345 34.9	30.744	117.163	1.6		B	
Nov 01	0255 57.4	30.754	117.176	0.8		A	Near ML 2.1 event
INNER NETWORK WITHDRAWN ON 2 NOV 1983							
Nov 04	1652 59.7	30.729	117.107	4.1	1.5	C	Near ML 2.4 event
Nov 06	0741 38.6	30.823	117.094	4.1	1.2	C	
Nov 08	0233 02.5	30.707	117.121	9.1	1.1	C	6 km N of Cadoux
Nov 09	1931 12.4	30.769	117.121	6.5		C	
Nov 10	1510 13.8	30.837	117.088	1.0	1.4	C	
Nov 13	0605 11.5	30.835	117.087	9.0	1.3	C	7.5 km SSW of Cadoux
Nov 22	0616 29.0	30.754	117.116	2.7		C	3 km WSW of Cadoux
Nov 25	1223 14.4	30.797	117.102	5.5	1.7	C	4.5 km SSW of Cadoux
Dec 03	1948 52.1	30.749	117.142	1.5	1.5	C	Cumming Fault
Dec 05	1010 06.9	30.745	117.150	4.4	1.3	C	
Dec 06	2247 21.6	30.784	117.035	1.5		C	10 km WSW of Cadoux
Dec 14	1000 33.0	30.841	117.103	0.8	2.3	C	8 km SSW of Cadoux

[1] Western Australian standard time
[2] A ±1.0 km in latitude/longitude, ±2 km depth
B ±3.0 km in latitude/longitude, ±4 km depth
C >±3.0 km in latitude/longitude, >±4 km depth

from Ballidu, Kellerberin and Mundaring. Table 3 shows the MGO locations, and compares them with the locations computed using the EQLOCL earthquake location program, with additional data provided by the survey.

The higher velocities of the model used routinely by the Mundaring observatory have the effect of reducing the apparent travel times, and causing the earthquake epicentres to be drawn towards the nearest station, Ballidu, by about 5 km. Because there were insufficient data to allow reliable depth calculation, a standard depth of 10 km was adopted for observatory locations. The survey data has indicated that the actual depths of these three earthquakes were 3.9 ± 2.0 km, 1.6 ± 2.0 km and 0.8 ± 4.0 km respectively.

Table 3. Comparison of earthquake solutions.

Date (1983)	*Magnitude*	*Reference*[1]	*Time*[2]	*Latitude (°S)*	*Longitude (°E)*	*Depth (km)*	*Number of stations*
26 Oct	2.4	MGO	070602.3	30.72 ±0.05	117.08 ±0.05	10 G	5
		EQLOCL	070601.4	30.730 ± 0.01	117.112 ± 0.01	3.9	11
28 Oct	2.1	MGO	025622.2	30.71 ±0.05	117.12 ±0.05	10 G	4
		EQLOCL	025621.0	30.738 ± 0.01	117.167 ± 0.01	1.6	21
14 Dec	2.3	MGO	100033.5	30.80 ±0.05	117.09 ±0.05	10 G	3
		EQLOCL	100033.0	30.841 ± 0.01	117.103 ± 0.03	0.8	6

[1] MGO Epicentre prepared by Mundaring Geophysical Observatory; EQLOCL Epicentre computed using the EQLOCL earthquake location program
[2] Western Australian standard time
G Set at standard depth by MGO geophysicist

Spatial distribution of earthquake hypocentres

Earthquake locations in Western Australia for events of magnitude ML >2.0 are listed in the annual reports of the Mundaring Geophysical Observatory (e.g. Gregson & others, 1985). The solutions in these reports were based on observations from permanent seismographs only, and claimed accuracies are at best ±5 km. Earthquake solutions from these reports indicate only a diffuse north–south band of earthquakes in the general vicinity of the Cadoux fault.

Hypocentre relocations are presented in two figures. The first (Fig. 2) shows solutions for the first week, when the inner-

network was in place. These are the most accurate solutions from the survey, and have far better depth control than later events.

Most of the events in Figure 2 are smaller than magnitude ML 1.0. A significant proportion are clearly aftershocks of the magnitude ML 2.4 earthquake 5 km NNW of Cadoux which occurred just after recording began on 26 October, 1983.

The second epicentre plot (Fig. 3) shows earthquakes located from 2 November to 15 December, 1983, without the benefit of the inner network. This network, covering a larger area and longer time span, has given a better indication of the normal seismicity of the area. Many of the events located are south of Cadoux, and the epicentres are aligned parallel to and about 3 km west of the Robb fault. Seismicity is fairly uniformly distributed along the length of the fault complex.

Previously, epicentral plots of the Cadoux region (Lewis & others, 1981, fig. 5; Denham & others, 1987, fig. 2) indicated that most epicentres were on the eastern side of the fault. While the pattern of seismicity of the fault region might have changed significantly with time, it is more likely that the earlier locations are in error, because of the lack of close stations at the time. Routine locations were improved significantly after August 1982, when a permanent seismograph was established at Ballidu, 40 km northwest of Cadoux.

Earthquake depths

Earthquakes of accuracy A show a depth range of 1.3–4.1 km. The deepest earthquake located has a depth of 9.1 km, but an accuracy rating of only C.

Figure 4 shows the earthquakes of Table 2 projected on a cross-section normal to the Robb fault (section A–B on Fig. 3). The less accurately located events (accuracies B and C) show a fairly scattered pattern. The events of accuracy A are more tightly grouped. This plot demonstrates that the distribution of earthquake hypocentres is consistent with an active zone dipping to the west from the surface expression of the Robb fault, at an angle of between 45 and 60°.

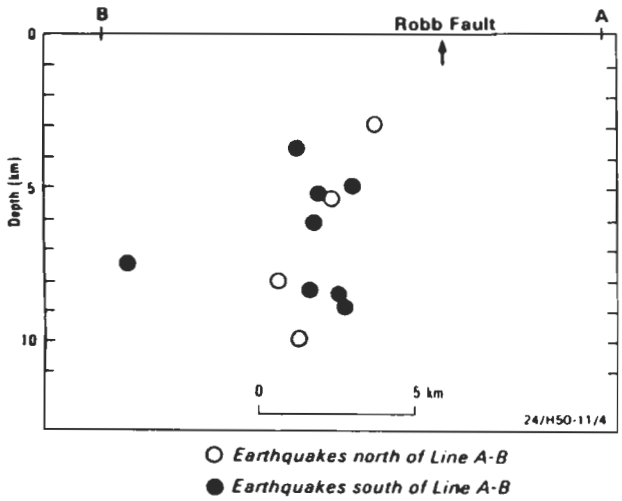

Figure 4. Earthquakes plotted on cross-section A–B of Figure 3. Closed circles indicate events north of A–B.

Conclusions

A collection of relatively precise earthquake hypocentres has been prepared from survey data (Table 2). The earthquakes show a clear trend parallel to the Robb fault, on its western side. This is consistent with the Robb fault being a west-northwest dipping thrust fault, with a dip angle of between 45 and 60 degrees.

Earthquakes located during the first week of the survey have excellent depth control, and indicate a focal depth range of 0.8–4.1 km. Although solutions for some events later in the survey indicated focal depths of up to 9 km, the depth control on these events was poor.

Acknowledgements

I would like to express my appreciation for the cooperation given to me by Barry Drummond, Ray Bracewell, and others in the Explosion Seismology Group of the BMR. I would also like to acknowledge the invaluable assistance given to me by David Denham, Peter Gregson and Kevin McCue (BMR) in the preparation of this paper.

References

Collins, C.D.N., 1988 — Seismic velocities in the crust and upper mantle of Australia. *Bureau of Mineral Resources, Australia, Report* 277.

Denham, D., Alexander, L.G., Everingham, I.B., Gregson, P.J., McCaffrey, R. & Enever, J.R., 1987 — The 1979 Cadoux Earthquake and intraplate stress in Western Australia. *Australian Journal of Earth Sciences*, 34, 507–521.

Dent, V.F., 1988 — The distribution of Cadoux aftershocks — additional data from temporary stations near Cadoux, 1983. *Bureau of Mineral Resources, Australia, Record* 1988/51.

Dent, V.F., 1989 — Computer generated crustal models for the South West Seismic Zone, Western Australia. *Bureau of Mineral Resources Australia, Record* 1989/43.

Dent, V.F., 1990 — Hypocentre relocations from temporary seismograph stations at Burakin and Wyalkatchem, Western Australia. *Bureau of Mineral Resources, Australia, Record* 1990/36.

Dent, V.F. & Gregson, P.J., 1986 — Cadoux Microearthquake Survey 1983. *Bureau of Mineral Resources, Australia, Record* 1986/22.

Everingham, I.B., 1968 — Seismicity of Western Australia. *Bureau of Mineral Resources, Australia, Report* 132.

Gregson, P.G. & Paull, E.P., 1979 — Preliminary report on the Cadoux earthquake, Western Australia, 2 June 1979. *Bureau of Mineral Resources, Australia, Report* 215; BMR Microform MF 100.

Gregson, P.J., Paull, E.P., Dent, V.F., Woad, G. & Page, B., 1985 — Mundaring Geophysical Observatory Twenty-fifth year 1983. *Bureau of Mineral Resources, Australia, Record* 1985/37.

Gordon, F.R. & Lewis, J.D. 1980 — The Meckering and Calingiri earthquakes October 1968 and March 1970. *Geological Survey of Western Australia, Bulletin* 126.

International Union of Geology & Geophysics, 1984 — International experimental sites for research on earthquake prediction. *International Union of Geology & Geophysics, Chronicle*, 1965, 29–31.

Jaeger, J.C. & Browne, W.R., 1958 — Earth tremors in Australia and their geological importance. *Australian Journal of Science*, 20(8), 225–228.

Lewis, J.D., Daetwyler, N.A., Bunting, J.A. & Moncrieff, J.S., 1981 — The Cadoux earthquake, 2 June 1979. *Geological Survey of Western Australia, Report* 11.

Mathur, S.P., 1974 — Crustal structure in southwestern Australia from seismic and gravity data. *Tectonophysics*, 24, 151–182.

BMR Journal of Australian Geology & Geophysics, 12, 5–12

Observations on the geological origin of the 'C' horizon seismic reflection, Eromanga Basin

I.H. Lavering[1]

Seismic exploration throughout the Eromanga Basin has identified several regionally-extensive seismic reflection horizons. The 'C' horizon, at the boundary of the Wallumbilla and Cadna-owie Formations, is one of the most significant. A difference in the petrophysical properties of these two formations is evident from sonic, density, gamma ray and resistivity well log data, and indicates that the amplitude of the 'C' horizon reflection is related to a sequence of low-density (undercompacted) shales in the basal part of the Wallumbilla Formation. The properties of the shales appear to be a consequence of rapid subsidence ('undercompaction') and burial. The empirical relationships between the 'C' horizon reflection amplitude, formation density and reflection coefficient are discussed, and geological implications for petroleum prospectiveness of the Eromanga Basin are outlined.

Introduction

The Cooper and Eromanga Basins of central and eastern Australia (Fig. 1) have been Australia's most active areas for onshore petroleum exploration and development. The early discovery of Cooper Basin gas and oil fields in the 1960s and 1970s and subsequent discovery of hydrocarbons over a significant area of the Eromanga Basin by a number of exploration groups have contributed to the rapid development of the region.

The geological character of the Eromanga Basin has contributed to a lag between hydrocarbon discovery in the Cooper Basin (1964, Gidgealpa gas) and Eromanga Basin (1978, Strzelecki oil) (Sprigg, 1986).

Figure 1. Location map of the Cooper and Eromanga Basins.

Initial perception of the Eromanga Basin's prospectivity focused on the relatively uniform character of the basin's stratigraphy and limited structuring, as evident from early seismic reflection data. The 1964 Coopers Creek seismic survey in the central part of the basin indicated that there were several major seismic reflection horizons in the Cooper Basin and overlying Eromanga Basin sequences (Smith, 1983). Three of the seismic reflection events were proved by later drilling to be major geological boundaries: a Permo-Carboniferous unconformity ('Z' horizon), a near top Permian event ('P' horizon), and the 'C' horizon, which is a high amplitude reflection generated near the boundary of the Wallumbilla Formation/ Bulldog Shale and Cadna-owie Formations (Fig. 2). The Wallumbilla–Bulldog is a shale-rich marine sequence and the Cadna-owie is a nearshore to marginal-marine sequence of sandstone, siltstone and shale.

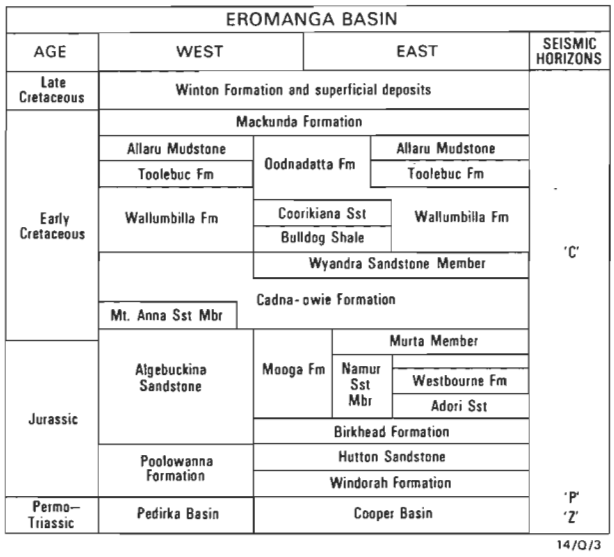

Figure 2. Regional stratigraphic relationships in the Eromanga Basin.

BMR regional seismic data were collected during a multidisciplinary study of the eastern part of the basin between 1980 and 1983. Interpretation of the data, and of wireline log data from petroleum exploration wells, indicates that the large amplitude of the 'C' seismic horizon reflector is the product of a marked contrast in acoustic impedance between the basal part of the Wallumbilla Formation and the upper part of the Cadna-owie Formation. Although the 'C' horizon reflection has been the subject of general discussion (Smith, 1983; Moore & Pitt, 1984), the geological factors which appear to affect its character and amplitude have not been specifically discussed. The lower part of the Wallumbilla Formation is rich in organic matter and corresponds to a low interval velocity zone evident on sonic log data (Moore & Pitt, 1984). This zone of low interval velocity causes much of the acoustic impedance contrast between the formations. If the 'low velocity' shale was absent from the sequence, a much smaller amplitude 'C' horizon reflection would be evident. The purpose of this paper is therefore to outline factors affecting the amplitude and continuity of the 'C' horizon and the geological sequence from which it originates.

[1] Petroleum Resource Assessment Program, Bureau of Mineral Resources, Geology & Geophysics, Canberra ACT 2601.

Geological origin of the 'C' horizon reflection

The Eromanga Basin extends over an area of approximately one million square kilometres of central and eastern Australia (Fig. 1). The basin contains Early Jurassic to Cretaceous sediments and is underlain by a series of Cambro-Ordovician and Late Carboniferous to Late Triassic basins as well as metamorphosed basement. The most significant hydrocarbon-bearing sequence underlying the Eromanga Basin is that of the Cooper Basin.

The regional stratigraphy of the Eromanga Basin is shown in a general form in Figure 2. The oldest sediments of the Windorah Formation (Passmore & Burger, 1986) are sandstone, siltstone and shale deposited as a discontinuous and patchy sequence. In the western part of the basin interbedded sandstone, siltstone, shale and coal were deposited as the Poolowanna Formation (cf. Moore, 1986). Subsidence in the Early to Middle Jurassic led to widespread sedimentation of a braided fluviatile sandstone sequence — the Hutton Sandstone in the central and eastern Eromanga Basin.

Reduced stream gradients at the end of the Hutton Sandstone deposition resulted in the development of floodplains, swamps and lakes where shale, siltstone and minor sandstone and coal of the Birkhead Formation were deposited (Paton, 1982). A high-energy environment followed, in which braided-fluviatile sediments of the Algebuckina and Adori Sandstones, and the lower part of the Namur Sandstone Member of the Mooga Formation were deposited.

Low-energy sedimentation followed, forming floodplain, swamp and lake areas over the east and central parts of the basin — the Westbourne Formation. This was succeeded by braided-fluvatile sedimentation of either the Namur Sandstone Member of the Mooga Formation, or the upper part of the Algebuckina Sandstone.

A return to low-energy conditions deposited the Murta Member of the Mooga Formation. Initial floodplain, swamp and lacustrine conditions in the Murta gave way to deltaic progradation in the upper part of the sequence with laterally equivalent braided-fluvial feeder channels (Ambrose & others, 1982, 1986) and possibly some marine influence.

The coarsening-upwards nature of the sandstone, siltstone and shale of the overlying Cadna-owie Formation indicates basin-wide regression, but some marine to marginal-marine influence is evident in the eastern part of the basin (John & Almond, 1987). The Mt Anna Sandstone Member on the basin's western margin is considered to be fluvio-deltaic (Wopfner & others, 1970). The Wyandra Sandstone which comprises the upper part of the Cadna-owie Formation is mainly marine (Ambrose & others, 1982; Burger, 1982) and includes beach-face (Senior & others, 1978) and low-energy shoreface deposits, although marsh and backswamp sediments are evident in parts of southeast Queensland (John & Almond, 1987).

A major early Aptian transgression is evident from the contact of the Wallumbilla Formation or Bulldog Shale with the underlying Cadna-owie Formation or 'Transition Beds'. While this boundary is laterally persistent and structurally uncomplicated, in some areas of the central and eastern parts of the basin the 'C' horizon exhibits an undulating seismic pattern related to listric faulting and submarine channelling (Moore & Pitt, 1984; Newton, 1986; Bauer & Harrison, 1987).

Marine shale and siltstone make up much of the Bulldog Shale, Wallumbilla and Oodnadatta Formations and Allaru Mudstone. The basal part of the Wallumbilla Formation is a 3–10 m thick interval of dark organic shales (total organic content (TOC) 1–1.5%). Moore & Pitt (1984) suggest that this corresponds to a low interval velocity zone evident on wireline log data. The question remains of whether the organic content of this part of the succession is the cause of the low interval velocity, or whether other factors (such as water build-up in the sequence) are responsible.

The upper part of the Wallumbilla–Bulldog succession is organically richer than the basal part (TOC >1.5%) (Moore & Pitt, 1984, fig. 15; McKirdy & others, 1986), but does not produce high-amplitude, continuous seismic reflections similar to that of the 'C' horizon. I suggest that factors other than organic richness influence the origin of the low interval velocity zone.

The Coorikiana Sandstone is a coarsening-upwards unit of glauconitic sandstone and siltstone deposited in a shallow-marine shoreface environment. The Toolebuc Formation consists of organic-rich shale, siltstone and limestone deposited in a very shallow epiric sea (Moore & Pitt, 1984). The Mackunda Formation consists of marginal-siltstone and calcareous sandstone, whereas the Winton Formation consists of shale, siltstone, sandstone and minor coal.

Structure and prospectivity

Regional studies of the Cretaceous sequence have emphasised the importance of the 'C' reflector as a major structural marker horizon in the Eromanga Basin (Moore & Pitt, 1984; Moore & others, 1986). The timing of Jurassic, Cretaceous and Tertiary deformation have been identified by Pitt (1986) as important for assessing the petroleum prospectivity of the Eromanga sequence.

Structures which developed in the Tertiary are generally considered to be less prospective than older features and are commonly identified by the symmetry of the 'C' reflection with older Eromanga and Cooper seismic reflectors. Pre-Cretaceous structures which formed before Eromanga and Cooper Basin source-rock sequences reached oil-maturity are generally more prospective. An exception to this is those areas with 'cooler' thermal histories where the oil generation threshold was reached after Tertiary structuring occurred in the Oligocene (Wopfner, 1960; Pitt, 1982, 1986).

Cretaceous and Jurassic growth structures are identified by a lack of symmetry between major marker horizons such as the 'C' horizon and other prominent seismic reflections. Such features are considered to have better prospectivity than younger structures, as the growth of potential traps predates oil generation in much of the Eromanga sequence (Moore & Pitt, 1984), and possibly even oil generated from the older underlying Cooper Basin sequence. The 'C' horizon is a major stratigraphic marker, and a key to assessing the timing of development of potential traps in the Eromanga sequence and their petroleum prospectivity.

Seismic character of 'C' horizon

Between 1980 and 1983, the Bureau of Mineral Resources (BMR) carried out seismic reflection and refraction surveys in the Queensland part of the central Eromanga Basin as part of a large-scale multidisciplinary study to investigate the structure, stratigraphy, geological evolution and petroleum potential of the region.

The reflection surveys recorded sixfold common depth point data to 20 s of two-way time (TWT) over 1400 line km of

seismic traverses. Single traverse lines up to 400 km long were recorded. An additional 2300 line km of analogue data from exploration company surveys were transcribed to digital format and reprocessed as an aid to detailed structural interpretation (Wake-Dyster & others, 1983).

The location of the major BMR seismic reflection traverse lines is shown in Figure 3 and the seismic section from Traverse 1 is shown in Figure 4. The reflection data in Traverse 1 show that the seismic character of the sediments of the Cooper and Eromanga Basins consists of a zone of extensive, coherent reflections to about 2.5 s TWT (3 km depth). Below this to 8 s (4–22 km) is a zone of no reflections which is interpreted as deformed and metamorphosed Early Palaeozoic rocks (Lock, 1983).

Seismic reflections within the Eromanga Basin sequence are generally flat-lying but exhibit some broad amplitude folds. The folds are associated with movement of basement blocks which developed faulting, folding and drape in the overlying Cooper and Eromanga Basin sequences (Lock, 1983). Results from the BMR surveys suggest that the lithological units which give rise to the major reflection horizons in the Eromanga Basin sequence must be thin, compared to their lateral extent, otherwise wide-angle reflections would be evident (Lock, 1983).

A closer view of the central part of Traverse 1 (Fig. 5) illustrates the 0–2 s record (TWT) for a 6 km length of the central part of the traverse east of the Mt Howitt 1 well. The record contains apparent discontinuous reflections from coal-bearing sediments of the Winton Formation — a product of low quality, near surface data, or discontinuous coals. Reflections in the Toolebuc Formation are somewhat discontinuous and 'channelled' on the record for similar reasons. The 'C' horizon and Hutton Sandstone reflections are continuous and of high amplitude even though the quality of this data is not as good as higher fold records from exploration company surveys in the same area. The typical character and continuity of the 'C' seismic reflection is that of a high amplitude and relatively continuous reflection shown in Figure 5. Torkington & Micenko (1988) suggest that the nature of the 'C' horizon

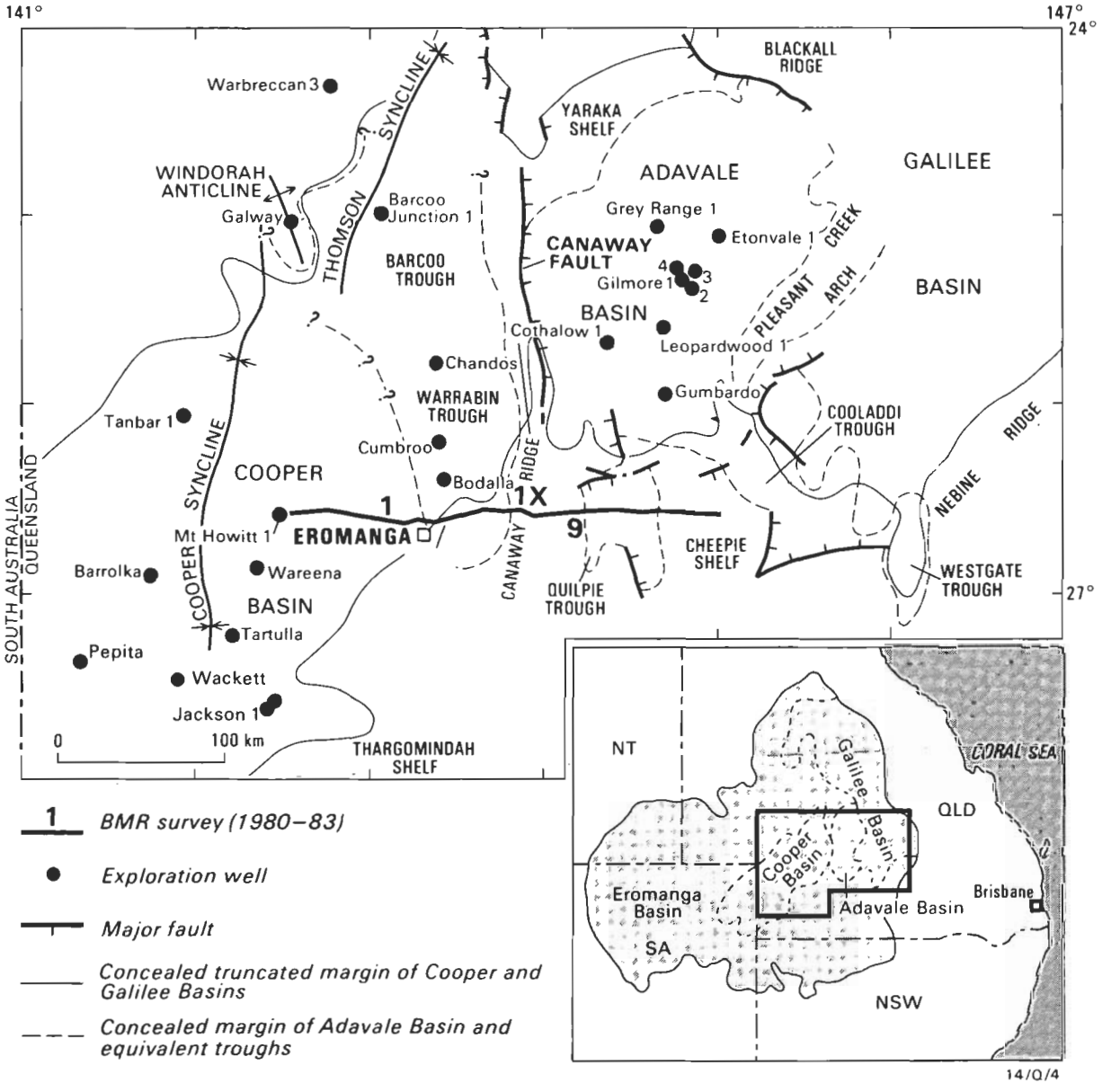

Figure 3. Location of the central Eromanga Basin area, petroleum exploration wells and BMR seismic traverses (1980–83).

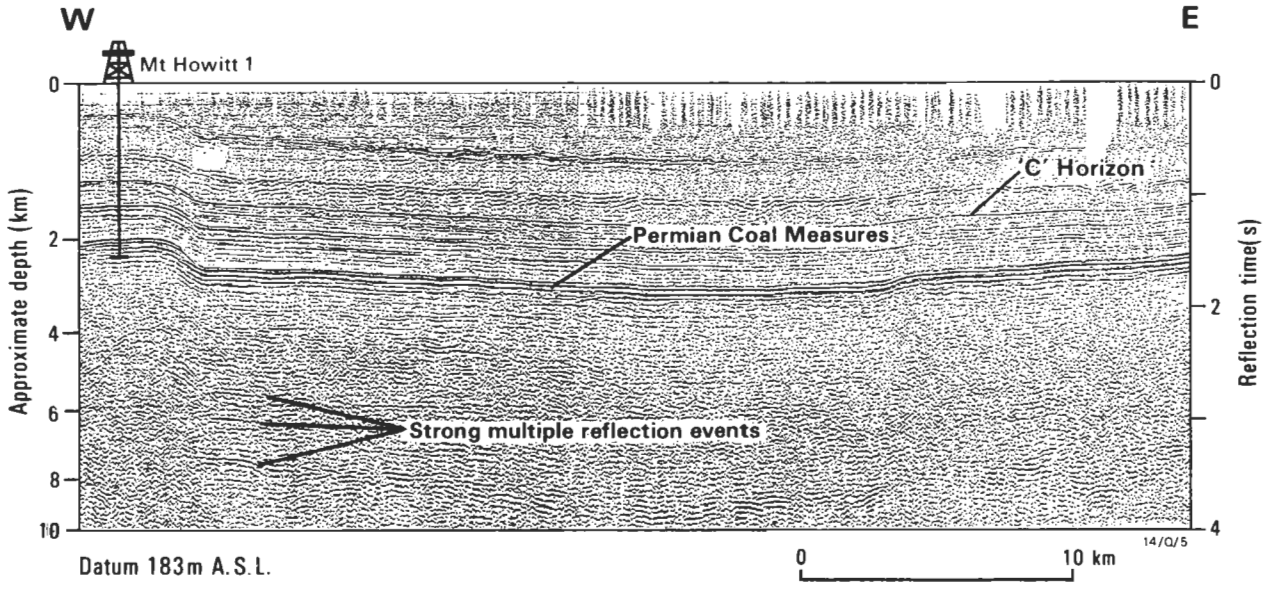

Figure 4. BMR seismic section east of Mt Howitt 1 well showing the 'C' seismic horizon reflection and Permian Cooper Basin coal measures (Traverse 1).
Data shown in Figure 5 are also indicated. After Wake-Dyster & others (1983).

reflection precludes study of its finer characteristics. The limited dynamic range available from some seismic data is one reason why these authors have been unable to model the Wyandra Sandstone oil reservoir which is immediately below the 'C' horizon in the Talgeberry field.

Petrophysical characteristics of the 'C' horizon

Wireline log data from wells in that part of the Eromanga Basin examined by the BMR (1980–83) reveal the typical character of the geological sequence in the basal part of the Wallumbilla/ Bulldog sequences and Cadna-owie Formation.

Wells such as Innamincka 1 and Mt Howitt 1 (Ryan, 1961; Wake-Dyster & others, 1983) show that the Wallumbilla Formation and Bulldog Shale consist of dark fissile shale and that the Cadna-owie Formation is a sequence of fine-grained subangular quartz sandstone with some hard splintery shale. Resistivity (deep) and interval velocity data from these two wells are shown in Figures 6 and 7.

The resistivity log from Innamincka 1 (Fig. 6) shows a pattern which indicates that a buildup or change in formation water salinity is present. Resistivities of about 140 ohm mm/m in the middle and upper part of the formation give way to a zone of as low as 80 ohm mm/m in the basal part. An increase to 200 ohm mm/m is present in the upper part of the Cadna-owie Formation. As sequences above and below the 'C' horizon were deposited in marine or marginal marine conditions, a build-up of water in the sequence, rather than a change in salinity, appears to be the reason for the log data.

The petrophysical data from Mt Howitt 1 and Innamincka 1 also indicate that the features of the basal part of the Wallumbilla Formation are not due to the presence of high concentrations of organic matter (high TOC). Higher than normal resistivity readings would be evident if high TOCs were present, but resistivity readings are lower. The low interval velocity and low density suggest that the sequence is 'under-compacted'.

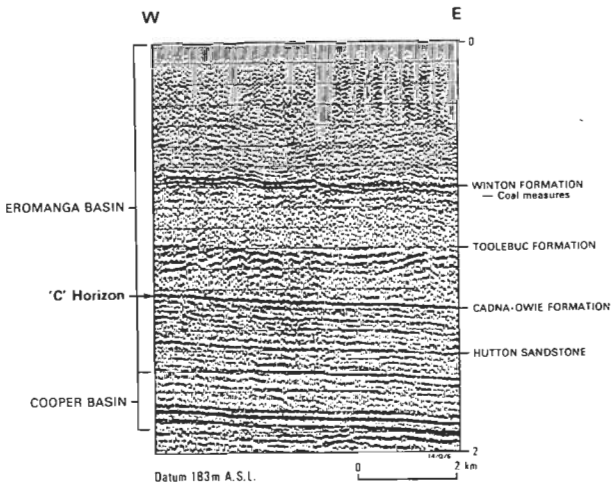

Figure 5. Part of BMR Traverse 1 showing prominent seismic reflections in the Eromanga Basin sequence.
After Wake-Dyster and others (1983).

The interval velocities in Lower Cretaceous and Upper Jurassic sequences of the Eromanga Basin, including the Wallumbilla Formation and Bulldog Shale, increase with depth. Interval velocity in the sequences intersected by the Mt Howitt 1 well (Figure 7) shows a general increase with depth. The basal parts of the Wallumbilla and Bulldog sequences display a lower interval velocity than expected from the depth-interval velocity.

The significant change in velocity between the Wallumbilla and Cadna-owie Formations can also be seen in the reflection coefficient at the 'C' horizon (Fig. 7). Acoustic impedance (the product of density and velocity) also indicates the origin of the 'C' horizon reflection. A plot of the gamma ray, sonic and density logs for the Merrimelia 9 well (Fig. 8; Smith, 1983) shows the petrophysical features of a part of the Eromanga sequence, including the Wallumbilla/Cadna-owie boundary.

There is a density difference of approximately 0.3 gm/cc between the basal part of the Wallumbilla and Cadna-owie Formations. The density difference combines with the change

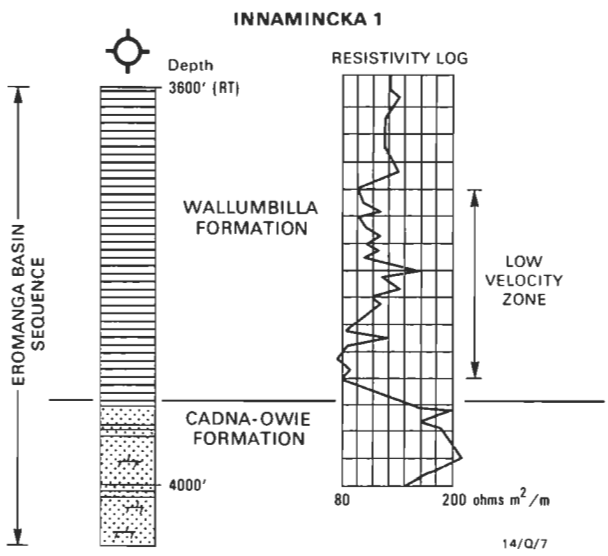

Figure 6. Lithology and resistivity of the lower Wallumbilla and upper part of the Cadna-owie Formations in the Innamincka 1 well. The lowermost part of the Wallumbilla Formation exhibits a lower formation resistivity than the overlying part of the sequence. Data from Ryan (1961).

in sonic velocity between the two formations to produce a major contrast in acoustic impedance, which is expressed on seismic reflection data in the form of the 'C' horizon.

Geohistory and origin of the 'C' horizon reflection

The Eromanga Basin began as a broad depression in the Late Triassic and Early Jurassic, overlying and extending well beyond the limits of the Cooper Basin. Structural development in the early history of the basin involved drape and differential compaction over basement-related features such as highs, as well as graben and half-graben structures. There was some fault growth around the margins of major troughs (Smith, 1983).

The thickness of sediments intersected in petroleum exploration wells provides an indication of the rate of subsidence sedimentation and therefore the nature of basin development through time. Subsidence curves derived from well intersections have been constructed for many parts of the Eromanga Basin. Cook (1982), Kanstler & others (1986), Passmore & Boreham (1986) and Pitt (1982, 1986) discussed the significance of subsidence curves in the Cooper and Eromanga Basins; some of the curves are illustrated in Figure 9. Subsidence/sedimentation rates can been calculated from these and other wells for major structural elements of the basin.

The term subsidence/sedimentation rate is used here to measure deposition of vertical 'compacted' thickness of sediment in m/Ma. Decompacting the shale-rich units such as the Wallumbilla sequence would significantly increase present measured thickness.

Although sea level changes exert an important influence over the pattern and extent of sedimentation in the basin, porosity-depth trends show that basin subsidence rate is the main contributor to the thickness of sedimentary fill.

The Eromanga Basin contains up to 1000 m of Jurassic fluvial, lacustrine and coal-measure sediments which were deposited in a broadly subsiding basin. Subsidence/sedimentation rates were highest in the major structural depressions such as the Patchawarra, Poolowanna and central Nappamerri Troughs, where up to 20 m/Ma of sediment was deposited. Rates of 3–15 m/Ma are evident in the Jurassic sequence for other areas.

In the Early Cretaceous, during deposition of the Wallumbilla succession, subsidence/sedimentation rates increased dramatically to approximately 30 m/Ma, and to peak rates of 65–120 m/Ma in the Cenomanian during deposition of the Winton Formation (Poolowanna 1, Cuttapirrie 1, Beanbush 1, Moomba 3 and Tartulla 1). Subsidence ceased in the Late Cretaceous, and was followed by Early Tertiary tectonism including uplift, wrenching and folding (Pitt, 1986).

Sediment compaction within the Early Cretaceous sequence of the Eromanga Basin can be deduced from the change in wireline log measurements with depth. As the Wallumbilla and Bulldog units contain a large thickness of shale, little or no allowance has to be made for the different compaction rates of shale, siltstone and sandstone when correlating changes of wireline log properties with depth.

Sonic velocity increases with depth in the marine Cretaceous sequence, including the Wallumbilla and Bulldog units (Fig. 7). This increase is thought to be due to a reduction in sediment porosity with increasing depth and increased overburden pressure. The notable exception to the trend is in the basal part of the Wallumbilla/Bulldog sequence.

The rapid deposition of the basal Wallumbilla/Bulldog succession indicates that a permeability seal formed soon after deposition of the sequence. Such a permeability seal would prevent normal dewatering from taking place, and has been maintained as overburden pressure increased.

Implications for exploration

Errors which are apparent in predicting depth to the 'C' horizon are more significant in petroleum exploration now than modelling of the 'C' reflection. Bauer & Harrison (1987) reviewed the results of 11 wildcat and 10 appraisal wells drilled in ATP 269P(1) between 1980 and 1986. They noted an average error in depth prediction to the 'C' horizon of 2.7% in wildcat wells and 0.5% in appraisal wells. They suggested that there is considerable local variation, although there is an average error of 2.7% in 'C' horizon depth prediction over the whole region.

One of the main sources of depth prediction error outlined by Bauer & Harrison (1987) is unexpected velocity variations. They note a 'C' horizon velocity difference of about 50 ms between the Bodalla South wells and Kyra 1, and a velocity gradient of 6 ms/km between these wells. This velocity gradient alters the interpretation of geological structure, reducing closure by about 10 m or half the expected closure height, and greatly reduces potential trap volume. As estimates of the Eromanga fields and trap volumes are sensitive to velocity changes around the level of the 'C' horizon, it is important to improve understanding of factors which influence seismic character and velocity-depth relationships.

The origin of the velocity variations in the sequence down to the 'C' reflection may not be clearly assigned to a single cause. However, if the petrophysical features of the lower part of the Wallumbilla Formation/Bulldog Shale are the product of 'undercompaction', they may contribute to the velocity gradient in the 'C' horizon observed by Bauer & Harrison (1987). 'Undercompaction' could have resulted in entrapment of fluid (water) in the lowermost parts of the Wallumbilla and Bulldog sequences.

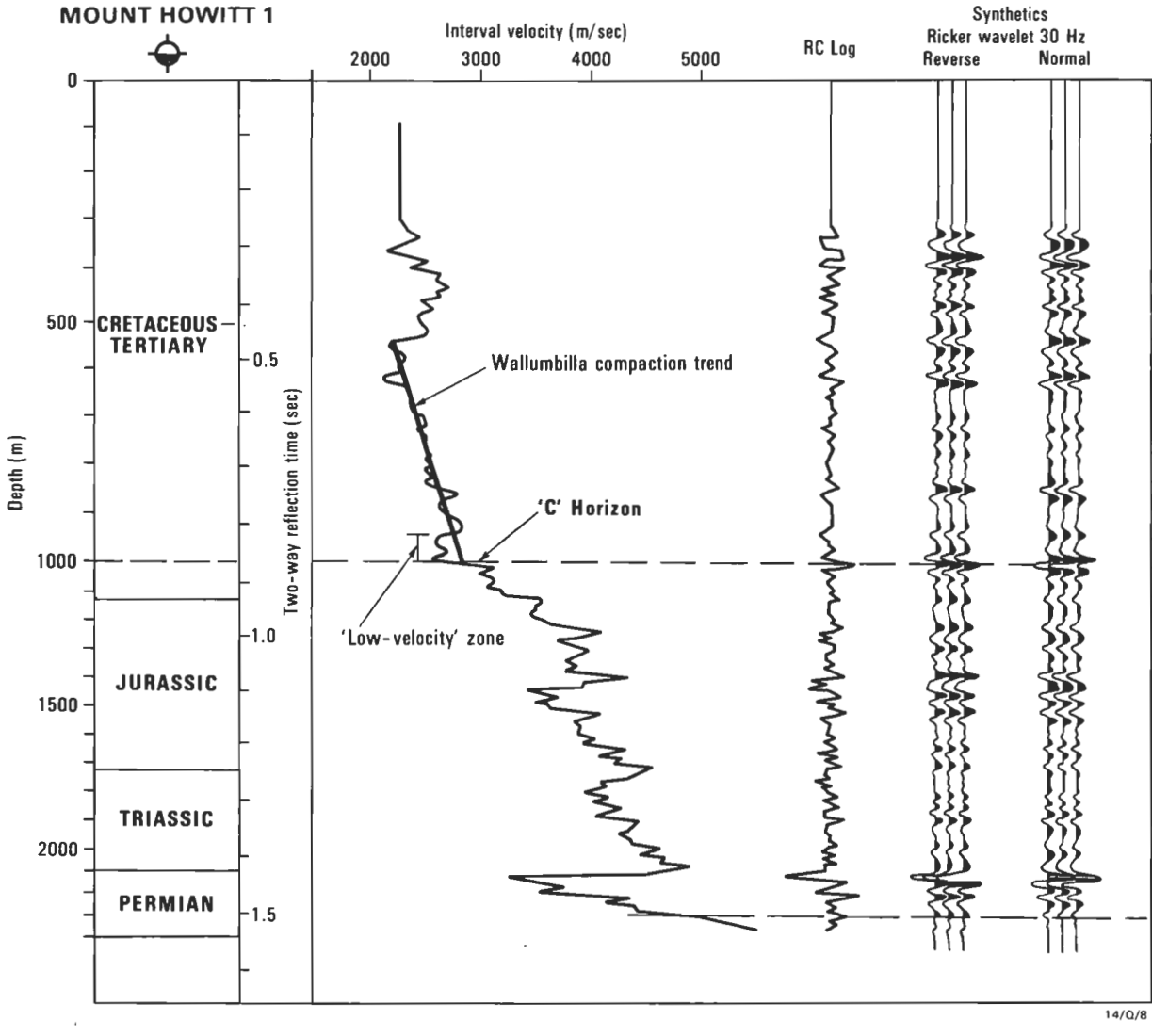

Figure 7. Synthetic seismogram from the Mt Howitt 1 well showing the increase in interval velocity with depth in the Wallumbilla Formation, a low velocity zone at the base of the Wallumbilla, a major reflection coefficient at the Wallumbilla–Cadna-owie boundary and synthetic seismogram traces produced from the well data.
After Wake-Dyster & Pinchin (1981).

The low velocity zone in the basal part of the Wallumbilla Formation which is responsible for the amplitude of the 'C' reflection may be irregular in its vertical thickness and areal extent. The most significant effects of changes in the thickness, extent and magnitude of the low velocity zone are on the depth to the 'C' horizon as well as the shape of depth converted structure contours at this and underlying levels. Local well control (velocity surveys) and detailed velocity analysis of seismic data during processing may help minimise problems associated with depth prediction.

Conclusions

Seismic exploration surveys throughout the Eromanga Basin have confirmed that the 'C' horizon is a major seismic marker and one of the most important for identifying structural trends in the prospective Jurassic and Early Cretaceous parts of the Eromanga sequence.

It has been commonly assumed (such as by Lock, 1983) that the strong amplitude and good continuity of the 'C' horizon reflection is the product of a contrast in rock properties between the Wallumbilla and Cadna-owie Formations. Inspection of log and seismic data in part of the Eromanga Basin investigated during the BMR (1980–83) study suggests that lithology alone is not sufficient to generate the amplitudes displayed by the 'C' horizon reflection.

Petrophysical data examined in this study indicate that the basal part of the Wallumbilla Formation has a lower density than similar sediments in the upper part of the formation and is 'undercompacted'. A buildup of formation fluid in the 'undercompacted' sequence is interpreted on interval velocity (sonic), formation density and resistivity logs. Subsidence curves from wells in the Eromanga Basin suggest that the Wallumbilla Formation, and equivalent Bulldog sequence, were deposited at a time of rapidly increasing basin subsidence. As a result, the basal parts of these units were buried at depths of more than 1 km without being greatly compacted by the weight of overburden. The development of sealing shales in the middle and upper parts of the units in many places may have trapped fluid (water) in the basal part of the sequence, causing an 'undercompacted' zone to be preserved.

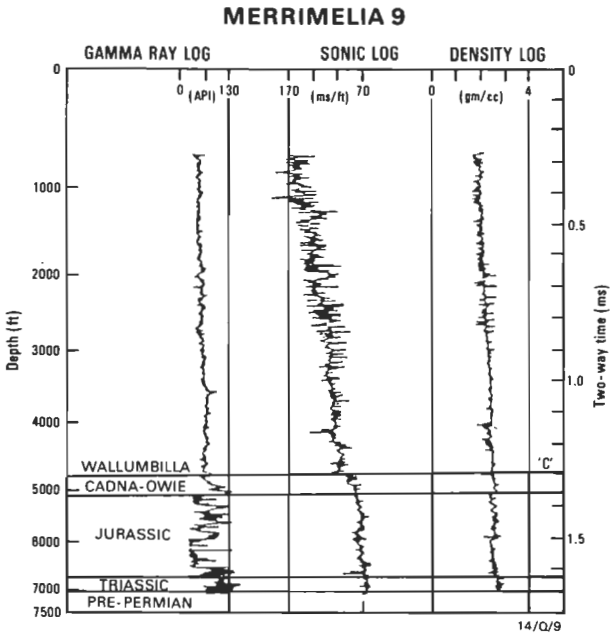

Figure 8. Gamma ray, sonic and density logs from Merrimelia 9 displayed on a time scale.
Data from Smith (1983).

Future seismic data gathering could be oriented towards a more sophisticated analysis of the character and nature of the 'C' horizon reflection. Such work should not be restricted to structure mapping. It should look at the nature and quality of rock properties which affect acoustic impedance contrast, the formation of effective permeability seals, and the implications of these factors for the prospectivity of the Eromanga Basin sequence.

Acknowledgements

The assistance of R. Smit (Santos), A. Waldron (SAGASCO), J. Bauer (Lasmo), A. Williams and V. Passmore (BMR) in guiding the development of some of the concepts in this paper is gratefully acknowledged. D. Gravestock (SADME), J. Hunt (Esso) and A. Guthrie (Esso) provided useful comments on the text and figures.

References

Ambrose, G., Suttill, R. & Lavering, I., 1982 — A review of the early Cretaceous Murta member in the southern Eromanga Basin. *In* Moore, P.S. & Mount, T.J. (compilers), Eromanga Basin Symposium, summary papers. *Geological Society of Australia and Petroleum Exploration Society of Australia, Adelaide*, 92–109.

Ambrose, G., Suttill, R. & Lavering, I., 1986 — The geology and hydrocarbon potential of the Murta Member (Mooga Formation) in the southern Eromanga Basin. *In* Gravestock, D.I., Moore, P.S. & Pitt, G. (editors), Contributions to the geology and hydrocarbon potential of the Eromanga Basin. *Geological Society of Australia Special Publication* 12, 71–84.

Bauer, J.A. & Harrison, P.L., 1987 — Seismic aspects of recent oil discoveries in the Bodalla Block, Cooper/Eromanga Basins, Queensland. *Bulletin of the Australian Society of Exploration Geophysicists*, 18(1/2), 6–10.

Burger, D., 1982 — A basal Cretaceous dinoflagellate suite from north-eastern Australia. *Palynology*, 6, 161–192.

Cook, A.C., 1982 — Organic facies in the Eromanga Basin. *In* Moore, P.S. & Mount, T.J. (compilers), Eromanga Basin Symposium, summary papers. *Geological Society of Australia and Petroleum Exploration Society of Australia, Adelaide*, 234–257.

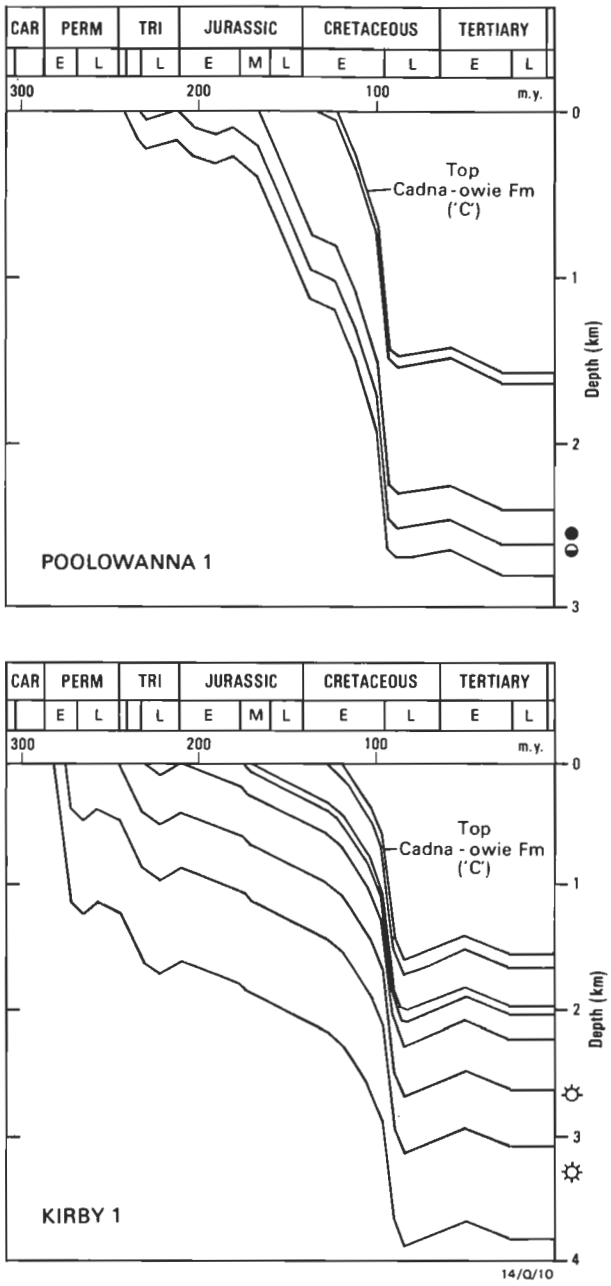

Figure 9. Subsidence history curve for Poolowanna 1 (Poolowanna Trough) and Kirby 1 (Nappamerri Trough).
After Kanstler & others (1986).

John, B.H. & Almond, C.S., 1987 — Lithostratigraphy of the Lower Eromanga Basin sequence in south-west Queensland. *The APEA Journal*, 27(1), 196–214.

Kanstler, A.J., Cook, A.C. & Zwigulis, M., 1986 — Organic maturation in the Eromanga Basin. *In* Gravestock, D.I., Moore, P.S. & Pitt, G. (editors), Contributions to the geology and hydrocarbon potential of the Eromanga Basin. *Geological Society of Australia Special Publication* 12, 305–322.

Lock, J., 1983 — Velocity/depth modelling using reflection and refraction data recorded in the central Eromanga Basin, Queensland, Australia. *Tectonophysics*, 100, 175–184.

McKirdy, D.M., Emmett, J.K., Mooney, B.A., Cox, R.E. & Watson, B.L., 1986 — Organic geochemical facies of the Cretaceous Bulldog Shale, western Eromanga Basin, South Australia. *In* Gravestock, D.I., Moore, P.S. & Pitt, G. (editors), Contributions to the geology and hydrocarbon potential of the Eromanga Basin. *Geological Society of Australia Special Publication* 12, 287–304.

Moore, P.S., Hobday, D.K., Mai, H. & Sun, Z.C., 1986 — Comparison of selected non-marine petroleum-bearing basins in Australia and China. *The APEA Journal*, 26(1), 258–309.

Moore, P.S. & Pitt, G., 1984 — Cretaceous of the Eromanga Basin — implications for hydrocarbon exploration. *The APEA Journal*, 24(1), 358–376.

Newton, C., 1986 — The Tintaburra oilfield. *The APEA Journal*, 26(1), 334–352.

Passmore, V.L. & Boreham, C.J., 1986 — Source rock evaluation and maturation history of the central Eromanga Basin. *In* Gravestock, D.I., Moore, P.S. & Pitt, G. (editors), Contributions to the geology and hydrocarbon potential of the Eromanga Basin. *Geological Society of Australia Special Publication* 12, 221–241.

Passmore, V.L. & Burger, D., 1986 — The effects of eustatic sea-level changes on Early Jurassic deposition in the eastern Eromanga Basin, Australia. *In* Sediments Down Under. *12th International Sedimentological Congress, Canberra*, 237.

Paton, I., 1982 — The Birkhead Formation: a Jurassic petroleum reservoir. *In* Moore, P.S. & Mount, T.J. (compilers), Eromanga Basin Symposium, summary papers. *Geological Society of Australia and Petroleum Exploration Society of Australia, Adelaide*, 346–355.

Pitt, G., 1982 — Geothermal gradients in the Eromanga–Cooper Basin region. *In* Moore, P.S. & Mount, T.J. (compilers) — Eromanga Basin Symposium, summary papers. *Geological Society of Australia and Petroleum Exploration Society of Australia, Adelaide*, 262–283.

Pitt, G., 1986 — Geothermal gradients, geothermal histories and the timing of thermal maturation in the Eromanga–Cooper Basins. *In* Gravestock, D.I., Moore, P.S. & Pitt, G. (editors), Contributions to the geology and hydrocarbon potential of the Eromanga Basin. *Geological Society of Australia Special Publication* 12, 323–351.

Ryan, J.C., 1961 — Innamincka No 1 well, South Australia, well completion report. *Petroleum Search Subsidy Acts (Department of National Development), Publication No.* 9.

Senior, B.R., Mond, A. & Harrison, P.L., 1978 — Geology of the Eromanga Basin, Queensland, Australia. *Bureau of Mineral Resources, Australia, Bulletin* 167.

Smith, B.L., 1983 — Seismic investigation of the Merrimelia Field. *The APEA Journal*, 23(1), 192–202.

Sprigg, R., 1986 — The Eromanga Basin in the search for commercial hydrocarbons. *In* Gravestock, D.I., Moore, P.S. & Pitt, G. (editors), Contributions to the geology and hydrocarbon potential of the Eromanga Basin. *Geological Society of Australia Special Publication* 12, 305–322.

Torkington, J. & Micenko, M., 1988 — A stratigraphic analysis of the Talgeberry oilfield. *The APEA Journal*, 28(1), 113–122.

Wake-Dyster, K., Moss, F.J. & Sexton, M.J., 1983 — New seismic reflection results in the central Eromanga Basin, Queensland, Australia: the key to understanding its tectonic evolution. *Tectonophysics*, 100, 147–162.

Wake-Dyster, K. & Pinchin, J., 1981 — Central Eromanga Basin seismic survey, Queensland, 1980. *Bureau of Mineral Resources, Record* 1982/22.

Wopfner, H., 1960 — On some structural developments in the central part of the Great Artesian Basin. *Royal Society of South Australia Transactions*, 83, 179–193.

Wopfner, H., Freytag, I.B. & Heath, G.R., 1970 — Basal Jurassic–Cretaceous rocks of western Great Artesian Basin, South Australia: stratigraphy and environment. *American Association of Petroleum Geologists, Bulletin* 54(1), 383–416.

BMR Journal of Australian Geology & Geophysics, 12, 13–24

Inverted transtensional basin setting for gold and copper and base metal deposits at Cobar, New South Wales

R. A. Glen[1]

The Cobar Basin in western New South Wales formed by sinistral transtension in the latest Silurian to late Early Devonian and evolved through a syn-rift phase of brittle upper crustal faulting and subsidence followed by a post-rift sag phase of passive subsidence which can also be recognised in other Early Devonian stratotectonic elements in western New South Wales. Basin evolution was controlled by regional faults splaying off the Gilmore Suture and the Kiewa Fault. The Cobar Basin was largely inverted ~400 Ma ago with reversal of movement (dextral transpression) on synsedimentary north–northwest-trending strike-slip/oblique-slip faults and on west–northwest-trending dip-slip faults. These faults controlled the partitioning of deformation in surface rocks into a high-strain Zone 1 developed above a half positive flower structure in the eastern part of the basin, and a lower strain Zone 2 developed above a flat detachment in the central part of the basin. Shortcut faults developed during inversion are the most likely structural targets for sulphide and gold accumulation which is structurally controlled and syntectonic metahydrothermal in origin. Some of these faults have experienced strike-slip faulting as well as contractional movement.

Introduction

The Cobar region in western New South Wales is one of the most prospective parts of the Lachlan Fold Belt for gold and base metal exploration. Major mining centres in the region are those around Cobar itself (the Cobar Mining Field) as well as those of Canbelego, Nymagee, Shuttleton and Mount Hope (Fig. 1). All deposits in these fields occur in Early Devonian rocks belonging to the Cobar Supergroup. The largest group of deposits is the Cobar Mining Field, which extends some 60 km from Elura Mine in the north to the Queen Bee Mine in the south. Historical and indicated reserves of this field amount to more than 431 000 t copper, 1 600 300 t lead, 2 500 000 t zinc, 4050 t silver and 56 t gold.

Recent work in the Cobar region by the Geological Survey of New South Wales has resolved to a considerable degree previous uncertainties and contradictions about stratigraphy, ages of units, deformation styles and ages, and the relationships of orebodies to regional structures and stratigraphic units. In the area around Cobar, published and unpublished work has produced a new tectonic model for the opening, filling and closure of the Cobar Basin. Structures developed during the inversion of the basin have in places acted as focusing pathways and traps for mineralising solutions.

Despite the new available surface mapping, the poor outcrop, lack of relief, monotonous lithologies and sparse fossil data create major uncertainties when trying to extrapolate surface data to depth, and act as major constraints on any tectonic and ore genesis models for the field. In order to solve this problem a consortium of government and mining/exploration companies has been formed to carry out deep seismic reflection studies in the area, under the aegis of the Australian Consortium of Refraction Profiling (ACORP). The consortium comprises the Bureau of Mineral Resources, the New South Wales Department of Minerals and Energy through the NSW Geological Survey, and three companies — Pasminco Limited, Geopeko and CRA Exploration Pty Ltd. The aims of the studies are:

1. to define major, possibly prospective structures which developed both within the basin and along its margins; and thereby
2. to test tectonic models which may have a significant impact on the prospectivity of both the Cobar Basin and other similar basins within the Lachlan Fold Belt.

The Cobar ACORP study marks a major attempt to apply the seismic reflection technique to deformed sedimentary basins within the fold belt. Up to now, the method has been applied mainly to undeformed basins; successful results from this project will establish seismic as a major regional mapping tool in fold belts. Because of company involvement, these results will be proprietary for two years after the end of data acquisition.

Because of the novelty in interpreting seismic data from folded rocks at Cobar, great care has been taken to define the parameters of the study, which must be able to pass judgement on the existing tectonic models of the area. This paper briefly describes the 'pre-seismic' tectonic and ore genesis models, which serve as a framework for seismic work and can later be compared with 'post-seismic' models. Modifications to these 'pre-seismic' models will come as no surprise.

Regional setting

Regional crustal extension of the Lachlan Fold Belt in western New South Wales in the latest Silurian to Early Devonian led to the widespread development of deepwater[2] troughs and basins and shallow-water flanking shelves. In the Cobar region, four deepwater elements are recognised (Glen & others, 1985) — the Cobar Basin to the north, the Mount Hope and Rast troughs joining it to the south and the poorly known Melrose Trough further to the southeast (Fig. 1).

The Cobar Basin, Mount Hope and Rast troughs form the eastern part of the Darling Basin (Glen & others, 1985). Shallow-water elements flanking deepwater structures (Fig. 1) include:

1. the Kopyje Shelf (Lochkovian in age; Sherwin, 1985) which lies east and north of the Cobar Basin, east of the Rast Trough and around the northern part of the Melrose Trough. The volcanic-rich eastern part of this shelf is the Canbelego–Mineral Hill Belt;
2. the Winduck shelf (mainly Pragian in age with some Lochkovian elements; Sherwin, 1985) which lies west of the Cobar Basin and Rast Trough, and
3. the Walters Range Shelf (Pragian in age; Sherwin, 1985) which lies between the Mount Hope and Rast troughs.

The regional Devonian extension event in western New South Wales followed:

1. deposition of the Girilambone Group. Limited palaeontological control indicates a late Darriwilian to earliest Gisbornian (Lower Ordovician) age at least in part (Stewart

[1] Geological Survey of New South Wales, PO Box 536, St Leonards NSW 2065

[2] The term 'deepwater' is used for water depths of greater than fair-weather wave base.

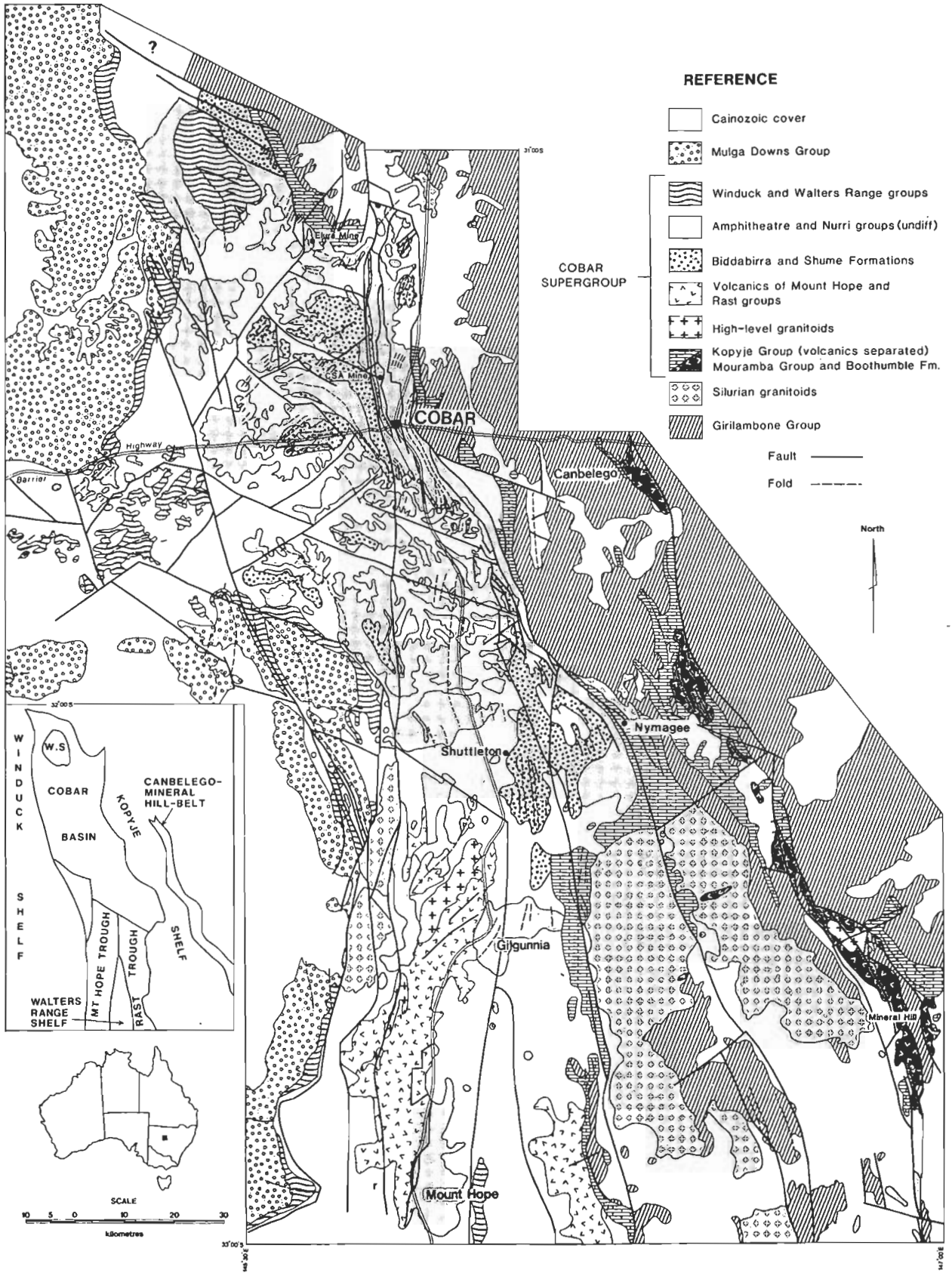

Figure 1. Location map, showing main geological units in the Cobar region.
Inset shows Devonian extensional elements. Based on mapping by Geological Survey of New South Wales (work by Glen, MacRae, Pogson, Scheibner and Trigg).

& Glen, 1986). This is consistent with the suggestion that deposition occurred in the northern part of the Wagga Basin (Pogson, 1982).

2. deformation of Girilambone Group rocks to greenschist–low amphibolite grades in the latest Ordovician–earliest Silurian (Pogson, 1982).
3. emplacement of granitoids during the Silurian, commencing with rare foliated granites at around 440 Ma (Pogson & Hilyard, 1981) but consisting mainly of post-tectonic Late Silurian granitoids at around 420 Ma (e.g. Thule Granite 422 ± 6 Ma, Pogson & Hilyard, 1981; Erimeran Granite ~419 Ma, S. Shaw, Macquarie University, & D. Pogson, Geological Survey of New South Wales, personal communication, 1985; Wild Wave Granodiorite 418 ± 2 Ma, Glen & others, 1983).

The youngest Palaeozoic events in the Cobar region were the deposition of the ~4 km thick fluviatile Mulga Downs Group from the late Early Devonian to earliest Carboniferous, and its subsequent deformation, presumably in the Carboniferous (Glen, 1982).

There is no widespread angular unconformity between the Mulga Downs Group and rocks of the underlying Winduck Shelf. Relations are generally paraconformable, although they range from disconformable to locally angular unconformable (Glen, 1982).

Elements of fill of the Cobar Basin

The Cobar Basin was filled by siliceous clastic sediments which show clear subdivision into syn-rift and post-rift packets (Figs 2, 3a). Although almost all of this fill is turbiditic, the syn-rift packet commenced with deposition of alluvial fan and shallow-water sequences on an unstable shelf (Mouramba Group; MacRae, 1987), which is now restricted to (or only developed in) the southeastern corner of the basin. Turbiditic sedimentation commenced soon after, with deposition of the Nurri Group (shed off land to the east) and lower parts of the Amphitheatre Group shed off varying sources to the northwest, west, southwest and southeast (Glen & others, 1985; Glen, 1987a; MacRae, 1987; Glen, in press). Variation in source direction, recognition of multiple submarine fan systems (Glen 1987a, MacRae 1987), major cyclic changes in bed thicknesses (sandstone beds up to 1 m) within the sequence (see below), and significant thickness changes across early syndepositional faults (see below) all indicate that the synrift packet continued into the Pragian, at or near the top of the Biddabirra Formation (Glen, 1989, 1990). Volcanics form only an insignificant part of the outcropping syn-rift packet, although they may be more common at depth, possible accounting for the increased gravity anomaly developed over the extended crust overlain by the Cobar Basin (Bureau of Mineral Resources, 1970; cf. Scheibner, 1982).

The post-rift packet comprises the Pragian upper Amphitheatre Group. Deposition in a quieter tectonic environment is reflected by reversion to thinner bedded turbidites (with sandstone beds generally less than 5 cm thick, but up to 10 cm), by a more consistent palaeocurrent direction to the southeast (Glen, 1987a, 1990, in press) and by less dramatic changes in thickness across the basin. This post-rift sag phase of subsidence was more widespread than the syn-rift phase of extension and, as a result, large areas of basement and even old shelf west of the Cobar Basin became submerged below the Pragian Winduck Shelf. As subsidence of the Cobar Basin slowed, sediments of the upwardly shallowing Winduck Shelf prograded eastwards across the old basin edge and before erosion probably interfingered with and overlay the post-rift

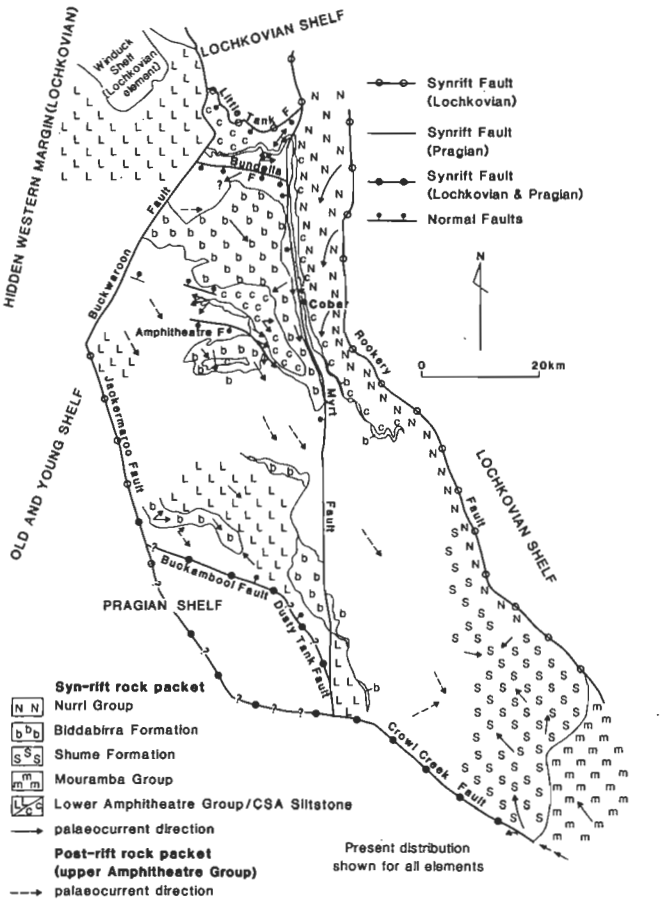

Figure 2. Interpretative diagram, using present rock distribution of the deformed Cobar Basin, showing syn-depositional faults and syn-rift and post-rift rock packets.

West–northwest-trending faults are inferred to be extensional largely dip slip. Meridional to northwest-trending faults on east (?and west) margins are inferred to be oblique to strike-slip faults. Palaeocurrent directions represent variable sized groups of data presented in MacRae (1988) for the southeast of the basin and Glen (1987a, in press) for the rest of the basin.

basin sediments of the upper Amphitheatre Group (Glen, 1987a). Whereas the syn-rift phase of formation was synchronous with limited crustal extension to the east (leading to formation of the Kopyje Shelf, see below), there was no equivalent post-rift sag phase subsidence east of the Cobar Basin (unless of course *all* evidence of Pragian sediments there was removed by later deformation and erosion). Sag phase subsidence thus seems to be asymmetrical in character, with syn-rift and post-rift packets outlining a 'half steer-head' structure rather than a symmetrical 'steer-head'.

The syn-rift and post-rift phases of formation of the Cobar Basin can be recognised throughout the Cobar region in the Mount Hope and Rast troughs, in the development of the Winduck and Walters Range shelves and in the Canbelego–Mineral Hill Belt (Glen, 1990). In the Mount Hope Trough (Fig. 3b), block-faulted felsic volcanics and interbedded sediments (Mount Hope Group; Scheibner, 1985) form the syn-rift packet. Deposition was originally fluviatile (Mount Kennan Volcanics; Scheibner, 1987) but became turbiditic thereafter. The siltstone-rich 'distal' Pragian turbidites of the Broken Range Group (Scheibner, 1987) and the surrounding shallow-water Winduck and Walters Range groups (Scheibner, 1987) represent post-rift, sag-phase deposition. In the Canbelego–Mineral Hill Belt (Fig. 3c), Lochkovian volcanics and clastics (including the debris flow Talingaboolba Formation (Pogson & Felton, 1978) are all syn-rift, and are unconformably overlain

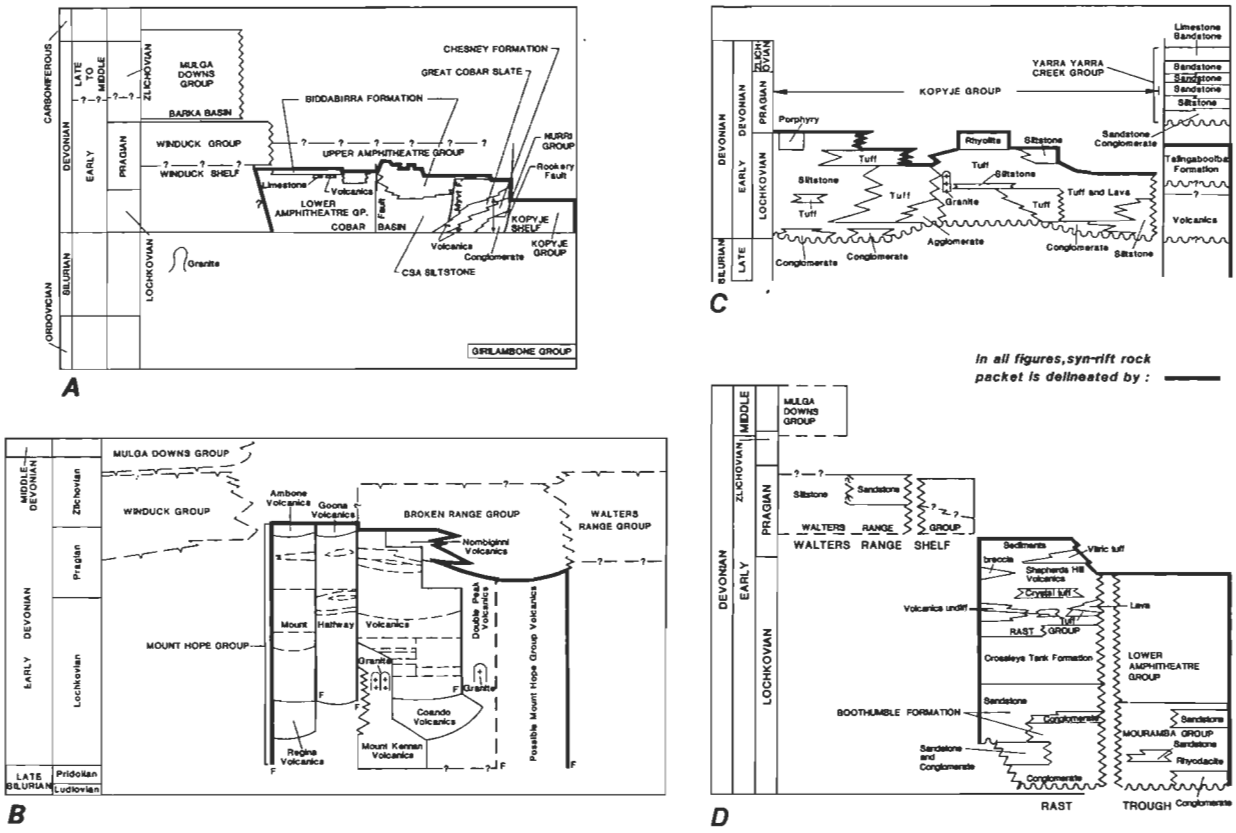

Figure 3. Rock relation diagrams showing syn-rift and post-rift elements for Devonian extensional elements in the Cobar Basin. **A,** Cobar Basin, modified from Glen (1987a). **B,** Canbelego–Mineral Hill Belt, simplified from Pogson (in press). **C,** Mount Hope Trough, simplified from Scheibner (1985). **D,** Rast Trough, modified from Trigg (1987).

to varying degrees by the post-rift Yarra Yarra Creek Group, consisting of shallow-water clastics and limestones (Pogson & Felton, 1978). In the Rast Trough (Fig. 3d), shallow-water to alluvial fan deposits (Boothumble Formation, Mouramba Group; Trigg, 1987) mark the start of the syn-rift phase. The mixed volcaniclastic and siliclastic, turbiditic Rast Group occupies the remainder of the syn-rift pocket, and probably extends up only into the Early Pragian (L. Sherwin, New South Wales Geological Survey, personal communication, 1988) rather than Zlichovian as thought by Trigg (1987). No outcropping post-rift sequence has yet been recognised from this trough, but sag-phase subsidence next to the Rast Trough led to formation of the shallow-water Winduck and Walters Range groups.

Indications thus are of large scale upper crustal processes acting roughly synchronously over 25 000 km^2 of western New South Wales. The superposition of syn-rift and post-rift phases of basin formation, the presence of abundant volcanics in the Mount Hope and Rast troughs and in the Canbelego–Mineral Hill Belt of the Kopyje Shelf, and the possible presence of volcanics either at the base of the Cobar Basin or in middle crustal levels beneath it, all suggest that processes leading to upper crustal extension and sag phase subsidence were concentrated in the same area over time. This has implications for the geometry and mechanism of crustal scale extension, which are outside the scope of this paper.

Cobar Basin architecture

Assessment of the syndepositional architecture of the Cobar Basin is complicated by poor outcrop, monotonous lithologies and the recognition that present boundaries and internal faults formed during basin inversion. Syndepositional faults are recognised by major, abrupt changes in facies and/or thickness across these inversion structures. Characteristics of faults identified this way are shown in Table 1. Their distribution and age constraints suggest that the Cobar Basin was fault-bounded on all sides (Fig. 2), although there is a lack of data about the Little Tank Fault along the northern edge.

Activity along the faulted eastern margin (Rookery Fault) was greatest at basin initiation. The upward-fining cycle of the Lochkovian Nurri Group indicates that activity on this fault (i.e. relief) diminished about the end of the Lochkovian (Glen, 1987a). This coincided with a switch of basin-margin tectonism to the western side of the Cobar Basin, which in part was the Jackermaroo Fault, and which in part lies hidden below post-rift rocks. Uplift and fault activity along this edge sent huge submarine fan lobes across the entire basin, and this is reflected in the upward thickening and coarsening cycle of the lower parts of the Amphitheatre Group (CSA Siltstone and lower Amphitheatre Group and up to the top of the Biddabirra Formation) (Glen, 1987a). Lessening of activity on the Rookery and Little Tank faults around the Lochkovian/Pragian boundary coincided with the development of new faults basinwards of them — the Myrt and Bundella faults respectively — which dammed the Amphitheatre Group to the west and south. As a result of this damming, shallow-water shelf-rocks at the start of syn-rift phase of subsidence were only thinly covered, and are now exposed on the eastern edge of the basin. How long these faults were active for is unknown. If there was no sag-phase subsidence east of the Cobar Basin (see above), fault activity must have persisted into post-rift time.

Synchronous activity on faults with different orientations constrains their movement histories. In the absence of direct

Table 1. Nature and age of synsedimentary faulting in the Cobar Basin.

Fault	*Demonstrated age*	*Activity*	*Type of fault*
Rookery	Lochkovian	Separates shelf from basement. W facing scarp. E edge of Cobar Basin in north, hinge zone overlapped by interfingering facies in SE corner. Intrabasinal conglomerates and slumped blocks of limestone in basin sediments attributed to faulting.	strike-slip, oblique-slip
Little Tank	Lochkovian (inferred)	Separates shelf from basin.	extensional
Jackermaroo	Lochkovian	Separates basal Lochkovian shelf sediments from basal Lochkovian turbidites. Extension to north underwent local early inversion, putting Lochkovian shelf over Lochkovian turbidites.	?strike-slip, oblique-slip
Myrt	Pragian	W facing scarp. Dramatic thinning of CSA Siltstone and Biddabirra Fault. Inactive before end of Biddabirra deposition.	strike-slip, oblique-slip
Bundella	Pragian	S-facing scarp, dams Biddabirra Formation to south.	extensional
Crowl Creek	Lochkovian to ?Pragian	Separates volcanics on south from clastics on north. Used as feeder channel for Shume fan. Dams Shume Fm to north.	extensional
Buckwaroon	Pragian	Biddabirra Formation thicker to east.	?

evidence for fault movement, information must come from the pattern of contractional faults. The braided nature of the faulted eastern margin, its length, and cross-sections indicating the presence of fore and back thrusts (see below and Glen 1990) all suggest that this basin edge is now a positive half-flower structure above a strike-slip fault. These inferences suggest that the original north–northwest trending edge of the Cobar Basin was marked by transtensional structures, and this in turn means that the west–northwest trending faults were extensional faults. The mainly hidden western margin of the basin was probably also transtensional, but data are scarce and limited to the southern section where a ramping, largely east-dipping thrust system developed in the Carboniferous (not Devonian as in the east — see below). Transtensional faults commonly contain areas of local uplift where changes in fault orientations lead to localised shortenings, and further evidence for these features in the basin history supports the transtensional faulted nature of the eastern and western boundaries. Along the eastern margin such syn-sedimentary uplifts led to deposition of intraformational conglomerate (Glen, 1987a). Along the western margin, uplift led to local inversion with Lochkovian shelf rocks lying above Lochkovian turbidites (Glen, in press). The Cobar Basin thus formed as a transtensional basin, opening under left-lateral shear coupled with extension.

Structures formed during basin inversion

Basin inversion was caused by right-lateral transpression. Subdivision of structures into zones of varying intensity and geometry (Glen, 1985) reflects the partitioning of deformation into largely strike-slip plus compressional components (Structural Zone 1) along the eastern edge and into purely compressional components elsewhere (Zone 2) (Fig. 4).

Structural Zone 1 lies along the eastern edge of the former basin and widens southward. Its structural style is characterised by a series of steep east and west dipping thrust faults at the surface, which are inferred to shallow with depth as part of a linked thrust system and merge into a floor thrust which itself steepens into a strike-slip fault (Fig. 5; Glen, 1988, 1989, 1990). These thrust faults are best recognised in the northern and middle parts of Zone 1, which they divide into three thrust plates. From west to east, these are:

- the steeply west-dipping Cobar Plate (imbricated at CSA Mine) and bounded to the east by the west-dipping Cobar Fault;
- a central strongly imbricated triangle zone (Chesney Plate) between the Cobar Fault and the east-dipping Great Chesney Fault;
- eastern pop-up zones (the Queen Bee Plate in the south between the Queen Bee and Rookery faults) and the northern part of the Rookery Plate in the north between the Great Chesney Fault and the west-dipping Rookery Fault (Figs 4, 5).

Geometries of these features are discussed more fully in Glen (1990). The Myrt and Rookery faults are interpreted to be reactivated syn-sedimentary faults. The other faults have no demonstrable early history and developed as short-cut structures during thrusting, as movement on the steepening reactivated faults became inhibited by increasing friction, causing them to become locked up. Major folds in Zone 1 are interpreted to be thrust related — as ramp (fault-bend) folds or as fault-propagation folds — which were subsequently overprinted by a regional shortening event which led to development of a subvertical S_1 cleavage (overprinting a local earlier fabric). S_1 commonly transects F_1 folds (Glen, 1985, 1990) and contains a subvertical extension lineation (L_1).

Structural Zone 1 also contains evidence of a strike-slip component of deformation which was active throughout the zone both during ductile cleavage formation, and also on individual faults during brittle deformation. Large-scale left-lateral ductile movement is indicated by transected relations between F_1 folds and S_1 cleavage (Fig. 4, and Glen, 1985, 1990) and by the variation in angles between S_1 and bounding faults (Fig. 4). This left-lateral movement is especially marked north of the latitude of Cobar. Evidence of strike-slip movement on individual faults within Zone 1 is indicated by the braided pattern of the Rookery Fault, by jogs and quartz vein arrays in and adjacent to the Great Chesney Fault (Glen 1987a), and by shallow plunging striae on steeply east-dipping shears which overprint dip-slip striae both at the CSA Mine and at The Peak in the Blue Shear. At The Peak, the pattern of braided faults (mapping by M. Hinman, James Cook University, personal communication, 1989) and the presence of steep folds in chlorite-talc schist also indicate strike-slip movement. While most of the strike-slip movement in Zone 1 was left-lateral, a right-lateral component of vertical movement on the Great Chesney Fault has been documented (Glen, 1987a). Right-lateral movement on the Myrt Fault is also suggested from the angular relations between that fault and D_1 structures in Zone 2 to the west (Fig. 4). Together these apparently contradictory movements are best interpreted in terms of the northern part of Zone 1 being translated southward, underthrusting the southern part (Glen, 1990).

Structural Zone 2 is of lower D_1 strain than Zone 1. Local relatively high strain parts do occur (e.g. the Bundella Block) but even here strain is less than in Zone 1. D_1 structures in Zone 1 include west–northwest trending F_1 folds, steep faults (inferred to be thrusts which shallow and merge at depth into a flat detachment; Fig. 6) and a subvertical S_1 cleavage which is best developed in the Bundella Block where it contains a down dip extension lineation L_1 (Schmidt, 1980). At Elura mine, de Roo (1989) showed that this S_1 overprints an earlier fabric which K.

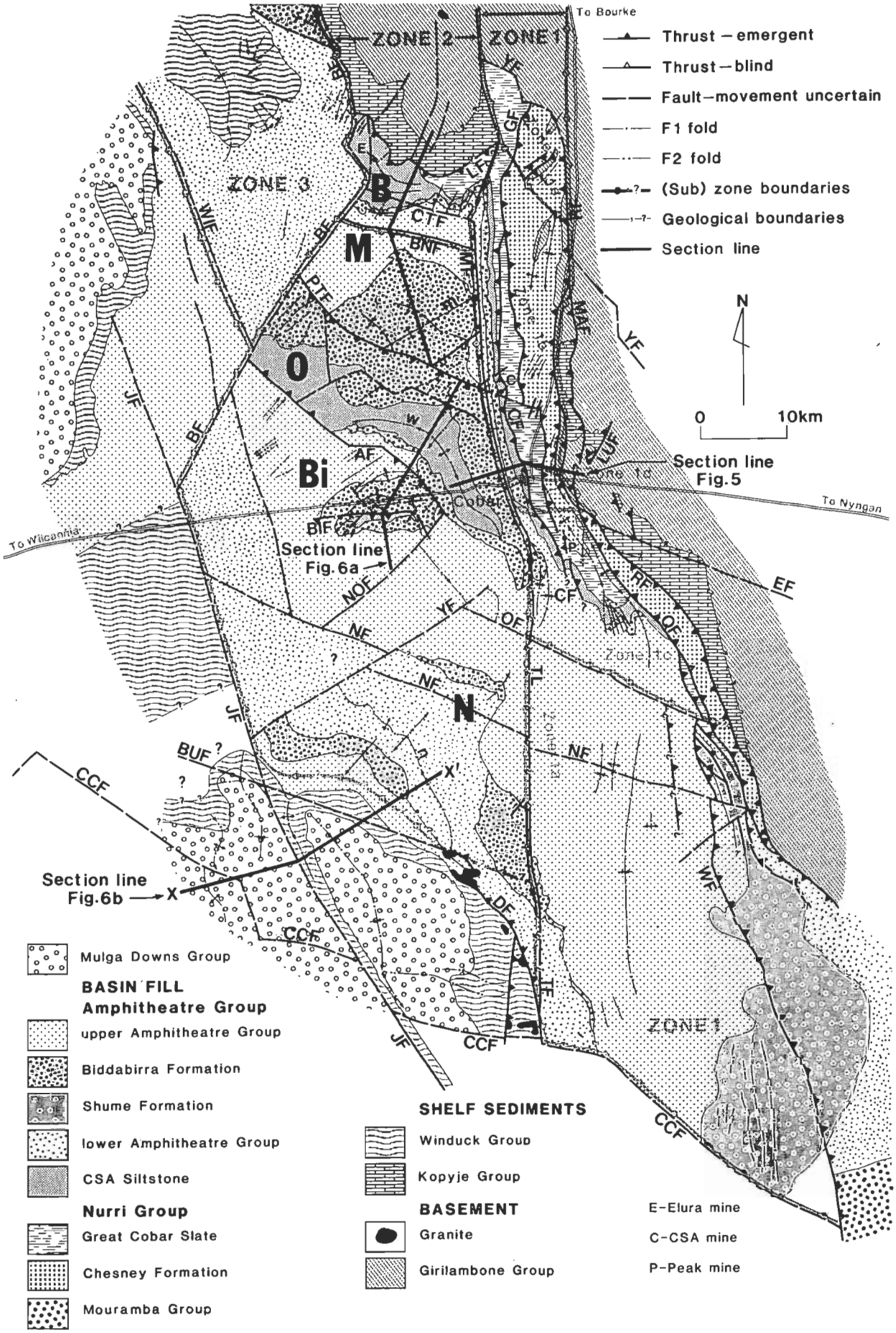

Figure 4. Map of deformed Cobar Basin, showing stratigraphic units, subdivision into structural zones, subzones and blocks, regional folds and contractional faults.

Block names (Zone 2): B Bundella, M Maryvale, O Oakden, Bi Biddabirra, N Nullawarra. Other abbreviations refer to faults and selected folds in Structural Zone 2. **Faults:** AF Amphitheatre Fault, BF Buckwaroon Fault, BIF Biddabirra Fault, BNF Bundella Fault, BUF, Buckambool Fault, CF Cobar Fault, CCF Crowl Creek Fault, CTF Cougar Tank Fault, DF Dusty Tank Fault, EF Elliston Fault, GF Great Chesney Fault, JF Jackermaroo Fault, LF Little Tank Fault, LUF Lucknow Fault,

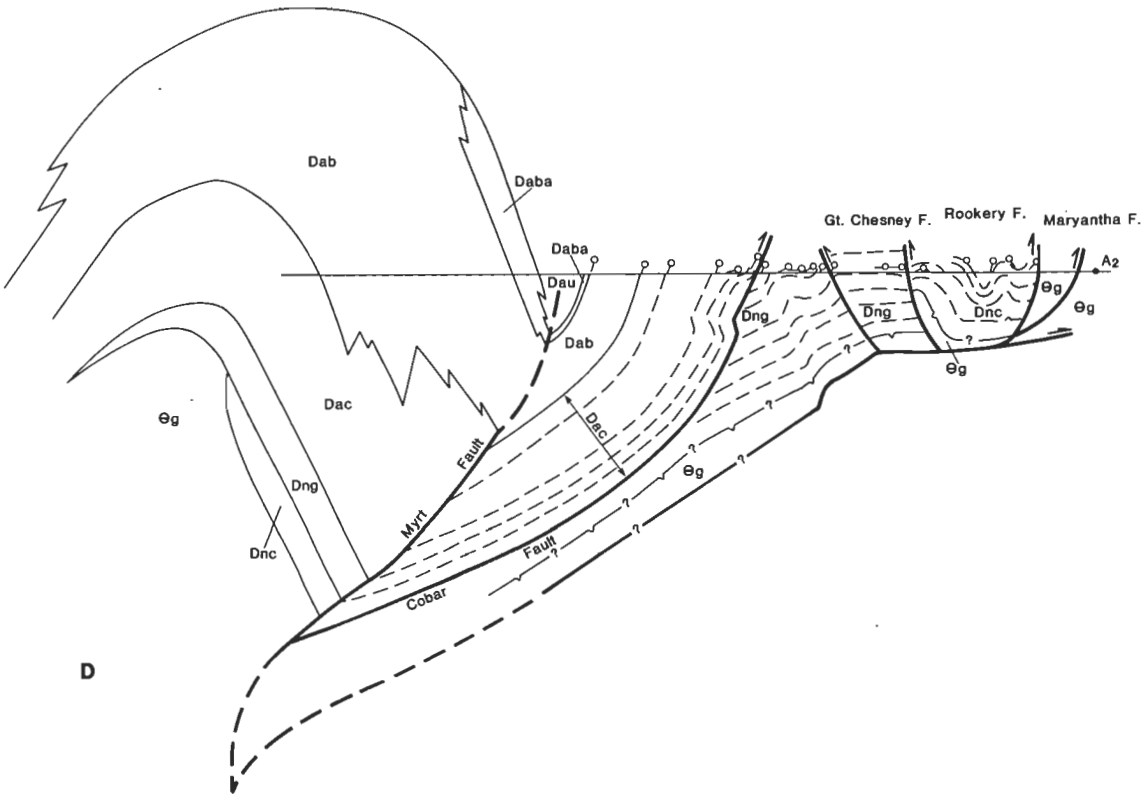

Figure 5. Representative cross-section through Structural Zone 1 and extending locally to the east and west.
This section is not unique, given lack of relief and absence of subsurface data, and could be significantly changed if there were other units (e.g. volcanics) at depth.

Lawrie (James Cook University, personal communication, 1989) has suggested in low strain localities is flat-lying and thrust related rather than steep as suggested by de Roo (1989). D_2 structures overprinting D_1 structures include regional north-east trending, variably plunging folds and variably developed S_2 cleavage.

Timing of inversion

Early workers (e.g. Rayner, 1969) suggested that regional deformation of rocks now known as the Cobar Supergroup was Devonian in age. Glen (1985) on the other hand suggested that this deformation was Carboniferous, on the basis of a general absence of unconformable relations between the Winduck and Mulga Downs groups, on the Carboniferous deformation of the latter unit, and on congruence of folds between the Mulga Downs and Amphitheatre groups. However, a joint BMR–Geological Survey of NSW age dating project (Black & Glen, 1983), followed by $^{39}Ar/^{40}Ar$ age dating (Glen & others, 1986; R.D. Dallmeyer, University of Georgia, written communication, 1989) showed that the cleavage deformation in Zone 1 was late Early Devonian (~400 Ma), with no sign of any Carboniferous overprint. These data suggest that the eastern margin and main bulk of the Cobar Basin underwent regional inversion in the late Early Devonian, in an event which largely bypassed the western edge of the basin except for minor block uplifts documented by Glen (1982). The main inversion event along the western edge of the basin and in the adjoining Winduck Shelf was in the Carboniferous, and was accompanied by deformation of the overlying Mulga Downs Group. This apparent paradox, with opposite basin margins undergoing inversion at different times, is best understood in a regime of strike-slip deformation, with the strike-slip system controlling evolution of the central and eastern parts of the basin (see below) having a somewhat different independent history from that controlling the western part of the basin.

Structural setting of mineral deposits

Structural Zone 1

All deposits of the Cobar Mineral Field, except for Elura, occur in a regional high-strain zone (Zone 1) characterised by a regional subvertical cleavage and down-dip elongation lineation. Thomson (1953) showed that deposits within Zone 1 lie in three zones of strong deformation, and mapping by Glen (Glen & others, 1985; Glen, 1987b, in press) has shown that these zones correspond with mapped thrusts (Fig.7). Gold–copper deposits (e.g. New Cobar, Chesney, New Occidental) lie on the Great Chesney Fault, an east-dipping backthrust, or in imbricates in the immediate footwall (Glen 1987b, in press). Copper mineralisation lies in east-dipping thrusts within the Great Cobar Slate (e.g. Great Cobar deposit) (Glen, in press). Copper–lead–zinc–silver deposits lie in steeply east-dipping imbricates (chlorite shears) in the CSA Siltstone (Barton, 1977; Glen, in press) east of the Footwall Fault of Kapelle (1970). In the Great Chesney line of mineralisation, and at the CSA deposits, faults are brittle-ductile structures with both dip-slip and strike-slip movement. Mineralisation at The Peak (Hinman & Scott, in press) appears to be related to syn-D_1 high-strain zones on the contact between felsic volcanics and the Chesney Formation which lie at depth along the line of the Great Peak Fault. Hinman (1989) suggested that mineralisation predated late development on these faults (see also Plibersek, 1982), although previously mined deposits appeared to lie in these structures. The Drysdale Group of gold deposits appears to be controlled by thrusting and blind thrusting within the Chesney Formation (Glen, in press).

Early workers (e.g. Andrews, 1913; Sullivan, 1951; Thomson, 1953; Mulholland & Rayner, 1961) showed that deposits along the Queen Bee and Great Chesney Faults consisted of steep lenses which lie oblique to bedding. For the CSA deposit,

MAF Maryantha Fault, MF Myrt Fault, MOF, Mopone Fault, NF Nymagee Fault, NOF Norwood Fault, O Oakden Fault, PTF Plug Tank Fault, QF Queen Bee Fault, RF Rookery Fault, TF(L) Thule Fault (Lineament), WF Woorara Fault, WIF Wiltagoona Fault, YF Yanda Creek Fault.
Folds: m Maryvale Anticline, w Western Anticline, n Nullawarra Anticline.
Cross-section line for figure 6 also marked.

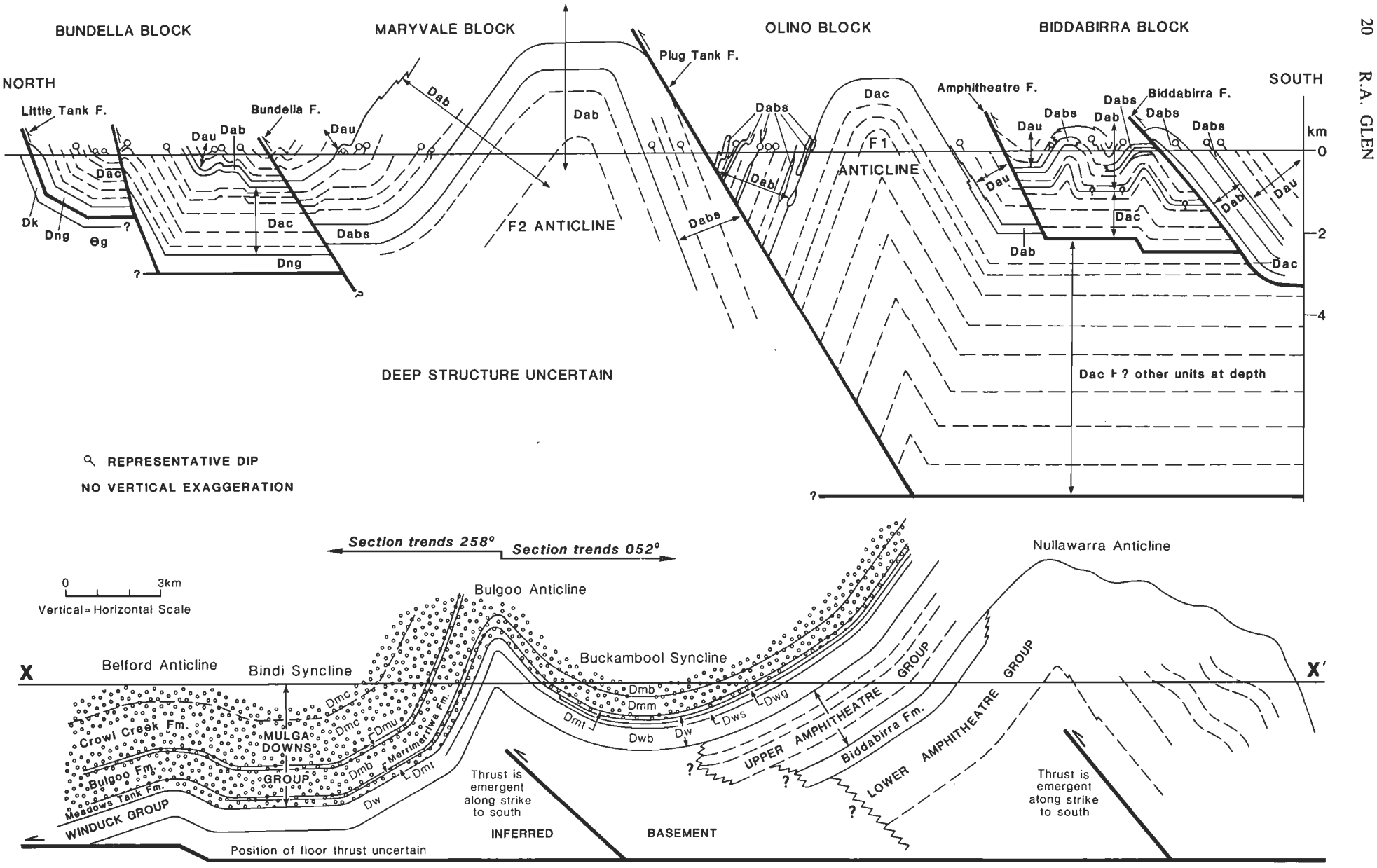

Figure 6. a, Cross-section through northern part of Zone 2. Southernmost boundary (Norwood Fault) shown as vertical for convenience. b, Cross-section through southwestern part of zone showing detachment with ramp and splay related folds.

Note the Bindi and Buckambool Synclines and Bulgoo and Bedford Anticlines are Carboniferous structures. The age of the Nullawarra Anticline is inferred to be Devonian. Thrusting thus propagated from east to west.

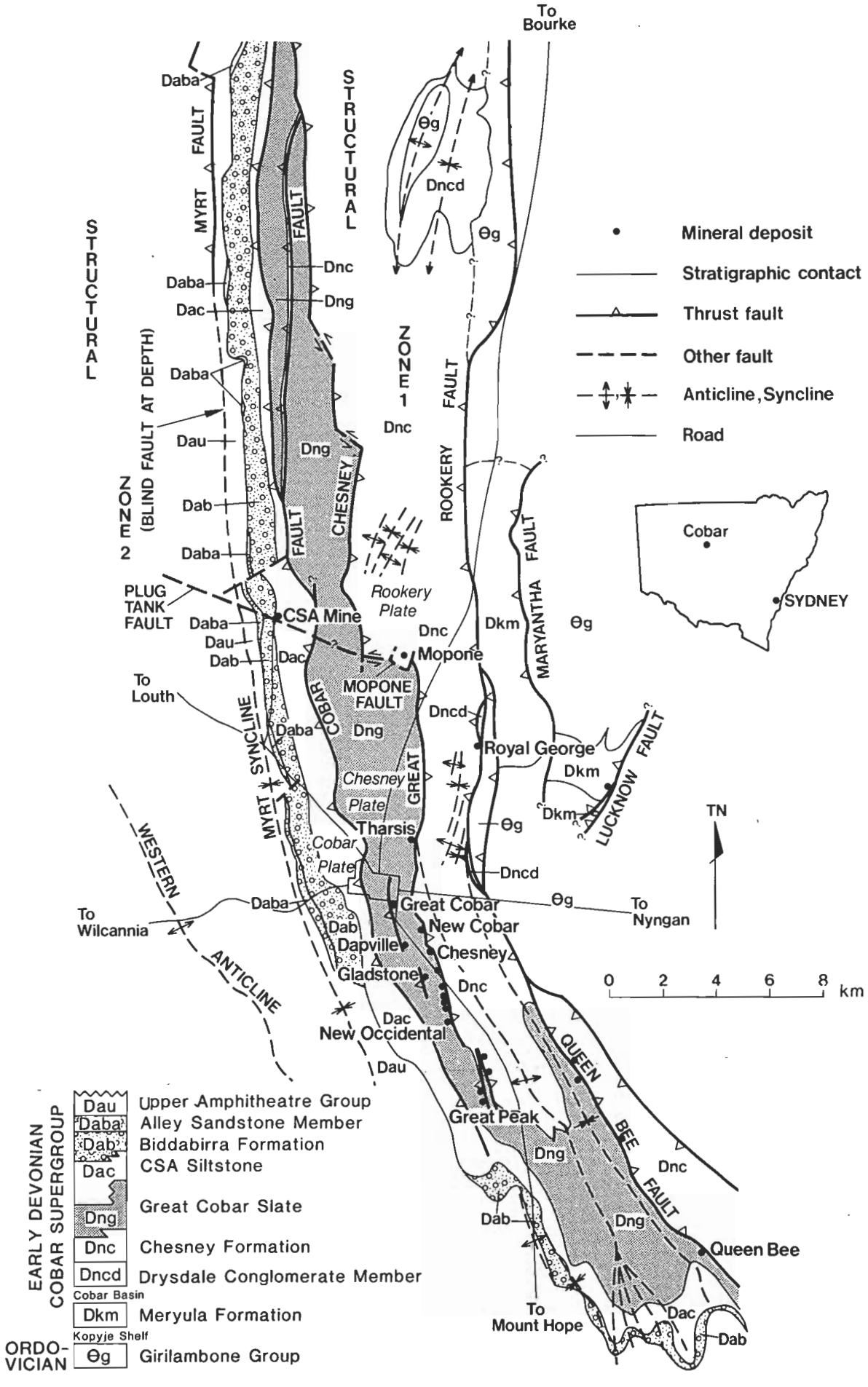

Figure 7. Relationship between mineral deposits and major faults in central part of Zone 1.

Robertson (1974) and O'Connor (1980) showed that mineralisation lay close to east-dipping cleavage in orientation and oblique to west-dipping bedding. All these deposits are associated with areas of silicification (quartz veining and formation of elvan), chloritisation, and formation of carbonate alteration haloes (Mulholland & Rayner, 1961; Robertson, 1974). Thus, in addition to lying in or next to major faults, the lenses making up individual deposits are themselves structurally controlled. For this reason, early workers (e.g. Andrews, 1913; Sullivan, 1951; Thomson, 1953; Mulholland & Rayner, 1961) suggested that the deposits were epigenetic and of replacement origin. More recent workers (Glen, 1987a; Brill, 1988; de Roo, 1989; Hinman, 1989 and, to some extent, Robertson, 1974) suggested a syn-deformational, metahydrothermal origin, with deposits occupying dilatant sites in the country rock.

Structural Zone 2

To date, Elura is the only known deposit in Structural Zone 2. Elura is a concentrically zoned pipe-like deposit localised by a north–northwest trending anticline (D_1 of this study, D_2 of de Roo, 1989) (Schmidt, 1980, 1983; de Roo, 1989). Additional orebodies north of the main pod also occur in domal culminations along this anticline (Lawrie, 1990). De Roo (1989) and Lawrie both suggested that Elura formed as a syntectonic orebody by a combination of replacement and emplacement in dilatant sites.

Towards a model of ore genesis

The association of major structures and orebodies suggests an ore genesis model involving the migration of ore-bearing fluids towards major faults, the focusing of those fluids up these structures and the precipitation therein of gangue minerals, sulphides and native metals (cf. Cox & others, 1986). Glen (1987a) suggested that these fluids were metamorphic in origin and Brill (1988) has demonstrated this for the CSA deposit. This in turn implies that basin sediments had already been dewatered before deformation and ore emplacement. Of critical interest to exploration and to more specific ideas on ore formation is why only particular parts of major structures are mineralised. In this regard, the following points can be made:

1. The absence of any deposit worthy of mention on reactivated syn-depositional faults may be due either to lack of favourable traps on these major structures and/or a time difference between movement on these faults and on the later short-cut faults, which were synchronous with cleavage formation and fluid circulation.
2. Deposits associated with the Great Chesney Fault are associated with left-stepping jogs in the fault which formed either as tear faults during thrusting or as dilational jogs during left-lateral strike-slip movement. As suggested by Sullivan (1951), Mulholland & Rayner (1961) and Glen (1987b), these areas are marked by intersections between north–northwest and west–northwest-trending major fracture systems, with consequent development of significant fault-induced permeability in the imbricated footwall of the fault itself. The greater presence of carbon in the footwall rocks probably also played a major role in the precipitation of gold (cf. Wall & Ceplecha, 1976).
3. The CSA group of deposits lies within the CSA siltstone in the imbricated hanging wall of the Footwall Fault (Barton, 1977; Glen, in press) and just north of west–northwest trending beds in the short limb of a sinistral south-plunging fold (O'Connor, 1980). Mapping by Glen (in press) suggests that this fold is a ductile manifestation of the Plug Tank Fault (see also Fig. 7)
4. The work of Hinman (Hinman, 1989; Hinman & Scott, in press) suggests that The Peak deposits occur where deformation has been partitioned around the contact between sediments of the Nurri Group and silicified felsic volcanics which have been intersected in deep drill holes.
5. The localisation of orebodies by folding at Elura appears anomalous in the context of the Cobar Mining Field where all other deposits are localised by faults. The simplest way to explain this anomaly is to suggest that the major anticline at Elura is developed above a blind thrust. In such cases, deposition of sulphides would occur in an area of reduced permeability above the tip line of the thrust.
6. Metal zoning of the Cobar field has long been enigmatic. Gold + copper deposits occur on the Queen Bee and Great Chesney faults, gold + copper + base metal deposits occur on faults in the Great Cobar Slate and also at The Peak, and base metal + /-copper deposits occur in the CSA Siltstone at Elura and at CSA. In the model of syn-deformational metahydrothermal ore genesis outlined above, wherein metals are scavenged from small traces in rocks at depth, this zoning may in part be explicable in terms of fault geometry and stratigraphy intersected by faults at depth. The Queen Bee and Great Chesney faults, associated with gold + copper mineralisation, dip east (Figs 5, 7) and penetrate relatively thin basin fill (Nurri Group) in addition to Ordovician basement. Faults in the CSA Siltstone (e.g. at the CSA Mine) lie in the imbricated Cobar Plate, in the hanging wall of the west-dipping Cobar Fault which penetrates large volumes of basin sediments of the Amphitheatre Group (Fig. 5). Faults in the Great Cobar Slate and at The Peak cut through a moderate amount of thin-bedded Nurri Group as well as Ordovician basement (Fig. 5). It would thus appear that gold + copper mineralisation may reflect metal sources in easterly derived basin sediments as well as in the underlying basement, whereas base metal + /-copper deposits may reflect metal sources within the deeper parts of the basin, either within sediments or from a mixture of sediments plus possible volcanics at depth.

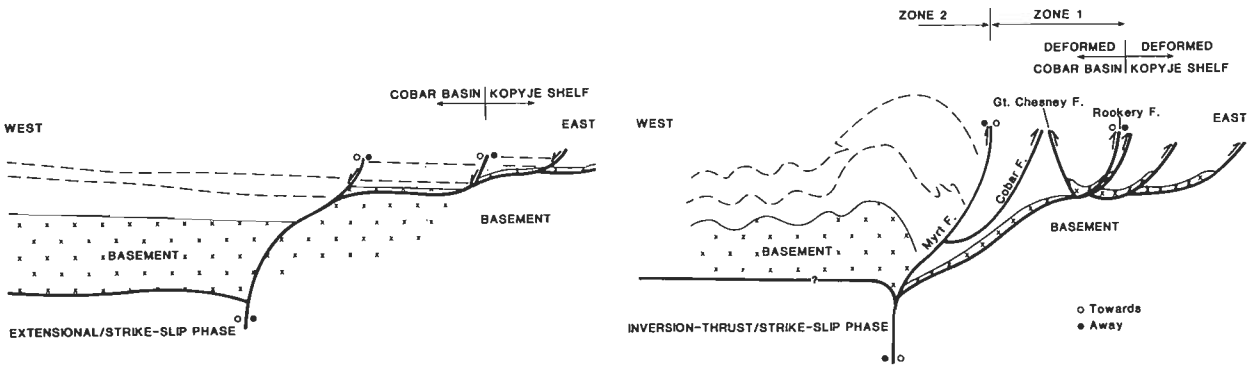

Figure 8. Sketch of extensional and contractional phases on the eastern side of the Cobar Basin, showing asymmetrical negative and positive flower structures.

Synthesis

The Cobar Basin developed as a left-lateral transtensional basin in the latest Silurian–Early Devonian (~410 Ma) and persisted till the late Early Devonian (~400 Ma) before undergoing the first stage of regional inversion in a right-lateral transpressional regime (Fig. 8). During the roughly 10 Ma of its existence, the basin was filled by both syn-rift and post-rift sediments.

Using aeromagnetic data and satellite imagery, D. Pogson (New South Wales Geological Survey, personal communication, 1989) has shown that the faults bounding the eastern margin of the Cobar Basin and margins of the Rast Trough can be traced hundreds of kilometres to the south, where they join the Gilmore Suture (Fig. 9). The eastern boundary fault of the Canbelego–Mineral Hill Belt also coincides for much of its length with the Gilmore Suture (Fig. 9). The Jackermaroo–Thule–Blue Mountain fault system has similarly been traced southward below alluvium (D. Pogson & E. Scheibner, New South Wales Geological Survey, personal communication, 1989) and may extend under the Murray Basin to link into the Kiewa Fault in eastern Victoria.

The Gilmore Suture and less certainly the Kiewa Fault are probably the controlling strike-slip faults in this part of the Lachlan Fold Belt (Glen, 1990), with movement on them and their splays leading to transtensional opening and transpressional closing of the Cobar Basin as discussed above. Regional relations suggest that the Gilmore Suture is in fact one of the master faults controlling end-Ordovician deformation, Silurian granite emplacement and Devonian to Carboniferous basin evolution in western New South Wales. This suture was active as an oblique collisional boundary between the Molong Volcanic Arc and the Wagga Basin at the end of the Ordovician (Scheibner, 1982). It underwent left-lateral strike-slip in the late Silurian (revealed by the en echelon arrangement of granitoids to the west) (Scheibner, 1982), and also controlled evolution of the Tumut Trough — opening in the mid Silurian by right-lateral movement[3] (Powell, 1983; P. Stuart-Smith, BMR, personal communication, 1989) and closing by left-lateral movement at the end of the Silurian (P. Stuart-Smith, BMR, personal communication, 1989). Interestingly, this end-Silurian left-lateral sense of movement at Tumut is the same as that inferred in the Cobar region, for the Cobar Basin and for the Canbelego–Mineral Hill Belt (Glen, 1990). Structures in the northern part of the Mount Hope Trough lie oblique to bounding Scotts Craig Fault (MacRae, 1989), thereby implying some component of strike-slip deformation. The main part of the Mount Hope Trough (and the Rast Trough to the east), however, shows no obvious structural evidence of transpression with ductile structures mapped parallel to bounding faults, and it is not known whether they evolved in a strike-slip regime or orthogonally. Some strike-slip movement is suggested, however, along the Sugarloaf Fault in the Mount Hope Trough where the cross and parallel faults mapped adjacent to it by Scheibner (1985) may be parts of a braided system with jogs. Movement on the Jackermaroo–Thule–Blue Mountain fault system was transpressional in the Carboniferous, with the strike-slip component varying locally from dextral to sinistral depending on fault orientation and local block movement (Glen, 1990).

Acknowledgements

Data from the Mount Hope and Rast troughs and the Kopyje Shelf are based on mapping by E. Scheibner, G. MacRae, S.

[3] L. Wyborn (1977) suggested that the Tumut Trough opened by left-lateral movement on the Long Plain–Indi Fault.

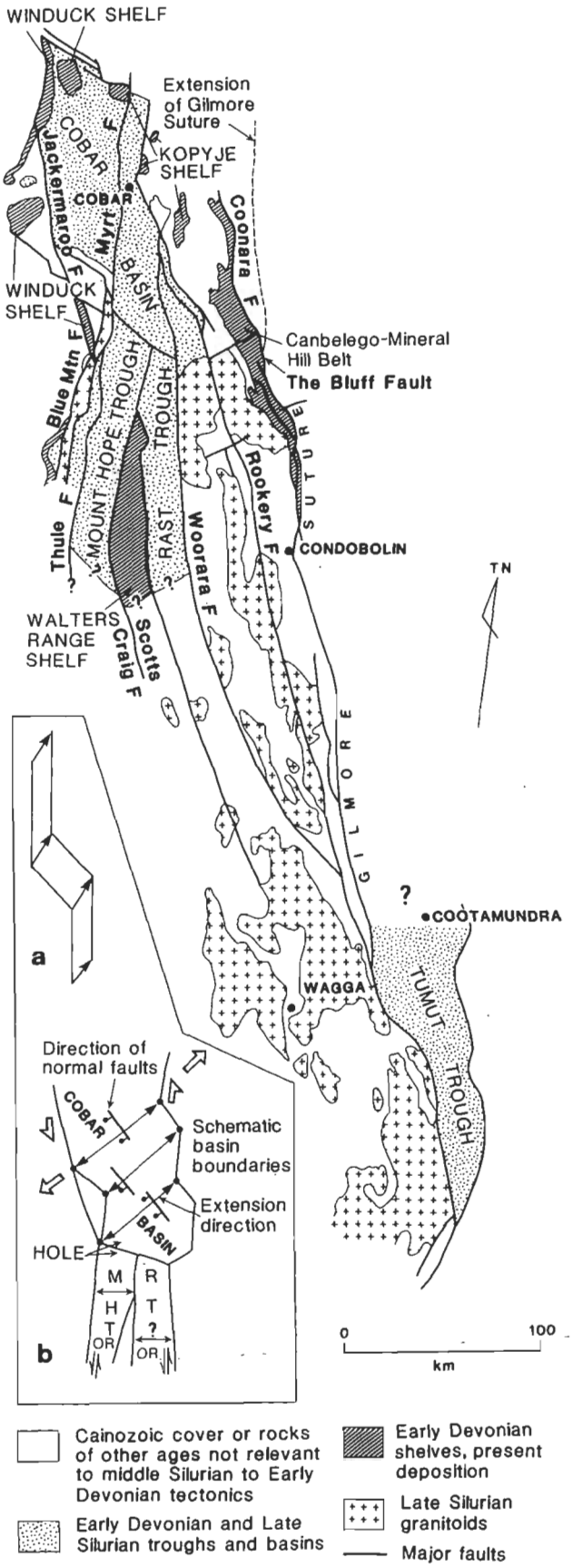

Figure 9. Regional relations in western New South Wales, showing middle Silurian to Early Devonian depositional elements, late Silurian granitoids and major faults. Simplified from Pogson (1972).

Note: all faults except Woorara have both syn-rift and post-rift depositional histories. Inset shows (a) model for oblique extension of an irregularly shaped basin, and (b) application to Cobar region. Holes formed at major changes in amount or direction of extension are filled by volcanics or shallow-level granites.

Trigg and D. Pogson, all of the New South Wales Geological Survey. Discussion with D. Pogson is gratefully acknowledged. M.G. Duba and M. Aresh of the New South Wales Geological Survey are thanked for typing and cartography, respectively. Published with the permission of the Director-General, New South Wales Department of Minerals and Energy.

References

Andrews, E.C., 1913 — Report on the Cobar Copper and Gold-field. Part 1. *Mineral Resources* 17. *New South Wales Department of Mines, Sydney.*

Barton, C.M., 1977 — A geotechnical analysis of rock structure and fabric in the CSA Mine, Cobar, New South Wales. *CSIRO Division of Geomechanics, Technical Paper*, 24, 30 pp.

Black, L.P. & Glen, R.A., 1983 — Cobar geochronology. *Bureau of Mineral Resources, Australia, 1982 Annual Report*, 107–108.

Brill, B.A., 1988 — Geochemistry and genesis of the CSA Cu–Pb–Zn deposit, Cobar, NSW, Australia. *Ph.D. thesis, University of Newcastle, New South Wales.*

Bureau of Mineral Resources, 1970 — Bouguer Anomalies, Cobar 1:250 000 sheet. H55/B2–14. *Bureau of Mineral Resources, Australia.*

Cox, S.F., Etheridge, M.A. & Wall, V.J., 1986 — The role of fluids in syntectonic mass transport, and the localization of metamorphic vein-type ore deposits. *Ore Geology Reviews*, 2, 65–86.

de Roo, J.A., 1989 — The Elura Ag–Pb–Zn mine in Australia — ore genesis in a slate belt by syndeformational metasomatism along hydrothermal fluid conduits. *Economic Geology*, 84, 256–278.

Glen, R.A., 1982 — Nature of late-Early to Middle Devonian tectonism in the Buckambool area, Cobar, New South Wales. *Journal of the Geological Society of Australia*, 29, 127–138.

Glen, R.A., 1985 — Basement control on the deformation of cover basins: an example from the Cobar district in the Lachlan Fold Belt, Australia. *Journal of Structural Geology*, 7, 301–315.

Glen, R.A., 1987a — Geology of the Wrightville 1:100 000 geological sheet 8034, explanatory notes. *Geological Survey of New South Wales, Sydney*, 257 pp.

Glen, R.A., 1987b — Copper and gold rich deposits in deformed turbidites at Cobar, Australia: their structural control and hydrothermal origin. *Economic Geology*, 82, 124–140.

Glen, R.A., 1988 — Basin inversion, thrusts and ore deposits at Cobar, New South Wales: a preliminary report. *Geological Survey of New South Wales, Quarterly Notes*, 73, 21–26.

Glen, R.A., 1989 — Basin inversion, thrusts and ore deposits at Cobar, New South Wales. *Geological Society of Australia, Abstracts*, 24, 54–55.

Glen, R.A., 1990 — Formation and inversion of transtensional basins in the western part of the Lachlan Fold Belt, with emphasis on the Cobar Basin. *Journal of Structural Geology*, 12, 601–620.

Glen, R.A., in press — Geology of the Cobar 1:100 000 geological sheet 8035 (second edition), explanatory notes. *Geological Survey of New South Wales, Sydney.*

Glen, R.A., Dallmeyer, R.D. & Black, L.P., 1986 — Preliminary report on new isotopic evidence for, and implication of, an Early Devonian deformation at Cobar. *Geological Survey of New South Wales, Quarterly Notes*, 64, 26–29.

Glen, R.A., Lewington, G.L. & Shaw, S.E., 1983 — Basement/cover relations and a Silurian, I-type intrusive from the Cobar Lucknow area, Cobar, New South Wales. *Journal and Proceedings of the Royal Society of New South Wales*, 116, 25–32.

Glen, R.A., MacRae, G.M., Pogson, D.J., Scheibner, E., Agostini, A. & Sherwin, L., 1985 — Summary of the geology and controls of mineralization in the Cobar region. *Geological Survey of New South Wales, Report GS 1985/203 (unpublished)*, 91 pp.

Hinman, M.C., 1989 — Syntectonic precious and base metal mineralization controlled by deformation partitioning during an Early Devonian Orogeny at Peak, Cobar, NSW. *Geological Society of Australia, Abstracts*, 24, 71–72.

Hinman, M.C. & Scott, A.K., in press — Geology of the Peak Gold Deposit, Cobar N.S.W. *In* The geology of Australian ore deposits. *Australasian Institute of Mining & Metallurgy, Melbourne.*

Kapelle, K., 1970 — Geology of the CSA Mine, Cobar, New South Wales. *Australasian Institute of Mining and Metallurgy, Proceedings*, 233, 79–94.

Lawrie, K., 1990 — Exploration for syntectonic massive sulphide deposits based on structural and microstructural analysis of drill core. *Geological Society of Australia, Abstracts*, 25, 179.

MacRae, G.P., 1989 — Geology of the Nymagee 1:100 000 sheet 8133. *Geological Survey of New South Wales, Sydney*, 137 pp.

Mulholland, C.St.J. & Rayner, E.O., 1961 — The gold-copper deposits of Cobar, New South Wales: central section (Great Cobar to New Occidental). *New South Wales Department of Mines, Technical Report* 1958, 6, 28–49.

O'Connor, D.P.H., 1980 — Discussion: Evidence of an exhalative origin for deposits of the Cobar district, New South Wales. *BMR Journal of Australian Geology & Geophysics*, 5, 70–72.

Plibersek, P.F., 1982 — Structure, stratigraphy, wall; rock alteration and mineralization of 'The Peak' near Cobar, New South Wales. *B.Appl.Sci. thesis, New South Wales Institute of Technology, Sydney.*

Pogson, D.J., 1972 — Geological map of New South Wales, 1:1 000 000. *New South Wales Geological Survey, Sydney.*

Pogson, D.J., 1982 — Stratigraphy, structure and tectonics: Nymagee–Melrose, central western New South Wales. *M.Appl.Sci. thesis, New South Wales Institute of Technology, Sydney.*

Pogson, D.J. & Felton, E.A., 1978 — Reappraisal of the geology, Cobar–Canbelego–Mineral Hill region, central western New South Wales. *Geological Survey of New South Wales, Quarterly Notes*, 33, 1–14.

Pogson, D.J. & Hilyard, D., 1981 — Results of isotopic age dating related to Geological Survey investigations, 1974–1978. *Geological Survey of New South Wales, Records*, 20, 251–273.

Powell, C.McA., 1983 — Tectonic relationship between the Late Ordovician and Late Silurian palaeogeographies of southeastern Australia. *Journal of the Geological Society of Australia*, 30, 353–373.

Rayner, E.O., 1969 — The copper ores of the Cobar Region, New South Wales. *Geological Survey of New South Wales, Memoir* 10.

Robertson, I.G., 1974 — The environmental features and petrogenesis of the mineral zones of Cobar, New South Wales. *Ph.D. thesis, University of New England, Armidale.*

Scheibner, E., 1982 — Some aspects of the geotectonic development of the Lachlan Fold Belt. *Geological Survey of New South Wales, Report* GS 1982/062 *(unpublished).*

Scheibner, E., 1985 — The Mount Allen 1:100 000 geological sheet 8032. *Geological Survey of New South Wales, Sydney.*

Scheibner, E., 1987 — Geology of the Mount Allen 1:100 000 geological sheet 8032. *Geological Survey of New South Wales, Sydney*, 220 pp.

Schmidt, B.L., 1980 — Geology of the Elura Ag–Pb–Zn deposit, Cobar district, NSW. *M.Sc. thesis, Australian National University, Canberra.*

Sherwin, L., 1985 — Biostratigraphy. *In* Glen, R.A., MacRae, G.M., Pogson, D.J., Scheibner, E., Agostini, A. & Sherwin, L., 1985 — Summary of the geology and controls of mineralization in the Cobar region. *Geological Survey of New South Wales, Report* GS 1985/203 *(unpublished)*, 91 pp.

Stewart, I.R. & Glen, R.A., 1986 — An Ordovician age for part of the Girilambone Group at Yanda Creek, east of Cobar. *Geological Survey of New South Wales, Quarterly Notes*, 64, 23–26.

Sullivan, C.J., 1951 — Geology of New Occidental, New Cobar and Chesney mines, Cobar, New South Wales. *Bureau of Mineral Resources, Australia, Report* 6, 45 pp.

Thomson, B.P., 1953 — Geology and ore occurrences in the Cobar district: *5th Empire Mining & Metallurgy Congress, Australia & New Zealand*, 1, 863–896.

Trigg, S.J., 1987 — Geology of the Kilparney 1:100 000 sheet 8132. *Geological Survey of New South Wales, Sydney*, 131 pp.

Wall, V.J. & Ceplecha, J.C., 1976 — Deformation and metamorphism in the development of gold-quartz mineralization in slate belts. *25th International Geological Congress, Abstracts*, 1, 142–143.

Wyborn, L.A.I., 1977 — Aspects of the geology of the Snowy Mountains region and their implications for the tectonic evolution of the Lachlan Fold Belt. *Ph.D. thesis, Australian National University, Canberra.*

BMR Journal of Australian Geology & Geophysics, 12, 25–33

NOAA satellite data in natural oil slick detection, Otway Basin, southern Australia

W.J. Perry[1], P.E. Williamson[2] & C.J. Simpson[3]

Crude petroleum in the form of thick oil or bitumen seeps in places from the sea floor off southeast South Australia, and periodically strands on the coasts of South Australia, western Victoria and western Tasmania. In this pilot study, National Oceanic and Atmospheric Administration (NOAA) Advanced Very High Resolution Radiometer data acquired by the NOAA-9 satellite, during the period from 13 days before to 1 day after a reported stranding of 1000 t on Kangaroo Island, was studied to try to detect the floating crude, map its drift path, and determine the location of the seepages. The study's failure to detect any oil slick on the ocean surface is attributed to the prevailing high percentage of cloud cover, and the calculated small area occupied by the slick in relation to the spatial resolution of the sensor, particularly after the oil had been degraded to bitumen. In the study area, continuing monitoring of locations and timing of strandings, and the associated meteorological conditions, are needed if the sites of oil seepage are to be determined. In such cloud-prone areas, monitoring of petroleum slicks by remote sensing could require sensors operating in the microwave part of the electromagnetic spectrum, but in areas with clearer skies the use of NOAA satellite data should be further investigated. If the locations of oil seeps can be thus identified, they may define locations of petroleum fields. Consequently, this type of investigation may be a relatively inexpensive exploration method in some offshore areas.

Introduction

Over the past two decades, satellite and aircraft remote sensing techniques have been evaluated for their ability to detect and monitor oil slicks on the sea surface. Most research has taken place in the northern hemisphere, owing to the intensity of petroleum shipment activity there. In April 1988, the British Government began a program of anti-pollution aerial surveillance patrols over the North Sea and other coastal waters. In May 1988, the Institute of Petroleum, London, organised an international meeting to review the remote sensing of oil slicks (Lodge, 1989), particularly with aircraft sensing methods.

In Australia, investigations of sensing of oil slicks have not been driven by the same environmental concerns as in the northern hemisphere. Nevertheless, some significant studies have been undertaken. In 1981, Ypma (1985) conducted airborne remote sensing research in Nepean Bay (north Kangaroo Island), South Australia, using Fraunhofer discrimination techniques to detect sunlight ultraviolet radiation excited luminescence of oil on sea water. His work demonstrated the feasibility of this approach, which offers promise for future satellites with very narrow (0.025–0.050 micrometre) bandwidth sensing capability.

In 1982, the CSIRO Division of Mineral Physics assessed the feasibility of using the Landsat multispectral scanner (MSS) for the detection of offshore oil seepage on the northwest, west and southeast coasts of Australia (Churchill, 1982). That report, as well as reviewing overseas experiences, documented the areas of known natural oil slick occurrence in Australia and their likely characteristics, and included comments on the chemical alteration processes of hydrocarbons under different ocean conditions.

The study reported here was proposed in 1988 after an oil slick-like feature was observed on the surface of the sea some 90 km northwest of Perth during special processing of Landsat data for BMR marine survey operations (Landsat 2 image WRS 120–082 of 19 November 1980; Fig. 1). The possible oil slick was 1 to 2 km wide and 16 km long. Given the size of the feature, it was proposed to attempt to use satellite data to track natural oil slicks in the offshore Otway Basin (a region of known seepage and an area under investigation by BMR).

Crude petroleum exudes from seepages on the continental slope in the western Otway Basin (Sprigg & Woolley, 1963; Sprigg, 1964; McKirdy & Horvath, 1976) and strands on the coast of South Australia, particularly in the southeast, on Kangaroo Island, and in western Victoria and western Tasmania. From recorded locations of strandings and from drift bottle experiments, Sprigg (1964, p. 62) concluded that:

- winter strandings are most likely on the coasts of southeast South Australia and western Victoria;
- until December, strandings occur about Encounter Bay (off Victor Harbor and the Murray mouth) and eastern Kangaroo Island; and
- summer strandings occur further west onto the southern Yorke and Eyre Peninsulas.

He postulated that seepage occurs on steep continental slopes opposite southeastern South Australia, about collapsing submarine canyon walls and active seafloor faults, and that winter storms and earthquakes activate the seeps.

The South Australian Department of Mines & Energy (D. Gravestock, personal communication, 1988) reported a stranding of an estimated 1000 t of crude oil near Seal Bay on the south coast of Kangaroo Island on 7 December 1986, after earthquakes of magnitude 2. Australian Mineral Development Laboratories (AMDEL) analysed samples and concluded the substance was naturally occurring oil (D.M. McKirdy, Department of Geology & Geophysics, University of Adelaide, personal communication, 1986). This particular stranding was targeted for the satellite tracking study reported here.

Geology and petroleum potential

The Otway Basin lies west of the Bass and Gippsland basins. It trends northwest–southeast, straddling the western Victorian and eastern South Australian coastlines for 500 km. The stratigraphy and structure of the Otway Basin are discussed by many authors, including Bouef & Doust (1975), Denham & Brown (1976), Megallaa (1986), Exon & others (1987a,b) and Williamson & others (1987, 1988).

The basin developed initially by rifting in the latest Jurassic to earliest Cretaceous as part of the rifting between Australia and Antarctica. It was part of the extensive Bassian rift, which continued eastwards into the Bass and Gippsland Basins,

[1] 39 Creswell Street, Campbell ACT 2601
[2] Marine Geoscience & Petroleum Geology Program, Bureau of Mineral Resources, Geology & Geophysics, GPO Box 378, Canberra ACT 2601
[3] Minerals & Land Use Program, Bureau of Mineral Resources, Geology & Geophysics, GPO Box 378, Canberra ACT 2601

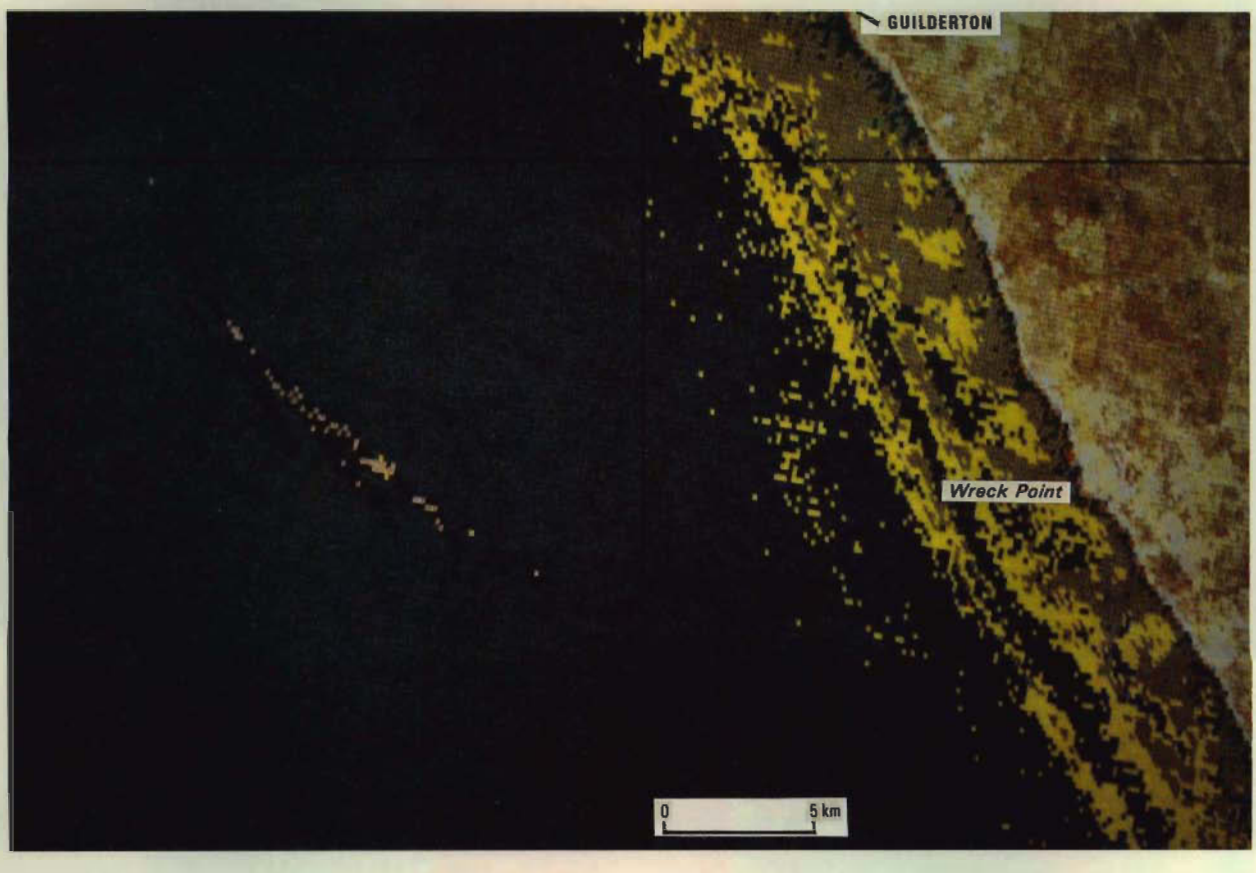

Figure 1. Extract from Landsat 2 MSS image WRS 120–082, dated 19/11/1980, located northwest of Perth and processed for depth of water penetration.
This shows an offshore oil slick-like feature (pink/black) some 1–2 km wide and 16 km long.

across the north–south-trending Palaeozoic structures. A second phase of rifting in the mid-Cretaceous established the present structural grain of the offshore Otway Basin, which consists predominantly of normal faults downthrown to the continent–ocean boundary and displacing landward dipping Cretaceous strata. Tertiary and younger reactivation of these faults is common, especially in parts of the western Otway Basin.

The continental shelf of the Otway Basin consists of three tectonic provinces: the Mussel Platform in the east, the Voluta Trough in the centre, and the Crayfish Platform in the west (Fig. 2). The likely region of origin for seeps encompasses the Crayfish Platform and the western Voluta Trough, around the margins of the platform.

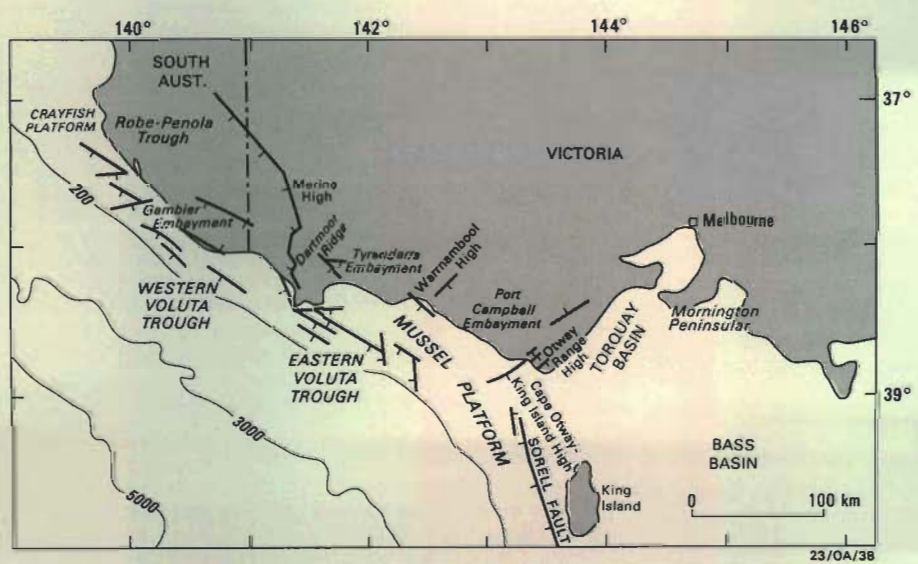

Figure 2. Structural elements of the offshore Otway Basin (after Williamson & others, 1987).

The oldest sediments drilled in this region belong to the Otway Group, a terrestrial sequence which ranges in age from latest Jurassic to latest Early Cretaceous (Fig. 3). The Otway Group has been divided into two formations: a basal fluviatile porous sandstone sequence, the Pretty Hill Sandstone, which is overlain by impermeable alluvial plain to lacustrine chloritic sandstone, mudstone and shale of the Eumeralla Formation.

Four 'dry' petroleum exploration wells have been drilled on the Crayfish Platform. However, geochemical studies on samples from exploration drilling (McKirdy & others, 1986) and analyses of hydrocarbons in water bottom sediments of the Otway Basin (O'Brien & Heggie, 1989) indicate that mature petroleum source rocks are present near the base of the Pretty Hill Sandstone in the region. This interval appears to be the most likely source for oil strandings on the adjacent South Australian and Victorian coastline. Structural definition of the Crayfish Platform region by Williamson & others (1987, 1988) reveals fault-dependent structural traps into which hydrocarbons could migrate (Fig. 4). The breaching of an oil field in one such trap by renewed fault movement could release the oil which forms the strandings on the coastline. The observation that strandings are often correlated with earthquake activity, and hence fault movement, in the region, supports this proposal.

Method

The usefulness of satellites to track natural oil slicks back to their unknown site of discharge is more complex than simply monitoring the movement of a spill from a known point source. In most cases the natural seep is reported only when it strands onshore. It may be difficult to determine accurately, if at all, many of the factors necessary to simplify back-tracking. These factors include the actual date and time of stranding, the composition (oil or bitumen), the direction of travel, the prevailing currents and winds (which determine the speed of

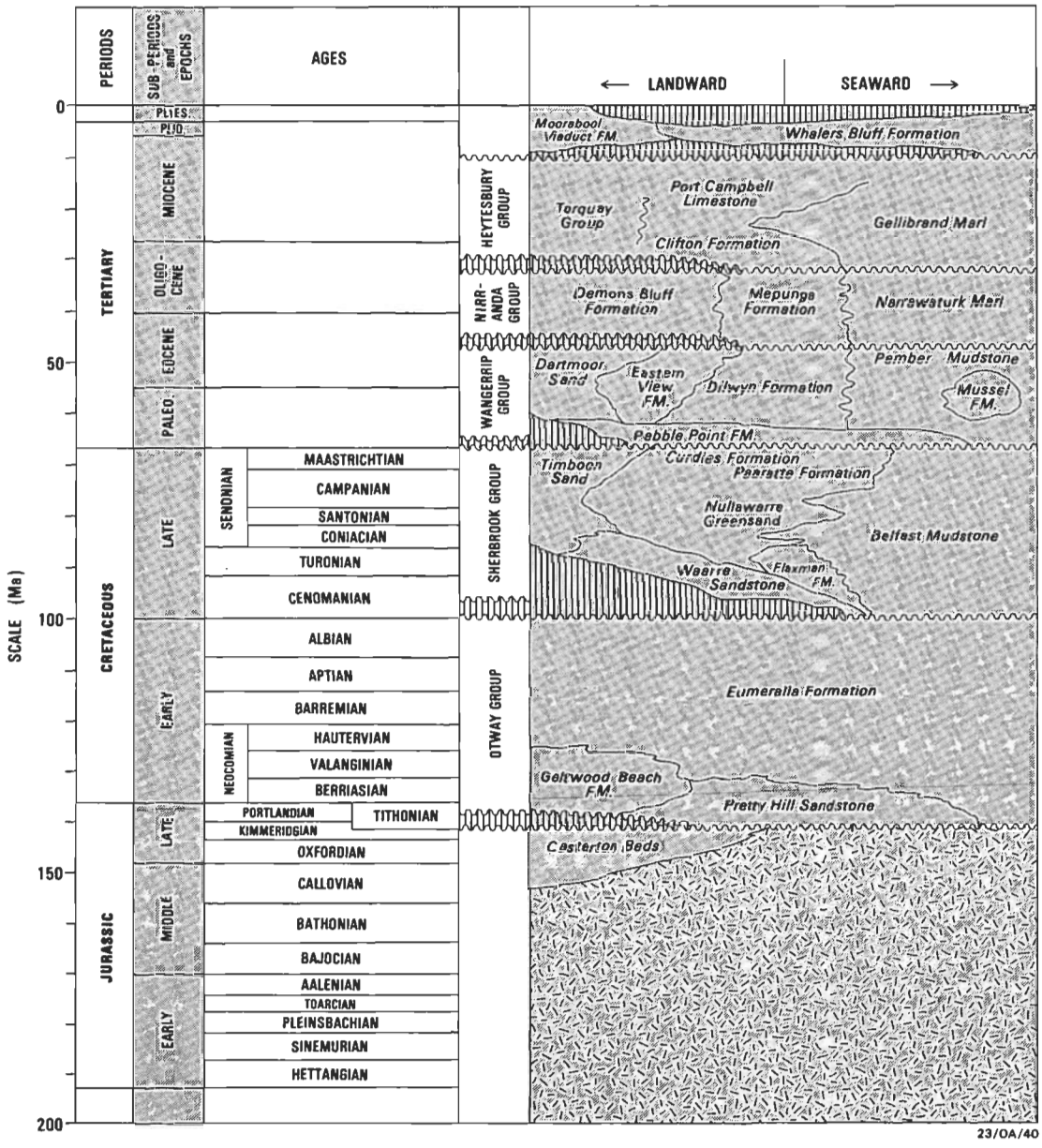

Figure 3. Generalised stratigraphy of offshore Otway Basin.

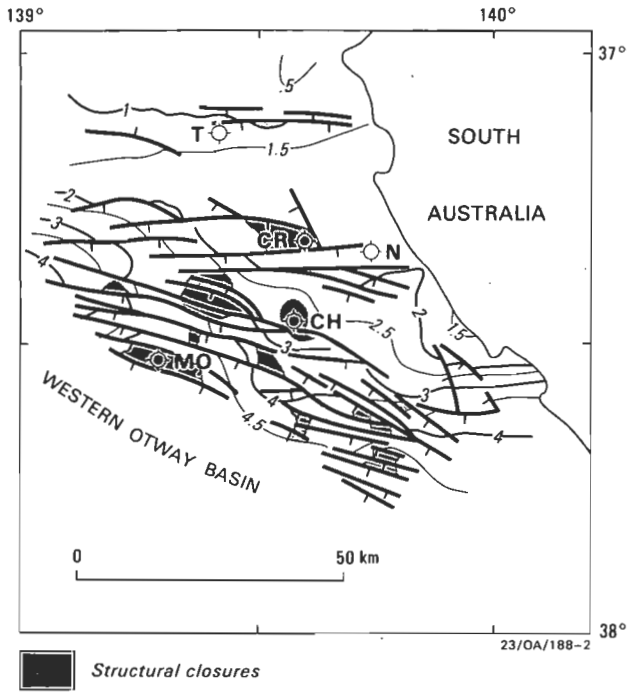

Figure 4. Structure contours on top of Pretty Hill Sandstone on Crayfish Platform proper showing structural traps (after Williamson & others, 1987, 1988).
Wells are identified as Trumpet (T), Crayfish (CR), Chama (CH), Neptune (N) and Morum (MO).

drift), and the likely time that the oil was on the sea surface before stranding (hours, days, weeks).

It is apparent that a satellite with a very frequent return-visit cycle (hours rather than days) and a high spatial resolution capability (metres rather than hundreds of metres) is preferable. Currently no spacecraft meeting the optimum criteria records data over Australia. At the time of the study the only spacecraft for which reasonable recorded data were archived in Australia were the Landsat and National Oceanic and Atmospheric Administration (NOAA) satellites.

Because of the 18-day cycle of Landsats 1 to 3 or the 16-day cycle of Landsats 4 and 5, Landsat coverage was somewhat inadequate for the present study. Surface ocean current velocity estimated (Sprigg, 1964, p. 61) from drift bottles dropped during winter south of Kangaroo Island was 0.7 knots. At this velocity, material on the sea surface could move more than 500 km in the 16-day period between overpasses. This renders the Landsat impractical for purposes of tracking an observed stranding back to its source. For this reason, and because of the twice daily coverage by the NOAA-9 satellite, trials were carried out with NOAA data despite the disadvantage of the NOAA–Advanced Very High Resolution Radiometer (AVHRR) resolution at nadir of 1.1 km. (The smallest AVHRR picture element or 'pixel' is a square with sides 1.1 km long, compared with the Landsat Multispectral Scanner (MSS) resolution of 80 m). Besides the frequent overpass cycle, the NOAA also has the advantage that the swath width is about 2415 km at the nominal altitude of 829 km (Griersmith & Kingwell, 1988).

Other investigators have successfully used AVHRR data to detect sea surface slicks. Asanuma & others (1986) investigated the use of NOAA-7 data for detecting oil slicks in the Persian Gulf after oil drilling rigs were damaged in March, 1983, during the Iran–Iraq war. They computed albedo and brightness temperatures by using calibration parameters on Local Area Coverage (LAC) tapes for the visible and thermal channels. The apparent thermal inertia, computed from the difference of sea surface temperature between day and night, showed the possibility of detecting oil slicks, as oil slicks have a small apparent thermal inertia, whereas sea water has a large one. It was difficult to recognise oil slicks from the temperature difference between oil slicks and sea water in a single observation. In addition, LAC data tapes of areas outside the direct readout range of US receiving stations have to be specially requested.

Asanuma and his colleagues were dealing with a large quantity of oil on the water surface. Pickett & others (1984) estimated the amount as about 2000 barrels/day in March 1983, possibly rising a few weeks later to as much as 18 000 barrels/day. For a crude oil of 26 A.P.I. (American Petroleum Institute) gravity, 2000 barrels/day is equivalent to about 285 t/day; in the form of a thin film (e.g. 10 micrometres thick) this would occupy about 26 pixels. These authors reported that the NOAA-7 satellite visible and infrared bands on 29 March, 1983 showed a dark, warm streak heading southeast, probably the oil slick from the damaged rigs.

The oil spill into Prince William Sound, Alaska from the tanker Exxon Valdez was identified using both NOAA-11 and Landsat (Anon, 1989) data. The grounding of the Exxon Valdez occurred on 24 March 1989, and the interpreted slick had moved 250 km by 7 April 1989. The suspected slick feature was observed in the NOAA–AVHRR thermal infrared image and had a radiant temperature of 1.5–2.0°C cooler than the surrounding water (Stringer & others, 1989).

For the pilot study, BMR requested from the CSIRO Division of Oceanography digital tapes of the best cloud-free scenes of the area of the western Otway Basin and around Kangaroo Island (35–41°S, 136–144°E) imaged by the AVHRR on NOAA-9 during the period 23 November to 8 December 1986. Such a time sequence of scenes gave the possibility of interpreting material on the ocean surface by the changing position of subtle features on successive scenes, features which on single images might not be recognised as having any significance. Table 1 shows the wavelength intervals corresponding to each of the five channels of the AVHRR. The locations of scenes used in the study are shown in Figure 5.

Table 1. NOAA-AVHRR channel number and wavelengths recorded.

Channel	*Wavelength(μm)*	*Radiation type*
1	0.58–0.68	Visible
2	0.73–1.10	Near infrared
3	3.55–3.93	Reflected infrared
4	10.30–11.30	Thermal infrared
5	11.50–12.50	Thermal infrared

Perry (1989) discusses the image processing equipment used, and details of the NOAA scenes examined are listed in Table 2. The processing of NOAA data was aimed at testing relatively simple image processing techniques to try to detect oil slicks on the ocean surface. This approach was adopted for, if it proved successful, the longer term aim was to set up a mechanism for routine processing of all NOAA overpasses of regions of interest. Such an approach currently requires that relatively simple processing routines are applicable if total monitoring is to be successful on a cheap routine basis for all Australian offshore basins. More advanced processing, involving principal component and inverse principal component methods, was undertaken to try to isolate oil slicks before testing simpler processing techniques.

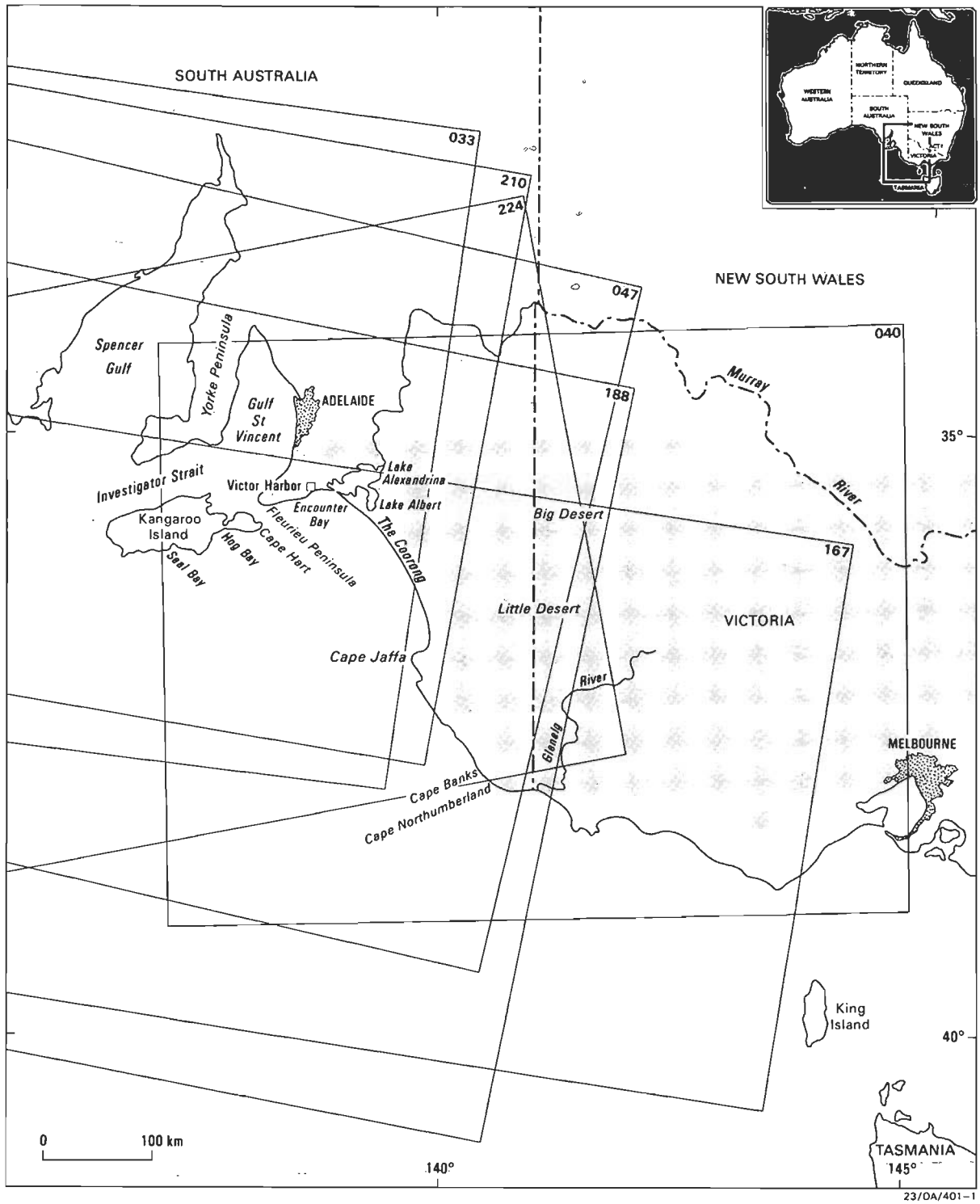

Figure 5. Locality diagram showing coverage of windows of NOAA-9 satellite AVHRR scenes used in this study.

The following routine procedure was adopted for studying images:

1a. Calculation of histograms for full screen image;
b. adjustment of function memories for maximum discrimination;
c. photography of images (both single channels and composites).

2. Selection of training area of sea, and repetition of steps 1a–c (this was not successful on some images owing to cloud cover).

3. Computation of principal component analysis of channels 3, 4 and 5, then enhancement of the resulting images before photography (as in steps 1b and 1c above).

Table 2. NOAA-9 scenes examined.

Image number	*Date acquired*	*Universal time*	*Local time & date (CSDST)*	*Estimated percentage cloud cover*	*Observations*
NOA033	23/11/1986	1701	0331 on 24/11/86	20	13 days before stranding. Only channels 3–5 available. Channel 5 plus pseudocolour shows good discrimination within the sea water. No anomalous areas were recognised.
NOA040	24/11/1986	0521	1551 on 24/11/86	10 (over sea)	13 days before stranding; channels 1–5 available. A principal component analysis of channels 3–5 displayed as PC3 red, PC2 green, PC1 blue, plus a small area stretch, provided good discrimination within the sea water. No anomalous areas were recognised.
NOA047	24/11/1986	1653	0323 on 25/11/86	35	12 days before stranding. A dark patch of water surrounding a smaller lighter area is visible on channels 3 and 5 (between the eastern side of Fleurieu Peninsula and the River Murray mouth where it leaves Lake Alexandrina). The darker area is some 29 x 32 pixels in area, and the lighter area (possibly due to slightly warmer river water and/or suspended sediment) occupies about 20 x 11 pixels.
NOA167	03/12/1986	0525	1555 on 03/12/86	15	4 days before stranding. A principal component analysis of channels 3–5 with a small area stretch displayed as PC3 red, PC2 green, PC1 blue showed good discrimination in the water which suggests a current drift from southeast toward Kangaroo Island. No anomalous areas were recognised.
NOA188	04/12/1986	1642	0312 on 05/12/86	20	2 days before stranding. Good water discrimination in channel 5 indicates probable current movement from southeast to the northwest. No anomalous areas were recognised.
NOA210	06/12/1986	0635	1705 on 06/12/86	75	The day before stranding. No anomalous areas were recognised.
NOA224	07/12/1986	0624	1654 on 07/12/86	40	The day of stranding. PC3 (of a principal component analysis of channels 2–4) plus pseudocolour showed a dark blue hue flanking the coast in St Vincent Gulf, and along the Coorong between Fleurieu Peninsula and Cape Jaffa; it is interpreted as being due to sea grass. No other anomalous areas were recognised.

Images examined

The NOAA-9 images examined are listed in Table 2, which shows scene acquisition date and time (both universal time — UT — and central standard daylight saving time — CSDST). An example of each scene is illustrated (Figs 6–12), to show various processing effects and the problems posed by the cloud cover encountered. Full descriptive details of each image examined are given in an unpublished report to the BMR Division of Marine Geoscience & Petroleum Geology (Perry, 1989).

Discussion

This pilot study showed no features that could be identified as oil slicks. Cloud cover was a major problem. The region has a very high incidence of cloud, as borne out by the NOAA-9 scenes examined (Figs 6–12), and confirmed by examination of the catalogue of Landsat acquisitions of a typical scene in the area. The Landsat 4 and 5 scene which includes Kangaroo Island (WRS path 098 row 085) has been recorded by the Australian Landsat Station every 16 days from September 1982 to March 1989. During that 6.5 year period 143 scenes were recorded, of which only three were cloud-free (24 November 1982, 30 April 1985 and 30 January 1987). Table 3 shows that 70% of all Landsat scenes acquired at that path-row point have >70% cloud cover content. Though such information indicates that any study will have little chance of success because of the high incidence of cloud, it does not allow specific satellite data to be dismissed as unusable. Digital processing techniques may allow slicks to be enhanced and detected between cloud gaps or through thin cover.

A review of relevant literature (Sprigg & Woolley, 1963, p. 70) also indicates that the material most commonly found on the shore of the South Australian coastline is brownish-black lumpy crude bitumen, usually rolled and somewhat incorporated with beach sand on the outer surface. Blocks of 50 lb (23 kg) or more have been reported; some have pedicular barnacles attached. Sprigg & Woolley collected almost half a ton (510 kg) after a single storm during 1961. They wrote that in very localised areas fresh seepage material was semi-liquid (tacky) black bitumen that collapsed and flowed under its own weight. They also quoted from a 1914 paper by Loftus Hills, who described the bitumen washed up on the west coast of Tasmania as fragments ranging from a few inches in diameter to blocks 3 feet by 2 feet by 2 inches thick (90 by 60 by 5 cm), most pieces being flat and others roughly cubical with rounded edges.

30-15/21

Figure 6. Extract from NOAA-9 scene 033, 24 November 1986 (13 days before stranding). Channel 3.
KI Kangaroo Island, YP Yorke Peninsula, LA Lake Alexandrina, FP Fleurieu Peninsula. Cf. Figure 5.

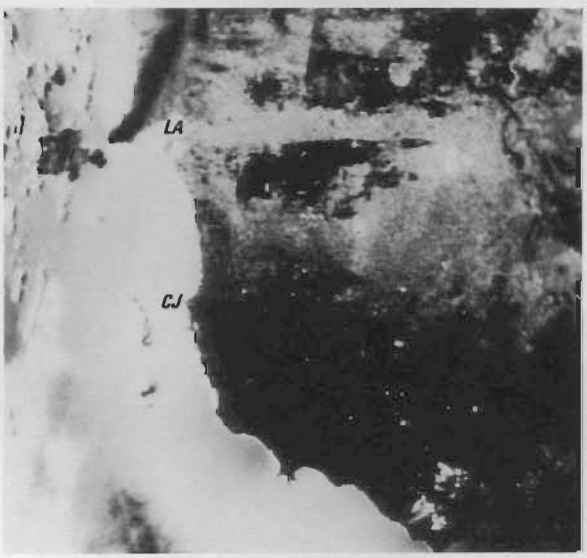

Figure 7. Extract from NOAA-9 scene 040, 24 November 1986 (13 days before stranding). Channel 4.
Geographic features as for Figure 6, plus CJ Cape Jaffa.

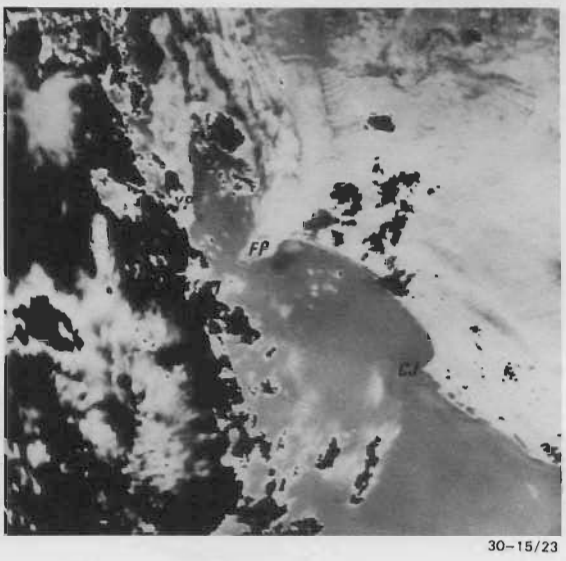

Figure 8. Extract from NOAA-9 scene 047, 25 November 1986 (12 days before stranding). Channel 3.

Figure 9. Extract from NOAA-9 scene 167, 3 December 1986 (4 days before stranding). Principal component 3 of channels 3–5.

Figure 10. Extract from NOAA-9 scene 188, 5 December 1986 (2 days before stranding). Channel 5.

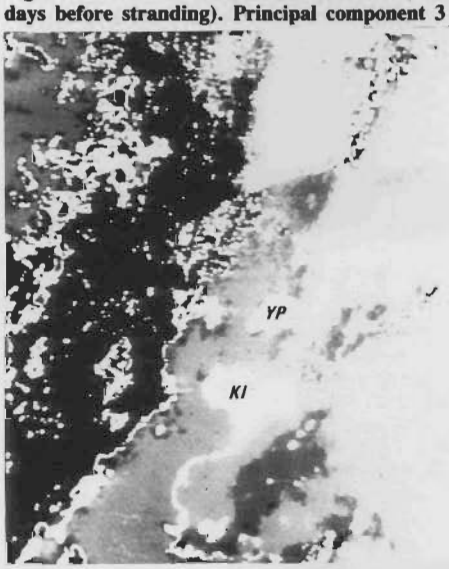

Figure 11. Extract from NOAA-9 scene 210, 6 December 1986 (the day before stranding). Principal component 3 of channels 3–5.

Figure 12. Extract from NOAA-9 scene 224, 7 December 1986 (the day of stranding). Ratios 4/5 red, 2/3 green, 1/2 blue.

Table 3. Number of Landsat scenes acquired and their percentage cloud cover content on WRS 098–085 (Kangaroo Island) for the period 6/9/1982 to 8/3/1989.

Percentage cloud cover	*Number of scenes*
0–9	4
10–19	4
20–29	6
30–39	3
40–49	8
50–59	9
60–69	9
70–79	25
80–89	32
90–99	43

Source: Australian Centre for Remote Sensing Landsat Data Catalogue.

Ward (1913, p. 13) recorded specific gravity determinations of bitumen samples ranging from 1.0041 for the soft pasty portions (found at the mouth of the Hog Bay River on the southeast coast of Kangaroo Island) through 1.017, 1.018, 1.035, 1.036 to 1.040 for the harder and more brittle parts. Other determinations reported by Ward (1913, p. 14) are 1.049, 1.066 and 1.075 for samples from various locations on the South Australian coast. He concluded that the specific gravity of sea water in the Southern Ocean off the coast of South Australia is about 1.0285, and hence the freshest bitumen, before the volatile ingredients have disappeared, is capable of floating on sea water.

Though seeps may not necessarily occur as bitumen, oil — after some degree of exposure — can be converted to bitumen by biological action. In these circumstances oil slicks will progressively become more difficult to detect using satellite data.

The volume occupied by the 1000 t of bitumen before stranding (assuming it was fresh with a specific gravity of 1.0041), would be 995.9 m^3. If we assume a thickness of 5 cm (in accordance with Loftus Hill's 1913 observation of 2 inches), the undispersed bitumen would cover the sea surface over an area of 19 918 m^2.

The area of one AVHRR pixel is 1 210 000 m^2, thus the bitumen before stranding would occupy only about one fiftieth of a pixel. Even with an assumed thickness of 1 mm, the surface area covered would be only 995 900 m^2, and would occupy about 80% of one pixel. This also represents the case of maximum detectability of the bitumen if it is assumed to remain as a continuous sheet. It seems clear therefore that a seepage of 1000 t would have to be in the form of an oil film to provide a target of sufficient size to be detectable by the AVHRR. The problem of a small target area caused by the crude petroleum being in the form of bitumen rather than liquid oil suggests that the average strandings of bitumen previously reported on the coast adjacent to the Otway Basin would not be detectable by the AVHRR, even under clear skies.

The unknown factor in this study is whether the slicks start out as a form of liquid oil and are then converted to bitumen in a given time after exposure, or whether they are discharged as bitumen. If they start out as oil and we assume an oil film thickness of the order of 10 micrometres, the area covered would be 99 590 000 m^2, equivalent to the area of 82 AVHRR pixels, in which case they would be detectable. Hurford (1989) states that layers of oil 50–500 micrometres thick appear cool when imaged in the thermal infrared (8–14 micrometre wavelength interval). This is because the oil, which is at the same physical temperature as the sea, has a lower emissivity than that of sea water. Layers of oil which are thicker than 500 micrometres will absorb solar radiation and on sunny days are physically hotter than the sea.

Conclusions and recommendations

Cloud cover in the latitudes of the target area is too high to allow successful use of this technology for routine monitoring. On the relatively cloud-free scenes studied, the failure to detect crude petroleum could be due to the coarseness of the resolution of the sensor relative to the small surface area occupied by oil of the tonnage reported, when it had been degraded to its bitumen phase.

The NOAA-9 twice-daily coverage of any area of interest is ideal for studies of this sort, whereas the 16 or 18-day return cycle of Landsat is clearly unsatisfactory. But the cloud cover that frequently masks the study area prevents optimum use of remote sensors operating in the visible, near infrared and thermal infrared regions of the electromagnetic spectrum, irrespective of their spatial resolution. The optimum satellite-borne remote sensing system for monitoring petroleum slicks in regions of high cloud cover would incorporate a cloud-penetrating microwave sensor with a spatial resolution in the tens of metres range, having a reasonably wide swath, mounted on a platform with preferably a daily return cycle, but certainly not greater than a few days. Until such a combination becomes available, the use of NOAA data to monitor petroleum slicks on the ocean surface should be further investigated in latitudes having clearer skies than those over the Southern Ocean. In latitudes with clearer skies the use of day and night thermal infrared data for the production of thermal inertia images should also be investigated.

In the Otway Basin study area, to try to determine the sites of the crude petroleum seepages it is necessary to continue documenting the location and timing of strandings, together with information about the effects of ocean surface currents on floating bitumen. Very large volume bitumen (or preferably liquid oil) strandings in this environment would still be worth examination using AVHRR imagery. In other areas with lesser cloud cover, however, satellite data sets may be useful in defining naturally occurring oil slicks and may assist in petroleum exploration.

Acknowledgements

W.J. Perry carried out this work under a contract initiated for the project by P.E. Williamson, and C.J. Simpson analysed the satellite images; P.E. Williamson contributed the petroleum geology component. The help given freely by staff of the Remote Sensing Group is gratefully acknowledged. NOAA imagery was supplied by the CSIRO Division of Oceanography, Hobart. The Landsat image was provided by the Australian Centre for Remote Sensing.

References

Anonymous, 1989 — Prince William Sound oil spill. *EOSAT Landsat Data Users Notes*, 4, 3–4.

Asanuma, I., Muneyama, K., Sasaki, Y., Iisaka J., Yasuda, Y. & Emori, Y., 1986 — Satellite thermal observation of oil slicks on the Persian Gulf. *Remote Sensing of Environment*, 19, 171–186.

Boeuf, M.S. & Doust, H., 1975 — Structure and development of the southern margin of Australia. *The APEA Journal*, 15, 33–43.

Churchill, J.N., 1982 — Feasibility trial for the use of LANDSAT for the detection of offshore oil seepage. NERDDP Report EG/83/205. *Department of Resources and Energy, Canberra.*

Denham, J.I. & Brown, B.R., 1976 — A new look at the Otway Basin. *The APEA Journal*, 16, 91–98.

Exon, N.F., Lee, C.S., & others, 1987a — Rig Seismic research cruise 1987: Otway Basin and West Tasmania sampling. *Bureau of Mineral Resources, Australia, Record* 1987/11.

Exon, N.F., Williamson, P.E. & others, 1987b — Rig Seismic research cruise 3: Otway Basin. *Bureau of Mineral Resources, Australia, Record* 1987/279.

Griersmith, D.C. & Kingwell, J., 1988 — Planet under scrutiny — an Australian remote sensing glossary. *Bureau of Meteorology, Canberra.*

Hurford, N. 1989 — Review of remote sensing technology. *In* Lodge, A.E. (editor), The remote sensing of oil slicks. *The Institute of Petroleum, John Wiley & Sons, London.*

Lodge, A.E. (editor), 1989 — The remote sensing of oil slicks. Proceedings of an International meeting organised by the Institute of Petroleum and held in London May 1988. *The Institute of Petroleum, John Wiley & Sons, London.*

McKirdy, D.M., Cox, R.E., Volkman, J.K. & Howell, V.J., 1986 — Botryococcane in a new class of Australian non-marine crude oils. *Nature*, 320, 57–59.

McKirdy, D.M. & Horvath, Z., 1976 — Geochemistry and significance of coastal bitumen from southern and northern Australia. *The APEA Journal*, 16, 123–135.

Megallaa, M., 1986 — Tectonic development of Victoria's Otway Basin — a seismic interpretation. *In* Glenie, R.C. (editor), Second southeast Australia oil exploration symposium, Melbourne. *Petroleum Exploration Society of Australia*, 201–218.

O'Brien, G.W. & Heggie, D.T., 1989 — Hydrocarbon gases in seafloor sediments, Otway and Gippsland Basins: implications for petroleum exploration. *The APEA Journal*, 29, 96–112.

Perry, W.J., 1989 — Pilot study of satellite data of sea surface in Bass Strait and Southern Ocean to see if natural oil slicks from deep reservoirs are detectable. *Report to BMR Division of Marine Geoscience & Petroleum Geology, June 1989 (unpublished).*

Pickett, R.L., Partridge, R.M. & Arnone, R.A., 1984 — The Persian Gulf via satellites. *Oceanographic Monthly Summary (U.S. Department of Commerce)*, 4(9), 3.

Sprigg, R.C., 1964 — The South Australian continental shelf as a habitat for petroleum. *The APEA Journal*, 4, 53–63.

Sprigg, R.C. & Woolley, J.B., 1963 — Coastal bitumen in southern Australia, with special reference to observations at Geltwood Beach, southeast South Australia. *Transactions of the Royal Society of South Australia*, 86, 67–103.

Stringer, J., Ahlnas, K., Royer, T.A., Kenneson, G.D. & Groves, J.E., 1989 — Oil spill shows on satellite image. *EOS*, May 2, 564.

Ward, L.K., 1913 — Possibilities of the discovery of petroleum on Kangaroo Island and the west coast of Eyre Peninsula. *Geological Survey of South Australia, Bulletin* 2.

Williamson, P.E., Exon, N.F., Swift, M.G., O'Brien, G.W., Heggie, D.T., McKirdy, D.M., Lee, C.S. & Stephenson, A.E., 1988 — Offshore Otway Basin study. *Bureau of Mineral Resources, Australia, Continental Margins Folio* 2.

Williamson, P.E., O'Brien, G.W., Swift, M.G., Felton, E.A., Scherl, A.S., Marlow, M., Lock, J., Exon, N.F. & Falvey, D.A., 1987 — Hydrocarbon potential of the offshore Otway Basin. *The APEA Journal*, 27, 173–195.

Ypma, P.J., 1985 — Airborne detection of natural marine oil seepage. NERDDP Report EG/85/492. *Department of Resources and Energy, Canberra.*

BMR Journal of Australian Geology & Geophysics, 12, 35–50

The Gilmore Fault Zone — the deformational history of a possible terrane boundary within the Lachlan Fold Belt, New South Wales

P.G. Stuart-Smith[1]

The Gilmore Fault Zone is a long-lived imbricate fault system separating the Wagga Metamorphic Belt from the Tumut Block in the Palaeozoic Lachlan Fold Belt. Structures within the fault zone indicate dominantly sinistral transpressional movements during regional deformation in the Siluro-Devonian and mid-Devonian and/or Carboniferous. These movements, in response to lateral compression, resulted in the Wagga Metamorphic Belt being thrust over the Tumut Block. Dextral strike-slip movement may be inferred during Early Silurian regional deformation and subsequent extension. Common structural and metamorphic histories, and lithological correlation of rock units straddling the fault zone, indicate that the Gilmore Fault Zone was not a terrane boundary in the Late Ordovician or Early Silurian. Differences in geophysical expression and crustal composition across the southern part of the zone would be explained if the zone is a reactivated basement fault which corresponds, in part, to an older terrane boundary. The fault zone is interpreted as a splay off a gently west-dipping mid-crustal detachment.

Introduction

The Gilmore Fault Zone (Crook & Powell, 1976; Basden, 1986), also referred to as the Gilmore Suture (Scheibner, 1985), is a major north–northwest-trending tectonic feature extending for several hundred kilometres in the southeastern part of the Lachlan Fold Belt. In its southern part, the zone separates Ordovician metasediments of the Wagga Metamorphic Belt in the west from Ordovician–Early Silurian[2] volcanosedimentary sequences of the Tumut Block to the east (Fig. 1).

The fault zone, well-defined by aeromagnetic and gravity patterns (Suppel & others, 1986; Wyatt & others, 1980), is interpreted as either (i) a terrane boundary, formed by collision and overthrusting of the Wagga–Omeo Terrane over the Ordovician Molong Volcanic Arc during the Early Silurian Benambran Orogeny (Scheibner, 1982, 1985; Degeling & others, 1986; Suppel & others, 1986), or (ii) a dextral (Cas & others, 1980; Powell, 1983a) or sinistral (Packham, 1987) strike-slip fault which has offset portions of the arc and its associated back-arc basin (Wagga–Omeo Terrane) during the Benambran Orogeny. The fault zone is thought to have been active throughout Silurian extension and the subsequent Siluro-Devonian Bowning Orogeny (Basden & others, 1987; Packham, 1987; Powell, 1983a). The age of the Bowning Orogeny, in the Tumut region, is poorly constrained between the Ludlovian (Blowering Formation) and Early to middle Siegenian (Minjary Formation, Barkas, 1976). Sediments and volcanics of the latter unit form relatively flat-lying strata unconformably overlying meridionally folded older units.

The origin and history of the Gilmore Fault Zone are important in any tectonic reconstruction of the Lachlan Fold Belt. Little detailed work has been done to support the various interpretations of the nature and timing of movements on the zone. This paper details structural investigations on the better exposed southern part of the zone. The oldest preserved structures indicate that the Wagga Metamorphic Belt was thrust over the Ordovician–Early Silurian volcanic sequences in a southeasterly direction during the Siluro-Devonian deformation. Farther north, the overall westward dip of the zone is supported by the gravimetric expression of the fault zone, which shows a westward displacement from the surface position (Suppel & others, 1986). Oblique-slip movement (sinistral reverse) also occurred in the mid-Devonian and/or Carboniferous.

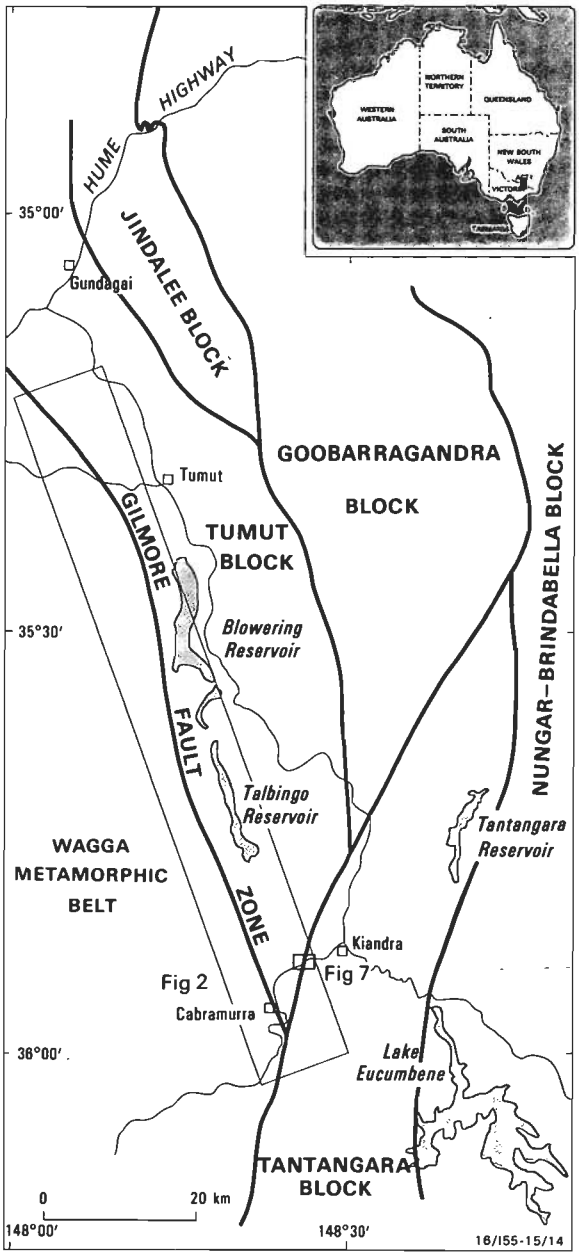

Figure 1. Locality map.
Geology modified after Owen & Wyborn (1979a). Note: The Tumut and Jindalee Blocks correspond to the Gocup and Jindalee Blocks, respectively, of Basden (1990) and the Tumut and Jindalee Terranes, respectively, of Basden & others (1987).

[1] Minerals and Land Use Program, Bureau of Mineral Resources, Geology & Geophysics, GPO Box 378, Canberra ACT 2601

[2] The Silurian timescale used here follows that of Strusz (1989), whereby the Silurian (435–410 Ma) is subdivided into Early and Late periods at the Wenlockian/Ludlovian boundary at about 420 Ma.

Rocks within the fault zone previously included in the Early to Late Silurian *Tumut Trough* (e.g. Basden, 1986) are here considered to be part of the Ordovician–Early Silurian volcanic sequence. Juxtaposition of these rocks with lithologically similar units west of the fault zone and common structural and metamorphic histories suggest that the Gilmore Fault Zone does not represent a terrane boundary in the Ordovician or Early Silurian. Rather, the Gilmore Fault Zone is interpreted as a reactivated basement fault which may, in part, correspond to a proposed Late Proterozoic–Early Palaeozoic basement terrane boundary suggested by Chappell & others (1988).

Geological setting

The geology of the region is described by Moye & others (1969a,b,c), Basden (1986), Wyborn (1977a) and Degeling (1975, 1977). The detailed geology of the southern part of the Gilmore Fault Zone is shown in Figure 2. A summary of stratigraphic units and relationships is given in Table 1 and Figure 3, respectively.

Ordovician–Early Silurian (Llandoverian) sediments and volcanics of the Molong Volcanic Arc, including the Nacka Nacka Metabasic Igneous Complex, Gooandra Volcanics and Kiandra Group, intertongue with the overlying laterally equivalent Bumbolee Creek Formation and the Tumut Ponds Beds. These units were deformed and metamorphosed during the Early Silurian (Late Llandoverian; Stuart-Smith, 1990a) Benambran Orogeny. They were then unconformably overlain by the Early to Late Silurian (Wenlockian–Ludloverian) Blowering Formation and Ravine Beds, during a period of extensional (transtensional) tectonics which resulted in uplift of Cambrian–Ordovician basement further to the east (Stuart-Smith, 1990b). The Tumut Ponds Serpentinite, present in the Gilmore Fault Zone, is here interpreted to represent part of this basement.

During the Siluro-Devonian Bowning Orogeny both the Ordovician and Silurian metasediments and volcanics were meridionally folded, metamorphosed and intruded by syn-kinematic granitoids (Wondalga and Green Hills Granodiorites, Rough Creek Tonalite and Gocup Granite). Early Devonian sediments and volcanics (Boraig Group, Byron Range Group and Minjary Volcanics) unconformably overlie older rocks and are mildly deformed in the fault zone. Outliers of flat-lying Tertiary basalt and minor sediments (common in the south as hill top cappings) overlie the fault zone, indicating a minimum of subsequent movement on the zone.

Fault zone structures

The Gilmore Fault Zone has three main structural units. From west to east these are:

(1) the deformed eastern margin of the Wagga Metamorphic Belt;
(2) a central belt of subparallel segments of Ordovician–Early Silurian metasediments and volcanics, with faulted allochthonous slivers of serpentinite and tonalite; and
(3) the folded and faulted western margin of the Tumut Block, comprising Ordovician, Silurian and Early Devonian rocks.

Although sharing some common aspects, each of the three structural units has a different structural history. Together, these reveal the long-lived deformation history of the fault zone.

Schematic structural profiles through the Gilmore Fault Zone are given in Figure 2. Stereoplots of the main structural elements are shown in Figure 4. Up to four phases of folding (F_{1-4}) and associated S surfaces (S_{1-4}) affect Ordovician–Early Silurian strata in the Tumut region (Stuart-Smith, 1990a). Only the later two fold phases and surfaces are preserved in the deformed margin of the Wagga Metamorphic Belt and in the central belt.

Margin of the Wagga Metamorphic Belt

The eastern margin of the Wagga Metamorphic Belt, consisting of the Wondalga and Green Hills Granodiorites and a narrow screen of Gooandra Volcanics, is marked by a deformed zone up to 1300 m wide.

Both the metasediments and the normally massive granodiorites are typified in the zone by a variably developed foliation which dips steeply to the west in the north and is subvertical in the south. The intensity of deformation in the granodiorites progressively increases towards the faulted contact with the central belt, from moderately foliated to strongly foliated with ultramylonite (nomenclature after Wise & others, 1984) zones several metres wide at the contact. Apart from deformed and fractured feldspar grains, the rocks are totally recrystallised, with the foliation defined by aligned muscovite, biotite, ribbon-quartz mosaic and polygonised quartz lenses. In the south, most of this zone was differentiated by earlier workers (e.g. Moye, 1953) as the 'Rough Creek Gneissic Granite'.

A mineral-elongation lineation is commonly present and plunges moderately to the northwest (Figs 4a,b). In mylonitic granodiorite, relic deformed primary biotite and muscovite 'fish' (Fig. 5), and asymmetrical lenses or tails of fine-grained polygonised quartz on deformed coarser feldspar grains, consistently indicate oblique-slip movement (sinistral transpressional). In places an *S-C* fabric (Berthé & others, 1979) is well developed between a slightly shallower and more southwest-dipping shear plane and the foliation (Fig. 4c). The intersection of these planes is orthogonal to the mineral lineation, in keeping with a true *S-C* fabric. The shear planes parallel the major fault trend, thus representing synthetic shears, whereas the foliation is slightly oblique to the main fault trend and parallels the S3 cleavage in the adjacent metasediments (Fig. 4e).

The metasedimentary screen of Gooandra Volcanics between Gilmore and Buddong Falls appears to be transitional with amphibolite facies rocks north of the Nacka Nacka Metabasic Igneous Complex to the west (Figs 2, 6). Garnet- and andalusite-bearing schists within 500 m of the complex grade through muscovite-biotite schist to phyllite at 1000 m. This metamorphic zoning is preserved at Valley View, where the screen is at its greatest width but is truncated by the Gilmore Fault Zone to the south and north. There is little evidence of major faulting at the contact between the metasediments and the complex or granodiorites. At Valley View, the metasediments pass from schist to gneiss approaching the complex; minor quartz-feldspar leucosome appears within 100 m of the contact. The structure of the metasediments and the Nacka Nacka Metabasic Igneous Complex, like the deformed granodiorites (Fig. 4a), is dominated by a steeply west-dipping schistosity with an associated northwest-plunging mineral elongation lineation. Compositional banding in the metasediments and mafic rocks mostly parallels the schistosity, which is axial plane to rare gently-plunging isoclinal fold closures. The schistosity, formed during peak metamorphic conditions, is defined by aligned but unstrained micas.

The development of schistosity and peak metamorphism within the deformed margin of the Wagga Metamorphic Belt is

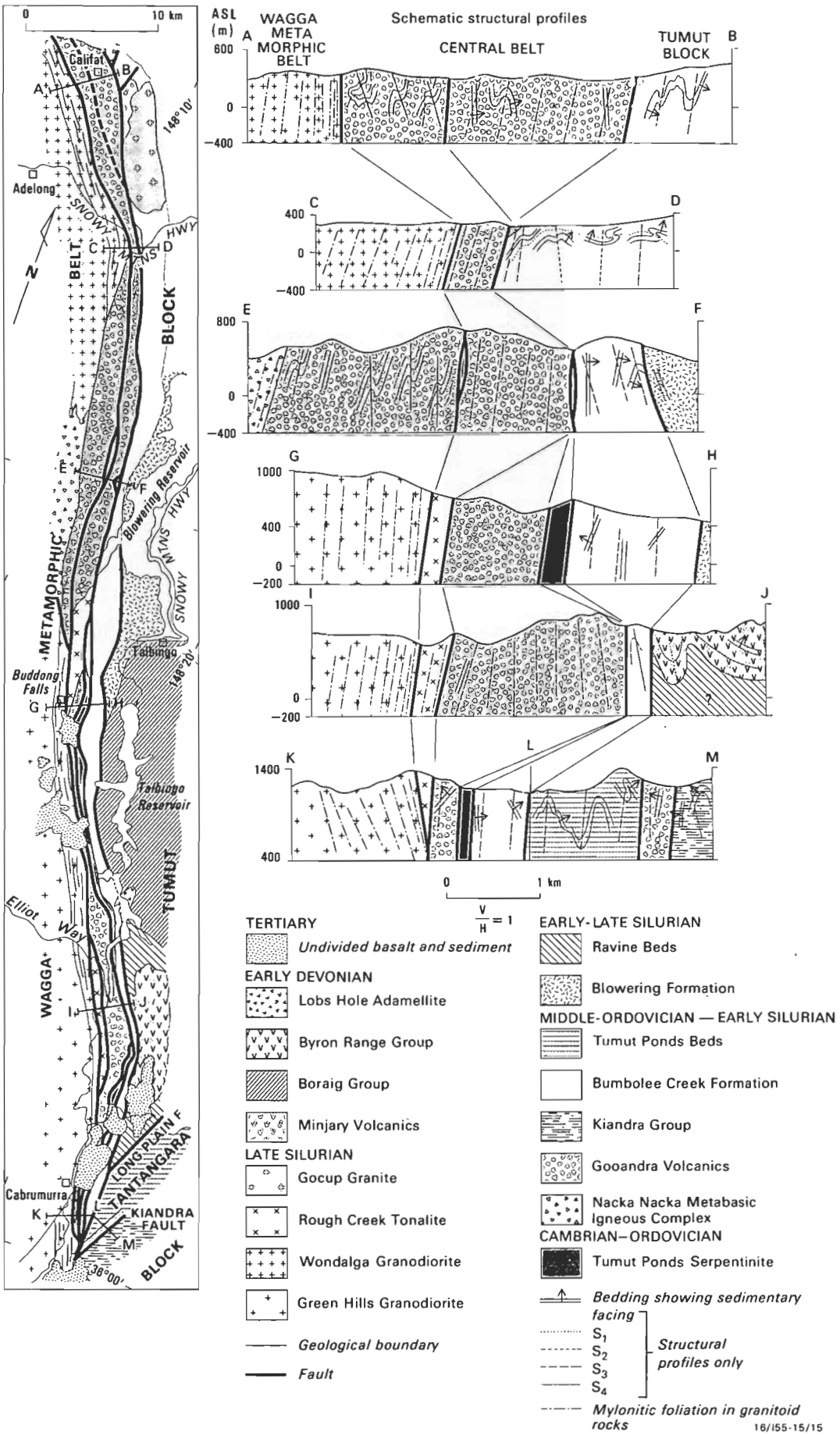

Figure 2. Generalised geology of the southern part of the Gilmore Fault Zone.

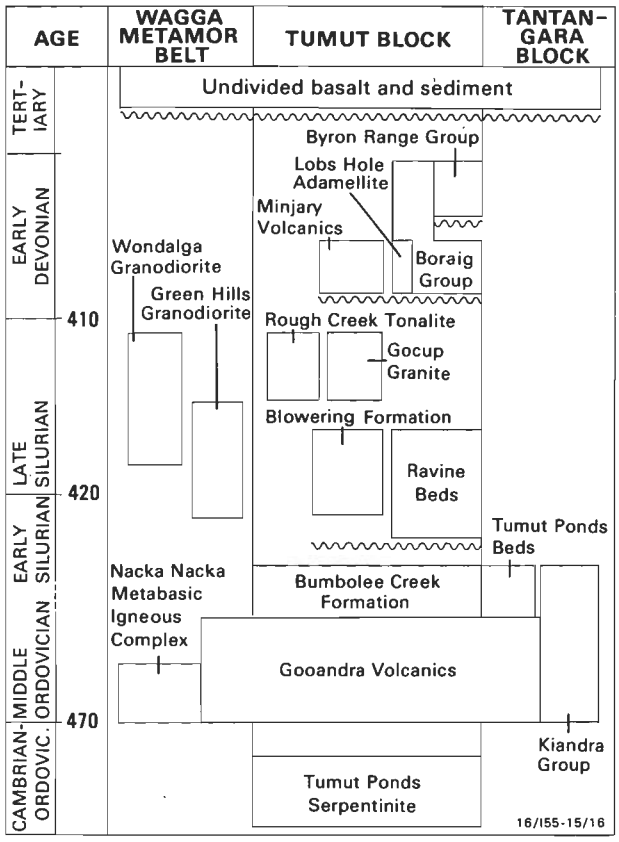

Figure 3. Diagrammatic stratigraphy of units within the Gilmore Fault Zone.

probably Siluro-Devonian. The presence of undeformed late-stage pegmatoid veins cross-cutting foliated phases of granodiorite (Dobos, 1971) indicates that the Late Silurian (Basden, 1986) granodiorite intrusions were emplaced during the deformation. No earlier structures are preserved in either the metasediments or granodiorites. The age, geometry and morphology of the schistosity suggest it is equivalent to the S_3 cleavage in Bumbolee Creek Formation sediments in the Tumut Block to the east (Stuart-Smith, 1990a).

The main metamorphic fabric within the deformed zone of the Wagga Metamorphic Belt is locally overprinted by later deformation spatially associated with the Gilmore Fault Zone. In the Cabramurra area, the mylonitic fabric in the Green Hills Granodiorite is deformed by cataclastic fault zones and subparallel chloritic shear zones with subvertical to gently S-pitching slickenlines. The mineral elongation associated with the mylonitic fabric is rotated (all of the S-plunging lineations on Fig. 4 come from the Cabrumurra area) within the fault and shear zones, both of which are commonly associated with localised chlorite and muscovite alteration. Slickenlines indicate that movement on the chloritic shear zones was mostly reverse (either east or west side up) with a dextral strike-slip component. In the Valley View area, the metamorphic foliation in the metasediments is tightly folded by a steep east-dipping, closely spaced, S_4 crenulation cleavage within 700 m of the fault (Fig. 4d). The cleavage, associated with east-verging folds, may be related to later reverse (i.e. west side up) movements of the Gilmore Fault Zone. The age of both this cleavage and the cataclasis mentioned above is unknown, but is probably either mid-Devonian or Carboniferous (see below).

Central belt

The central belt is mainly metasediments and volcanics of the Gooandra Volcanics, with narrow discontinous allochthonous slivers of Rough Creek Tonalite and Tumut Ponds Serpentinite along the bounding faults. The belt, up to 3 km wide in the north, narrows southwards and pinches out about 4 km south of Cabramurra. All the units are characterised by a foliation or cleavage which parallels the foliation (both S_3 in Fig. 4a and S plane in Fig. 4b) in the Wagga Metamorphic Belt to the west and the S_3 cleavage (Fig. 4k) in metasediments of the Tumut Block to the east.

Rough Creek Tonalite

Massive, fractured and extensively chloritised bodies of equigranular coarse-grained biotite tonalite occur along the western margin of the central belt. Mostly, the margins of the tonalite bodies are converted to mylonite with structural elements (only limited data) parallel to mylonites in the adjacent deformed granodiorites (Fig. 4i). The mylonitic foliation consists of broken feldspar and quartz grains in a strongly foliated phyllonitic matrix of muscovite, chlorite and ribbon quartz. South of Cabramurra, this fabric is rotated and crosscut by secondary foliated chlorite-rich and muscovite-rich zones. Slickenlines on the latter zones pitch steeply or shallowly to the south (Fig. 4i). Both fabrics may have been the result of either continuous mylonitisation or two separate deformations as is indicated in the adjacent Green Hills Granodiorite.

Although only tectonic contacts were found, the presence of foliated fine-grained aplitic margins to the northernmost body of tonalite possibly represent chilled margins, indicating the tonalite may intrude the Gooandra Volcanics.

Tumut Ponds Serpentinite

Numerous slivers of ultramafic and mafic rocks (up to 600 m wide and 25 km long) occur along the length of the central belt within the major fault zones. The rocks include mostly massive to schistose serpentinite, and minor meta-pyroxenite, serpentinised harzburgite (Van Der Oever, 1984), talc schist, metabasalt and amphibolite. Typically, the margins of the bodies are schistose serpentinite with a well-developed *S-C* fabric. This fabric is dominated by a subvertical *C* plane, which parallels the major faults and the main foliation (S_3 cleavage) in adjacent rocks (Figs 4g,h). A subhorizontal mineral elongation is present on the *C* plane orthogonal to the intersection of the plane and a vertical north–northeast-trending flattening foliation (S plane). The orientation of the fabric indicates mostly sinistral strike-slip movement with a minor reverse component, the *C* planes forming synthetic shears to the main faults.

The metamorphic grade of the mafic and ultramafic rocks is lower greenschist facies, similar to tonalite, metasediments and volcanics within the central belt. Pyroxenites are altered to actinolite/tremolite, and mafic rocks to chlorite + epidote assemblages. Near Section Creek, 7 km north of Cabramurra, the western margin of the main serpentinite body consists of a chloritic breccia containing rotated clasts of massive meta-pyroxenite and foliated hornblende amphibolite. The body therefore represents an allochthonous sequence which may have been derived from a Cambrian–Ordovician basement similar to that proposed for other serpentinite bodies in the region (Stuart-Smith, in press).

Metasediments and volcanics

Metasediments and volcanics of the Gooandra Volcanics occupy most of the central belt. The rocks are characterised by a steeply west-dipping penetrative slaty cleavage or schistosity which parallels the foliation in adjacent granitoids slightly

Table 1. Summary of stratigraphy of units within the Gilmore Fault Zone.

	Unit	*Description*	*Field relationships*	*Remarks*
TERTIARY	T	Basalt, minor limonitic pebble conglomerate and sandy clay at base.	Unconformably overlies older units	Forms flat-lying capping
EARLY DEVONIAN	Lobs Hole Adamellite (Dgl)	Porphyritic granophyric leucogranite	Intrudes Dlv.	Subvolcanic intrusion comagmatic with Dlv (Barkas, 1976).
	Byron Range Group (Dls)	Shale, limestone and arenite.	Unconformably overlies Ssr and basal part of Dlv Faulted against Oub.	Shallow-marine (Moye & others, 1969c).
	Boraig Group (Dlv)	Rhyolite, rhyolitic tuff, siltstone, shale, volcanilithic arenite and cobble conglomerate.	Unconformably overlies Ssr and Sbd. Unconformably overlain by Dls (Moye & others, 1969c). Faulted against Oub.	Shield volcanic complex (Owen & others, 1982).
	Minjary Volcanics (Dvm)	Rhyolitic ignimbrite, tuff and minor polymictic conglomerate and arenite.	Unconformably overlies Oub and Sgc.	Shallow-marine to subaerial. Early to middle Seigenian brachiopods and corals (Barkas, 1976).
LATE SILURIAN	Gocup Granite (Sgc)	Pink coarse-grained muscovite-biotite granite.	Intrudes Oub. Unconformably overlain by Dvm.	Pre-dates Siluro-Devonian meridional upright folds. ?Deformation ages 409 ± 2 Ma [(K-Ar on muscovite) and 402 ± 2 Ma (Rb-Sr whole rock) (Richards & others, 1977).
	Rough Creek Tonalite (Sgr)	Coarse-grained equigranular chloritised biotite tonalite.	Allochthonous fault slices. Probably intrudes Ovg.	Synkynematic S-Type granitoid (Wyborn, 1977a).
	Wondalga Granodiorite (Sgw)	Medium-to-coarse-grained biotite granodiorite.	Intrudes On and Gisbornian Wagga Metamorphic Belt metasediments.	Synkynematic I-type granitoid (Basden, 1986).
	Green Hills Granodiorite (Sgg)	Coarse-grained equigranular muscovite-biotite granodiorite.	Intrudes On and Gisbornian Wagga Metamorphic Belt metasediments.	Late synkynematic S-type granitoid (Wyborn, 1977a; Basden, 1986). Ages 406 ± 6 Ma 419 ± 6 Ma, 422 ± 6 Ma (K-Ar on biotite; Webb, 1980).
EARLY SILURIAN	Ravine Beds (Ssr)	Shale, slate, chert, graded coarse-grained volcanilithic arenite and conglomerate.	Unconformably overlain by Dlv and Dls faulted against Oub.	Late Wenlockian to early Ludlovian (Labutis, 1969).
	Blowering Formation (Sbd)	Massive dacitic ignimbrite.	Uncomformably overlies and faulted against Oub. Unconformably overlain by Dlv.	Flows and subvolcanic intrusions. Coeval with 429 Ma Goobarragandra Volcanics (Owen & Wyborn, 1979a).
EARLY SILURIAN	Tumut Ponds Beds (Out)	Graded thickly bedded fine- to coarse-grained quartz-intermediate arenite, slate, and minor quartz-rich arenite.	Lateral equivalent of Oub ?Conformably overlies Ovg.	Deep-marine turbidite sequence.
	Bumbolee Creek Formation (Oub)	Phyllite, slate, silty slate, thinly bedded graded fine- to coarse-grained quartz-rich arenite, minor massive coarse-grained quartz-intermediate arenite and pebble conglomerate.	Lateral equivalent of Out. Conformably overlies Ovg (Stuart-Smith, 1988).	Deep-marine turbidite sequence.
	Kiandra Group (Ovk)	Fine- to coarse-grained and pebbly mafic volcaniclastic metasediments, silty slate.	Faulted against Ovg.	Deep- to shallow-marine, locally subaerial. Late Darriwilian to ?late Gisbornian (Owen & Wyborn, 1979a).
MIDDLE ORDOVICIAN	Gooandra Volcanics (Ovg)	Interbedded fine- to medium-grained mafic volcaniclastic metasediments, silty slate, metabasalt, minor quartz-rich arenite, quartz-intermediate arenite, laminated black chert, metarhyolite and polymictic pebble and cobble conglomerate.	Lateral equivalent of On. Conformably overlain by Oub and Out.	?Late Darriwilian to ?early Gisbornian (Owen & Wyborn, 1979a).
	Nacka Nacka Metabasic Igneous Complex (On)	Amphibolite, metagabbro.	Intruded by Sgw and Sgg. Lateral equivalent of Ovg.	Age 465 ± 6 Ma and 467 ± 6 Ma (K-Ar on hornblende, Webb, 1980).
CAMBRIAN ORDOVICIAN	Tumut Ponds Serpentinite (COs)	Serpentinite, talc schist, serpentinised harzburgite, metabasalt and amphibolite inclusions.	Faulted against other units.	Age unknown. Forms allochthonous tectonic slices within the Gilmore Fault Zone. ?Part of Jindalee Group.

oblique to the main fault trend (Fig. 4k). The cleavage is correlated with the S_3 cleavage in the units east of the fault, on the basis of its meridional trend and associated fold styles. The cleavage is axial plane to variably-plunging, upward-facing, steeply inclined, tight to isoclinal folds. The variation in fold plunge may be a result of either earlier recumbent folding such as occurs to the east in the Bumbolee Creek Formation, or of heterogeneities in strain or both. There is no evidence of downward-facing folds or older structures. However, this may be an artifact of the greater intensity of the deformation in the Gilmore Fault Zone. Within the belt, bedding is mostly parallel to cleavage and the degree of metamorphic recrystallisation and associated strain is higher than east of the fault zone. Conglomerate pebbles which are undeformed east of the Gilmore Fault Zone are flattened and stretched within the the S_3 surface (Fig. 7), forming a prominent elongation lineation which

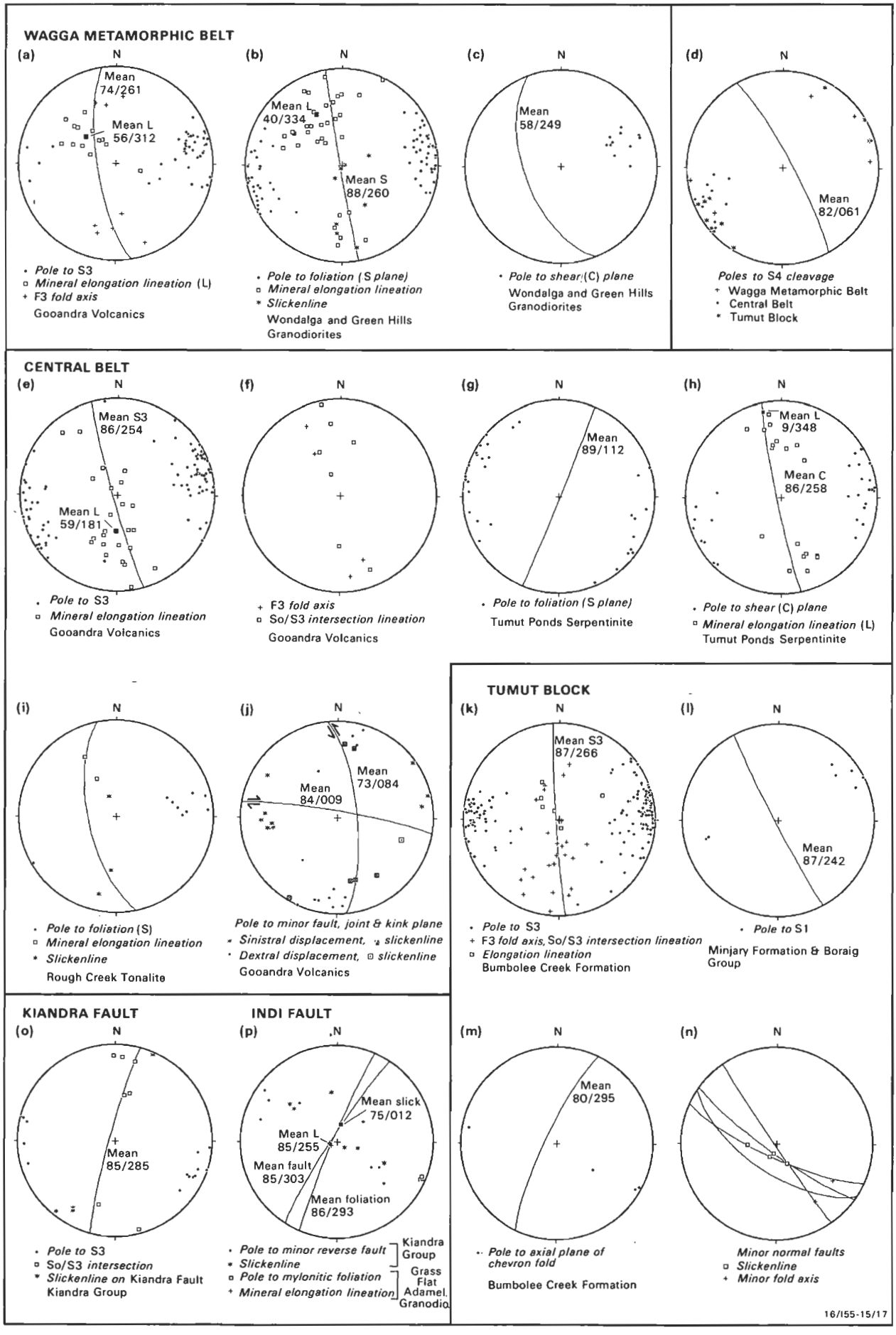

Figure 4. Equal area stereoplots of the main structural elements of all units within the Gilmore Fault Zone.

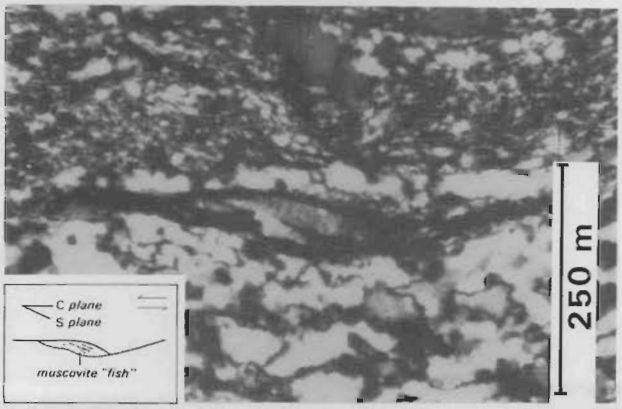

Figure 5. Photomicrograph of muscovite 'fish' in the mylonitic margin of the Wondalga Granodiorite, showing indicated movement direction.

plunges moderately to the south (Fig. 4e). This lineation is also marked by the extension direction of boudinaged quartz veins and a mineral-elongation lineation in quartz–feldspar porphyries (flows or dykes?). The lineation may reflect an earlier movement history not seen in the syn-kinematic Late Silurian granitoids or preserved in the serpentinite. This appears likely as, in several places approaching the fault contact with the Wondalga Granodiorite, the lineation in the metasediments is progressively rotated into parallelism with the lineation in the granodiorite. Older units in the belt are thrown against younger units east of the Gilmore Fault Zone, so the earlier movement history was probably reverse (i.e. west side up).

Metamorphic grade is greenschist facies, with meta-pelites and arenites typified by fine-grained foliated chlorite and muscovite, and metabasalts by actinolite + chlorite + epidote assemblages. Biotite is also common in metasediments north of Gilmore and south of Talbingo Reservoir (Fig. 6). In the latter area, S_3 micas are overgrown by randomly oriented muscovite and biotite indicating possible contact metamorphic overprinting.

Sinistral strike-slip movements are indicated by minor structures in the central belt which post-date the S_3 cleavage (Fig. 4j). Minor joints and faults are commonly present and parallel conjugate widely to closely spaced, steeply dipping kink bands (Fig. 4j). East-trending kink bands rotate the penetrative S_3 cleavage with a consistent dextral sense of shear, whereas those trending north have a sinistral symmetry. The symmetry and orientation of the conjugate kink bands is consistent with sinistral strike-slip movement on the Gilmore Fault Zone. This sense of movement is also supported by the presence of minor subhorizontal to northwest-dipping reverse faults and spatially associated with the kink bands. In the north, only the east-trending kink is present. The lack of a conjugate set in this area indicates that the kinks were not a result of layer-parallel shortening but rather may have been the result of sinistral shear on the Gilmore Fault Zone, which here forms an acute angle with the S_3 cleavage. In keeping with shear band experimental data of Harris & Cobbold (1984) and Williams & Price (1990), the kinks would have developed as R′ (P′) shear bands with P the most active shear paralleling the S_3 cleavage.

A steep east–northeast-trending S_4 crenulation cleavage (Fig. 4d) is locally present in the central belt, particularly next to the major faults where it is most intensely developed. The cleavage is axial plane to open F_4 folds, and F_3 folds are rotated into recumbent orientations. Consistent eastward-vergences, the spatial association of the cleavage and its parallelism to the main faults suggest that it is probably related to late reverse

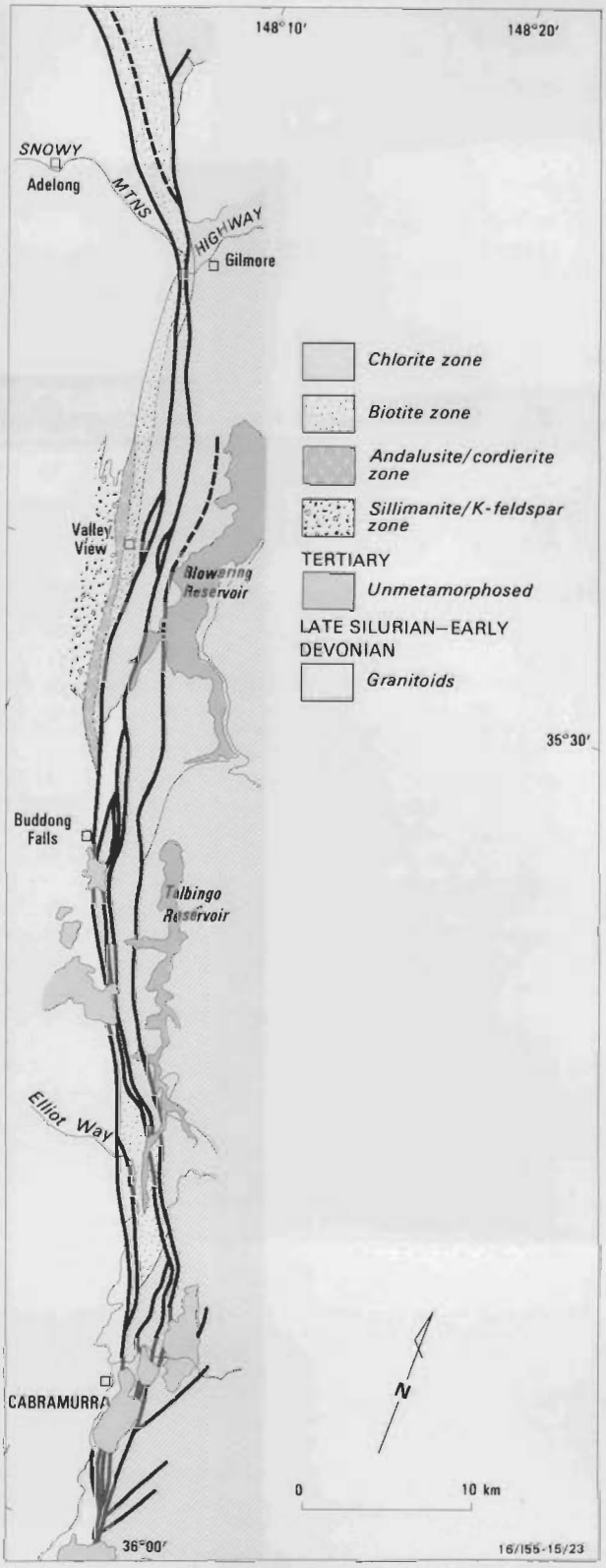

Figure 6. Metamorphic zones in Ordovician to Early Devonian strata.

Identification of zones is based on the mineralogical critera described by Wyborn (1977a). The zones correlate with zones established by previous workers in the region, as follows:

Chlorite Zone = Zone B of Wyborn (1977a); low grade zone of Vallance (1953, 1967) and Guy (1969); chlorite zone of Joplin (1947) and Rogerson (1977).

Biotite Zone = Zone C of Wyborn (1977a); biotite zone of Smith (1969).

Andalusite/cordierite Zone = Zone E of Wyborn (1977a); knotted schist zone of Joplin (1947), Vallance (1953) and Guy (1968); andalusite/cordierite zone of Rogerson (1977).

Sillimanite/K-feldspar Zone = Zone E of Wyborn (1977a); high grade zone of Vallance (1953), Guy (1968); K-feldspar zone of Rogerson (1977).

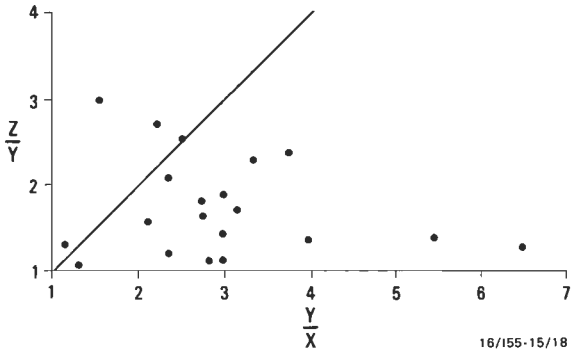

Figure 7. Flynn diagram of quartzite pebbles in Gooandra Volcanics conglomerate, Central Belt (Califat area).

movements on the fault zone. As there is no relationship between the cleavage and other minor structures, its age cannot be determined. The cleavage may be equivalent to a similarly trending crenulation in the Wagga Metamorphic Belt to the west and a spaced cleavage present in Early Devonian sediments abutting the Gilmore Fault Zone to the east.

Margin of the Tumut Block

In the study area, the western margin of the Tumut Block comprises poly-deformed flysch of the ?Ordovician–Early Silurian Bumbolee Creek Formation unconformably overlain by Silurian (Wenlockian–Ludloverian) and Early Devonian felsic volcanics and shallow-marine sediments. Within 2 km of the Gilmore Fault Zone, all the units are affected by deformation associated with movements on the zone.

Throughout the Tumut Block, the Bumbolee Creek Formation has a complex deformation history (Stuart-Smith, 1990a). Early recumbent east–west folds (F_1) are widespread, commonly with an associated axial-plane slaty cleavage (S_1). South of the Gocup Granite, the F_1 folds are refolded by coaxial open upright folds (F_2) with an axial crenulation cleavage (S_2). Both periods of folding pre-date intrusion of the Gocup Granite and are probably Early Silurian in age (Stuart-Smith, 1990). These early folds are refolded by Siluro-Devonian near meridional-trending upright folds (F_3) with a steep west-dipping penetrative axial spaced cleavage (S_3) (Fig. 4k).

The F_3 folds dominate regional structures in the area, particularly in the deformed margin against the Gilmore Fault Zone. Within this margin, F_3 folds are tight to isoclinal, whereas elsewhere they are tight to open. Except in the 'strain shadow' areas, immediately north and south of the Gocup Granite, there is little evidence of F_1 or F_2 folds in the deformed margin, owing to the intensity of the F_3 folding and the parallelism of the different S surfaces. Mostly beds are upright where younging is determined. F_3 axes plunge to the south and north, reflecting either or both earlier fold geometries and heterogeneity of strain. In the south, where the formation forms a narrow faulted-bounded strip adjacent to younger units, F_3 folds are isoclinal and plunge subvertically parallel to a pebble elongation lineation. This lineation, where present, parallels that in the adjacent central belt, suggesting a common origin. As with the central belt, the extension lineation may reflect an earlier movement history not present in Silurian (Wenlockian–Ludloverian) and younger units. Older units in the belt are thrown against younger units east of the Gilmore Fault Zone, so the earlier movement history was probably reverse (i.e. west side up). Anticlockwise rotation of the S_3 cleavage into the fault zone indicates a component of sinistral shear either during this or a later movement(s) on the fault zone.

The Silurian (Wenlockian–Ludloverian) and Early Devonian units are downthrown against either the Bumbolee Creek Formation or Gooandra Volcanics along the eastern margin of the Gilmore Fault Zone. Where exposed, this fault contact dips steeply (70°) to the west. The younger units east of the fault are tightly folded within 1 km of the fault, with a penetrative foliation locally present in the Silurian (Wenlockian–Ludloverian) units. Within the Early Devonian units, a spaced cleavage (Fig. 4l) parallels the main fault trend and may correlate with the S_4 cleavage in older units.

Slickenlines on minor steep west-dipping reverse faults in the Byron Range Group indicate a sinistral strike-slip component of displacement. Post-Early Devonian sinistral strike-slip movement is also indicated by normal faults in the Bumbolee Creek Formation and Minjary Volcanics in the Gilmore area (Fig. 4n). Post-S_3 sinistral strike-slip movement is also consistent with locally developed northeast-trending chevron folds, showing a sinistral symmetry, in the Bumbolee Creek Formation south of Cabramurra (Fig. 4m).

Relationship to Long Plain, Kiandra and Indi Faults

The Gilmore Fault Zone terminates in the south near the junction between the Long Plain, Kiandra and Indi Faults. The Long Plain and Indi Faults have previously been regarded as part of the one continous fault system (e.g. Wyborn, 1977a). However, this study establishes that the Gilmore Fault Zone truncates the Long Plain and Kiandra Faults east of Cabramurra (Fig. 2) and continues farther southwards where it becomes continuous with the Indi Fault.

The north–northeast-trending Long Plain Fault separates meridional-trending Silurian and Early Devonian rocks of the Tumut and Goobarragandra Blocks to the north from tightly folded north–northeast-trending Ordovician–Silurian volcanic and flysch sequences of the Tantangara Block (Owen & Wyborn, 1979a,c) to the south. The fault has been described as a west-dipping reverse fault farther to the north where its strike is more northerly (Wyborn, 1977b; Owen & Wyborn, 1979b). In the study area, a section through the fault was examined along the Cabramurra–Kiandra road.

At this locality (Fig. 8), tightly folded strata in the Tumut Ponds Beds east of the fault young westwards and become progressively overturned approaching the fault. Within 250 m of the fault, bedding, dipping 70° southeast, parallels a penetrative cleavage and the inferred fault contact. Northwest of the fault, the cleavage in slate of the Ravine Beds is rotated clockwise from a near vertical north-trending orientation into parallelism with the fault at the fault contact. Rare quartz-fibre lineations present on the cleavage surface pitch about 60° northeast. The above structures are all consistent with dextral reverse movement on the Long Plain Fault.

Mainly dextral strike-slip movement is also indicated for the Kiandra Fault, which parallels the Long Plain Fault about 3 km to the southeast. At Tumut Ponds Dam, the fault is marked by a siliceous breccia with subhorizontal slickenlines (Fig. 4o). The movement on both the Kiandra and Long Plain Faults is probably mid-Devonian and/or Carboniferous (see following section).

South of Cabramurra, the Gilmore Fault Zone swings southwards beneath a Tertiary basalt capping, emerging as the Indi Fault. The fault throws mylonitic rocks of the Green Hills Granodiorite against the Ordovician Kiandra Group. The contact between both units was examined where exposed along

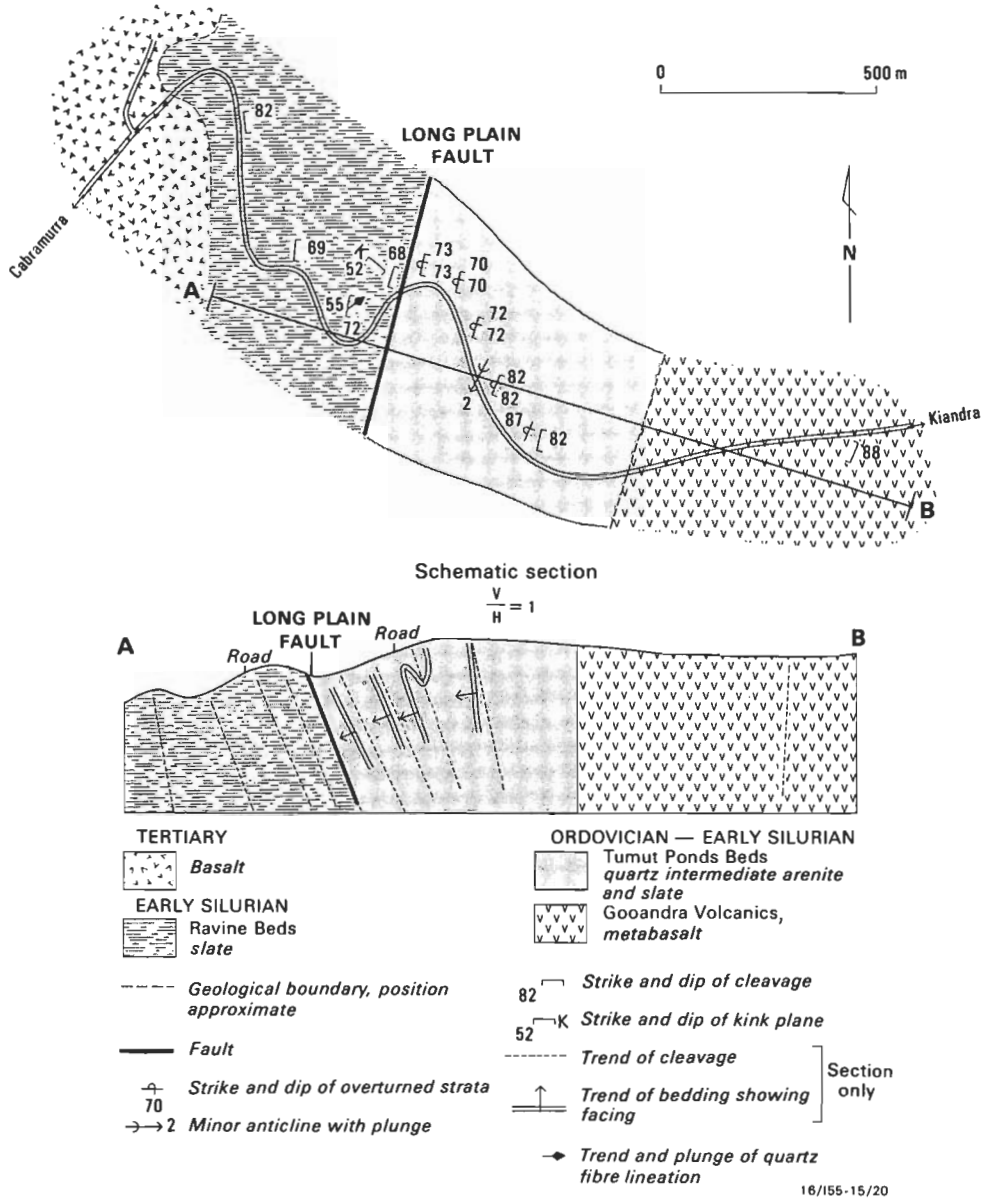

Figure 8. Geological sketch map and section across the Long Plain Fault, Cabramurra–Kiandra road.

the Geehi Dam access road (Locality A, Fig. 9). Here the fault dips steeply to the west and is marked by a 20 m wide ultramylonite zone in the granodiorite. Reverse movement is indicated by a near vertical mineral-elongation lineation (Fig. 4p) in the mylonite and slickenlines on minor synthetic shear zones in adjacent metabasalt of the Kiandra Group. There is no evidence to support interpreted sinistral displacement (Wyborn, 1977a) or large-scale dextral displacement (Vandenberg, 1978).

The indicated movement direction on the Indi Fault is close to that in the mylonitic zone within the Gilmore Fault Zone along the margin of the Wagga Metamorphic Belt, and is compatible with the interpreted east–west compression in southeastern Australia during Silurian (e.g. Chappell & White, 1976; Scheibner, 1976; White & others, 1976), mid-Devonian (Wyborn, 1977b; Powell, 1984) and Carboniferous (Powell & Veevers, 1984) times.

Discussion

Movement history

Pre-Siluro-Devonian

Owing to the penetrative nature of the Siluro-Devonian deformation (Bowning Orogeny) and the associated metamorphism, no earlier movement history is recorded in fault zone structures. However, it is likely, considering the structural history of the Wagga Metamorphic Belt and the Tumut Block, that the fault zone existed before this time. Folds pre-dating Silurian granitoid intrusion and trending 080° are present in both the Wagga Metamorphic Belt (e.g. Rogerson, 1977) and the Tumut Block. In the latter area they are recumbent, and zones of consistently south or north-facing folds are separated by minor faults which parallel the Gilmore Fault Zone (Stuart-Smith, 1988). These faults probably acted as accommodation structures (e.g. tear faults) during recumbent folding. The Gilmore Fault Zone may have been similarly active during the

Early Silurian deformation (Benambran Orogeny) when folding took place. The attitude of the folds, which also occur elsewhere in the Lachlan Fold Belt, is thought to be a result of dextral shear on the major fault zones (Cas & others, 1980; Powell, 1983a, 1984; Fergusson, 1987).

The Gilmore Fault Zone forms the western extent of Early Silurian north–south extension in the Tumut region (Stuart-Smith, 1990b). The partioning of this extension from the adjacent blocks requires strike-slip displacement on the bounding faults which parallel the extension direction. Movement on the Gilmore Fault Zone during this period may have been either dextral (Powell, 1983a, 1984) or sinistral (Packham, 1987).

Early Silurian

The earliest preserved structures within the Gilmore Fault Zone were synchronous with meridional folding of the Ordovician and Silurian rocks in the region during the Siluro-Devonian Bowning Orogeny. A subvertical elongation lineation, developed on the penetrative west-dipping cleavage (S_3) axial-plane to the folds, reflects an east–west principal compression direction and eastwards thrusting of the Wagga Metamorphic Belt over the Tumut Block. This accompanied thermal uplift associated with (and possibly postdating) widespread granitoid intrusion and regional metamorphism in the Wagga Metamorphic Belt. The Indi Fault, having an orientation orthogonal to the principal compression direction, became the thrust front as the Wagga Metamorphic Belt overrode the Tumut and Tantangara Blocks. Numerous lineaments parallel to the Indi Fault within the Wagga Metamorphic Belt (Fig. 9a) probably reflect smaller, but similar, reverse faults.

As deformation progressed, the principal compression direction rotated slightly to the northwest, creating transpressional conditions, and movement on the fault zone became oblique (sinistral reverse). The S_3 cleavage was rotated in an anticlockwise direction. In the mylonitic margin of the Wagga Metamorphic Belt and the adjacent central belt, the elongation lineation rotated from a steep westerly plunge to a more moderate northwesterly plunge. Only this latter orientation was preserved in allochthonous bodies of Rough Creek Tonalite and the margin of the Wagga Metamorphic Belt where thermal gradients were still high following granitoid intrusion.

Displacement does not appear to be confined to the boundary between the Wagga Metamorphic Belt and the Tumut Block at this time. Mylonitic rocks within the Wondalga Shear Zone (Basden, 1986), farther to the west within the Wagga Metamorphic Belt, are typified by a southwest-dipping foliation with an elongation lineation plunging 50° northwest (Veness, 1973). The parallelism of fabric elements in this zone to those in mylonites within the Gilmore Fault Zone suggests a common origin. Indeed, lineaments on Landsat images (Fig. 9a) indicate that the shear zone links up with the Gilmore Fault Zone. Thus the Wondalga Shear Zone and the Gilmore Fault Zone probably represent parts of a braided or imbricate oblique-slip (sinistral reverse) fault system.

Post-Early Devonian

Following deposition of Early Devonian shallow-marine sediments and volcanics, renewed southeast-directed thrusting of the Wagga Metamorphic Belt is indicated by downfaulting and folding of the Early Devonian rocks next to the Gilmore Fault Zone and the northwest pitch of rare slickenlines on minor faults. A crenulation cleavage (S_4), locally present in older units and parallel to a spaced cleavage in Early Devonian pelites, may have formed during this movement. The crenulation is axial plane to open east-verging folds.

The *S-C* fabric present in serpentinite bodies within the Gilmore Fault Zone and other minor structures such as kinks, joints, chevron folds and normal and reverse faults within Ordovician and Silurian metasediments and volcanics, forms a typical Riedel shear zone consistent with sinistral strike-slip movement on the Gilmore Fault Zone (Fig. 10). In the south, interaction with the north–northeast-trending Long Plain Fault Zone is interpreted to be the cause of minor retrograde cataclastic zones associated with dextral transpressional shear zones which deform the mylonitic fabric along the margin of the Wagga Metamorphic Belt.

The Riedel shear zone fabric of the Gilmore Fault Zone is also paralleled on a regional scale by the development of northwest-trending sinistral and northeast-trending dextral strike-slip faults and north-trending thrust faults throughout the southeastern part of the Lachlan Fold Belt (Fig. 9b). Such fabrics can be developed at any scale (Tchalenko, 1970). This is illustrated by the marked similarity of the strike-slip fault pattern in southeastern Australia (Fig. 9b) to that developed in a much larger area in eastern Turkey by the collision of the Arabian Plate with Eurasia (Fig. 11).

The movement history of the Gilmore Fault Zone is very similar to that outlined for the Mooney Mooney Fault Zone (Stuart-Smith, in press) and other faults in the region. In the Brindabella–Tantangara region, Wyborn (1977b) interpreted two periods of fault movement (one during the Late Silurian and the other post-mid Devonian) corresponding to episodes of lateral compression. Vandenberg (1978) describes both reverse and sinistral movement on the Kiewa Fault which parallels the Gilmore Fault Zone, forming part of the western margin of the Wagga Metamorphic Belt. However, recent work on the latter fault indicates that dextral strike-slip movement preceded mid-Devonian sinistral strike-slip movement (Gray & others, 1988). The only constraint on the timing of sinistral strike-slip movement on the Gilmore Fault Zone is that it post-dates the Siluro-Devonian S_3 cleavage. However, throughout the region deformation associated with east–west compression occurred during the mid-Devonian (Powell, 1983a, 1984) and Carboniferous (Powell & Veevers, 1984). All or most of the structures which post-date the Siluro-Devonian deformation in the Gilmore Fault Zone are therefore probably also either mid-Devonian and/or Carboniferous.

Serpentinite emplacement

S-C fabrics in allochthonous slices of ultramafic and mafic rocks (Tumut Ponds Serpentinite) within the Gilmore Fault Zone are consistent with the youngest structures found in the Ordovician and Silurian units. This does not necessarily imply a post-Siluro-Devonian age for their emplacement. Stuart-Smith (in press) found that successive deformations in the Coolac Serpentinite readily obliterated earlier fabrics. It is not suprising that *S* and *C* surfaces are the only Riedel shear elements present. In both the Coolac and Tumut Ponds Serpentinites, the *C* plane approximates the Y shear (Fig. 10) direction, which develops experimentally only during the residual stages of deformation (Tchalenko, 1970). The Tumut Ponds Serpentinite, like the Coolac Serpentinite, may well represent part of the Cambrian–Ordovician basement exposed elsewhere in the region as metamorphic core complexes (Stuart-Smith, 1990b) which were emplaced during Early Silurian extension in the region.

Crustal structure and terrane accretion

The crustal structure beneath the Gilmore Fault Zone in the Tumut region is poorly known. However, some interpretations can be made from limited seismic, gravity, surface structural and granitic source data available.

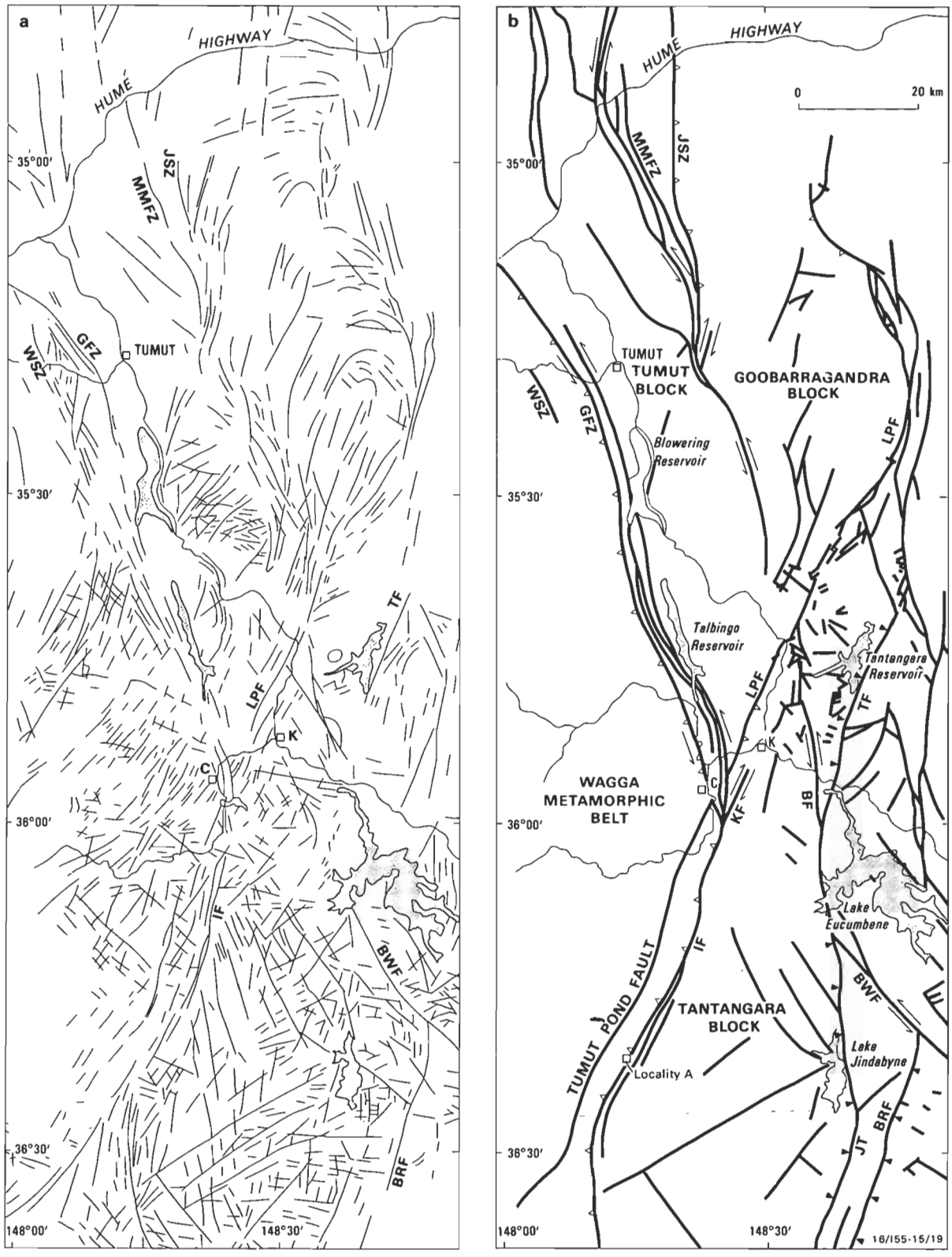

Figure 9. Sketch maps of (a) Landsat lineaments, (b) mapped faults (modified from Owen & Wyborn, 1979a,b; Owen & others, 1982; Wyborn, 1977b).

BRF Barneys Range Fault, BF Berridale Fault, C Cabramurra, GFZ Gilmore Fault Zone, IF Indi Fault, JT Jindabyne Thrust, JSZ Jugiong Shear Zone, K Kiandra, LPF Long Plain Fault, MMFZ Mooney Mooney Fault Zone, TF Tantangara Fault, T Tumut, TPF Tumut Ponds Fault, WSZ Wondalga Shear Zone.

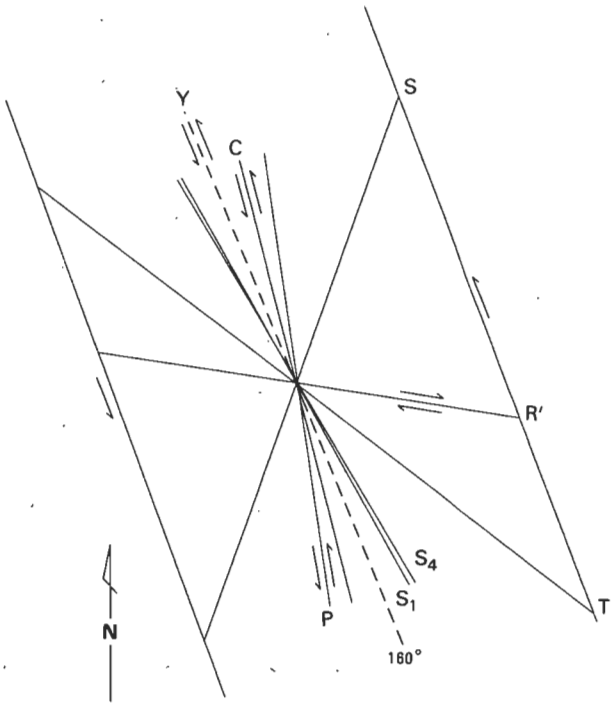

Y = *Y shear (trend of main fault zone)*

R′ = *Conjugate Riedel shear (minor faults, joints and kinks)*

T = *Tension fracture (normal faults)*

P = *P shear (minor faults and joints)*

S = *Foliation (S plane) in serpentinite*

C = *Synthetic shear (C plane) in serpentinite*

S_1 = *S_1 spaced cleavage in Early Devonian strata*

S_4 = *S_4 crenulation cleavage in Ordovician–Early Silurian strata*

16/155-15/22

Figure 10. Angular relations between mid-Devonian structural elements of the Gilmore Fault Zone.
Riedel terminology modified from Biddle & Christie-Blick (1985).

The Tumut seismic traverse (Leven & Rickard, 1987) provides limited information about the upper crust under the Tumut Synclinorial Zone and the adjacent Goobarragandra Block. Major fault zones traversed by the survey (e.g. Mooney Mooney Fault Zone) are represented as vertical non-reflective zones which separate different packages of reflectors (Leven & others, 1988a,b). Between 10 and 20 km depth, most reflectors dip eastwards and are truncated by strong continuous gently west-dipping reflectors. These latter reflectors, corresponding to a low velocity zone present on regional seismic refraction profiles at about 16–35 km depth (Finlayson & others, 1979), are interpreted as a mid-crustal detachment linking the Gilmore Fault Zone with the Mooney Mooney Fault Zone, Long Plain Fault and other major faults in the region (Fig. 12). Mid-crustal detachments have also been invoked in structural interpretations by Fergusson & others (1986) and Glen & Vandenberg (1987) for other areas of the Lachlan Fold Belt. The presence of a mid-crustal detachment could accommodate both the vertical and horizontal displacements indicated for the Gilmore Fault Zone. The seismic character of the vertical faults in the Tumut area (i.e. near vertical reflection-free zones terminating in a mid-crustal horizontal reflectors) is characteristic of intraplate strike-slip zones (Lemiski & Brown, 1988; Burchfiel & others, 1989) rather than continental transform zones which are represented by continuous through-going crustal fractures (Lemiski & Brown, 1988).

Allochthonous bodies of Cambrian–Ordovician greenstone sequences (e.g. Tumut Ponds Serpentinite) in the Gilmore Fault Zone and elsewhere in the Tumut region probably represent tectonic slices originally obducted onto a thin Late Proterozoic to Early Palaeozoic crust underlying Ordovician strata throughout the Lachlan Fold Belt (Wyborn, 1988). The extent of the greenstone sequence in the subsurface (shown in Figure 12) is based on correlation of packages of short reflectors similar to those recorded in the Bullawyarra Schist in the Jindalee Block. Gravity and magnetic profiles in the region, dominated by shallow Early Silurian tholeiitic intrusions and the large body of Coolac Serpentinite in the Mooney Mooney Fault Zone, do not enable distinction of Silurian, Ordovician and older basement rocks at depth (R. Musgrave, Australian National University, personal communication, 1989). However, short wavelength (<250 km) residual Bouguer gravity anomalies (Murray & others, 1989) and magnetic anomalies (Wellman, 1989) reflect major differences in the trends of deep crustal structures either side of the Gilmore Fault Zone over a 'reworked' zone up to 100 km wide (Wellman, 1989).

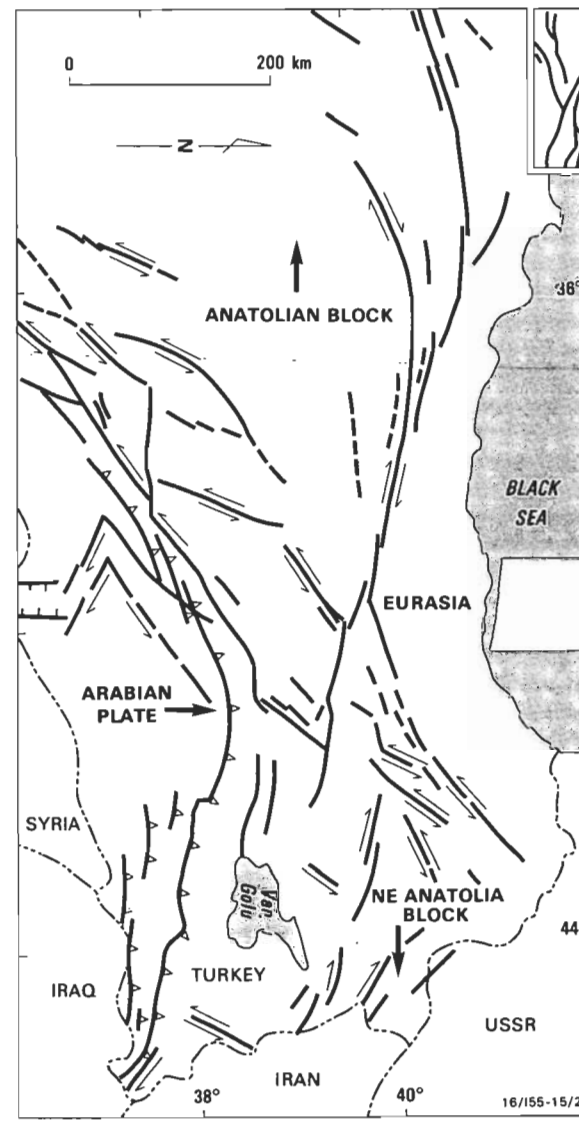

Figure 11. Fault patterns in eastern Turkey (modified from Barka & Kadinsky-Cade, 1988).
Inset shows Figure 9b simplified and reduced to same scale for comparison.

On the basis that granitoid source data may provide some information about the nature of the mid to lower crust in the region, Chappell & others (1988) interpreted Late Proterozoic to Early Palaeozoic terranes of different composition beneath the Lachlan Fold Belt. The boundary between their 'Kosciusko' and 'Wagga' basement terranes corresponds in part to the southern part of the Gilmore Fault Zone. Silurian S-type felsic volcanics and granitoids in the region were derived from partial melting of an immature feldspathic metasedimentary source (Chappell, 1984) at pressures of 5 to 6 kb (Wyborn & others, 1981). The source regions for these melts would be on the upper and lower plate, west and east respectively of the interpreted west-dipping Gilmore Fault Zone (Fig. 12). Thus the Gilmore Fault Zone may well represent an older reactivated basement fault separating Late Proterozoic–Early Palaeozoic terranes.

The Gilmore Fault Zone is unlikely to represent a terrane boundary in the Ordovician–Early Silurian formed by collision of the Wagga–Omeo Terrane with the Molong Volcanic Arc. Basden & others (1985) suggested that the Nacka Nacka Metabasic Igneous Complex (Wagga Metamorphic Belt) may be part of the volcanic arc. This study concurs with the suggestion of Basden & others; rocks here interpreted as Gooandra Volcanics occur on both sides of the fault zone, and are laterally continuous with the correlative Nacka Nacka Metabasic Igneous Complex. Thus volcanic rock units comprising the volcanic arc straddle the supposed terrane boundary. In addition, both 'terranes' share a common metamorphic (Wyborn, 1977a) and structural history.

Movement on the Gilmore Fault Zone has been demonstrated during the Late Silurian and post-Early Devonian (probably mid-Devonian and/or Carboniferous), and can be inferred as far back as the Early Silurian Benambran Orogeny. However, this movement cannot account for the differences in basement gravimetric and magnetic patterns and the inferred mid to lower crustal composition across the fault zone. The Gilmore Fault Zone therefore most likely represents a reactivated basement fault which corresponds, in part, to a Late Proterozoic–Early Palaeozoic terrane boundary interpreted by Chappell & others (1988).

Conclusions

The Gilmore Fault Zone is a long-lived imbricate fault system, up to 6 km wide, separating the Wagga Metamorphic Belt from the Tumut Block. Structures within the fault zone indicate two periods of dominantly sinistral transpressional movement: during regional deformation (Bowning Orogeny) in the Siluro-Devonian, and in the mid-Devonian and/or mid-Carboniferous. The movements, in reponse to lateral compression, resulted in the Wagga Metamorphic Belt being thrust over the Tumut and Tantangara Blocks. The Indi Fault, continuous with the

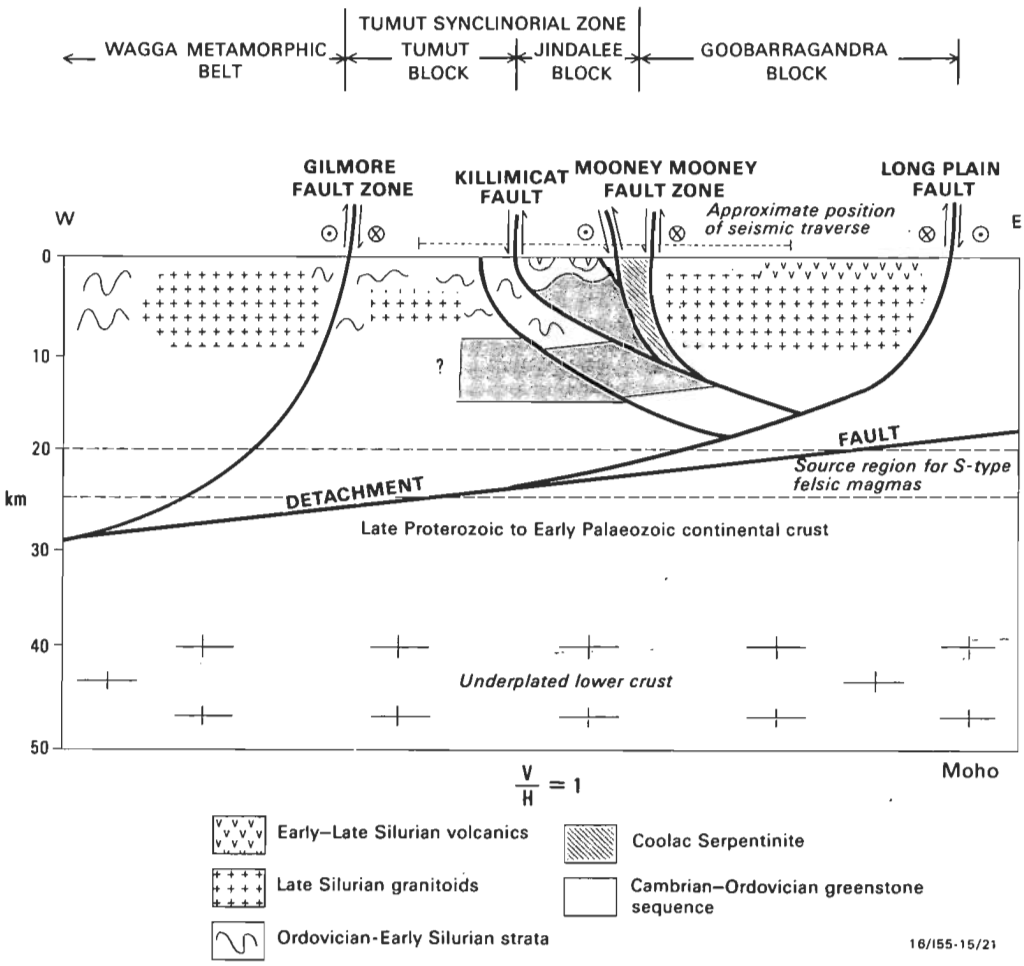

Figure 12. Schematic crustal profile for the Tumut region, showing relationship of major faults to interpreted mid-crustal detachment, based on the Tumut seismic traverse.

Gilmore Fault Zone, formed as a thrust front. An earlier strike-slip history is inferred during Early Silurian regional deformation (Benambran Orogeny) and subsequent Early Silurian extension.

Common structural and metamorphic histories, and lithological correlation of Ordovician–Early Silurian volcanic sequences straddling the fault zone, indicate that the Gilmore Fault Zone does not represent a terrane boundary in the Late Ordovician or Early Silurian as suggested by some previous workers. Differences in geophysical expression and crustal composition across the zone can be explained by the zone being a reactivated basement fault linked to a mid-crustal detachment.

Acknowledgements

M.J. Rickard, K.A.W. Crook, M.A. Etheridge and D. Wyborn are thanked for their helpful criticism of the manuscript. Personnel of the NSW National Parks and Wildlife Service (Tumut Branch) and the Snowy Mountains Authority at Cabramurra provided useful advice on access in the region. The figures were drawn by V. Ashby, BMR Cartographic Services Unit.

References

Barka, A.A. & Kadinsky-Cade, K., 1988 — Strike-slip fault geometry in Turkey and its influence on earthquake activity. *Tectonics*, 7, 663–684.

Barkas, J.P., 1976 — Early Devonian igneous activity and some stratigraphic correlations in the Tumut region, NSW. *Proceedings of the Linnean Society of New South Wales*, 101, 13–25.

Basden, H., 1986 — Tectonostratigraphic and geochemical development of the Tumut area. *M.Appl.Sci. thesis, New South Wales Institute of Technology, Sydney.*

Basden, H., 1990 — Geology of the Tumut 1:100 000 geological sheet 8527. *New South Wales Geological Survey, Sydney.*

Basden, H., Franklin, B.J., Marshall, B. & Waltho, A.E., 1985 — Tectonstratigraphy of the Tumut Trough and adjacent terranes. *In* Third Circum-Pacific Terrane Conference. *Geological Society of Australia, Abstracts*, 14, 16–21.

Basden, H., Franklin, B.J., Marshall, B. & Waltho, A.E., 1987 — Terranes of the Tumut district, southeastern New South Wales, Australia. *In* Leitch, E.C. & Scheibner, E. (editors), Terrane accretion and orogenic belts. *American Geophysical Union, Geodynamics Series*, 19, 57–66.

Berthé, D., Choukroune, P. & Jegouzo, P., 1979 — Orthogneiss, mylonite and non-coaxial deformation of granites: the example of the South Amorican Shear Zone. *Journal of Structural Geology*, 1, 31–42.

Biddle, K.T. & Christie-Blick, N., 1985 — Glossary — strike-slip deformation, basin formation, and sedimentation. *In* Biddle, K.T. & Christie-Blick, N. (editors), Strike-slip deformation, basin formation and sedimentation. *The Society of Economic Palaeontologists and Mineralogists, Special Publication*, 37, 375–386.

Burchfiel, B.C., Quidong, D., Molnar, P., Royden, L., Yipeng, W., Peizhen, Z. & Weiqi, Z., 1989 — Intracrustal detachment within zones of continental deformation. *Geology*, 17, 448–452.

Cas, R.A.F., Powell, C.McA. & Crook, K.A.W., 1980 — Ordovician palaeogeography of the Lachlan Fold Belt: a modern analogue and tectonic constraints. *Journal of the Geological Society of Australia*, 27, 19–31.

Chappell, B.W., 1984 — Source rocks of I- and S-type granites in the Lachlan Fold Belt, southeastern Australia. *Philosophical Transactions of the Royal Society, London*, 310, 693–707.

Chappell, B.W. & White, A.J.R., 1976 — Plutonic rocks of the Lachlan Mobile Zone. *International Geological Congress 25, Field Guide Excursion 13C*, 40 pp.

Chappell, B.W., White, A.J.R. & Hine, R., 1988 — Granite provinces and basement terranes in the Lachlan Fold Belt, southeastern Australia. *Australian Journal of Earth Sciences*, 35, 505–521.

Crook, K.A.W., 1980 — Fore-arc evolution in the Tasman Geosyncline: the origin of the southeast Australian continental crust. *Journal of the Geological Society of Australia*, 27, 215–232

Crook, K.A.W. & Powell, C.McA., 1976 — The evolution of the southeastern part of the Tasman Geosyncline. *Field guide for Excursion 17A, 25th International Geological Congress, Australia, 1976.*

Degeling, P.R., 1975 — Wagga Anticlinorial Zone. *In* Markham, N.L. & Basden, H. (editors), The mineral deposits of New South Wales. *New South Wales Geological Survey, Sydney*, 132–147.

Degeling, P.R., 1977 — Wagga Wagga 1:250 000 metallogenic map SI 55–15. *New South Wales Geological Survey, Sydney.*

Degeling, P.R., Gilligan, L.B., Scheibner, E. & Suppel, D.W., 1986 — Metallogeny and tectonic development of the Tasman Fold Belt System in New South Wales. *Ore Geology Reviews*, 1, 259–313.

Dobos, S., 1971 — The geology of an area north-west of Adelong N.S.W. *B.Sc.(Hons) thesis, University of Sydney.*

Fergusson, C.L., 1987 — Early Palaeozoic back-arc deformation in the Lachlan Fold Belt, southeastern Australia: implications for terrane translations in eastern Gondwanaland. *In* Leitch, E.C. & Scheibner, E. (editors), Terrane accretion and orogenic belts. *American Geophysical Union, Geodynamics Series*, 19, 39–56.

Fergusson, C.L., Gray, D.R. & Cas, R.A.F., 1986 — Overthrust terranes in the Lachlan Fold Belt, southeastern Australia. *Geology*, 14, 519–522.

Finlayson, D.M., Prodehl, C. & Collins, C.D.N., 1979 — Explosion seismic profiles, and implications for crustal evolution, in southeastern Australia. *BMR Journal of Australian Geology & Geophysics*, 4, 243–252.

Glen, R.A. & Vandenberg, A.H.M., 1987. Thin-skinned tectonics in part of the Lachlan Fold Belt near Delegate, southeastern Australia. *Geology*, 15, 1070–1073.

Gray, D.R., Allen, R.L., Etheridge, M.A., Fergusson, C.L., Gibson, G.M., Morand, V.J., Vandenberg, A.H.M., Watchhorn, R.B. & Wilson, C.J.L., 1988 — Structure and tectonics. *In* Douglas, J.G. & Ferguson, J.A. (editors), Geology of Victoria. *Geological Society of Australia, Victorian Division*, 1–36.

Guy, B.B., 1968 — Progressive and retrogressive metamorphism in the Tumbarumba–Geehi District, NSW. *Journal and Proceedings of the Royal Society of New South Wales*, 101, 183–196.

Guy, B.B., 1969. Granitic development and emplacement in the Tumbarumba–Geehi District, NSW. (ii) The massive granites. *Journal and Proceedings of the Royal Society of New South Wales*, 102, 149–156.

Harris, L.B. & Cobbold, P.R., 1984 — Development of conjugate shear bands during bulk simple shearing. *Journal of Structural Geology*, 7, 37–44.

Joplin, G.A., 1947 — Petrological studies in the Ordovician of NSW. (i) The northern extension of the north-east Victorian metamorphic complex. *Proceedings of the Linnean Society of New South Wales*, 72, 87–124.

Labutis, V., 1969 — Geology of the Yarrangobilly area. *B.Sc.(Hons) thesis, Australian National University, Canberra.*

Lemiszki, P.J. & Brown, L.D., 1988 — Variable crustal structure of strike-slip fault zones as observed on deep seismic reflection profiles. *Geological Society of America, Bulletin*, 100, 665–676.

Leven, J.H. & Rickard, M.J., 1987 — Tumut Trough seismic survey New South Wales. *Bureau of Mineral Resources, Australia, Record* 1987/62.

Leven, J.H., Stuart-Smith, P.G., Rickard, M.J. & Crook, K.A.W., 1988a — A deep seismic survey across the Tumut Trough, New South Wales. *Ninth Australian Geological Convention. Geological Society of Australia, Abstracts* 21, 247–248.

Leven, J.H., Stuart-Smith, P.G., Rickard, M.J. & Crook, K.A.W., 1988b — A deep seismic survey across the Tumut Trough, southeastern Australia. *International workshop and symposium on Seismic Probing of Continents and their Margins, Abstracts. Bureau of Mineral Resources, Australia, Record* 1988/21, 89.

Moye, D.G., 1953 — Report on the geology of Upper Tumut development. *Snowy Mountains Hydro-electric Authority* (unpublished report).

Moye, D.G., Sharp, K.R. & Stapledon, D.H., 1969a — Ordovician System: 3. Snowy Mountains Belt. *In* Packham, G.H. (editor), The geology of New South Wales. *Geological Society of Australia, Sydney*, 91–97.

Moye, D.G., Sharp, K.R. & Stapledon, D.H., 1969b — Silurian System: Snowy Mountains Region. *In* Packham, G.H. (editor), The geology of New South Wales. *Geological Society of Australia, Sydney*, 114–119.

Moye, D.G., Sharp, K.R. & Stapledon, D.H., 1969c — Devonian System — 1. Lower and Middle Devonian Series: Snowy Mountains Area. *In* Packham, G.H. (editor), The geology of New South Wales. *Geological Society of Australia, Sydney*, 143–146.

Murray, C.G., Scheibner, E. & Walker, R.N., 1989 — Regional geological interpretation of a digital coloured residual Bouguer gravity image of eastern Australia with a wavelength cut-off of 250 km. *Australian Journal of Earth Sciences*, 36, 423–449.

Owen, M. & Wyborn, D., 1979a — Geology and geochemistry of the Tantangara and Brindabella area. *Bureau of Mineral Resources, Australia, Bulletin* 204, 52 pp.

Owen, M. & Wyborn, D., 1979b — Brindabella (NSW and ACT) 1:100 000 geological map, first edition. *Bureau of Mineral Resources, Australia.*

Owen, M. & Wyborn, D., 1979c — Tantangara (NSW and ACT) 1:100 000 geological map, first edition. *Bureau of Mineral Resources, Australia.*

Owen, M., Wyborn, D. & Wyborn, L., 1982 — Kosciusko National Park and Environs (NSW and ACT) 1:250 000 geological map, preliminary edition. *Bureau of Mineral Resources, Australia.*

Packham, G.H., 1987 — The eastern Lachlan Fold Belt of southeastern Australia: a possible late Ordovician to early Devonian sinistral strike-slip regime. *In* Leitch, E.C. & Scheibner, E. (editors), Terrane accretion and orogenic belts. *American Geophysical Union, Geodynamics Series*, 19, 67–82.

Powell, C.McA., 1983a — Tectonic relationships between the late Ordovician and Late Silurian palaeogeographies of southeastern Australia. *Journal of the Geological Society of Australia*, 30, 353–373.

Powell, C.McA., 1983b — Geology of the N.S.W. south coast. *Geological Society of Australia. Specialist Group in Tectonics and Structural Geology, Field Guide* 1.

Powell, C.McA., 1984 — Silurian to mid-Devonian — a dextral transtensional margin. *In* Veevers, J.J. (editor), Phanerozoic earth history of Australia. *Clarendon Press, Oxford*, 309–348.

Powell, C.McA. & Veevers, J.J., 1984 — Termination of the Uluru Regime: the mid-Carboniferous lacuna. *In* Veevers, J.J. (editor), Phanerozoic earth history of Australia. *Clarendon Press, Oxford*, 348–350.

Richards, J.R., Barkas, J.P. & Vallance, T.G., 1977 — A Lower Devonian point on the geological timescale. *Geochemical Journal*, 11, 147–153.

Rogerson, R.J., 1977 — Metamorphism, folding and plutonism in the Wagga Metamorphic Belt of N.E. Victoria. *Australian Society of Exploration Geophysics Bulletin*, 7, 41–43.

Skempton, A.W., 1966 — Some observations on tectonic shear zones. *International Society of Rock Mechanics, Proceedings of the 1st Congress, Lisbon, 1966*, 1, 329–335.

Scheibner, E., 1976 — Explanatory notes on the Tectonic Map of New South Wales. *Geological Survey of New South Wales, Sydney.*

Scheibner, E., 1985 — Suspect terranes in the Tasman Fold Belt System, eastern Australia. *In* Tectonostratigraphic terranes in the Circum-Pacific region. *Circum-Pacific Council for Energy and Mineral Resources — Earth Science Series* 1, 493–514.

Smith, R.E., 1969 — Zones of progressive regional burial metamorphism in part of the Tasman Geosyncline, eastern Australia. *Journal of Petrology*, 10, 144–163.

Strusz, D.L., 1989 — Australian Phanerozoic timescales: Silurian. *Bureau of Mineral Resources, Australia, Record* 1989/33.

Stuart-Smith, P.G., 1988 — Surface geology and structure of the Tumut seismic traverse, Lachlan Fold Belt, New South Wales. *Bureau of Mineral Resources, Australia, Record* 1988/27.

Stuart-Smith, P.G., 1990a — Structure and tectonics of the Tumut region, Lachlan Fold Belt, southeastern Australia. *Ph.D. thesis, Australian National University, Canberra.*

Stuart-Smith, P.G., 1990b — Evidence for extension tectonics in the Tumut Trough, Lachlan Fold Belt, NSW. *Australian Journal of Earth Sciences*, 37, 147–167.

Stuart-Smith, P.G., in press — The emplacement and fault history of the Coolac Serpentinite, Lachlan Fold Belt, southeastern Australia. *Journal of Structural Geology.*

Suppel, D.W., Warren, A.Y.E., Watkins, J.J., Chapman, J., Tenison Woods, K. & Barron, L., 1986 — A reconnaissance study of the geology and gold deposits of the West Wyalong–Temora–Adelong District. *New South Wales Geological Survey, Quarterly Notes*, 64, 1–23.

Tchalenko, J.S., 1970 — Similarities between shear zones of different magnitudes. *Geological Society of America, Bulletin*, 81, 1625–1640.

Vandenberg, A.H.M., 1978 — The Tasman Fold Belt System in Victoria. *Tectonophysics*, 48, 267–297.

Van Der Oever, P., 1984 — The geology of the Tumut Ponds Serpentinite Belt near Talbingo, NSW. *B.Appl.Sci. thesis, New South Wales Institute of Technology, Sydney.*

Vallance, T.G., 1953 — Studies in the metamorphic and plutonic geology of the Wantabadgery–Adelong–Tumbarumba district, NSW. *Proceedings of the Linnean Society of New South Wales*, 78, 90–121.

Vallance, T.G., 1967 — Palaeozoic low pressure regional metamorphism in southeastern Australia. *Meddelesen Fra Dansk Geologisk Forrening*, 7, 494–503.

Veness, V.R., 1973 — Metamorphic and plutonic geology of the Wondalga area, NSW. *B.Sc.(Hons) thesis, Sydney University.*

Webb, A.W., 1980 — K/Ar analyses (Tumut area). The Australian Mineral Development Laboratories — Report AC 5446/80. *New South Wales Geological Survey Report GS 1980/444 (unpublished).*

Wellman, P., 1989 — Structure and subdivision of the Tasman Orogen, on the basis of gravity and magnetic anomaly pattern. *Geological Society of Australia, Abstracts* 24, 165–166.

White, A.J.R., Williams, I.S., & Chappell, B.W., 1976 — The Jindabyne Thrust and its tectonic, physiographic and petrogenetic significance. *Journal of the Geological Society of Australia*, 23, 105–112.

Williams, P.F. & Price, G.P., 1990 — Origin of kinkbands and shear-band cleavage in shear zones: an experimental study. *Journal of Structural Geology*, 12, 145–164.

Wise, D.U., Dunn, D.E., Engelder, J.T., Geiser, P.A., Hatcher, R.D., Kish, S.A., Odom, A.L. & Schamel, S., 1984 — Fault-related rocks: suggestions for terminology. *Geology*, 12, 391–394.

Wyatt, B.W., Yeates, A.N. & Tucker, D.H., 1980 — A regional review of the geological sources of magnetic and gravity fields in the Lachlan Fold Belt of NSW. *BMR Journal of Australian Geology and Geophysics*, 5, 289–300.

Wyborn, D., 1977b — Discussion — The Jindabyne Thrust and its tectonic, physiographic and petrogenetic significance. *Journal of the Geological Society of Australia*, 24, 233–236.

Wyborn, D., 1988 — Ordovician magmatism, gold mineralisation, and an integrated tectonic model for the Ordovician and Silurian history of the Lachlan Fold Belt in NSW. *BMR Research Newsletter*, 8, 13–14.

Wyborn, D., Chappell, B.W. & Johnston, R.M., 1981 — Three S-type volcanic suites from the Lachlan Fold Belt, southeast Australia. *Journal of Geophysical Research*, 86, 10335–10348.

Wyborn, L.A.I., 1977a — Aspects of the geology of the Snowy Mountains region. *Ph.D. thesis, Australian National University, Canberra.*

BMR Journal of Australian Geology & Geophysics, 12, 51–64

Hydrochemistry of a groundwater–seawater mixing zone, Nauru Island, central Pacific Ocean

Jerzy Jankowski[1] & Gerry Jacobson[2]

Nauru Island is a karstified dolomitic limestone island in the central Pacific Ocean. A thin, discontinuous freshwater layer overlies a thick brackish water mixing zone. In the mixing zone, groundwater salinity increases gradationally downwards until seawater is encountered at about 70 m below sea level. Fresh HCO_3–Ca–Mg groundwaters evolve to seawater. Saturation indices for particular carbonate minerals increase with increased groundwater salinity. Supersaturation is achieved with dolomite at 300 mg/L total dissolved solids, with calcite at 5000 mg/L, and with aragonite at 6000 mg/L. As groundwaters in the mixing zone are saturated with dolomite there is potential for dolomitisation, and this probably occurs at low proportions of admixed seawater. Open and closed system trends can be defined, based on the partial pressure of CO_2. The open system, with lower partial pressure, comprises vadose waters, cave waters and the more saline mixing zone waters; in the latter, chemical evolution is controlled mainly by mixing with seawater. The closed system comprises the freshwater layer with low proportions of admixed seawater; its chemistry is controlled by ingassing of CO_2 and by dissolution and precipitation reactions. Theoretical calculations based on simple mixing between karst groundwaters and seawater are inadequate to describe actual chemical processes, which change with the degree of mixing.

Introduction

Nauru Island is a karst limestone island in the central Pacific Ocean at 0°32'S, 166°56'E (Fig. 1). The island land area is 22 km^2, of which about 15 km^2 constitutes a large surficial phosphate mine which is nearing the end of its life after nearly a century of mining. An investigation of the island's hydrogeology has recently been undertaken in order to assure water resources for land rehabilitation (Jacobson & Hill, 1988; Ghassemi & others, 1990). Groundwater samples were collected from wells and caves, and also obtained during drilling with a reverse-circulation drilling rig. The locations of drillholes are shown on Figure 2. Salinity profiles were established on site with an electrical conductivity meter, and pH and temperature were also measured. Samples were refrigerated until chemical analyses could be undertaken.

The investigation proved a thin, discontinuous layer of fresh groundwater, close to sea level in the limestone (Fig. 2). This is underlain by a brackish groundwater–seawater mixing zone with progressively more saline water at depth. Seawater is encountered at about 70 m below sea level. The mixing zone is unusually thick compared with that on other limestone islands of comparable size, such as Niue (Jacobson & Hill, 1980). In this paper, we document the hydrochemistry of the Nauru groundwater system, with special reference to the mixing zone. Hydrochemical processes are considered in terms of saturation levels based on thermodynamic calculations, a comparison with theoretical mixing of freshwater and seawater, and mass transfer calculations. The work was undertaken in the context of groundwater resources development, but has implications for the understanding of karstification and diagenesis.

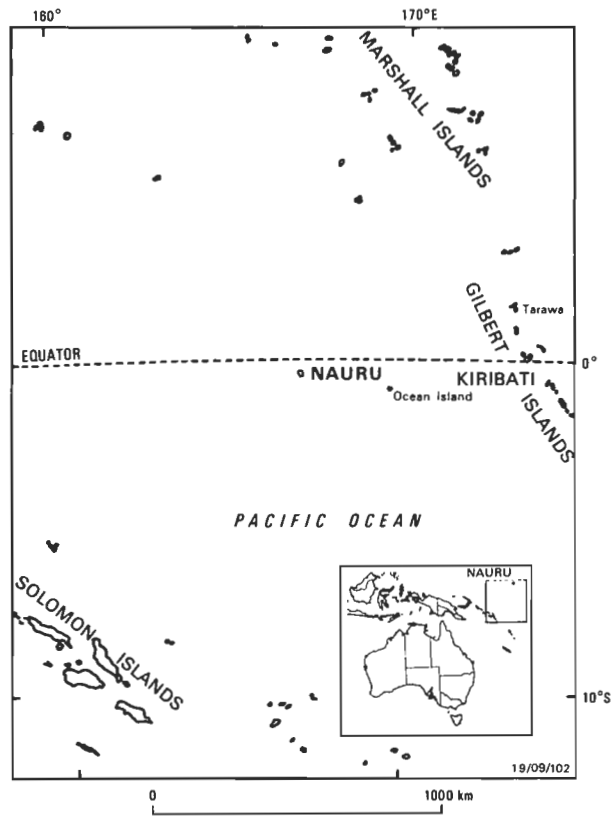

Figure 1. Location map.

Hydrogeology of Nauru Island

Nauru Island is a raised-coral atoll (Fig. 2) with a maximum elevation of 70 m above sea level. It is underlain by a volcanic seamount that rises 4300 m from the floor of the Pacific Ocean. The seamount is capped by about 500 m of dolomitised limestone of Miocene to Quaternary age (Hill & Jacobson, 1989). The limestone has been drilled in the present investigation to a depth of 55 m below sea level, and is intensely karstified to that depth, with phosphate cavity fillings. A terrace, 400 m wide, extends around the island's coastline at an elevation of a few metres above sea level.

Salinity measurements in drill holes show that Nauru is underlain by a discontinuous layer of freshwater (<1500 mg/L total dissolved solids, TDS), which averages 4.7 m thick and is up to 7 m thick (Fig. 3). This overlies a mixing zone of brackish water up to about 60 m thick, which in turn overlies seawater. The unusually thick mixing zone is due to high permeability in the limestone; open karst fissures allow intrusion of seawater beneath the island and consequent mixing.

Groundwater flow is radially outwards to the sea (Fig. 4) and is generated by the 0.30 m head differential between the inland watertable (average elevation relative to island datum 1.50 m) and mean sea level (elevation 1.20 m). Diurnal tidal oscillations of groundwater level have an amplitude of about 0.5 m. In the southwest, a freshwater lagoon, Buada Lagoon, is perched (water level elevation 2.40 m) above the general watertable, on impermeable phosphatic alluvium.

[1] Centre for Groundwater Management and Hydrogeology, University of New South Wales, PO Box 1, Kensington NSW 2033
[2] Groundwater Program, Bureau of Mineral Resources, Geology & Geophysics, GPO Box 378, Canberra ACT 2601

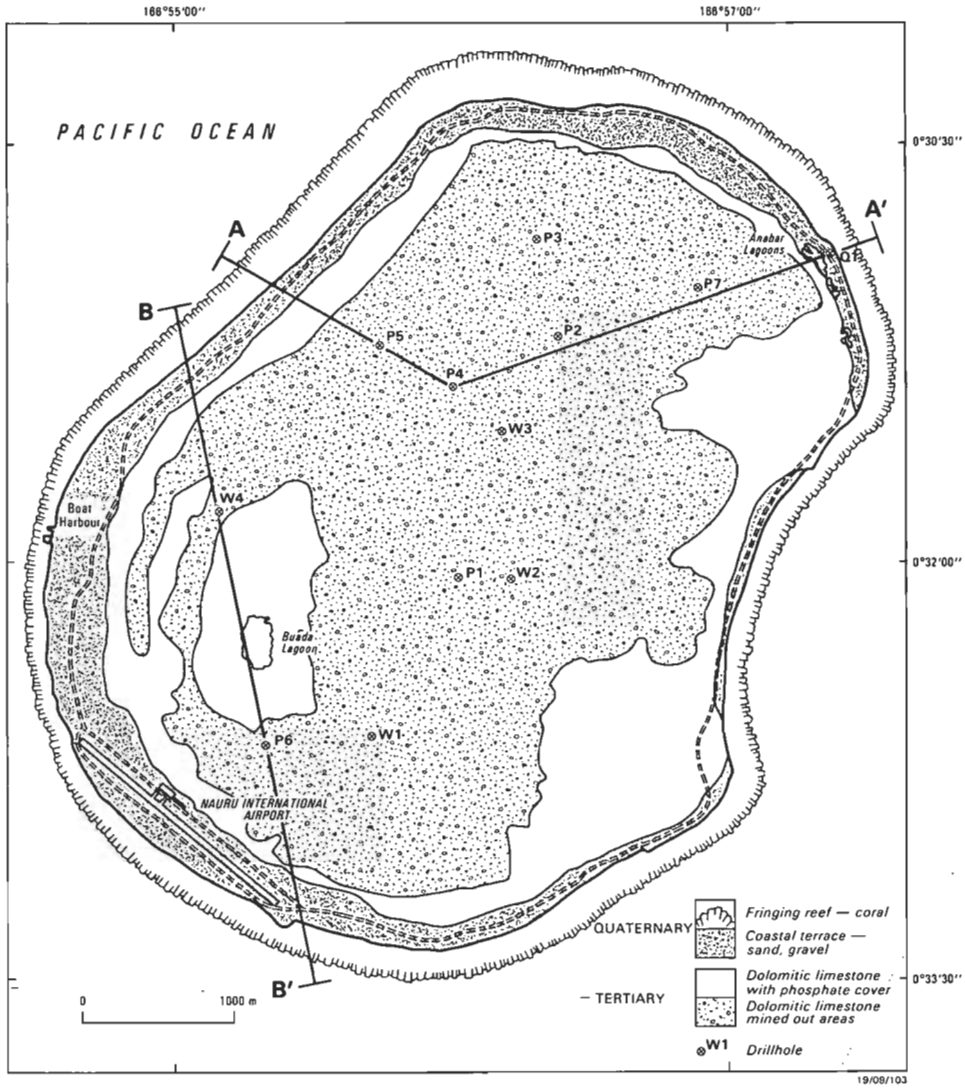

Figure 2. Geology and drillhole locations, Nauru Island.
Cross-sections are shown in Figure 3.

Measurements of Buada Lagoon water levels indicate that the lagoon is not tidal but that its level is affected by rainfall and evaporation.

Nauru rainfall records are available for 60 years from 1916 with some gaps, including the period of World War 2, when the island was occupied by the Japanese. They indicate a mean annual rainfall of 1994 mm, with a high degree of both annual and seasonal variability. High annual rainfalls commonly occur in the years corresponding to, or immediately following, major El Niño–Southern Oscillation events. Groundwater recharge is estimated as being about 40% of rainfall for the mostly bare karrenfeld surface of Nauru (Jacobson & Hill, 1988), and thus amounts to about 800 mm annually. Surface runoff is negligible, and evapotranspiration is estimated as close to 1200 mm annually. Groundwater discharges on the inner side of the coastal terrace, to the brackish water Anabar Lagoons, and also to springs in the reef (Fig. 4). Several caves are evident at the inland margin of the coastal terrace, and provide a window on the watertable close to the discharge end of the flow system. The largest of these is Maqua Cave in the southwest of Nauru.

Hydrochemistry: major ion concentrations

Chemical analyses of Nauru waters are listed in Table 1. Hydrochemical types are derived from a classification listing major ions constituting greater than 20% meq/L of total anions and cations, respectively. These are listed in order of anion dominance, then cation dominance (Alekin, 1970).

Nauru rainwater contains 10 mg/L TDS, and pH is 5.8–6.5. The dominant anions in the rainwater are HCO_3 and Cl, and the dominant cations Na and Ca. The Cl concentration, 1–4 mg/L, provides a source of Cl for the vadose zone groundwater.

Buada Lagoon was fresh when sampled in October 1987, with 155–200 mg/L TDS, but becomes brackish with evaporation in long dry periods. The lagoon water is alkaline, with dominant anions HCO_3 and Cl, and cations Ca and Na. The increased HCO_3 and Ca concentrations are probably due to dissolution of limestone, and the increased Cl and Na concentrations to evaporation of rainwater or dissolved ocean spray.

Table 1. Chemical analyses of water samples, Nauru Island.

Sample	*TDS*	*Na^+ mg/L*	*K^+ mg/L*	*Ca^{2+} mg/L*	*Mg^{2+} mg/L*	*HCO_3^- mg/L*	*CO_3^{2-} mg/L*	*SO_4^{2-} mg/L*	*Cl^- mg/L*	*pH*	*Hydrochemical types of waters*[1]
Rainwater											
	10	1	0.5	1	0.6	9		0.3	1	6.5	HCO_3-Ca-Mg-Na
	10	1	0.5	0.5	0.2	3.5		0.5	2	5.8	HCO_3-Cl-Na-Ca-Mg
	10	1.5	0.5	0.6	0.4	4.7		0.5	4	5.8	Cl-HCO_3-Na-Ca-Mg
Surface water											
Buada Lagoon	155	30	0.5	28	6.5	46.8	34.9	11	48	8.3	HCO_3-Cl-Ca-Na
Buada Lagoon	200	32	0.5	29	6.2	91.3	9.5	12	47	8.2	HCO_3-Cl-Ca-Na
Anabar Lagoon	5032	1431	40	85	175	187	15.7	353	2540	8.0	Cl-Na
Seawater (Nauru)	35410	10500	320	364	1220	113.3	23.5	2410	19611	8.5	Cl-Na
Vadose water											
P6 — 25.5 m*	85	16	0.5	14	4.8	70.7		5.2	23	6.8	HCO_3-Cl-Na-Ca-Mg
P6 — 21.5 m	145	20	0.5	20	7.5	93.8		6.3	31	6.85	HCO_3-Cl-Ca-Na-Mg
W1 — 20.5 m	160	18	0.5	23	12	131.2		5.5	25	7.10	HCO_3-Cl-Ca-Mg-Na
P4 — 36.5 m*	168	23	1	24	9.3	105.5		7.7	40	6.90	HCO_3-Cl-Ca-Na-Mg
W1 — 25.5 m*	295	36	0.5	22	13	121.3		10	55	7.30	HCO_3-Cl-Na-Ca-Mg
Anatan Cave*	310	52	0.5	26	26	177.4		13	79	7.30	HCO_3-Cl-Na-Mg-Ca
Anmara Well*	400	104	2	15	22	256.3		32	74	6.90	HCO_3-Cl-Na-Mg
Cave water											
Ijuw Cave — pool	730	182	5.5	32	37	210.9		66	272	6.58	Cl-HCO_3-Na-Mg
Maqua Cave — pool	1710	450	15	44	68	199.1		101	801	6.90	Cl-Na-Mg
Maqua Cave — pool	1760	466	16	42	68	186.5		103	838	7.10	Cl-Na
Groundwater											
Coastal terrace											
G. Apad's Well	290	6	0.5	85	12	337.7		2.4	4	6.84	HCO_3-Ca
Rudy's Well	520	68	0.5	73	36	467.5		52	36	6.94	HCO_3-Ca-Na-Mg
Odn-aiwo Well	3245	830	32	105	125	403.2		195	1532	6.95	Cl-Na
Heine's Well	740	145	4	86	35	327.8		42	240	6.84	Cl-HCO_3-Na-Ca-Mg
Reweru's Well	1755	374	12	135	71	529.7		65	715	6.81	Cl-HCO_3-Na-Ca-Mg
Clodamar's Well	1475	370	12	68	65	282.2		110	652	6.89	Cl-Na-Mg
Meneng Well	1690	422	15	71	70	295.9		144	722	6.70	Cl-Na-Mg
Botelenga's Well	430	26	3	93	22	357.2		16	35	6.82	HCO_3-Ca-Mg
Jeremiah's Well	1090	253	7	70	50	345.4		94	413	6.83	Cl-HCO_3-Na-Mg
Rydell's Well	615	138	8	34	36	330		88	123	6.92	HCO_3-Cl-Na-Mg
Engar's Well	730	167	7	37	36	211.2		49	268	6.86	Cl-HCO_3-Na-Mg
Ijuh Well	1420	365	11	72	56	347.6		163	534	6.88	Cl-HCO_3-Na
Retow's Well	1520	390	16	62	67	308		119	646	6.92	Cl-Na-Mg
Anabar Cemetery Well	1140	265	8.5	67	56	471.6		133	355	6.78	Cl-HCO_3-Na-Mg
Anatan Well	1490	358	14	96	56	430.7		119	567	6.70	Cl-HCO_3-Na
Dannang's Well	730	120	0.5	90	40	434		33	177	6.80	HCO_3-Cl-Na-Ca-Mg
Kayser's Well	360	44	1.5	69	19	314.6		22	48	6.91	HCO_3-Ca-Na-Mg
Benjamin's Well	465	96	6	52	33	283.8		36	129	6.88	HCO_3-Cl-Na-Mg-Ca
Itsimera's Well	1195	257	10	96	51	390.5		73	424	6.85	Cl-HCO_3-Na-Ca-Mg
Menke's Well	1650	400	15	90	60	334.4		111	703	7.09	Cl-Na
Tapau's Well	640	103	2	87	27	318.7		33	163	7.16	HCO_3-Cl-Na-Ca-Mg
Daniel's Well	460	70	1	72	23	351.7		33	80	6.96	HCO_3-Cl-Ca-Na-Mg
Seawater intrusion											
H10 — 33 m	1655	380	17	66	73	168.9		94	715	7.11	Cl-Na-Mg
Mixed water											
P4 — 39.5 m	2000	555	20	40	84	167.8		114	1018	7.8	Cl-Na-Mg
P5 — 31.5 m	2600	685	25	53	100	182.1		143	1291	7.4	Cl-Na
P3 — 11.2 m	5160	1605	45	90	203	154	26.3	390	2905	7.8	Cl-Na
H10 — 50 m	5920	1670	51	103	223	146.3	15.1	410	3138	7.9	Cl-Na
P5 — 43.5 m	8830	2500	60	103	305	143.6	23.5	595	4583	8.1	Cl-Na
W3 — 65 m	18490	5500	180	215	680	118.8	19.6	1300	10160	8.4	Cl-Na

[1] Classification after Szczukariew & Priklonski (Alekin, 1970)
* Top of lens

The Anabar Lagoons are brackish with about 5000 mg/L TDS. The dominant ions in these lagoon waters are Cl and Na; they also contain appreciable SO_4 and Mg. These waters are discharging groundwaters mixed with seawater.

Nauru groundwaters described in this study have been separated into vadose water and fresh groundwater at the top of the saturated zone, cave water in watertable pools, and groundwater in the saturated zone, which is fresh, brackish or saline depending on the depth of the well or bore and the pumping rate.

Samples from the vadose zone and top of the freshwater layer include those from drillholes P6, P4 and W1 (Fig. 2) and Anatan Cave and Anmara Well. Analyses are shown in Table 1. Sample salinity is 85–400 mg/L TDS, and samples are HCO_3-rich with Na and Ca as dominant cations. Their chloride, 23–79 mg/L, is probably derived from rainwater and dissolved ocean spray. Concentrations of SO_4 and K are low. This water percolates through the karst fissure system, and dissolution of limestone causes an increase in Ca and Mg concentrations. The pH is close to neutral, 6.8–7.3, and groundwater temperature is 25–26°C.

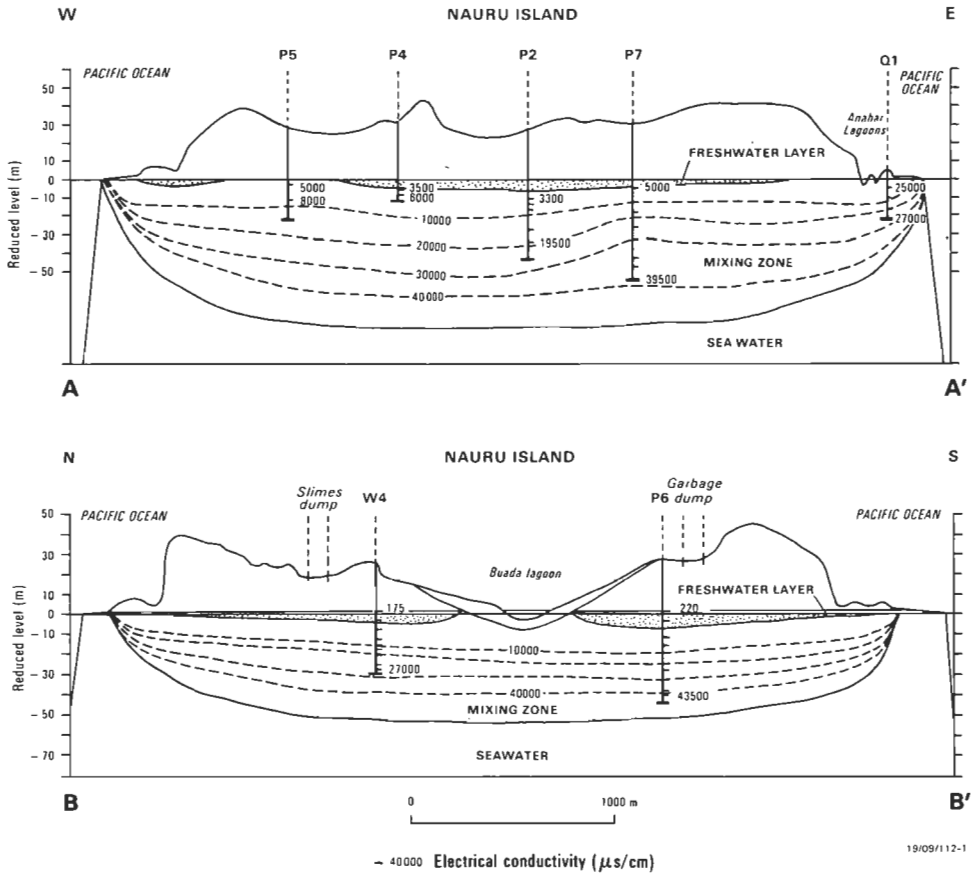

Figure 3. Cross-sections showing freshwater layer and mixing zone, Nauru Island.
For location see Figure 2.

Groundwater sampled in the coastal terrace has 290–3245 mg/L TDS. The variation in salinity is due to variation in the depth of the well and the pumping rate. Chemical composition ranges from HCO_3-rich with Ca and Mg in the fresher coastal-terrace water, through HCO_3–Cl and Cl–HCO_3 water, to Cl-dominant with Na in the saltier water. The pH is 6.0–7.2, and the temperature is constant at 28°C.

Groundwater samples from the investigation drillholes (P4, H10, P5, P3, W3) become increasingly saline with depth. The pH is 7.1–8.0. With increasing salinity the groundwater approaches seawater composition and changes from a Cl–Na–Mg water to a Cl–Na water.

The major ion composition of Nauru groundwaters is shown as a trilinear diagram (Fig. 5). With increasing salinity, cations show a trend from the Ca corner through Ca–Mg dominant water towards the Na–K corner. The more saline samples have 15–30% Mg. The anions show a trend from the HCO_3–CO_3 corner through to the Cl corner, with concentrations of SO_4 generally less than 10%. These evolutionary trends are characteristic of karst groundwater mixing with seawater, for example, on the Yucatan Peninsula (Back & Hanshaw, 1970).

Major ion relationships of the Nauru groundwaters are shown in dilution diagrams (Figs 6, 7), where individual major ion concentrations are plotted against Cl concentrations for particular waters. Concentrations of Na show a linear relationship with Cl (Fig. 6) throughout the evolution from freshwater to seawater. Samples from the vadose zone and the fresher groundwater plot above the mixing line, owing to the limited influence of seawater. Concentrations of Mg also increase relative to Cl, but this plot is rather scattered for the fresher waters, becoming linear in the more saline waters. This is probably due to the dissolution of dolomite in relatively fresh groundwater, which releases Mg; the relationship approaches equilibrium with mixing in the more saline waters. Concentrations of Ca remain constant with increasing Cl in the vadose waters and karst groundwaters, but increase linearly relative to Cl in more saline waters. All the fresher groundwater samples plot above the mixing line in the Ca versus Cl diagram, reflecting the dissolution of carbonate rocks which release Ca. Vadose waters and groundwaters at the top of the freshwater layer are grouped where the Ca:Cl ratio is close to unity. Deeper karst groundwaters are grouped separately, with higher Ca concentrations than the vadose waters.

Alkalinity (HCO_3 + CO_3) and SO_4 concentrations are plotted against Cl concentrations (Fig. 7). Vadose waters show a general increase in alkalinity with increasing Cl, reflecting the open nature of the system. However the fresh groundwaters have constant alkalinity with increasing Cl, reflecting closed system conditions. Alkalinity then decreases slightly in more saline waters due to precipitation of carbonate minerals. Concentrations of SO_4 increase steadily with increasing Cl. On the SO_4 versus Cl plot, most karst groundwaters plot above the dashed line, suggesting dissolution of gypsum, although there is no field evidence that this occurs.

The relationship between Ca and Mg concentrations is shown in Figure 8. Most vadose waters and fresher phreatic groundwaters plot on the Ca side of the equilibrium line, reflecting dissolution of limestone. The more saline waters plot on the Mg side, on a mixing line, suggesting that some precipitation of Ca takes place concurrently with seawater mixing.

Figure 9 shows the relationship between alkalinity (HCO_3 + CO_3) and hardness (Ca + Mg). Vadose waters and fresh phreatic groundwaters are close to equilibrium on this plot: the

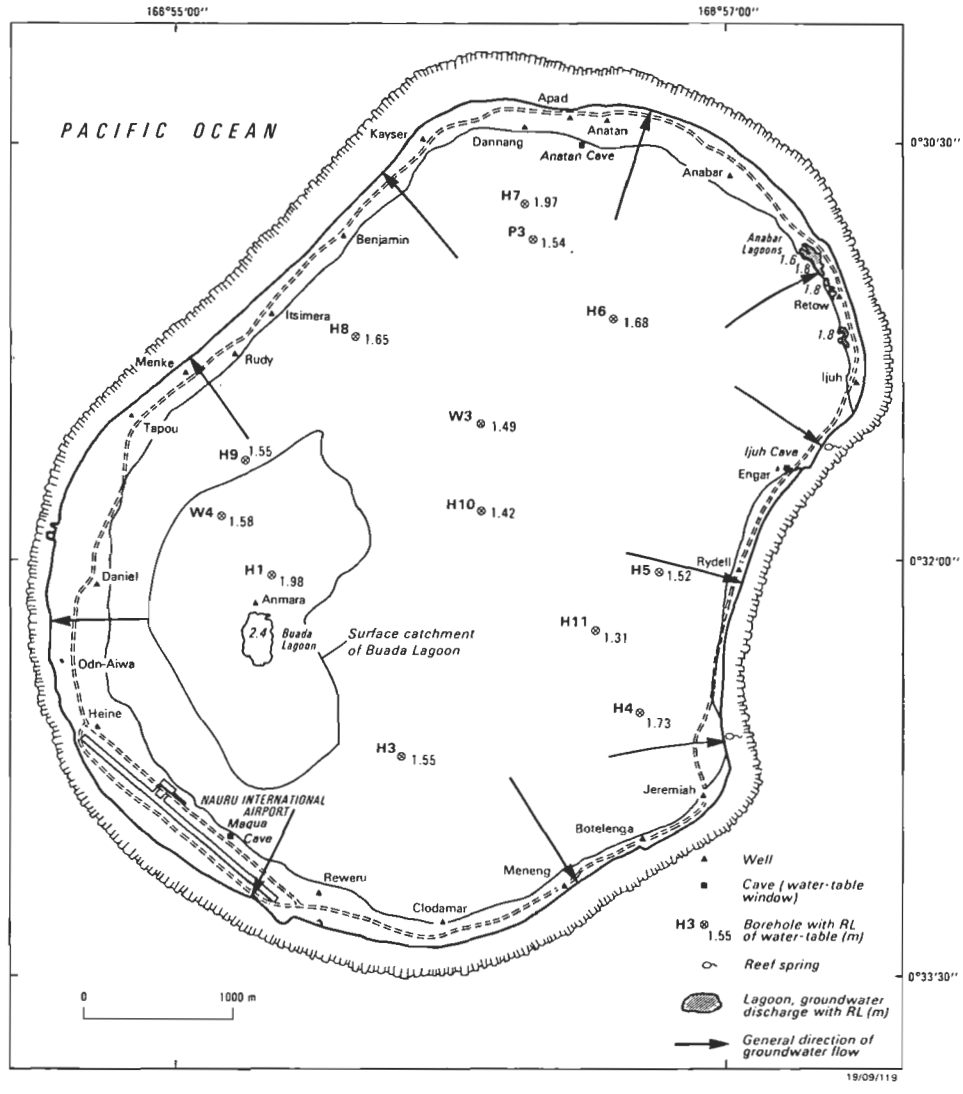

Figure 4. Groundwater flow system and well locations, Nauru Island.

ratio of alkalinity to hardness is between 0.5 and 1, and the regime is one of dissolution. For mixed waters the ratio of alkalinity to hardness is less than 0.5, and this ratio decreases with the trend towards seawater. This suggests precipitation of carbonate minerals, taking up available alkalinity, concurrently with the addition of Ca and Mg from seawater. The grouping of most karst groundwaters in this diagram suggests closed system conditions.

Figure 10 shows the relationship between the Mg:Ca ratio and the $SO_4 : HCO_3 + CO_3$ ratio. Fresher Nauru groundwaters tend to have $HCO_3 > SO_4$; with seawater mixing this changes to SO_4 HCO_3. The increase in the $SO_4 : HCO_3 + CO_3$ ratio reflects the precipitation of carbonate minerals and addition of sulphate from seawater. In the fresher groundwaters the Mg:Ca ratio increases markedly (dashed line, Fig. 10) but in more saline waters it increases slowly (solid line, Fig. 10). The slow increase in the Mg:Ca ratio through the mixing zone probably reflects some precipitation of dolomite and/or dolomitisation.

Solution chemistry

Thermodynamic properties of the ionic components of Nauru groundwaters have been calculated using an ion interaction model based on Pitzer's equations (Pitzer, 1973) and developed by Harvie & Weare (1980) and Harvie & others (1984). A computer program called PITZ (Hanor & others, 1988) has been used to calculate saturation indices for dolomite, calcite, aragonite, and gypsum, and the partial pressure of CO_2. Saturation indices (SI) are calculated from ion activities according to:

$SI = IAP/Ks$

where IAP is the ionic activity product of the appropriate ions, and Ks is the solubility product of the mineral.

Values taken for the solubility products of dolomite, calcite, aragonite and gypsum are:

$\log K_D = -18.14$,
$\log K_C = -8.34$,
$\log K_A = -8.16$, and
$\log K_G = -4.58$.

Saturation indices for Nauru groundwaters (Table 2) are shown as a function of salinity in Figure 11. Saturation indices for dolomite increase with salinity. Vadose zone waters are undersaturated for dolomite, but saturation is achieved at about 300 mg/L TDS so that most groundwater and mixed water is supersaturated. Saturation indices increase from about 1500 mg/L TDS (3.5% seawater) along a mixing line trending towards seawater.

The vadose waters and fresher groundwaters are undersaturated for calcite. Saturation is achieved at about 5000 mg/L TDS, and more-saline waters are supersaturated. Most Nauru water is undersaturated for aragonite, and saturation is achieved at about 6000 mg/L TDS (16% seawater). All Nauru water is

Table 2. Saturation indices for dolomite, calcite, aragonite and gypsum, and log P_{CO_2} for water samples, Nauru Island.

Sample	Saturation index SI_D	SI_C	SI_A	SI_G	log P_{CO_2}
Rainwater					
	-6.47	-3.96	-4.14	-5.59	-2.52
	-9.45	-5.36	-5.54	-5.66	-2.23
	-8.83	-5.16	-5.36	-5.59	-2.10
Surface water					
Buada Lagoon	1.30	0.13	-0.05	-2.79	-3.62
Buada Lagoon	1.27	0.13	-0.05	-2.74	-3.23
Anabar Lagoon	2.61	0.31	0.13	-1.46	-2.81
Seawater (Nauru)	4.10	0.93	0.75	-0.64	-3.63
Vadose water					
P6 — 25.5 m[1]	-2.05	-1.63	-1.81	-3.35	-2.01
P6 — 21.5 m	-1.53	-1.39	-1.57	-3.15	-1.87
W1 — 20.5 m	-0.50	-0.95	-1.13	-3.17	-1.97
P4 — 36.5 m[1]	-1.18	-1.22	-1.40	-3.00	-1.87
W1 — 25.5 m[1]	-0.18	-0.81	-0.99	-2.95	-2.21
Anatan Cave[1]	0.45	-0.61	-0.79	-2.82	-2.05
Anmara Well[1]	-0.37	-1.11	-1.29	-2.69	-1.50
Cave water					
Ijuw Cave — pool	-0.75	-1.25	-1.43	-2.16	-1.28
Maqua Cave — pool	0.05	-0.91	-1.09	-1.99	-1.64
Maqua Cave — pool	0.37	-0.76	-0.94	-2.01	-1.87
Groundwater					
Coastal terrace					
G. Apad's Well	0.26	-0.28	-0.46	-3.08	-1.31
Rudy's Well	1.04	-0.16	-0.34	-1.89	-1.28
Odn-aiwo Well	1.21	-0.27	-0.45	-1.51	-1.41
Heine's Well	0.54	-0.37	-0.55	-1.96	-1.34
Reweru's Well	1.21	-0.09	-0.27	-1.74	-1.13
Clodamar's Well	0.52	-0.5	-0.75	-1.76	-1.48
Meneng Well	0.20	-0.74	-0.92	-1.65	-1.27
Botelenga's Well	0.52	-0.26	-0.44	-2.26	-1.27
Jeremiah's Well	0.55	-0.49	-0.67	-1.76	-1.32
Rydell's Well	0.35	-0.68	-0.86	-1.99	-1.42
Engar's Well	-0.13	-0.90	-1.08	-2.22	-1.55
Ijuh Well	0.64	-0.46	-0.64	-1.56	-1.37
Retow's Well	0.62	-0.54	-0.72	-1.77	-1.47
Anabar Cemetery Well	0.72	-0.44	-0.62	-1.64	-1.14
Anatan Well	0.59	-0.42	-0.60	-1.58	-1.10
Dannang's Well	0.79	-0.26	-0.44	-2.04	-1.18
Kayser's Well	0.41	-0.35	-0.53	-2.23	-1.48
Benjamin's Well	0.33	-0.57	-0.75	-2.17	-1.44
Itsimera's Well	0.83	-0.28	-0.46	-1.75	-1.29
Menke's Well	1.14	-0.18	-0.36	-1.65	-1.60
Tapau's Well	1.09	-0.03	-0.21	-2.02	-1.67
Daniel's Well	0.67	-0.25	-0.43	-2.06	-1.42
Seawater intrusion					
H10 — 33 m	0.55	-0.59	-0.77	-1.85	-1.92
Mixed water					
P4 — 39.5 m	1.70	-0.15	-0.33	-2.02	-2.62
P5 — 31.5 m	1.11	-0.43	-0.61	-1.86	-2.19
P3 — 11.2 m	2.16	0.06	-0.12	-1.43	-2.70
H 10 — 50 m	2.34	0.16	-0.02	-1.37	-2.82
P5 — 43.5 m	2.78	0.31	0.13	-1.32	-3.05
W3 — 65 m	3.60	0.70	0.52	-0.92	-3.47

[1] Top of lens

undersaturated for gypsum, although gypsum saturation indices generally increase with salinity.

The plots of saturation indices versus salinity (Fig. 11) show considerable scatter in Nauru karst groundwaters. This probably reflects varying degrees of seawater mixing, and also the dissolution process. There is a distinct decrease or levelling off of saturation indices with salinity of 1500–2000 mg/L TDS (2–4% seawater). Most vadose water and karst groundwater plots above the dashed lines (Fig. 11) which join the freshest vadose water with seawater. This reflects the dissolution of carbonate rocks, which appears to be a more important process than seawater mixing in this salinity range. Mixing becomes more significant at greater salinities.

Saturation indices for dolomite and calcite are plotted relative to each other in Figure 12. Fresher water (rainwater and vadose water) is undersaturated for both minerals. With increasing salinity, the groundwaters become supersaturated with respect to dolomite, but not calcite, suggesting that dolomitisation is occurring. More saline, mixed waters are supersaturated for both minerals. The trend for saline waters diverges from the dashed line ($SI_D = SI_C$) showing a greater degree of saturation for dolomite than calcite.

Saturation indices for calcite and aragonite are shown in relation to $C0_2$ partial pressure (Fig. 13). Evolution from vadose water to karst groundwater involves increasing saturation indices with increasing P_{CO2} along a closed-system line. The increase in Ca concentration in the closed system is due to the dissolution of calcite but saturation for calcite is not achieved. This phenomenon is known from other karst groundwater systems (Thrailkill & Robl, 1981). In the mixing-zone waters, P_{CO_2} decreases towards its atmospheric value, $10^{-3.5}$ This coincides with increasing saturation and suggests that the mixing zone can be considered as an open system. Saturation for calcite and aragonite is achieved in the more saline waters.

The dashed line (Fig. 13) is projected from the mixing line in order to define open and closed system chemistry. The chemical evolution of the fresher, closed system, waters is controlled by dissolution and precipitation processes, and by ingassing of CO_2. The brackish, open system waters evolve mainly by seawater mixing and outgassing of CO_2 (cf. Hanor, 1978; Back & others, 1986).

Karst groundwaters generally increase in P_{CO_2} with increasing $CaCO_3$ concentration (Fig. 14), reflecting a closed system trend. In the mixed waters, P_{CO_2} decreases with increasing $CaCO_3$ through to its atmospheric value in seawater, showing an open system trend.

Groundwater–seawater mixing

Figure 15 shows the observed concentration of major ions relative to the increasing salinity as freshwater mixes with seawater. The TDS, Cl, SO_4 and Na concentrations increase steadily from freshwater to seawater. Concentrations of K and Mg increase with an increasing proportion of seawater, but not at a steady rate. The Ca concentration and alkalinity initially increase as a result of dissolution of carbonate rock. When the seawater proportion is about 5%, Ca concentration and alkalinity decrease and then increase again, reflecting the processes of dolomite precipitation and seawater mixing. Beyond 15% seawater, the Ca concentration increases, partly owing to dissolution of calcite, whereas alkalinity decreases to a stable level in more saline waters. The latter effect is due to the precipitation of dolomite, followed by calcite and aragonite.

The degree of mixing has also been calculated as proportions of two initial waters, with Cl considered as the conservative parameter in the mixing process (Back & others, 1979; Plummer & Back, 1980). The two initial waters were taken as the top of the freshwater layer (drillhole P4) and seawater. The fraction of each initial water in the mixture was calculated, as:

$$X = 100 \times \frac{Cl_{mix} - Cl_2}{Cl_1 - Cl_2}$$

where X is the percentage of water 1 in the mixture, Cl_{mix} is the concentration of Cl (mmol/kg H_2O) in the mixed water, and Cl_1 and Cl_2 are the concentrations of Cl (mmol/kg H_2O) in the initial waters 1 and 2 respectively (Badiozamani, 1973; Plummer, 1975; Wigley & Plummer, 1976).

The effects of the observed and the calculated mixing conditions are compared by plotting saturation indices for dolomite,

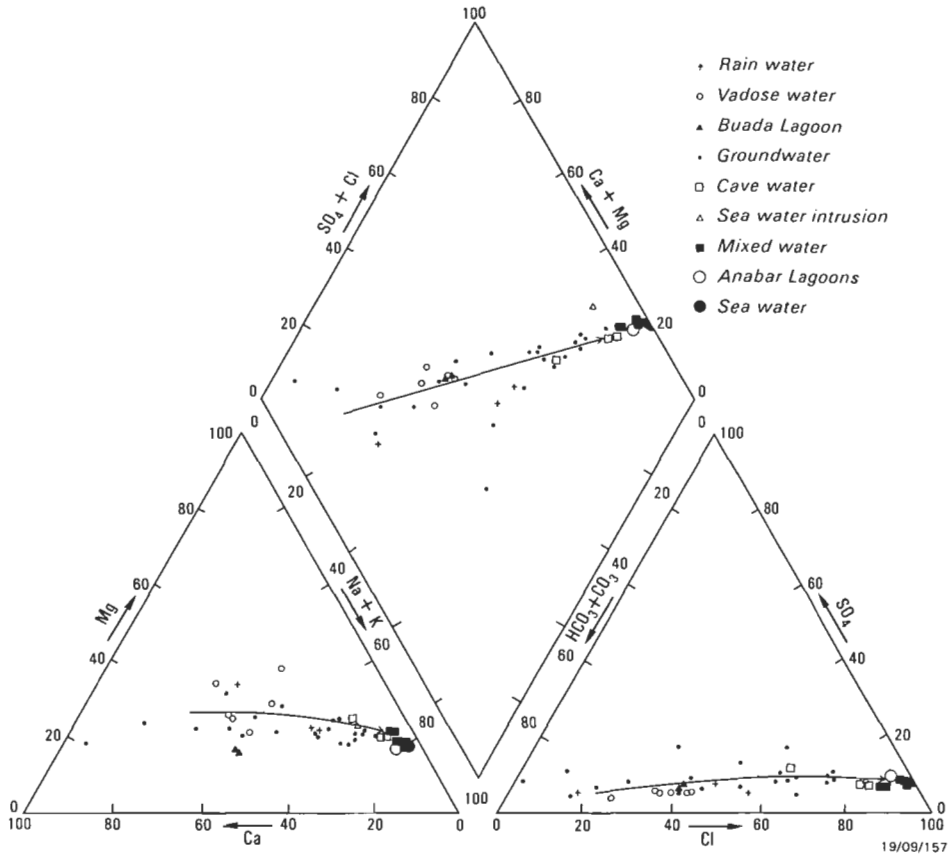

Figure 5. Trilinear diagram showing chemical composition of groundwaters, Nauru Island.

calcite and aragonite against percentage seawater (Fig. 16). The calculated mixing conditions diverge considerably from those observed. Theoretically, mixtures containing less than 57% seawater are undersaturated for calcite, mixtures containing less than 65% seawater are undersaturated for aragonite, and mixtures containing less than 9% seawater are undersaturated for dolomite. A mixture of 9–57% seawater is theoretically favourable for dolomitisation of calcite, and 57–65% seawater is theoretically favourable for dolomitisation or calcitisation of aragonite (dashed lines with arrows on Fig. 16).

However, the observed saturation indices derived from Nauru water analyses indicate that mixtures containing less than 12% seawater are undersaturated for calcite, mixtures containing less than 18% seawater are undersaturated for aragonite, and fresh groundwater is already supersaturated for dolomite. The three curves for observed values indicate that dolomitisation of calcite and aragonite occurs with less than 18% of seawater in the mixture (continuous lines with arrows on Fig. 16). This narrower band of mixing zone conditions for replacement, and the generally higher saturation indices in the natural waters, indicate that processes other than simple mixing are significant and determine saturation levels in Nauru groundwaters.

Mass transfer

Mass transfer is the net amount of each mineral or gas transferred from one phase (solid, aqueous or gas) to another (Plummer & Back, 1980). Mass transfer calculations are used to define reactions that simulate the observed water chemistry, and thereby increase understanding of the chemical evolution of the natural water system. These relationships give independent results to those derived from thermodynamic calculations, and help identify controlling chemical reactions. In this study we used the computer program 'BALANCE' to calculate mass transfer for Nauru groundwaters (Parkhurst & others, 1982), for mineral phases considered as plausible in this system.

Amounts of calcite, dolomite and gypsum dissolved or precipitated during the hydrochemical evolution of groundwaters can be estimated by chemical mass balance relations as follows:

$\Delta Ca = \Delta cal + \Delta dol + \Delta gyp$

$\Delta Mg = \Delta dol$

$\Delta SO_4 = \Delta gyp$

$\Delta CO_2 = \Delta cal + 2\,\Delta dol + \Delta CO_{2gas}$

where Δ indicates change in the number of moles of the dissolved constituent between initial and final water (Parkhurst & others, 1982; Back & others, 1983). The initial water was taken as the top of the freshwater layer (P4), and the final water as Nauru seawater. Table 3 shows calculations of mass transfer for Nauru groundwaters.

Mass transfer calculations for dolomite, calcite and gypsum (Fig. 17) show that dolomite dissolves and that the degree of dissolution tends to increase with increasing seawater in the mixture. In fresher Nauru groundwaters (less than 3% seawater), the amount of calcite precipitation is variable, and results from a few samples indicate some dissolution. Calcite precipitates in more saline water, deeper in the mixing zone. Gypsum, if present, dissolves except between 6% and 8% seawater, where it apparently precipitates.

In the closed system groundwaters, values of ΔCO_{2gas} are variable, but are greater than 1. The high P_{CO_2} (calculated from thermodynamic properties), together with high positive values of ΔCO_{2gas} (calculated from mass transfer), indicates that ingassing of CO_2 is the main chemical reaction in the closed system. The karst groundwaters are slow to reach saturation for calcite. In the open system, where groundwaters mix with

Table 3. Mass transfer calculations for mixed waters, Nauru Island.

		Percent seawater	Na^+ mmol/L	K^+ mmol/L	Ca^{2+} mmol/L	Mg^{2+} mmol/L	Alk mmol/L	SO_4^{2-} mmol/L	Cl- mmol/L	Mass transfer[2] Δ cal	Δ dol	Δ gyp	CO_{2gas}
P4 — 36.5 m (top of lens)		0	1.000	0.026	0.599	0.383	1.729	0.080	1.128				
Seawater (Nauru)		100	456.725	8.185	9.082	50.195	2.249	25.089	553.155				
Ijuw Cave-pool[1]	O	1.18	7.917	0.141	0.798	1.522	3.456	0.687	7.672				
	C		6.377	0.123	0.699	0.970	1.736	0.375	7.672	–0.764	+0.552	+0.312	+1.380
Maqua Cave	O	3.88	19.574	0.384	1.098	2.798	3.263	1.051	22.593				
— pool[1]	C		18.682	0.343	0.928	2.316	1.749	1.051	22.593	–0.313	+0.482	+0.000	+0.863
Maqua Cave	O	4.07	20.270	0.409	1.048	2.798	3.057	1.072	23.637				
— pool[1]	C		19.548	0.358	0.945	2.410	1.751	1.097	23.637	–0.258	+0.388	–0.025	+0.788
Coastal terrace													
Odn-aiwo Well	O	7.61	36.103	0.818	2.620	5.143	6.608	2.030	43.212				
	C		35.692	0.647	1.244	4.173	1.768	1.983	43.212	+0.359	+0.970	+0.047	+2.541
Heine's Well	O	1.02	6.307	0.102	2.146	1.440	5.372	0.437	6.770				
	C		5.649	0.109	0.686	0.891	1.734	0.335	6.770	+0.810	+0.549	+0.102	+1.730
Reweru's Well	O	3.44	16.268	0.307	3.368	2.921	8.681	0.677	20.168				
	C		16.677	0.307	0.890	2.096	1.746	0.941	20.168	+1.916	+0.825	+0.264	+3.399
Clodamar's Well	O	3.12	16.094	0.307	1.697	2.674	4.625	1.145	18.391				
	C		15.219	0.280	0.863	1.937	1.745	0.860	18.391	–0.189	+0.737	+0.285	+1.595
Meneng Well	O	3.48	18.356	0.384	1.771	2.880	4.849	1.499	20.365				
	C		16.859	0.310	0.894	2.117	1.747	0.950	20.365	–0.436	+0.763	+0.59	+2.012
Jeremiah's Well	O	1.90	11.005	0.179	1.747	2.057	5.661	0.979	11.649				
	C		9.659	0.182	0.761	1.330	1.739	0.555	11.649	–0.165	+0.727	+0.424	+2.633
Rydell's Well	O	0.42	6.003	0.205	0.848	1.481	5.408	0.916	3.469				
	C		2.914	0.060	0.634	0.593	1.731	0.186	3.469	–1.406	+0.888	+0.730	+3.307
Engar's Well	O	1.16	7.264	0.179	0.923	1.481	3.461	0.510	7.559				
	C		6.286	0.121	0.697	0.961	1.735	0.370	7.559	–0.434	+0.520	+0.140	+1.120
Ijuh Well	O	2.52	15.877	0.281	1.796	2.304	5.697	1.697	15.062				
	C		12.484	0.231	0.813	1.638	1.742	0.710	15.062	–0.669	+0.666	+0.987	+3.292
Retow's Well	O	3.09	16.964	0.409	1.547	2.757	5.048	1.239	18.221				
	C		15.082	0.278	0.861	1.922	1.745	0.853	18.221	–0.535	+0.835	+0.386	+2.168
Anabar Cemetery	O	1.61	11.527	0.217	1.672	2.304	7.729	1.385	10.013				
Well	C		8.337	0.158	0.735	1.185	1.737	0.483	10.013	–1.085	+1.119	+0.902	+4.839
Anatan Well	O	2.69	15.572	0.358	2.395	2.304	7.059	1.239	15.993				
	C		13.259	0.245	0.827	1.723	1.742	0.753	15.993	+0.501	+0.581	+0.486	+3.654
Dannang's Well	O	0.70	5.220	0.013	2.246	1.646	7.113	0.344	4.993				
	C		4.190	0.083	0.659	0.732	1.733	0.255	4.993	+0.584	+0.914	+0.089	+2.968
Kayser's Well	O	0.04	1.914	0.038	1.722	0.782	5.156	0.229	1.354				
	C		1.183	0.029	0.603	0.403	1.729	0.090	1.354	+0.602	+0.379	+0.139	+2.067
Benjamin's Well	O	0.45	4.176	0.153	1.297	1.358	4.651	0.375	3.639				
	C		3.051	0.063	0.637	0.607	1.731	0.192	3.639	–0.273	+0.751	+0.183	+1.691
Itsimera's Well	O	1.96	11.176	0.256	2.395	2.098	6.400	0.760	11.959				
	C		9.932	0.185	0.765	1.360	1.739	0.570	11.959	+0.701	+0.738	+0.190	+2.484
Menke's Well	O	3.38	17.399	0.384	2.246	2.469	5.480	1.156	19.829				
	C		16.403	0.302	0.886	2.067	1.747	0.925	19.829	+0.759	+0.402	+0.231	+2.170
Tapau's Well	O	0.63	4.480	0.051	2.171	1.111	5.223	0.344	4.598				
	C		3.871	0.078	0.652	0.697	1.732	0.238	4.598	+0.998	+0.414	+0.106	+1.665
Daniel's Well	O	0.20	3.045	0.026	1.796	0.946	5.764	0.344	2.257				
	C		1.911	0.042	0.616	0.482	1.730	0.130	2.257	+0.502	+0.464	+0.214	+2.604
Seawater intrusion													
H10 — 33 m	O	3.47	16.529	0.435	1.647	3.003	2.768	0.979	20.168				
	C		16.813	0.309	0.893	2.112	1.747	0.948	0.168	–0.169	+0.891	+0.031	–0.592
Mixed water													
P4 — 39.5 m	O	5.01	24.141	0.512	0.998	3.456	2.750	1.187	28.714				
	C		23.832	0.435	1.024	2.879	1.755	1.332	28.714	–0.453	+0.577	–0.145	+0.299
P5 — 31.5 m	O	6.40	29.796	0.639	1.322	4.114	2.984	1.489	36.414				
	C		30.166	0.548	1.142	3.571	1.762	1.680	36.414	–0.171	+0.543	–0.191	+0.307
P3 — 11.2 m	O	14.61	69.814	1.151	2.246	8.352	2.962	4.060	81.939				
	C		67.582	1.218	1.838	7.660	1.805	3.733	81.939	–0.610	+0.692	+0.327	+0.383
H10 — 50 m	O	15.80	72.641	1.304	2.570	9.175	2.650	4.268	88.512				
	C		73.005	1.315	1.939	8.253	1.811	4.032	88.512	–0.528	+0.922	+0.236	–0.477
P5 — 43.5 m	O	23.17	108.744	1.535	2.570	12.549	2.790	6.194	129.270				
	C		106.591	1.916	2.564	11.925	1.849	5.875	129.270	–0.938	+0.624	+0.319	+0.631
W3 — 65 m	O	51.60	239.237	4.604	5.364	27.978	2.274	13.534	286.577				
	C		236.154	4.236	4.976	26.086	1.997	12.984	286.577	–2.053	+1.892	+0.550	–1.454

[1] Cave water

[2] Δ cal, Δ dol, Δ gyp, Δ Co_2 in mmol/L, calculated from mass balance between computed values in mixture and observed values in samples. Positive values indicate dissolution, negative values indicate precipitation.

O observed value in sample, C calculated value of mixture between fresh groundwater (P4 — 36.5 m top of lens) and seawater (Nauru).

seawater, Δ CO_{2gas} is less than 1 (drillholes P3, P4, P5, Table 3). With an increasing proportion of seawater, the value drops to a negative value (drillholes H10, W3, Table 3), indicating rapid mixing and outgassing of CO_2. Saturation is quicker with lower values of P_{CO_2} and Δ CO_{2gas}, and therefore precipitation is more important than dissolution in the open system.

Discussion

Chemical analyses of Nauru Island water samples show that the vadose waters are undersaturated for calcite (Fig. 11). Vadose waters percolate down to the freshwater layer, where there is an increase in TDS, ionic concentrations, and pH. The fresher

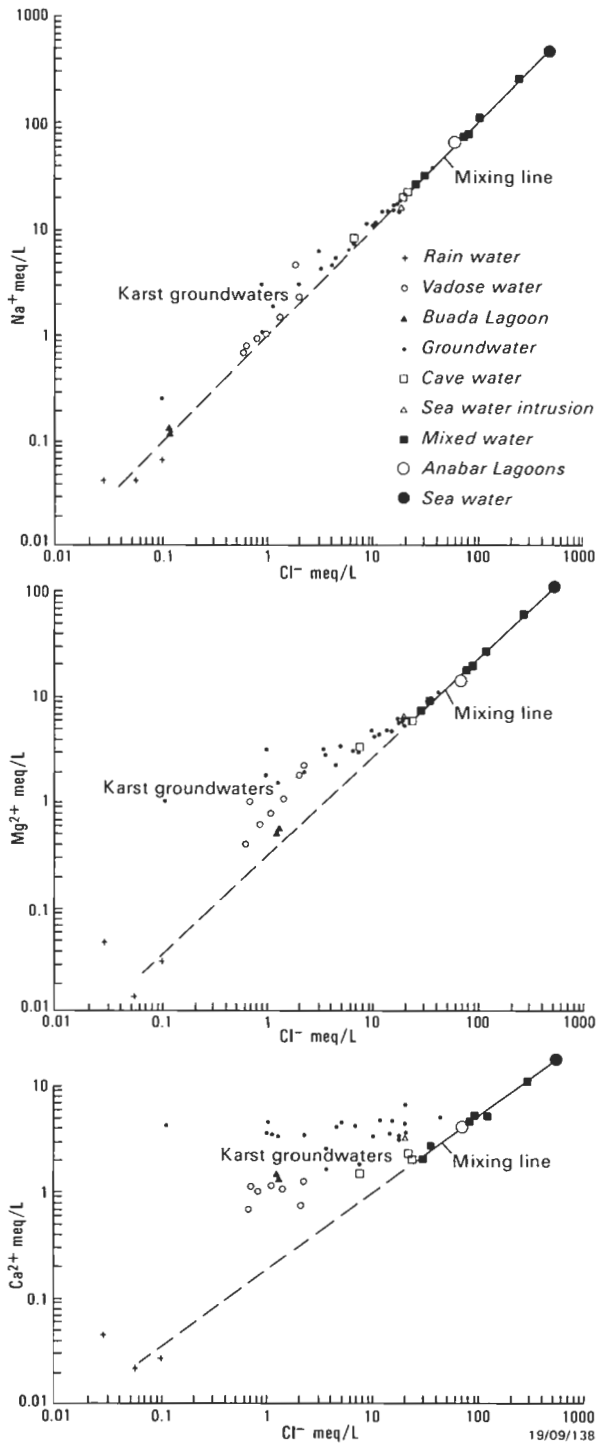

Figure 6. Relationship of concentrations of individual major cations to that of chloride for Nauru groundwaters.
Solid line shows mixing between karst groundwaters and seawater. Dashed line joins points of initial freshwater composition with mixing line.

groundwaters are undersaturated for calcite but rapidly achieve saturation for dolomite.

In the early phase of groundwater/seawater mixing, the groundwater is chemically unstable. Saturation indices for calcite and dolomite vary, but the groundwater remains undersaturated for calcite and supersaturated for dolomite. With an increasing proportion of seawater in the mixture (>7%), saturation indices level out; mixed water becomes saturated for calcite at 12% seawater, and for aragonite at 18% seawater. Saturation indices for dolomite increase throughout the mixing process.

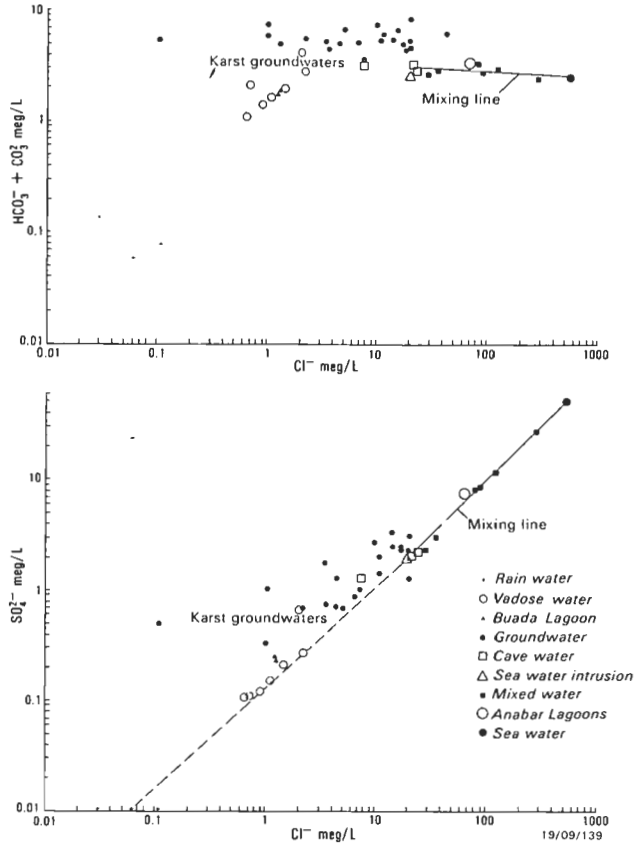

Figure 7. Relationship of concentrations of individual major anions to that of chloride for Nauru groundwaters.
Solid line shows mixing between karst groundwaters and seawater. Dashed line joins points of initial freshwater composition with mixing line.

Theoretical calculations of the mixing of fresh karst groundwater with seawater give saturation for dolomite at 9% seawater, saturation for calcite at 57% seawater, and saturation for aragonite at 65% seawater. These results differ significantly from saturation indices calculated from chemical analyses of waters in the natural environment. The same differences were noted in the Bermuda mixing zone (Plummer & others, 1976). The differences show that in the early phase of mixing between carbonate groundwaters and seawater, the dominant processes are in fact dissolution and precipitation reactions rather than mixing. It is also inferred that dolomitisation may be limited in

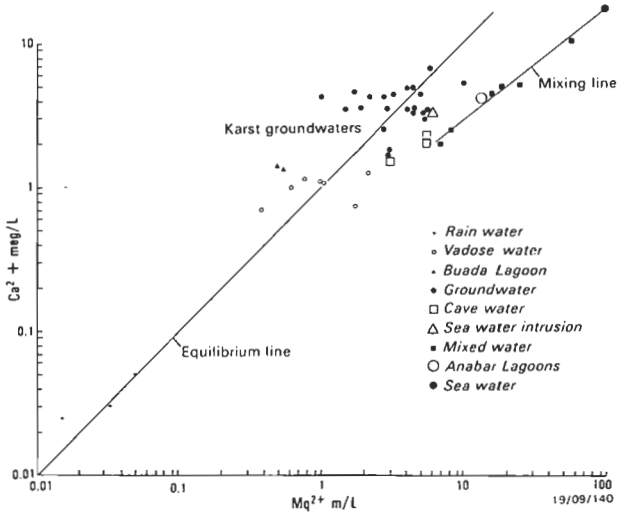

Figure 8. Relationship between Mg and Ca concentrations in Nauru groundwaters.

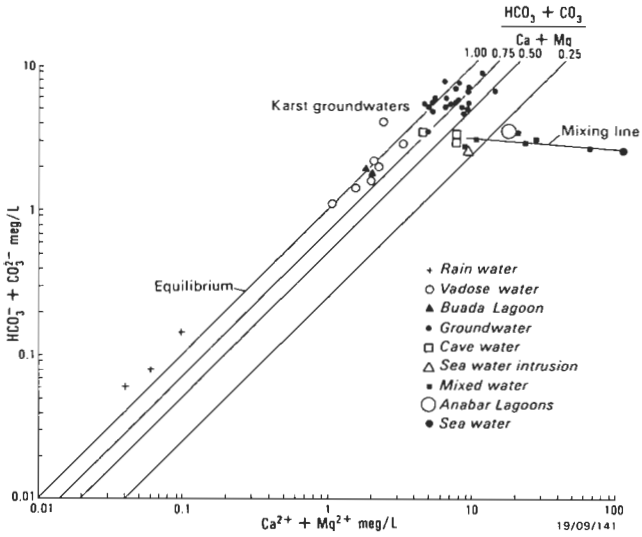

Figure 9. Relationship between alkalinity (HCO_3 + CO_3) and hardness (Ca + Mg) for Nauru groundwaters.

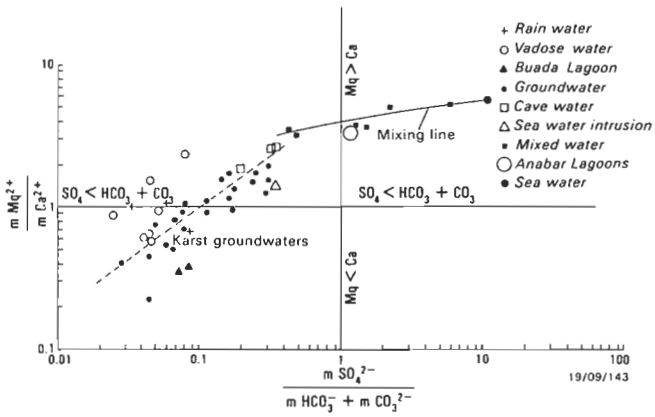

Figure 10. Relationship between the molar Mg/Ca and SO_4/(HCO_3 + CO_3) ratios for Nauru groundwaters.

the natural environment to a narrower band of mixing zone conditions than theoretical calculations suggest (cf. Badiozamani, 1973; Hardie, 1986; Smart & others, 1988).

The significant differences between the results obtained from Nauru and those from other localities (Table 4) are possibly due to the extremely undersaturated nature of the Nauru freshwater end-member for calcite (S.I. = –1.22). This may be caused by phosphate in the vadose zone fissures. In comparison, freshwater on Bermuda is near equilibrium (Plummer & others, 1976) for calcite, and that on the Yucatan Peninsula is slightly supersaturated (Back & others, 1986; Stoessell & others, 1989).

Thermodynamic calculations suggest that conditions are favourable for dolomitisation in the early stages of mixing, up to the beginning of calcite saturation. However, mass transfer calculations suggest that Mg (dolomite) is dissolved in mixed waters up to 51.6% seawater. To reconcile these differences, we infer that dissolution of calcite in the early stages of mixing is a more effective process than dolomitisation and/or precipitation of dolomite and the creation of Mg-rich calcite. The dissolution of limestone is evident in the increased porosity and permeability of carbonate aquifers (cf. Plummer, 1975; Sanford & Konikow, 1989); in Nauru, modern karstification is demonstrated by the development of caves in the coastal terrace. The limestone is extensively dolomitised, but there is no evidence that this is related to the modern mixing zone.

Conclusions

1. In the mixing zone on Nauru Island, fresh HCO_3–Ca groundwater with high P_{CO_2} and low pH mixes with Cl–Na seawater with low P_{CO_2} and high pH. In the early stages, the carbonate groundwater is undersaturated for calcite; mixing with seawater, which is saturated, produces undersaturated

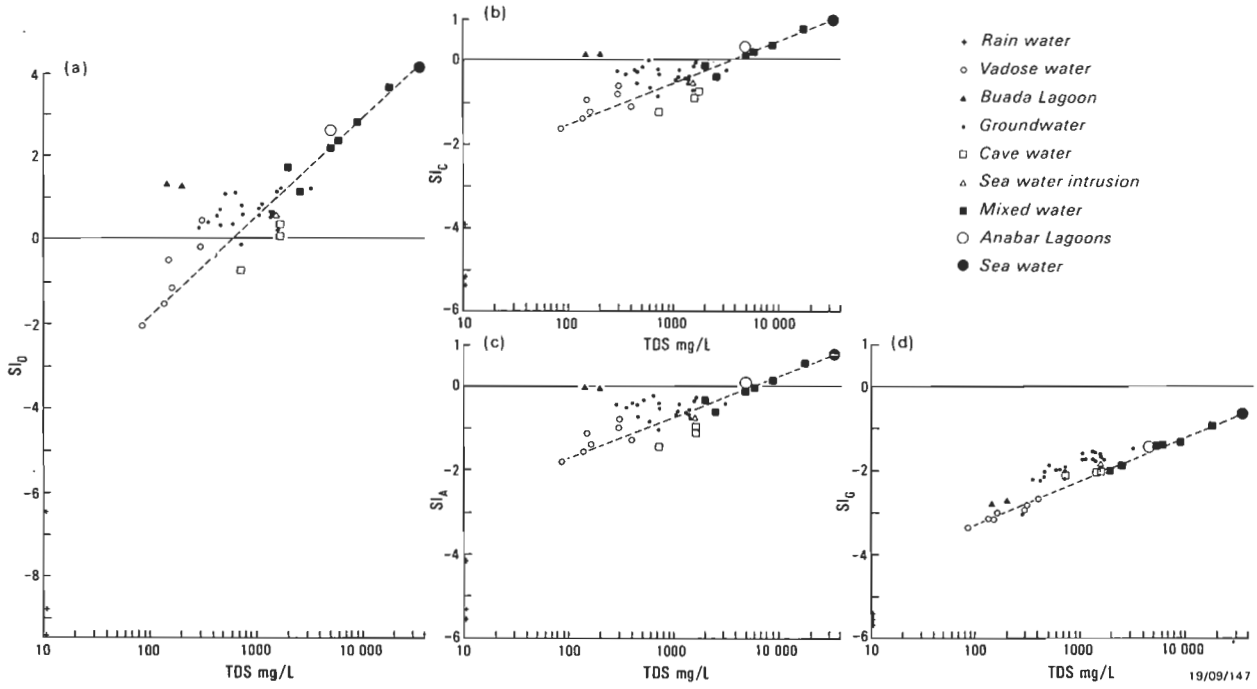

Figure 11. Saturation indices for (a) dolomite, (b) calcite, (c) aragonite, and (d) gypsum, plotted as a function of salinity for Nauru groundwaters.

Lines of mixing are shown, joining points of initial freshwater composition with seawater.

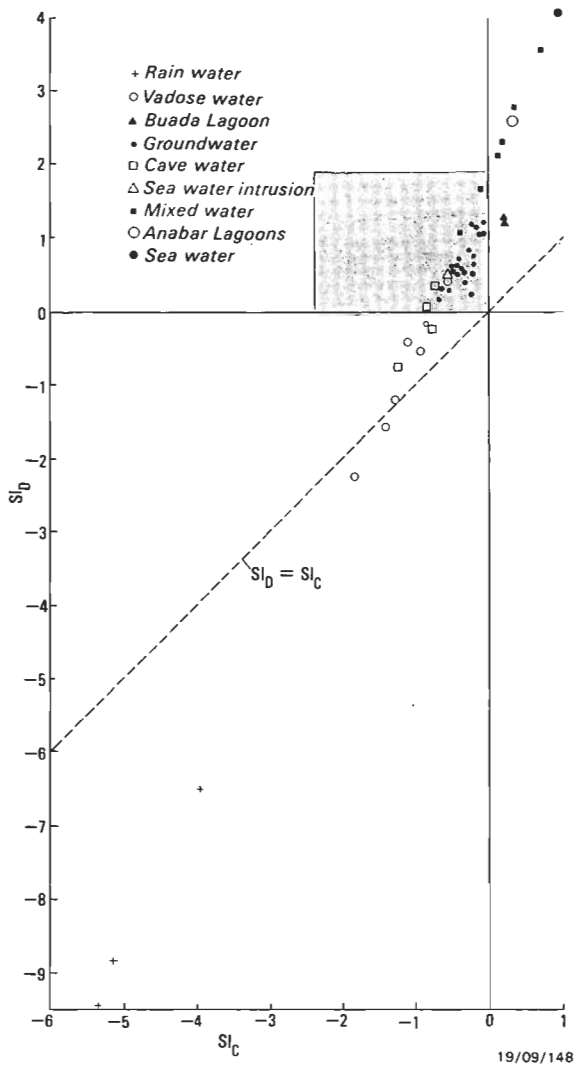

Figure 12. Relationship of saturation indices for calcite(SI_C) and dolomite(SI_D) for Nauru groundwaters.
The shaded area defines a region favourable for dolomitisation.

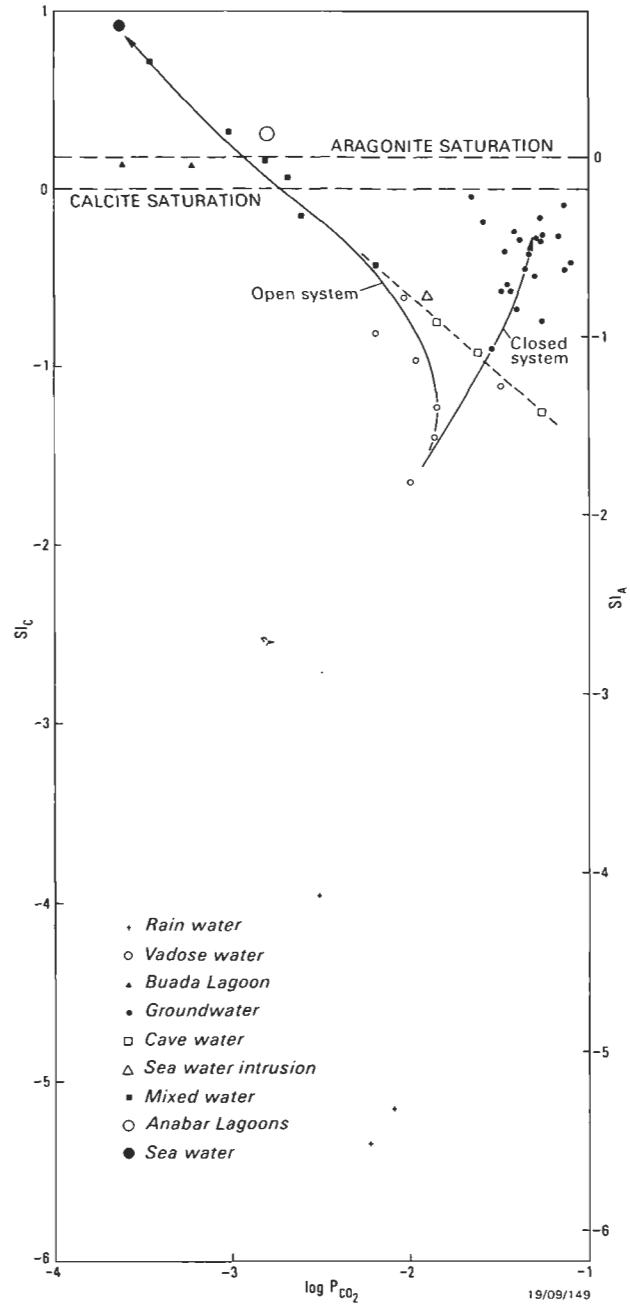

Figure 13. Relationship between saturation indices for calcite and aragonite, and log P_{CO2} in groundwaters, Nauru Island.
Evolutionary trends for closed and open systems are shown. Dashed line projects open system trends from cave waters to mixing zone.

groundwaters with the capacity to dissolve limestone. The effect of dissolution is to develop and increase porosity and permeability, i.e. karstification. Sea-level fluctuations result in fluctuations in the level of the mixing zone, and this increased permeability is the cause of the thick, modern mixing zone on Nauru.

2. The top of the freshwater layer is recharged by vadose zone waters, and forms a closed system in which chemistry is controlled by dissolution and precipitation reactions and especially by ingassing of CO_2.

3. The cave waters and brackish mixed waters form an open system in which saturation for calcite is achieved; the degree of saturation increases with the increasing proportion of seawater in the mixture. Chemical evolution is controlled mainly by seawater mixing, but other operative processes are dissolution, precipitation and outgassing of CO_2.

4. Saturation for dolomite is attained early in the fresh groundwaters; the Ca/Mg ratio is less than 0.5. The early stage of mixing, up to 12% seawater, is favourable for the dolomitisation of calcite. From 12 to 18% seawater, conditions are favourable both for the dolomitisation of aragonite and the calcitisation of aragonite.

Table 4. Comparison between Nauru saturation levels and other determinations.

Location	*Saturation level (% seawater)* *Dolomite*	*Calcite*	*Aragonite*	*Source*
Nauru — natural	0	12	18	
— theoretical	9	57	65	
Bermuda — natural	—	scattered	—	Plummer &
— theoretical	—	37	—	others, 1976
Yucatan Peninsula				
— theoretical	10	50	60	Herman & Back, 1984; Back & others, 1986
— thermodynamic modelling	0	90	95	Stoessell & others,1989
Laura — theoretical	—	0–7 and 50	—	Anthony & others, 1989

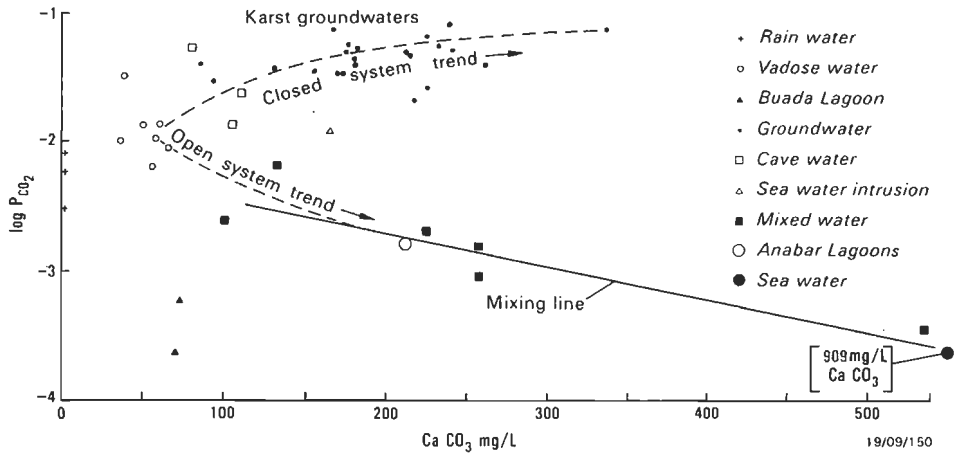

Figure 14. Relationship between log P_{CO_2} and $CaCO_3$ concentration in groundwaters, Nauru Island. Evolutionary trends for closed and open systems are shown.

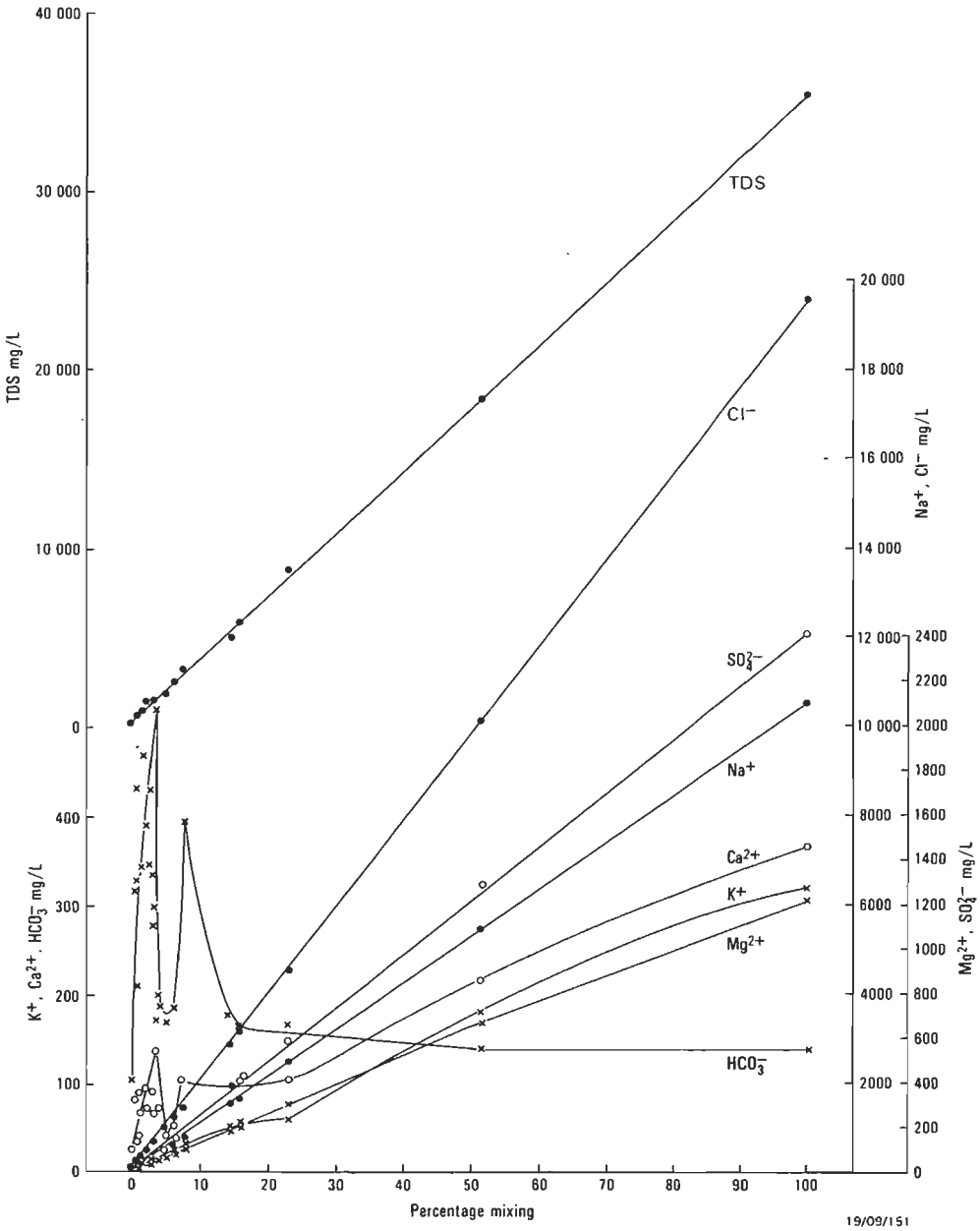

Figure 15. Ionic concentrations with different proportions of admixed seawater, Nauru Island.

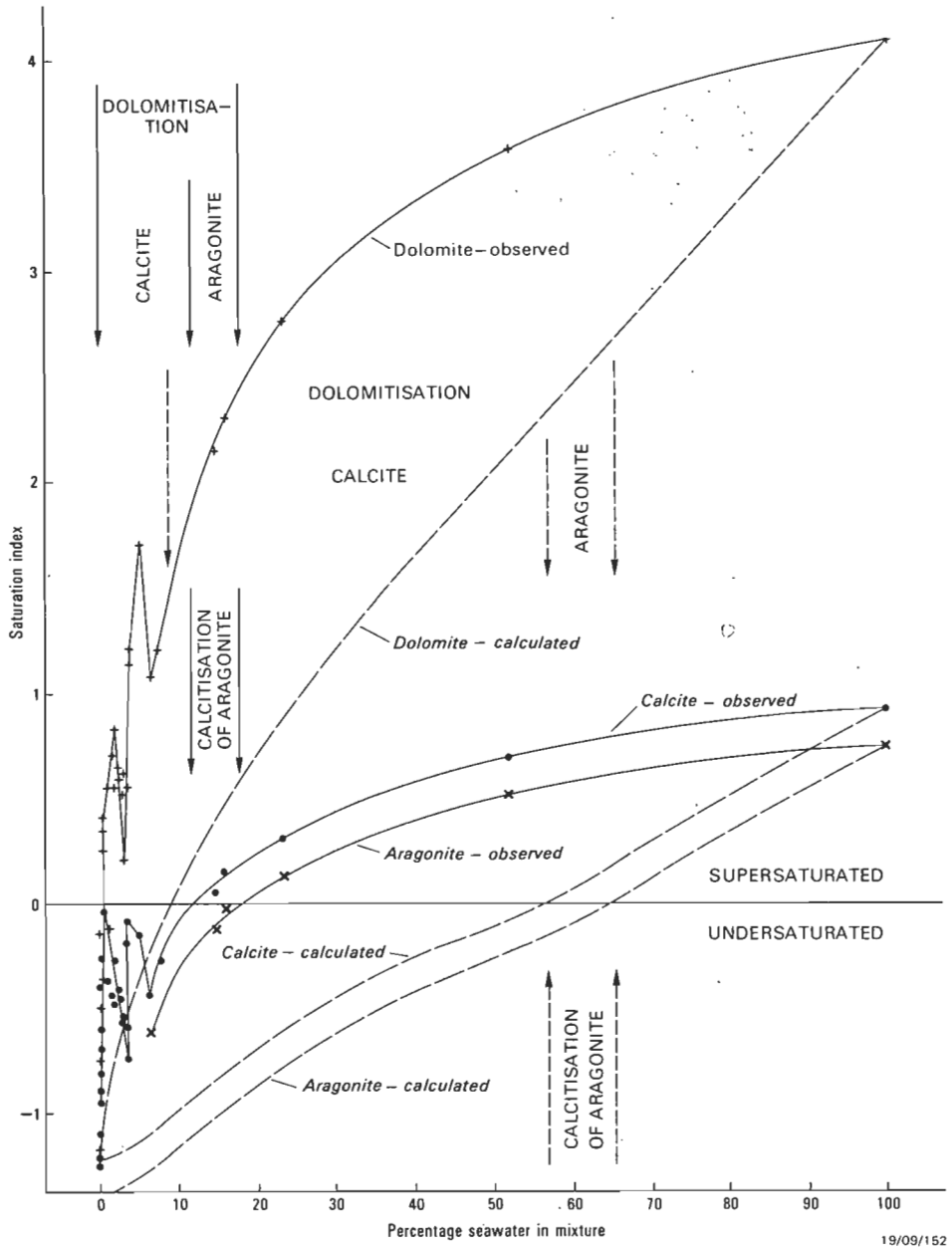

Figure 16. Relationship between saturation indices for dolomite, calcite and aragonite, and the proportion of admixed seawater for Nauru groundwaters.
Solid lines show observed trend, dashed lines show theoretical trend.

5. Theoretical calculations of the mixing of two initial waters, fresh Nauru groundwater and seawater, suggest that saturation for calcite should be attained at 57% seawater, and saturation with respect to dolomite at 9% seawater. However, processes in the mixing zone are more complex than those indicated by simple mixing calculations, and the processes change with the degree of mixing.

Acknowledgements

Hydrogeological investigation on Nauru was undertaken on behalf of the Commission of Inquiry into Rehabilitation of the Worked Out Phosphate Lands in Nauru. Peter Hill (BMR) was responsible for geophysical aspects of this investigation, and fieldwork was facilitated by the Nauru Phosphate Corporation. Chemical analyses of groundwater samples were undertaken by the Australian Mineral Development Laboratory in Adelaide, South Australia. For the computation of physical chemistry parameters we used the computer program 'PITZ' developed by Jeff Hanor and Ray Evans at the BMR. We thank Jim Ferguson of the BMR and two anonymous referees for comments on an earlier version of the manuscript, and Chris Knight, Joe Mifsud and Danuta Dlugosz of BMR's Cartographic Services Unit for the figures.

References

Alekin, O.A., 1970 — Osnovy hydrokhimii (Principles of hydrochemistry). *Hydrometeorologicheskoe Izdat., Leningrad*, 443 pp.

Anthony, S.A., Peterson, F.L., Mackenzie, F.T. & Hamlin, S.N., 1989 — Geohydrology of the Laura freshwater lens, Majuro atoll: a hydrogeochemical approach. *Geological Society of America, Bulletin*, 101, 1066–1075.

Back, W. & Hanshaw, B.B., 1970 — Comparison of chemical hydrogeology of the carbonate Peninsulas of Florida and Yucatan. *Journal of Hydrology*, 10, 330–368.

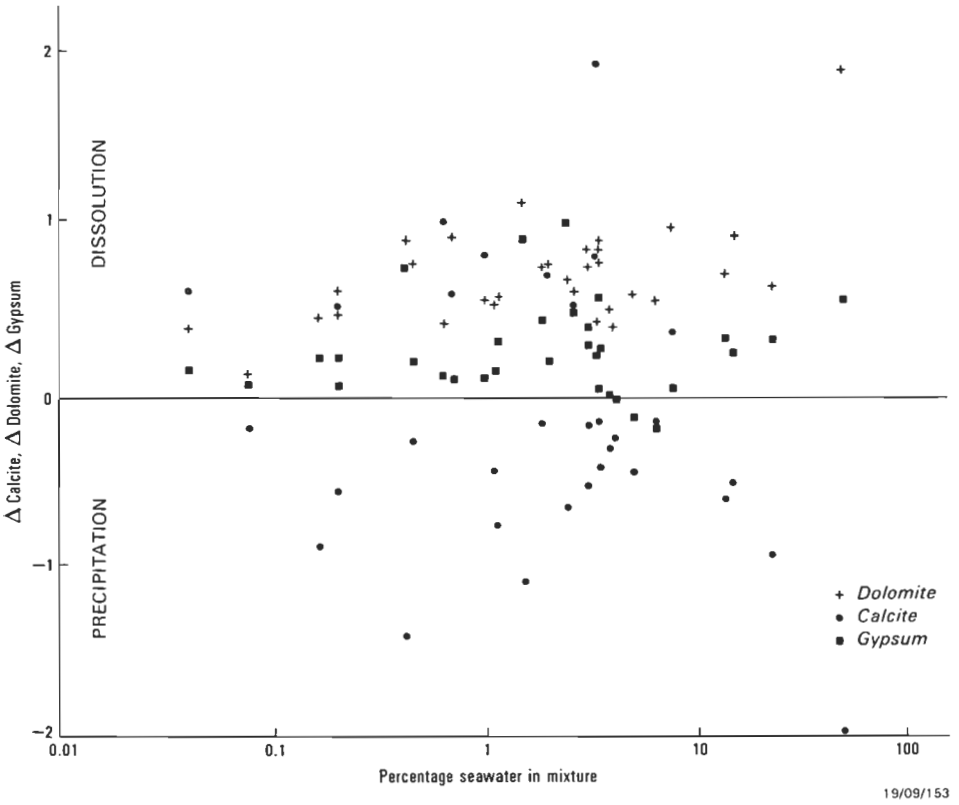

Figure 17. Mass transfer of calcite, dolomite and gypsum as a function of percentage of admixed seawater, Nauru Island.

Back, W., Hanshaw, B.B., Herman, J.S. & Van Driel, J.N., 1986 — Differential dissolution of a Pleistocene reef in the groundwater mixing zone of coastal Yucatan, Mexico. *Geology*, 14, 137–140.

Back, W., Hanshaw, B.B., Plummer, L.N., Rahn, P.H., Rightmire, C.T. & Rubin, M, 1983 — Process and rate of dedolomitization: mass transfer and ^{14}C dating in a regional carbonate aquifer. *Geological Society of America, Bulletin*, 94, 1415–1429.

Back, W., Hanshaw, B.B., Pyle, T.E., Plummer, L.N. & Weidie A.E., 1979 — Geochemical significance of groundwater discharge and carbonate solution to the formation of Caleta Xel Ha, Quintana Roo, Mexico. *Water Resources Research*, 15, 1521–1535.

Badiozamani, K., 1973 — The Dorag dolomitization model — application to the middle Ordovician of Wisconsin. *Journal of Sedimentary Petrology*, 43, 965–984.

Ghassemi, F., Jakeman, A.J. & Jacobson, G., 1990 — Mathematical modelling of sea water intrusion, Nauru Island. *Hydrological Processes*, 4, 269–281.

Hanor, J.S., 1978 — Precipitation of beachrock cements: mixing of marine and meteoric waters vs. CO_2-degassing. *Journal of Sedimentary Petrology*, 48, 489–501.

Hanor, J.S., Evans, W.R. & Tucker, A., 1988 — PITZ — a computer program for calculating activity coefficients and saturation indices. *Bureau of Mineral Resources, Australia (unpublished).*

Hardie, L.A., 1986 — Dolomitization: a critical view of some current views. *Journal of Sedimentary Petrology*, 57, 166–183.

Harvie, C.E., Moller, N. & Weare, J.H., 1984 — The prediction of mineral solubilities in natural waters: the Na–K–Mg–Ca–H–Cl–SO_4–OH–HCO_3–CO_3–CO_2–H_2O system to high ionic strengths at 25°C. *Geochimica et Cosmochimica Acta*, 48, 723–751.

Harvie, C.E. & Weare, J.H., 1980 — The prediction of mineral solubilities in natural waters: the Na–K–Mg–Ca–Cl–SO_4–H_2O system from zero to high concentration at 25°C. *Geochimica et Cosmochimica Acta*, 44, 981–997.

Herman, J.S. & Back, W., 1984 — Mass transfer simulation of diagenetic reactions in the groundwater mixing zone. *Geological Society of America, Abstracts with Programs*, 16, 537.

Hill, P.J. & Jacobson, G., 1989 — Structure and evolution of Nauru Island, central Pacific Ocean. *Australian Journal of Earth Sciences*, 36, 365–381.

Jacobson, G. & Hill, P.J., 1980 — Hydrogeology of a raised coral atoll — Niue Island, South Pacific Ocean. *BMR Journal of Australian Geology & Geophysics*, 5, 271–278.

Jacobson, G. & Hill, P.J., 1988 — Hydrogeology and groundwater resources of Nauru Island, central Pacific Ocean. *Bureau of Mineral Resources, Australia, Record* 1988/12, 87 pp.

Parkhurst, D.L., Plummer, L.N. & Thorstenson, D.C., 1982 — BALANCE — A computer program for calculating mass transfer for geochemical reactions in ground water. *United States Geological Survey Water-Resources Investigation*, 82–14, 29 pp.

Pitzer, K.S., 1973 — Thermodynamics of electrolytes. I: Theoretical basis and general equations. *Journal of Physical Chemistry*, 77, 268–277.

Plummer, L.N., 1975 — Mixing of sea water with calcium carbonate ground water. *In* Whitten, E.H.T. (editor), Quantitative studies in the geological sciences. *Geological Society of America, Memoir*, 142, 219–238.

Plummer, L.N. & Back, W., 1980 — The mass balance approach: application to interpreting the chemical evolution of hydrologic systems. *American Journal of Science*, 280, 130–142.

Plummer, L.N., Vacher, H.L., Mackenzie, F.T., Bricker, O.P. & Land, L.S., 1976 — Hydrogeochemistry of Bermuda: a case history of groundwater diagenesis of biocalcarenites. *Geological Society of America, Bulletin*, 87, 1301–1316.

Sanford, W.E. & Konikow, L.F., 1989 — Simulation of calcite dissolution and porosity changes in saltwater mixing zones in coastal aquifers. *Water Resources Research*, 25, 655–667.

Smart, P.L., Dawans, J.M. & Whitaker, F., 1988 — Carbonate dissolution in a modern mixing zone. *Nature*, 335, 811–813.

Stoessell, R.K., Ward, W.D., Ford, B.H. & Schuffert, J.D., 1989 — Water chemistry and $CaCO_3$ dissolution in the saline part of an open-flow mixing zone, coastal Yucatan Peninsula, Mexico. *Geological Society of America, Bulletin*, 101, 159–169.

Thrailkill, J. & Robl, T.L., 1981 — Carbonate geochemistry of vadose water recharging limestone aquifers. *Journal of Hydrology*, 54, 195–208.

Wigley, T.M.L. & Plummer, L.N., 1976 — Mixing of carbonate waters. *Geochimica et Cosmochimica Acta*, 40, 989–995.

BMR Journal of Australian Geology & Geophysics, 12, 65–91

Upper Cretaceous and Tertiary stratigraphy of the Fremantle Canyon, South Perth Basin: a nannofossil assessment

Samir Shafik[1]

The nannostratigraphy of material dredged from the Fremantle Canyon, west of Perth (Western Australia), indicates that the Maastrichtian–Miocene section in the South Perth Basin is more complete than contemporaneous sections in the Perth Abyssal Plain and on the Naturaliste Plateau. The data point to a possible continuous sequence through most of the Paleocene and the entire Eocene in the Fremantle Canyon. In addition to the five rock units previously known to form the Maastrichtian–Miocene succession of the Perth Basin, two (or possibly three) new units have been discovered. The new units, yet to be named, are of Early Eocene and mid Oligocene age; in addition a previously unreported Lower Paleocene sequence could be the lower extension of the Kings Park Formation offshore. The unnamed new Lower Eocene unit fills the stratigraphic gap between the (mainly) Upper Paleocene Kings Park Formation and the Middle Eocene Porpoise Bay Formation. The unnamed new mid (upper Lower) Oligocene unit fits between the 'Upper Eocene' Challenger Formation and the Lower–Middle Miocene Stark Bay Formation, still leaving a large stratigraphic gap between these two formations. The lithological evidence, supported by nannofossil data, indicates that the Porpoise Bay and Challenger Formations merge into a single unit along the canyon walls. This unit is similar to the Lower Eocene and Paleocene carbonates there. A widespread Late Maastrichtian transgression over the Carnarvon and Perth Basins, reaching the Great Australian Bight Basin as an ingression, is seen in the Fremantle Canyon as occurrences of nannofossil association characteristic of the Upper Maastrichtian Breton Marl onshore. Several lines of evidence are discussed to suggest that the onshore Kings Park Formation represents a rapid sea level rise and culmination of the Paleocene transgression over the Perth Basin. Indications of a previously reported significant Middle Eocene reworking episode are recorded at the right level in the Fremantle Canyon succession. Middle Eocene microplanktic components found in the newly reported mid Oligocene of the canyon are thought to have been derived from the Naturaliste Plateau during a major Oligocene erosional event, whose effects have been recorded previously in several DSDP sites in the Southwest Pacific region.

Introduction

With the exception of the Upper Paleocene–Lower Eocene Kings Park Formation, the Upper Cretaceous–lower Tertiary marine sequence in the Perth Basin (Western Australia) was poorly known biostratigraphically until fairly recently. Two unnamed Eocene units containing calcareous nannofossils and/or planktic foraminiferids have been recently discovered: a Middle Eocene unit in the Rottnest Island Bore (Fig. 1) investigated by Shafik (1978), who recorded its calcareous nannofossils, and an 'Upper Eocene' unit in the Challenger No. 1 well (Fig. 1) investigated by Quilty (1978), who documented its planktic foraminiferids. Cockbain & Hocking (1989) proposed the names Porpoise Bay and Challenger Formations for these Eocene units. More recently, Shafik (1990a) discovered an Upper Maastrichtian marine unit in two coreholes at Breton Bay (31°10′36″S, 115°24′06″E), rich with abundant calcareous nannofossils, which he named the Breton Marl.

Material examined in the present study came from the Fremantle Canyon in the offshore South Perth Basin (Fig. 2). It fills most of the nannofossil biostratigraphic gap between the type sections of the Upper Paleocene–Lower Eocene Kings Park Formation and the Middle Eocene Porpoise Bay Formation, and includes records of several other new nannofossil-bearing levels within the Palaeogene and Miocene (see Fig. 3). Equivalents of the previously known five lithostratigraphic units, which form the marine Maastrichtian–Miocene sequence in the Perth Basin (Fig. 3), are identified, based on occurrences of their nannofossil assemblages in the material studied.

The study is based on dredge samples recovered during BMR Cruise 80 by R/V *Rig Seismic*. Dredging during this survey was successful at 17 stations. Calcareous nannofossil-bearing sediments came from 14 stations along the walls of the Fremantle Canyon and also from one station (80DR/003) on the continental slope north of the canyon. Water depths at these stations, and their locations, are given in Table 1. The continental slope west of Perth is fairly smooth, but it is incised occasionally by submarine canyons and gullies. Notable among these canyons is the Fremantle Canyon, whose head is near the

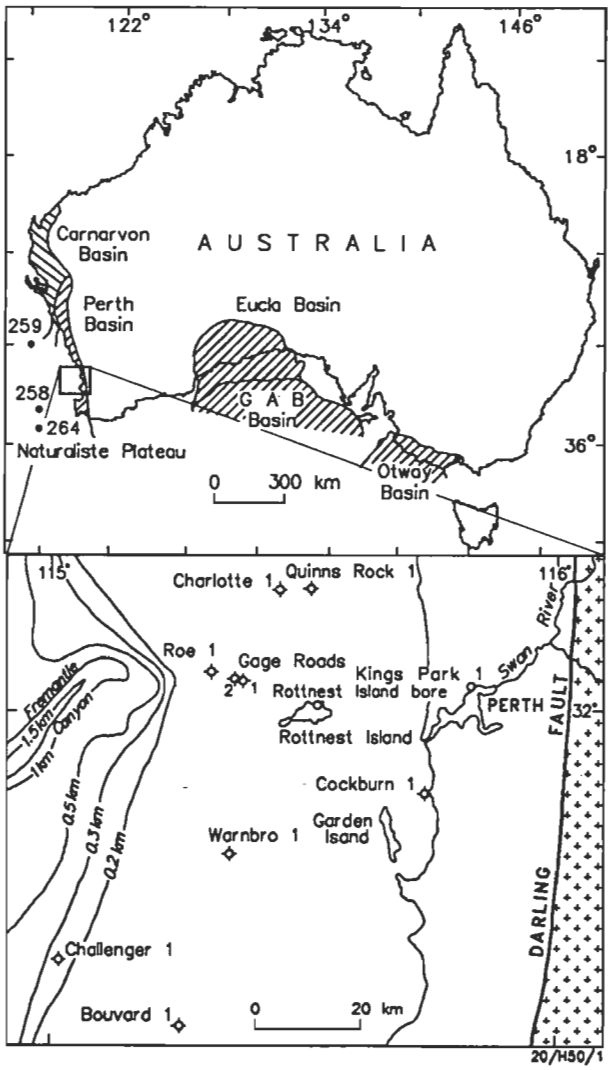

Figure 1. South Perth Basin, Western Australia, showing location of relevant wells.

[1] Marine Geoscience & Petroleum Geology Program, Bureau of Mineral Resources, Geology & Geophysics, GPO Box 378, Canberra ACT 2601

shelf break directly off Perth. This canyon is about 160 km long, and consists of three discrete segments of similar length (Fig. 2; see Marshall & others, 1989; Quilty & others, in press). Initially, the canyon trends southwesterly for about 50 km, to an axial depth of 1700 m, where it suddenly changes direction to join a northwesterly-trending arm. This northwesterly arm of the canyon extends for about 60 km, to an axial depth of 3000 m, before abruptly changing direction to a westerly orientation. The canyon extends in this direction to a depth of 4600 m where it opens out onto a submarine fan.

Table 1. Location of dredge stations where nannofossil-bearing Maastrichtian and Tertiary sediments outcrop, and water depth at these stations.

Dredge station	*Latitude (°S)*	*Longtitude (°E)*	*Depth (m)*
80DR/003	31°13.64′	114°35.96′	2415
80DR/005	32°00.70′	114°58.00′	730–1350
80DR/007	32°03.30′	115°01.13′	650–850
80DR/008	32°02.50′	115°00.30′	850–1150
80DR/009	32°01.70′	114°58.60′	1200–1650
80DR/013	32°03.60′	114°45.00′	1940–2500
80DR/014	32°03.10′	114°45.50′	1135–1965
80DR/016	32°06.05′	114°43.00′	1750–2470
80DR/017	31°57.40′	114°44.20′	1800–2814
80DR/018	31°59.80′	114°39.50′	2400–2810
80DR/019	32°00.00′	114°38.00′	1600–2700
80DR/020	31°50.05′	114°37.60′	2420–3000
80DR/021	31°48.00′	114°39.00′	1420–2650
80DR/022	31°51.80′	114°36.30′	2310–2970
80DR/023	31°53.40′	114°34.50′	1920–2520

Detailed lithological descriptions and other relevant data concerning the samples examined in this study are given by Marshall & others (1989). In general, the lithologies of the Tertiary samples reflect carbonate deposition on the outer shelf and upper continental slope.

Previously known Maastrichtian and early Tertiary calcareous microplankton biostratigraphy of the Perth Basin

Shafik (1990a) detailed the Late Cretaceous nannofossil biostratigraphy of onshore parts of the Perth Basin. The documentation of Late Maastrichtian assemblages, from what was referred to as the Breton Marl, is relevant to the present study. These assemblages are characterised by the occurrence of *Nephrolithus frequens*, *Lithraphidites quadratus* and *Cribrosphaerella daniae*.

The Breton Marl is best known from the Breton Bay corehole No. 1 (31°10′36″S, 115°24′06″E). There, it consists of an approximately 6 m thick section of soft marl. The underlying Lancelin Formation is about 60 m thick in Breton Bay corehole No. 1, and is separated from the Breton Marl by an intra-Maastrichtian disconformity. The Breton Marl is a part of a wide Late Maastrichtian transgression which occurred in both the Perth and Carnarvon Basins (Shafik, 1990a), and reached the Great Australian Bight Basin as a marine ingression (Shafik, 1990b).

The Kings Park Formation (Fairbridge *in* Coleman, 1952; amended Quilty, 1974a,b) has the oldest Tertiary marine sediments in the onshore Perth Basin. Its type section is 275 m thick in the Kings Park No. 2 Bore (Perth metropolitan area) (Fig. 1), but a thickness of more than 500 m has been reported elsewhere in the Perth area (Playford & others, 1975). The formation consists of grey, calcareous, mostly glauconitic shale and siltstone, containing bryozoans, foraminiferids, calcareous nannofossils, molluscs, ostracods and sponge spicules (McWhae & others, 1958; Shafik, 1978). McGowran (1964, 1968) revised the age of the Kings Park Formation to Late Paleocene, and correlated its planktic foraminiferids with his *Acarinina mckannai* zonule which roughly equates with zone P4. Cockbain (1973) recorded a foraminiferal assemblage of Late Paleocene to Early Eocene age from the formation, and Quilty (1974a,b) indicated that foraminiferids recovered from offshore are younger than Late Paleocene.

Shafik (1978) recorded the nannofossil assemblages of the Kings Park Formation in several boreholes as well as its type section, and correlated these assemblages with the Late Paleocene foraminiferal zones late P4 and P5, but also argued for an Early Eocene age (zone P6). Assemblages from the younger levels (Upper Paleocene–Lower Eocene) include the key species *Campylosphaera eodela*, *Chiasmolithus eograndis*, *Coccolithus* sp. cf. *C. formosus*, *Discoaster* sp. cf. *D. diastypus*, *D. multiradiatus* and *Transversopontis* sp. aff. *T. pulcher*, whereas those from the Upper Paleocene levels lack discoasters, but include the index species *Heliolithus kleinpellii* and *H. riedelii*, in addition to several species of *Fasciculithus*.

Shafik (1978) dated nannofossils from a unit in the Rottnest Island Bore, formally regarded as Kings Park Formation, as Middle Eocene in age. He recommended that this unit be given separate lithostratigraphic status, because it was deposited during a separate sedimentary cycle from that which produced the Kings Park Formation. Subsequently, Cockbain & Hocking (1989) named the unit in the Rottnest Island Bore the Porpoise Bay Formation. The type section of the Porpoise Bay Formation consists of 382 m of brown calcareous shale and siltstone, unconformably overlying the Lower Cretaceous Leederville Formation.

According to data in Shafik (1978), the lower part of the type section of the Porpoise Bay Formation contains rich nannofossil assemblages which include *Braarudosphaera bigelowii*, *Chiasmolithus grandis*, *Coccolithus eopelagicus*, *Coccolithus formosus*, *Daktylethra punctulata*, *Discoaster tanii nodifer*, *Helicosphaera lophota*, *Lanternithus minutus*, *Micrantholithus procerus*, *Pemma basquensis*, *P. papillatum*, *P. rotundum*, *Pontosphaera multipora*, *P. ocellata*, *Reticulofenestra dictyoda*, *R. scrippsae*, *R. umbilicus* and *Zygrhablithus bijugatus*. The key species *Chiasmolithus solitus*, *Cyclicargolithus reticulatus* and *Helicosphaera reticulata* are also present, suggesting correlation with the Middle Eocene foraminiferal zone P12. Several species of planktic foraminiferids from the type section of the Porpoise Bay Formation, indicating Early Eocene age (zone P6), were recorded earlier by Quilty (1974a), and later augmented (Quilty, 1978) by others including a few index forms indicative of Middle Eocene age (P11–P13 zonal interval) from the same section. Quilty (1978) accepted the Middle Eocene age which was supported by both nannofossil and dinoflagellate data.

Quilty (1978) described an unnamed 'Upper Eocene' unit from the offshore South Perth Basin (in the Challenger No. 1 well, Fig. 1), in addition to recording its foraminiferids. This unit was named the Challenger Formation by Cockbain & Hocking (1989). The type section of the Challenger Formation in the Challenger No. 1 well consists of 67 m of chalk, calcarenite and chert, disconformably overlying the Kings Park Formation, and disconformably overlain by an unnamed Upper Miocene unit. The foraminiferal determinations (and consequently the age) of the type section of the Challenger Formation are based on two samples of ditch cuttings, taken at 15 m interval. According to Quilty (1978), the planktic foraminiferal species *Chiloguembelina cubensis*, *Hantkenina alabamensis*, *H. primitiva*, *Pseudohastigerina micra*, *Tenuitella gemma* (reported as *Globorotalia*), *Globorotalia*

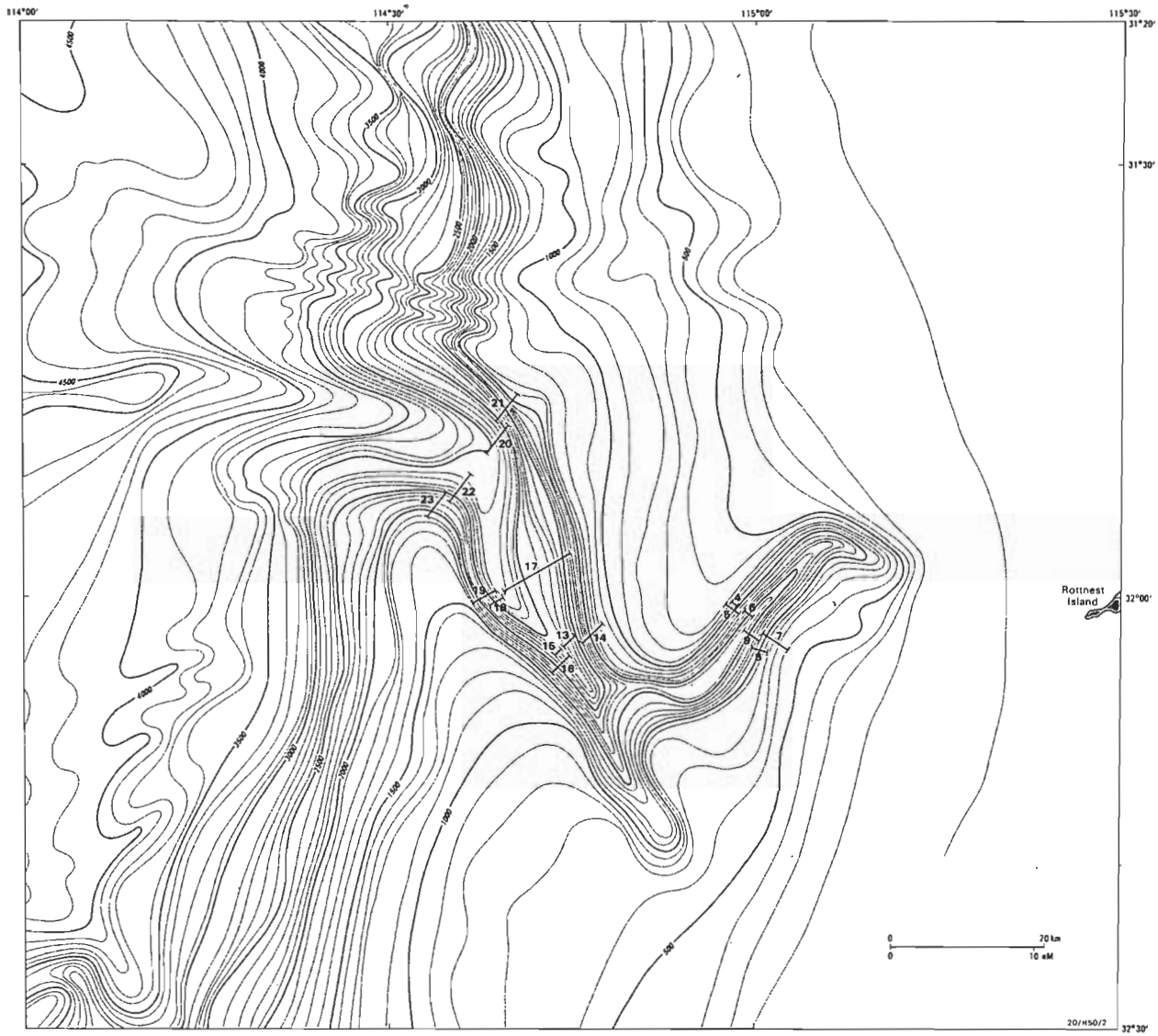

Figure 2. The Fremantle Canyon, South Perth Basin, showing location of dredge samples studied.

cerroazulensis, G. opima nana, Subbotina linaperta, Acarinina primitiva (reported as *Pseudoquadrina*), *Globorotaloides suteri* and *Catapsydrax pera* are restricted to the lower sample (which is probably from about 7 m from the base of the formation). *Globigerinatheka index index, G. subconglobatus luterbacheri, Globigerina corpulenta, G. eocenica* and *Subbotina angiporoides* occur in both samples (see Quilty, 1978, fig. 2). These faunal lists include not only Upper Eocene species and several other species known to range into the Upper Eocene (such as *Hantkenina primitiva* and *Globigerinatheka index index*; see, e.g., Blow, 1969, 1979; McGowran, 1978), but also species indicative of Middle Eocene age (see below).

The key species *Acarinina primitiva* is known to disappear below the Upper Eocene in southern Australia (McGowran, 1978; see also discussion in Shafik (1983) about correlating the extinction datum of this species within the Middle Eocene zone P13) and elsewhere (Blow, 1969, 1979; Stainforth & others, 1975; Jenkins, 1985; Toumarkine & Luterbacher, 1985). Significantly, it is among the species restricted to the lower sample. Because of the problems of downhole contamination associated with the study of ditch cuttings, it is generally accepted that the tops of species stratigraphic ranges are the best reliable biostratigraphic evidence. Consequently, the presence of *Acarinina primitiva* suggests that the basal part of the type section of the Challenger Formation is likely to be Middle Eocene (zone P13 or P14), in spite of the apparent association of species indicating a younger age (which can be attributed to downhole contamination).

The planktic foraminiferids restricted to the higher sample (15 to 30 m below the upper boundary of the type Challenger Formation) include *Globorotalia opima opima, Globigerina officinalis, G. praebulloides praebulloides, Catapsydrax martini martini* and *C. unicavus* (see Quilty, 1978, fig. 2). *Globorotalia opima opima*, an Oligocene species (Blow, 1969, 1979; Stainforth & others, 1975; Bolli & Saunders, 1985), cannot be regarded as a result of downhole contamination from the overlying unit because foraminiferids of the latter unit are Late Miocene as dated by Quilty (1978). Therefore, *G. opima opima* is regarded as a good indication that the uppermost part of the type section of the Challenger Formation is Oligocene. The presence of *Subbotina angiporoides* (in the higher sample, Quilty, 1978) may also support an (Early) Oligocene age. The type section of the Challenger Formation covers the Middle Eocene to the (Early) Oligocene (Fig. 3; see also below). *Hantkenina primitiva* has a very short range within the Upper Eocene of southern Australia, disappearing either late in zone

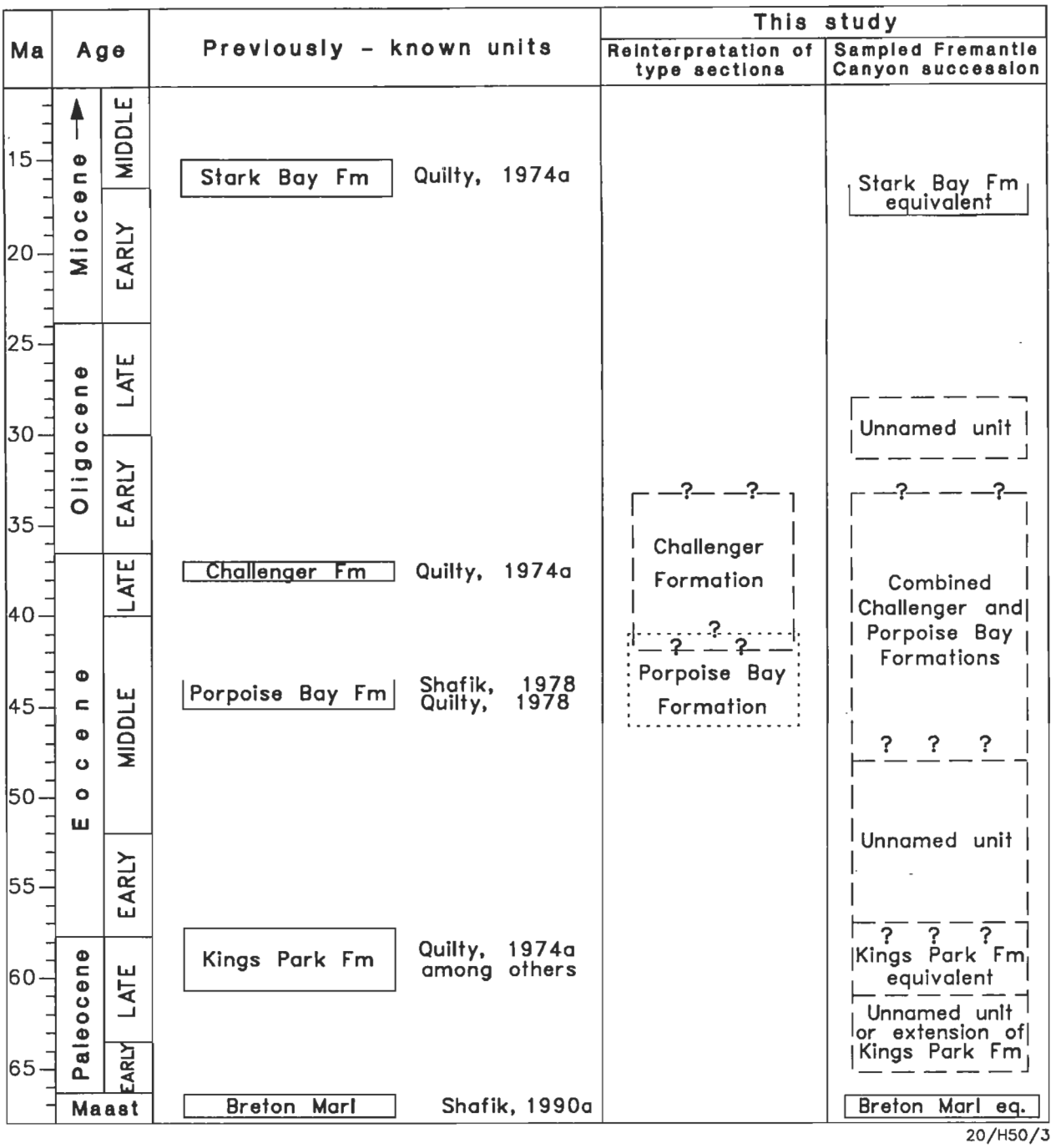

Figure 3. The Maastrichtian–Middle Miocene stratigraphy of the South Perth Basin.

P15 (McGowran, 1986) or within zone P16 (Shafik, 1981). Its presence in the lower sample (and absence from the higher sample) in the type section of the Challenger Formation in the Challenger No. 1 well (Quilty, 1978, fig. 2) suggests that the middle part of this section includes an Upper Eocene segment (probably spanning zones P15 and P16). (Because of its association with *Acarinina primitiva*, *Hantkenina primitiva* is regarded as a downhole contaminant from the middle part of the section, being absent from the higher sample.) *Globigerinatheka subconglobata luterbacheri* ranges elsewhere from the top of zone P13 to within zone P16 (Toumarkine & Luterbacher, 1985). Its presence in the lower sample supports the age assignment of Middle to Late Eocene for a substantial part of the type section of the Challenger Formation, as concluded above from the presence of both *Acarinina primitiva* and *Hantkenina primitiva*; correlation with the foraminiferal zonal interval P14–P16 can be thus demostrated. The occurrence of *Globigerina praebulloides praebulloides*, which is known to be restricted to the Late Eocene zonal interval P15–P16 (Blow, 1969, 1979) in the higher sample, shows an Upper Eocene part (P16 above the extinction of *Hantkenina primitiva*) extending to the level of the higher sample, and points to a thin Oligocene. Quilty (1978) correlated the planktic foraminiferids from the type section of the Challenger Formation with the Late Eocene P16 zone, though he referred the lower sample to the P15–P16 zonal interval in his figure 2.

It is my opinion that the choice of the type section of the Challenger Formation from the Challenger No. 1 well (Cockbain & Hocking, 1989) is unfortunate, because of the lack of adequate material to date it more precisely. This 67 m section was apparently not cored and probably not more than two

samples of ditch cuttings were taken. The Challenger Formation was originally intended as an Upper Eocene unit. Reinterpretation of its planktic foraminiferids indicates that it ranges from the Middle Eocene through to within the (Early) Oligocene (see Fig. 3).

Late Cretaceous to Early Oligocene nannofossil assemblages from the Fremantle Canyon

The distribution of the calcareous nannofossils recovered from most of the Fremantle Canyon dredges (Checklists 1, 2) and the illustrations in this paper (Figs 5, 6, 8–12) are based on optical microscopic examination of smear slides. In the discussion below, the assemblages are arranged in chronological order. Nannofossil biostratigraphic assignments made below (see also Figs 4, 5) are to datum intervals (DI) rather than zones, in order to avoid difficulties inherent in the usage of formally defined zonations; see Shafik (*in* Shafik & Chaproniere, 1978) and Shafik (1990a,b) on the reasons for preferring the use of the concept of datum interval. (The symbols * and + are used to denote lowest and highest occurrences of species respectively when naming a datum interval.) Correlations with the foraminiferal P and N zones are made when possible. This facilitates comparison of results obtained here with those based on planktic foraminiferids, either from the same material (Apthorpe *in* Marshall & others, 1989), or from other sections elsewhere in the Perth Basin (e.g. Quilty, 1974a, 1978).

Late Maastrichtian (Breton Marl equivalent)

Three samples (80DR/020–9 to -11; see Fig. 2 for location) of light to medium grey, fairly soft calcilutite were dredged from the northeastern wall of the Fremantle Canyon. These contained rich nannofossil assemblages (see Checklist 1). The presence of the age-diagnostic species *Nephrolithus frequens*, *Cribrosphaerella daniae* and *Lithraphidites quadratus* in all three samples suggests a Late Maastrichtian age, and that these samples are from the same stratigraphic unit. The overall composition of the assemblages suggests cool to cold surface waters, and deposition on the shelf or upper continental slope. The solution-prone *Kamptnerius magnificus* (Roth, 1973) is present in two of these samples.

Discussion. The evidence of age and depositional palaeoenvironment derived from the Fremantle Canyon samples matches similar evidence in land-based assemblages from the Breton Marl (Shafik, 1990a). The latter contain more solution-prone taxa (such as *Calculites obscurus* and *Acuturris scotus*), which suggests shallower depositional depths. Thus, the canyon samples represent the offshore equivalent of the Breton Marl, notwithstanding the more calcareous nature of these samples.

It is worth noting that the nannofossil key species for the latest Maastrichtian, *Micula prinsii* (Perch-Nielsen, 1979), was not found in either the onshore Breton Marl (Shafik, 1990a) or its offshore equivalent in the Fremantle Canyon. This apparent absence could indicate a hiatus at the Cretaceous/Tertiary boundary. *M. prinsii* was found in reworked Miria Marl at the base of the Paleocene Boongerooda Greensand, in the Giralia Anticline north of the Carnarvon Basin (Shafik, 1990a), but it is highly likely that this species preferred warmer waters than those in the South Perth Basin.

Early Paleocene (no known onshore equivalent)

Three assemblages, corresponding to three biostratigraphic levels, are described below.

Assemblage A. Sample 80DR/014–5, a grey friable to well-cemented glauconitic calcilutite dredged from the northern wall of the canyon (Fig. 2), yielded a fairly well-preserved nannofossil assemblage. The assemblage is an admixture of Late Cretaceous and Early Paleocene forms (see Checklist 1). The Late Cretaceous forms are diversified. They include Late Maastrichtian species, such as the key species *Nephrolithus frequens*. The Paleocene forms are fewer in number of species. They include *Cruciplacolithus asymmetricus* and *Ericsonia subpertusa*. *Thoracosphaera operculata* and *Markalius astroporus* are also present. The assemblage is assigned to the Early Paleocene biostratigraphic interval, immediately below the lowest occurrence of *Cruciplacolithus tenuis* (Fig. 4). A correlation with the foraminiferal zone late P1b is indicated.

Remarks. It is interesting to note that Apthorpe (*in* Marshall & others, 1989) assigned sample 80DR/014–5 an age of Late Campanian to Maastrichtian, based on the foraminiferal species *Gublerina cuvillieri*. Evidently the foraminiferids are extremely rare in this sample, and what Apthorpe picked was the reworked part. This is consistent with the nannofossil evidence of a high percentage of reworked Upper Cretaceous nannofossil elements in the sample.

Assemblage B. Sample 80DR/014–10, a grey soft calcilutite, contains a very rich, moderately well-preserved nannofossil assemblage, dominated by species of *Cruciplacolithus* but including a large number of rare reworked Late Cretaceous species. The assemblage is assigned to the Early Paleocene biostratigraphic DI:**Chiasmolithus inconspicuus*/**Ellipsolithus macellus* (see Fig. 4), on the presence of *C. inconspicuus* and *Cruciplacolithus tenuis* (see Fig. 5). This assignment suggests a correlation with the foraminiferal zone early P1c. The foraminiferal evidence of *Nuttallides truempi* and high planktic percentage (Apthorpe *in* Marshall & others, 1989), and the notable absence of pentaliths and other nannofossil shallow-water indicators, suggest that deposition was probably on the continental slope.

Assemblage C. Sample 80DR/020–08, a grey friable calcilutite dredged from the northeastern wall of the canyon (Fig. 2), contains a moderately well-preserved assemblage, with *Chiasmolithus edentulus* but without species of *Fasciculithus* and *Sphenolithus* (see Checklist 1). Reworked Upper Cretaceous forms are very rare, and are apparently confined to a few species. The assemblage is assigned to the Early Paleocene biostratigraphic DI:**Chiasmolithus edentulus*/**Fasciculithus tympaniformis* (Fig. 4), which correlates with the foraminiferal zonal interval P2–P3a.

Discussion. The three samples examined above are thought to represent biostratigraphic levels unknown from the onshore sequence of the Perth Basin. Our current knowledge confines the onshore Kings Park Formation to the Late Paleocene–Early Eocene interval. There are two alternative interpretations regarding these Lower Paleocene levels: (1) they are a new unit (or units) separate from the Kings Park Formation, or (2) they are a part of the offshore Kings Park Formation, i.e. the lower boundary of the Kings Park Formation becomes older offshore, suggesting that this formation is transgressive.

The apparent absence of basal Paleocene assemblages below the lowest occurrence of *Cruciplacolithus asymmetricus* (Fig. 4) lends some support to the notion of a biostratigraphic gap at the Cretaceous/Tertiary boundary.

Age	Calcareous nannofossil biostratigraphic events	(Foraminiferal P zones)	Dredges and Rock units	
Early Eocene	+*Fasciculithus* spp.	(early P6b)		
	* *Tribrachiatus bramlettei; Discoaster diastypus*		80DR/020-06	Kings Park Formation equivalent
Late Paleocene	* *Campylosphaera eodela*	(P5/P6 boundary)	80DR/021-05	
	* *Discoaster multiradiatus*	(late P4)	80DR/017-03	
	* *Discoaster nobilis;* * *Heliolithus riedelii*	(mid P4)	80DR/014-12 80DR/014-13	
			80DR/005-08 80DR/005-09 80DR/014-03 80DR/016-02 80DR/016-03 80DR/022-03	
	* *Discoaster mohleri*	(early P4)	80DR/004-02 80DR/014-08	
	* *Toweius pertusus*	(early P4)		
Early Paleocene	* *Cruciplacolithus frequens*	(late P3b)		Unnamed new unit(s) or old phase of Kings Park Formation
	* *Heliolithus kleinpellii*	(mid P3b)		
	* *Fasciculithus tympaniformis*	(P3a/P3b boundary)		
	* *Chiasmolithus edentulus*	(P2)	80DR/020-08	
	* *Ellipdolithus macellus*	(mid P1c)		
	* *Chiasmolithus inconspicuus*		80DR/014-10	
	* *Cruciplacolithus tenuis*	(earliest P1c)		
	* *Cruciplacolithus asymmetricus*	(late P1b)	80DR/014-05	
	* *Cruciplacolithus primus*	(early P1b)		
	* *Biantholithus sparsus*			
Late Maastrichtian	* *Micula prinsii*		80DR/020-09 80DR/020-10 80DR/020-11	Breton Marl
	* *Nephrolithus frequens*			
Middle Maastrichtian: A disconformity in the onshore sequence (Shafik,1990a)				

* *Lowest occurrence* + *Highest occurrence* 20/H50/6

Figure 4. Calcareous nannofossil biostratigraphic assignment of Fremantle Canyon dredges and their lithostratigraphic assessment — Late Cretaceous to Early Eocene.

Late Paleocene–Early Eocene (Kings Park Formation equivalent)

A large number of samples from several dredge stations yielded abundant nannofossils which are mainly Late Paleocene in age. Assemblages recorded from these samples (Checklist 1) are assignable to at least five nannofossil biostratigraphic datum intervals, being bracketed by the lowest occurrence of *Toweius pertusus* and the highest occurrence of species of *Fasciculithus*. These assemblages represent a fairly continuous nannofossil biostratigraphic sequence, which may be equated with the foraminiferal zonal interval P4–early P6b (Fig. 4). Consequently, they are regarded as the offshore equivalent of the Kings Park Formation, although some of these assemblages are slightly older than those recorded by Shafik (1978) from onshore occurrences. Reworking from Cretaceous source(s) is minimal, in terms of number of species and samples containing them. The assemblage from sample 80DR/014–8 includes a

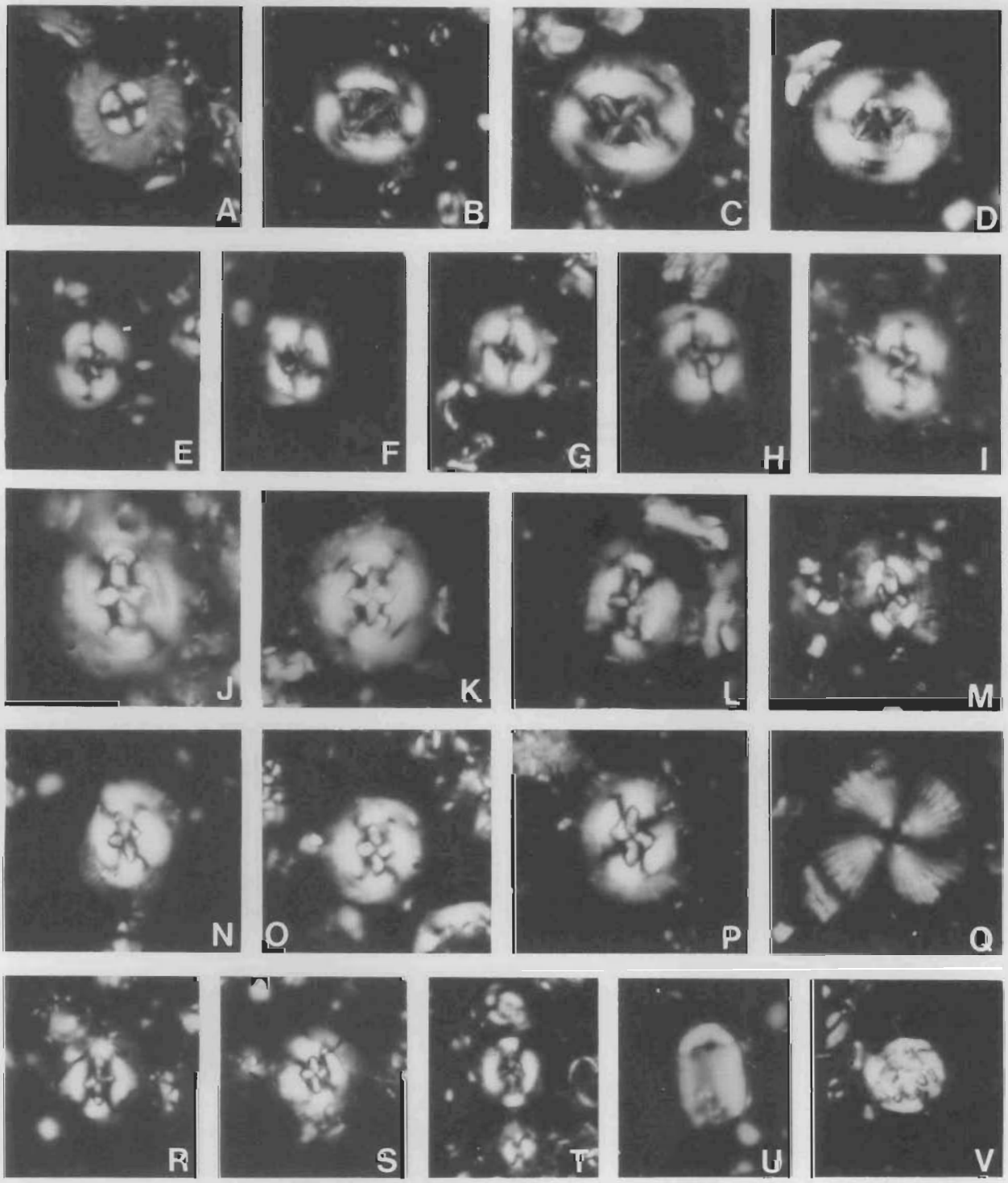

Figure 5. Optical microscopic micrographs of Palaeogene nannofossil taxa from the Fremantle Canyon, South Perth Basin.
A, *Markalius astroporus* (Stradner), CPC 30247 from 80DR/014–10; **B,** *Chiasmolithus edentulus* van Heck & Prins, CPC 30248 from 80DR/014–08; **C, D,** *Chiasmolithus bidens* (Bramlette & Sullivan), C, CPC 30249, D, CPC 30250, both from 80DR/005–08; **E–G,** *Chiasmolithus inconspicuus* van Heck & Prins, E, CPC 30251, F, CPC 30252, G, CPC 30253, all from 80DR/014–10; **H,** *Chiasmolithus edwardsii* (Romein), CPC 30254 from 80DR/014–10; **I,** *Chiasmolithus danicus* (Brotzen), CPC 30255 from 80DR/014–10; **J, K,** *Cruciplacolithus frequens* (Perch-Nielsen), J, CPC 30256, K, CPC 30257, both from 80DR/014–08; **L,** *Cruciplacolithus tenuis* (Stradner), CPC 30258 from 80DR/014–10; **M,** *Cruciplacolithus latipons* Romein, CPC 30259 from 80DR/014–05; **N–P,** *Cruciplacolithus asymmetricus* van Heck & Prins, N, CPC 30260 from 80DR/014–05, O, CPC 30261 from 80DR/014–10, P, CPC 30262 from 80DR/014–05; **Q,** *Heliolithus kleinpellii* Sullivan, CPC 30263 from 80DR/005–08; **R–T,** *Cruciplacolithus primus* Perch-Nielsen, R, CPC 30264 from 80DR/014–05, S, CPC 30265 from 80DR/014–05, T, CPC 30266 from 80DR/014–10; **U,** *Lapideacassis* sp., CPC 30267 from 80DR/014–05; **V,** *Thoracosphaera operculata* Bramlette & Martini, CPC 30268 from 80DR/014–10.
All specimens ×2000.

few reworked Upper Cretaceous species, but the exceptionally high abundance of *Placozygus sigmoides* suggests a possible reworking from a Lower Paleocene source as well.

Only one assemblage is possibly Early Eocene. This was recovered from sample 80DR/020–6. It is assigned to the (broad) Late Paleocene–Early Eocene DI:**Campylosphaera eodela*/+*Fasciculithus* spp. (Fig. 4), because there is uncertainty regarding the presence or absence of typical *Discoaster diastypus*. Nevertheless, the occurrence of both *Fasciculithus involutus* and *Transversopontis pulcher* in the presence of *Discoaster multiradiatus* and *Campylosphaera eodela* suggests proximity to the base of the Eocene. The assemblages of the other samples are Late Paleocene (see Fig. 4).

Warm-water species of the genus *Discoaster* are either rare or absent in those samples below the lowest occurrence of *Discoaster multiradiatus* in Figure 4. On the other hand, individual specimens of the species of the genera *Chiasmolithus* and *Cruciplacolithus*, which are thought of as more suited to cool surface waters, are abundant in most of the assemblages below sample 80DR/017–3 (as stacked in Fig. 4). These two observations suggest that, for most of the Late Paleocene, surface waters were cool in the Perth Basin. Conversely, specimens of *Discoaster* are abundant in the younger assemblages containing the index species *Discoaster multiradiatus*, suggesting some warming during the latest Paleocene and earliest Eocene in the basin. Similar evidence for this trend is apparent in assemblages from the onshore Kings Park Formation (Shafik, 1978).

Pentaliths (such as *Braarudosphaera bigelowii* and *Micrantholithus* spp.) and other hemipelagic species (such as *Hemihololithus kerabyi* or *Zygrhablithus bijugatus*) are common in most of the assemblages, suggesting that the offshore equivalent of the Kings Park Formation was deposited mainly on the shelf and upper slope (neritic to upper bathyal environments); the nannofossil evidence from onshore occurrences of the formation suggested nearshore environments (Shafik, 1978).

Discussion. The data presented above indicate that the offshore equivalent of the Kings Park Formation is widespread along the walls of the Fremantle Canyon. The presence in these offshore occurrences of levels older than the onshore (type) Kings Park Formation indicates that the formation is transgressive.

The samples representing the offshore equivalent of the Kings Park Formation in the present study (listed in Fig. 4) are grey

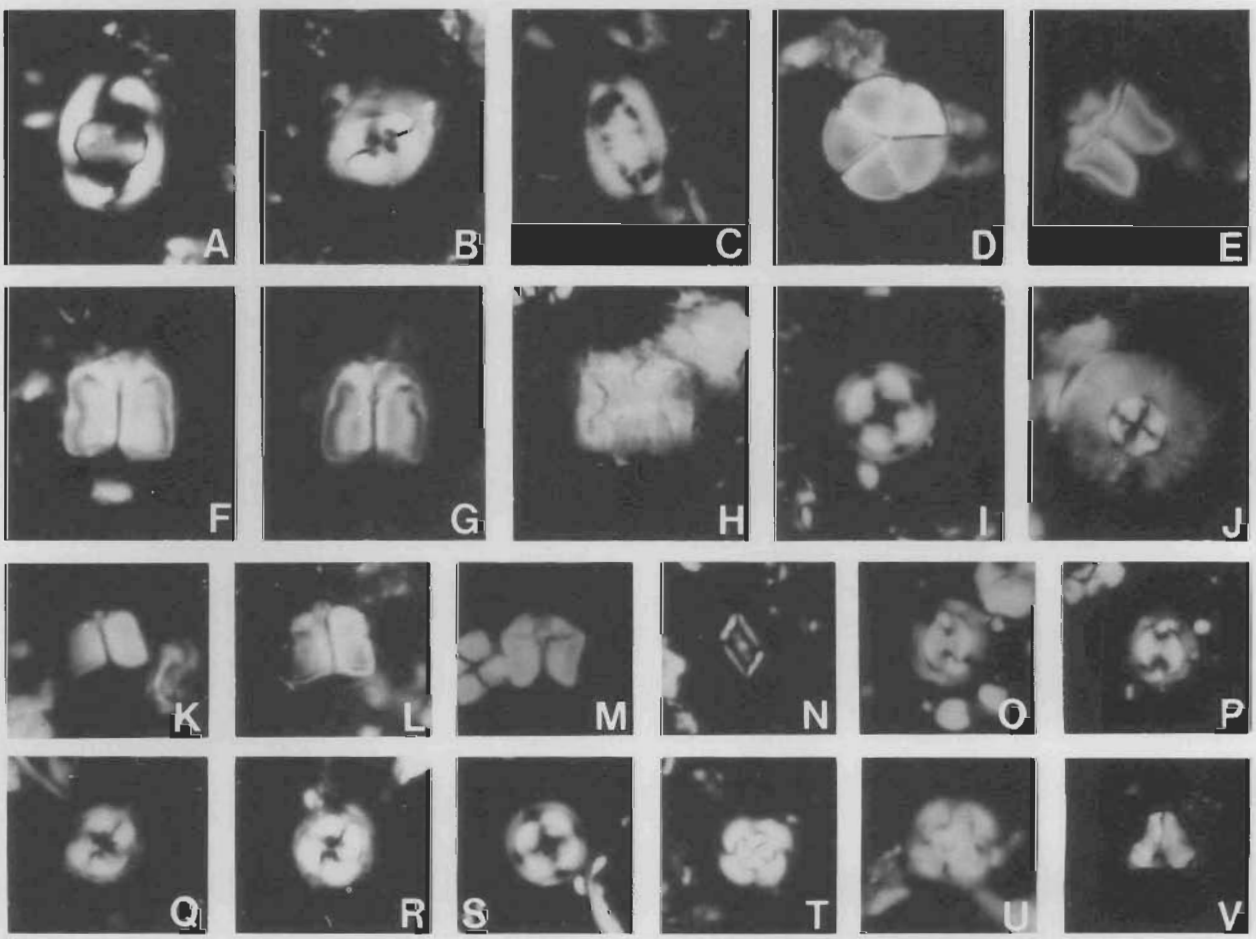

Figure 6. Optical microscopic micrographs of Paleocene nannofossil taxa from the Fremantle Canyon, South Perth Basin.
A, *Zygodiscus adamas* Bramlette & Sullivan, CPC 30269 from 80DR/005–08; **B**, *Toweius eminens* (Bramlette & Sullivan), CPC 30270 from 80DR/005–08; **C**, *Ellipsolithus distichus* (Bramlette & Sullivan), CPC 30271 from 80DR/005–08; **D**, *Braarudosphaera discula* Bramlette & Riedel, CPC 30272 from 80DR/005–08; **E, M**, *Fasciculithus ulii* Perch-Nielsen, E, CPC 30273, M, CPC 30274, both from 80DR/014–08; **F**, *Fasciculithus involutus* Bramlette & Sullivan, CPC 30275 from 80DR/005–08; **G, L**, *Fasciculithus bobii* Perch-Nielsen, G, CPC 30276, L, CPC 30277, both from 80DR/005–08; **H**, *Fasciculithus* sp., CPC 30278 from 80DR/005–08; **I, S**, *Ericsonia subpertusa* Hay & Mohler, I, CPC 30279, S, CPC 30280, both from 80DR/014–10; **J**, *Markalius astroporus* (Stradner), CPC 30281 from 80DR/014–10; **K**, *Fasciculithus tympaniformis* Hay & Mohler, CPC 30282 from 80DR/005–08; **N**, *Scapholithus rhombiformis* Hay & Mohler, CPC 30283 from 80DR/005–08; **O, P**, *Prinsius bisulcus* (Stradner), O, CPC 30284, P, CPC 30285, both from 80DR/020–08; **Q, R**, *Toweius pertusus* (Sullivan), Q, CPC 30286, R, CPC 30287, both from 80DR/005–08; **T**, *Cyclagelosphaera alta* Perch-Nielsen, CPC 30288 from 80DR/014–05; **U**, *Cyclagelosphaera reinhardtii* (Perch-Nielsen), CPC 30289 from 80DR/014–10; **V**, *Semihololithus kerabyi* Perch-Nielsen, CPC 30290 from 80DR/005–08.
All specimens ×2000.

calcilutites with some calcarenites, occasionally siliceous but mostly glauconitic, which vary mainly in their degree of induration. Thus the Kings Park Formation becomes siliceous and much more calcareous offshore.

The terrigenous aspect and the great thickness of the type section of the Kings Park Formation was viewed by Shafik (1978) as a result of a high rate of sedimentation, largely from the nearby mainland. This also explained the uniformity of the microfauna and microflora of the formation in the Perth metropolitan area. The terrigenous components were thought to be contributed by a river system (Shafik, 1978) which is probably related to the now submerged drainage system of the old Swan River (Quilty, 1974b; Playford & others, 1975, 1976). Evidently, these components did not reach the depositional sites now occupied by the Fremantle Canyon, where the formation is highly calcareous. This conclusion is consistent with the bathymetry of the shelf area west of Perth. There is no channel between the mouth of the Swan River (Perth area) and the head of the Fremantle Canyon which occurs at the shelf break (Fig. 1; see also Marshall & others, 1989; Quilty & others, in press). The onshore part of the Kings Park Formation may represent a rapid rise in sea level and culmination of the Paleocene transgression over the Perth Basin.

Samples from the offshore equivalent of the Kings Park Formation were recovered from water 700 m and 3000 m deep. As indicated above, these samples bear nannofossil elements which suggest deposition on the shelf or upper continental slope. An overall deepening is thus demonstrated since the Early Eocene in the area of the Fremantle Canyon.

Early to (early) Middle Eocene (no known onshore equivalent)

Nannofossil assemblages representing the Early to (early) Middle Eocene in the offshore succession in the South Perth Basin came from a large number of samples (Fig. 7, Checklist 2) collected from nine dredge stations, the youngest sample being 80DR/019–4. These assemblages seem to form a continuous nannofossil biostratigraphic sequence consisting of five biostratigraphic units. This sequence is bracketed by the disappearance of *Fasciculithus* spp. and the appearance of *Nannotetrina fulgens*, and may be correlated with the foraminiferal zonal interval P6b–P10 (see Fig. 7).

Biostratigraphic unit A. This is the oldest unit in the sequence. It is based on three samples (80DR/018–1, 80DR/014–14, 80DR/020–7; see Fig. 2 for location) of grey, soft to weakly-cemented calcilutite which were collected from the southern, northern and northeastern walls of the Fremantle Canyon. This unit predates the lowest occurrence of the index species *Tribrachiatus orthostylus* (see Fig. 7), and is characterised by the presence of several Eocene-originated species (such as *Chiasmolithus eograndis, C. grandis, Coccolithus formosus*) among a suite of Paleocene-originated species (such as *Ellipsolithus macellus, Toweius pertusus* and *T.? magnicrassus*). Forms transitional between *Discoaster multiradiatus* and *D. barbadiensis* are present. A correlation with the foraminiferal zone P6b is indicated (see Fig. 7). Very scarce reworked Cretaceous forms were noted among the assemblages of this biostratigraphic unit (see Checklist 2).

Biostratigraphic unit B. This unit is also based on three samples (80DR/020–5, 80DR/017–1, 80DR/003–6; see Fig. 2 for location) — chalky and weakly-cemented calcilutites — which were dredged from the northeastern wall of the Fremantle Canyon and from the continental slope to its north. Two other samples (80DR/003–1, 80DR/003–9), fairly well-cemented calcarenites from the continental slope to the north of Perth, should possibly be included in this unit. The reason for the uncertainty is the poor preservation of the already rare fossils in these two samples; the presence of abundant calcite rhombs indicates recrystallisation.

Assemblages forming this biostratigraphic unit predate the lowest occurrence of *Discoaster lodoensis*, and are characterised by the presence of the index species *Tribrachiatus orthostylus* (Figs 7, 8). Forms transitional between *Discoaster multiradiatus* and *D. barbadiensis* persist. Specimens of the genus *Discoaster* are appreciably more abundant than those of the genera *Chiasmolithus* and *Cruciplacolithus*, particularly in sample 80DR/017–1. This suggests some warming during the Early Eocene biostratigraphic DI:**Tribrachiatus orthostylus*/**Discoaster lodoensis* (foraminiferal zonal interval late P6b–late P7).

The index species *Tribrachiatus orthostylus* was not encountered in samples 80DR/003–1 and 80DR/003–9, but rare *Cyclicargolithus gammation* was found in the latter sample.

Biostratigraphic unit C. This unit is based on an assemblage recovered from sample 80DR/003–2, a greenish grey, glauconitic calcarenite from the continental slope north of Perth. This assemblage contained the index species *Discoaster lodoensis*, without *D. sublodoensis*.

Biostratigraphic units D and E. Based on the available data, by far the most widespread (and probably the thickest) part of the offshore Eocene succession in the Perth Basin is apparently that with the many nannofossil assemblages containing *Discoaster sublodoensis* (Fig. 7). This key species was found in the two highest biostratigraphic units of the Lower to basal Middle Eocene sequence under discussion. The younger of these units, being discriminated by the presence of *Rhabdosphaera inflata*, is based on an assemblage from sample 80DR/019–4, a grey, soft calcilutite dredged from the southwestern wall of the Fremantle Canyon (Fig. 2). The nannofossil assemblage from 80DR/019–4 is correlated with the Middle Eocene foraminiferal zone P10, whereas the assemblages from the older biostratigraphic unit (with *Discoaster sublodoensis*) are correlated with the Early Eocene foraminiferal zone P9.

The biostratigraphic unit with *Discoaster sublodoensis* and without *Rhabdosphaera inflata* is based on assemblages from six samples of grey calcarenite and calcilutite which were dredged from the southern and northeastern walls of the Fremantle Canyon (Fig. 2) and from the continental slope to its north. Of these, the assemblage in sample 80DR/023–1C is of particular interest: it includes forms transitional between *Discoaster sublodoenis* and *D. saipanensis*, with some being typical *D. saipanenis*. The vertical ranges of the latter species and of *D. sublodoensis* do not usually overlap. Other members of the assemblage in sample 80DR/023–1C (such as *Cyclicargolithus gammation, Campylosphaera dela, Discoasteroides kuepperi, Discoaster lodoensis, Lophodolithus* spp. and *Reticulofenestra dictyoda*) are those normally present in the biostratigraphic DI:**D.sublodoensis*/**Rhabdosphaera inflata*.

Discussion. The Early to early Middle Eocene biostratigraphic sequence discussed above has no known counterpart in onshore sections. Assemblages from the basal part of the Porpoise Bay Formation in the Rottnest Island Bore (data in Shafik, 1978) are referable to the biostratigraphic DI:**Reticulofenestra umbilicus*/**Cyclicargolithus reticulatus* and the slightly younger DI:**Cyclicargolithus reticulatus*/**Reticulofenestra scissura*. These assemblages together correlate with the foraminiferal zone late P12 and probably with early P13, and are substantially younger than the youngest level in the Lower–Middle Eocene sequence discussed above. This sequence,

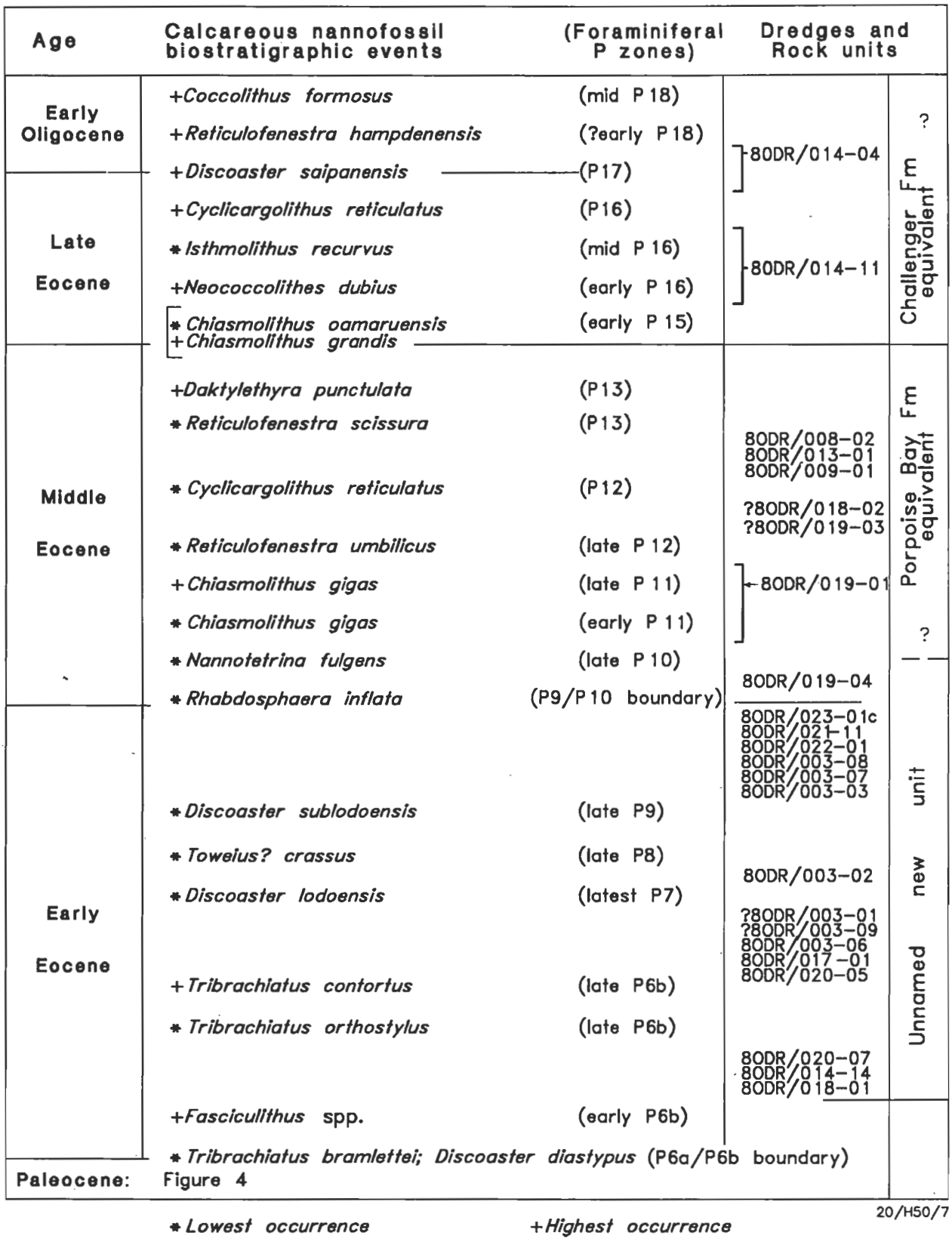

Figure 7. Calcareous nannofossil biostratigraphic assignment of Fremantle Canyon dredges and their lithostratigraphic assessment — Early Eocene to Early Oligocene.

therefore, is considered to represent an unnamed new unit, consisting of calcilutites and calcarenites. The nannofossil evidence given above suggests that it is exposed at many locations in the Fremantle Canyon and also on the continental slope to its north.

Differentiation between this unnamed new unit and the offshore equivalent of the Kings Park Formation may pose a problem, because of similar lithologies. A good nannofossil working criterion for the separation of these two formations is the disappearance (highest occurrence) of species of the genus

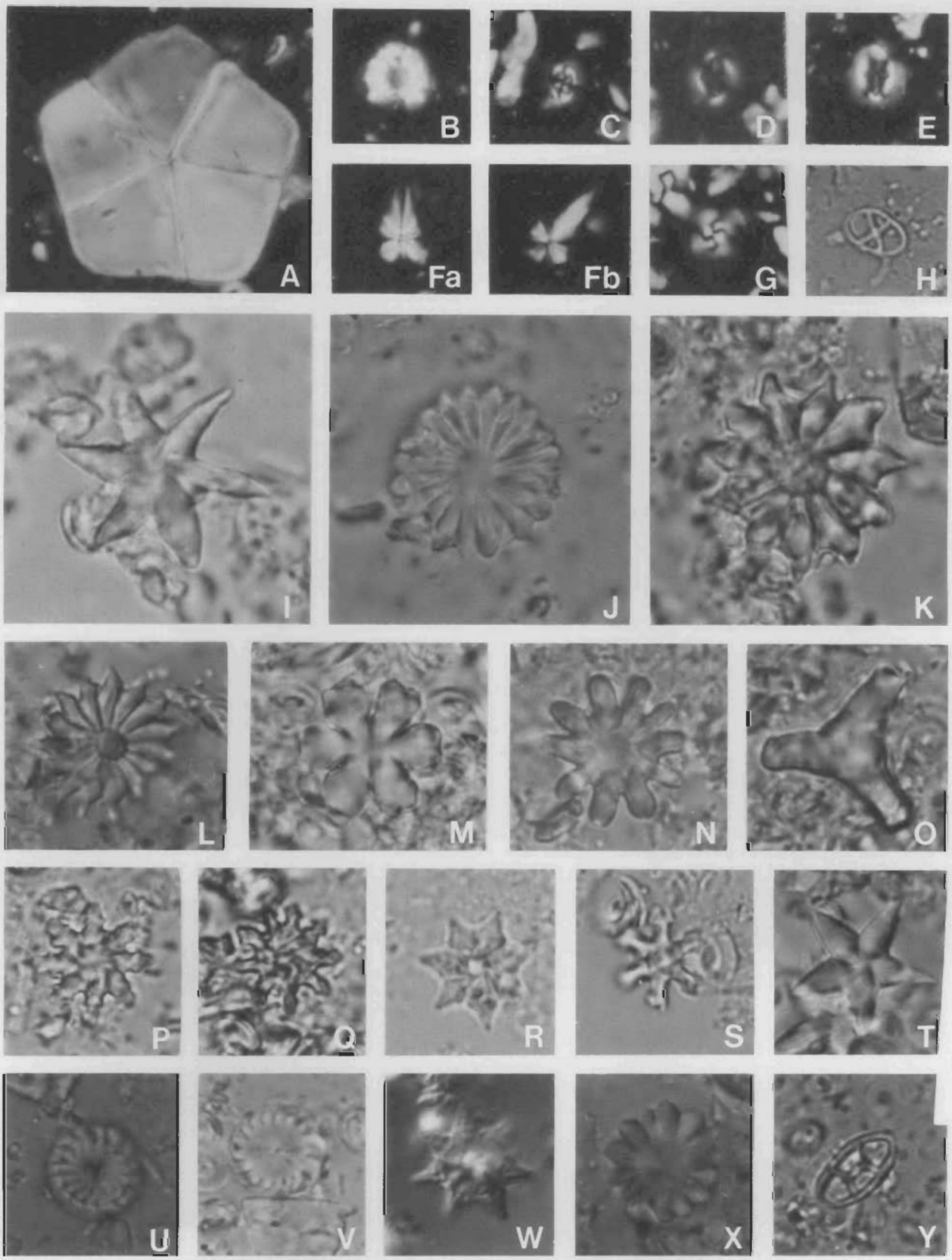

Figure 8. Optical microscopic micrographs of Palaeogene nannofossil taxa from the Fremantle Canyon, South Perth Basin.
A, *Braarudosphaera bigelowii* (Gran & Braarud), CPC 30291 from 80DR/020–05; **B,** *Daktylethra punctulata* Gartner, CPC 30292 from 80DR/009–01; **C,** *Chiasmolithus titus* Gartner, CPC 30293 from 80DR/003–03; **D, E,** *Cruciplacolithus* sp., D, CPC 30294 from 80DR/020–05, E, CPC 30295 from 80DR/003–06; **Fa, Fb,** *Sphenolithus radians* Deflandre, CPC 30296 from 80DR/019–01; **G,** *Cyclicargolithus gammation* (Bramlette & Sullivan), CPC 30298 from 80DR/003–03; **H,** *Neococcolithes protenus* (Bramlette & Sullivan), CPC 30297 from 80DR/020–05; **I,** *Discoaster lodoensis* Bramlette & Riedel, CPC 30299 from 80DR/003–03; **J,** a form transitional between *Discoaster multiradiatus* Bramlette & Riedel and *D. barbadiensis* CPC 30300 from 80DR/003–06; **K, L,** *Discoaster barbadiensis* Tan Sin Hok, K, CPC 30301 from 80DR/003–06, L, CPC 30302 from 80DR/020–05; **M,** *Discoaster deflandrei* Bramlette & Riedel, CPC 30303 from 80DR/022–04; **N,** *Discoaster mediosus* Bramlette & Sullivan, CPC 30304 from 80DR/003–06; **O,** *Tribrachiatus orthostylus* Shamarai, CPC 30305 from 80DR/003–06; **P, Q,** *Discoaster binodosus* Martini, P, CPC 30306, Q, CPC 30307, both from 80DR/020–05; **R, W,** *Discoaster saipanensis* Bramlette & Riedel, R, CPC 30308 from 80DR/014–11, W, CPC 30313 from 80DR/019–01; **S,** *Discoaster distinctus* Martini, CPC 30309 from 80DR/019–01; **T,** *Discoaster sublodoensis* Bramlette & Sullivan, CPC 30310 from 80DR/003–08; **U, V,** *Discoaster* sp., U, CPC 30311, V, CPC 30312, both from 80DR/020–05; **X,** *Discoaster mohleri* Bukry & Percival, CPC 30314 from 80DR/005–08; **Y,** *Neococcolithes dubius* (Deflandre), CPC 30315 from 80DR/020–05.
All specimens ×2000.

Fasciculithus. The Kings Park Formation, as it is currently known, contains species of *Fasciculithus*, which are notably absent from assemblages of the unnamed new (mainly) Lower Eocene unit; species of *Fasciculithus* are also absent from the new Lower Paleocene levels described above (see Fig. 4).

Minor reworking from Cretaceous and probably Paleocene sources can be detected in the unnamed new (mainly) Lower Eocene unit, particularly among the assemblage from sample 80DR020–5.

Middle Eocene (Porpoise Bay Formation equivalent)

Several Middle Eocene assemblages were extracted from samples obtained from four dredge stations in the Fremantle Canyon (Checklist 2). These are assignable to three biostratigraphic units.

Biostratigraphic unit A. Sample 80DR/019–1, a grey, soft calcilutite from the southwestern wall of the canyon (Fig. 2), yielded a particularly well-preserved assemblage. This included the key Middle Eocene species *Nannotetrina fulgens* and abundant *Chiasmolithus* spp. but not *C. gigas*. The short vertical range of *C. gigas* is used to subdivide the biostratigraphic interval between the lowest occurrences of *Nannotetrina fulgens* and *Reticulofenestra umbilicus* into three biostratigraphic divisions (Fig. 7; see also Bukry, 1973). However, it is difficult to determine whether this assemblage belongs to the biostratigraphic division below or above the range of *Chiasmolithus gigas*. The assemblage from 80DR/019–1 is correlated with the foraminiferal zonal interval P11–P12 (Fig. 7).

Biostratigraphic unit B. Samples 80DR/019–3 and 80DR/018–2, well-cemented calcilutites from the southwestern wall of the canyon (Fig. 2), yielded moderately well-preserved assemblages which included Middle Eocene species of *Nannotetrina* and forms of *Reticulofenestra* approaching the typical *R. umbilicus*. These assemblages are tentatively placed in the biostratigraphic DI:**Reticulofenestra umbilicus*/**Cyclicargolithus reticulatus* (foraminiferal zone P12). Deposition was on the shelf or upper continental slope, as indicated by the presence of several species including *Zygrhablithus bijugatus crassus*.

In the assemblage of 80DR/019–3, specimens of *Chiasmolithus solitus* are more abundant than specimens of *Discoaster*. This suggests conditions for cool to cold surface-waters.

Biostratigraphic unit C. Assemblages recovered from the calcarenites and calcilutites of samples 80DR/009–1, 80DR/013–1 and 80DR/008–2, which were obtained from the southeastern and northern walls of the canyon (Fig. 2), are diverse. They contain the index species *Cyclicargolithus reticulatus* (see Checklist 2 and Fig. 9). These assemblages are assigned to the biostratigraphic DI:**Cyclicargolithus reticulatus*/**Reticulofenestra scissura*, and a correlation with the foraminiferal zonal interval late P12–early P13 is made (see Fig. 7). Each of these assemblages has a large number of Upper Cretaceous nannofossil species, suggesting a substantial reworking episode from Cretaceous source(s). This contrasts with the levels above and below, where reworked nannofossils are non-existent, very minor, or from Paleocene rather than from Upper Cretaceous sources.

Species indicative of deposition on the shelf or upper continental slope (neritic or upper bathyal environments) are common in the assemblages from samples 80DR/009–1, 80DR/013–1 and 80DR/008–2. These include *Braarudosphaera bigelowii, Daktylethra punctulata, Lanternithus minutus, Micrantholithus procerus, Pemma papillatum, Pontosphaera plana* and *Zygrhablithus bijugatus crassus*. As the samples were dredged over a range of present-day water depths from 850 m to 2500 m, deepening must have occurred since the Middle Eocene at the sites of these dredge stations (Fig. 2), probably mainly due to subsidence of the seafloor.

Discussion. The basal metre of the type section of the Porpoise Bay Formation, as defined by Cockbain & Hocking (1989), was not studied by Shafik (1978) who reported on the lower part of that section. The nannofossil content of the lower part of the Porpoise Bay Formation in the Rottnest Island Bore is therefore known except for that single metre at the base. The recorded assemblages from the Rottnest Island Bore equate well with the assemblages from the Fremantle Canyon samples 80DR/009–1, 80DR/013–1 and 80DR/008–2. The older Middle Eocene assemblages from samples 80DR/019–1, 80DR/019–3 and 80DR/018–2 (see above; Fig. 7) either equate with the unknown assemblages of the basal metre, or have no counterparts in the type section of the Porpoise Bay Formation, because they are older. The assemblage from sample 80DR/019–4, dated as earliest Middle Eocene, is still older than the assemblage from sample 80DR/019–1, and is thought to represent the upper part of an unnamed (mainly Lower Eocene) unit, underlying the equivalent of the Porpoise Bay Formation (see Fig. 7).

The type section of the Porpoise Bay Formation in the Rottnest Island Bore consists of brown calcareous shale and siltstone, whereas the Middle Eocene equivalent of the formation (samples 80DR/009–1, 80DR/013–1 and 80DR/008–2) in the canyon succession is apparently a sequence of intercalating fine calcarenites and calcilutites. Obviously, the formation becomes more calcareous further offshore, and probably cannot be discriminated lithologically from both the underlying and overlying carbonates in the Fremantle Canyon succession.

Based on occurrences of Upper Cretaceous nannofossils in the lower part of the type section of the Porpoise Bay Formation, as well as at contemporaneous levels elsewhere along the western and southern margins of Australia (Carnarvon, Eucla and Otway Basins), Shafik (1985) indicated a widespread reworking episode during the Middle Eocene. This was linked to some important events occurring south of Australia, such as major acceleration in the seafloor spreading rate and initiation of a short-lived strong bottom current. The occurrence of a large number of reworked Upper Cretaceous nannofossils in the Middle Eocene equivalent of the Porpoise Bay Formation in

Figure 9. Optical microscopic micrographs of Eocene nannofossil taxa from the Fremantle Canyon, South Perth Basin.
A, *Coccolithus eopelagicus* (Bramlette & Riedel), CPC 30316 from 80DR/009–01; **B, H,** *Toweius?* sp. cf. *T. crassus* (Bramlette & Sullivan), B, CPC 30317, H, CPC 30318, both from 80DR/003–06; **C,** *Coccolithus formosus* (Kamptner), CPC 30319 from 80DR/009- 01; **D,** *Nannotetrina cristata* (Martini), CPC 30320 from 80DR/019–01; **E,** *Cyclicargolithus reticulatus* (Gartner & Smith), CPC 30321 from 80DR/008–02; **F,** *Reticulofenestra dictyoda* (Deflandre), CPC 30322 from 80DR/019–01; **G,** *Cyclicargolithus gammation* (Bramlette & Sullivan), CPC 30323 from 80DR/003–03; **I,** *Pontosphaera plana* (Bramlette & Sullivan), CPC 30324 from 80DR/003–06; **Ja, Jb,** *Rhabdosphaera solus* Perch-Nielsen, CPC 30325 from 80DR/003–03; **K, L,** *Blackites spinulus* (Levin), K, CPC 30326, L, CPC 30327, both from 80DR/019–01; **M,** *Transversopontis fimbriatus* (Bramlette & Sullivan), CPC 30328 from 80DR/019–01; **N,** *Naninfula* sp., CPC 30329 from 80DR/003–06; **O,** *Zygrhablithus bijugatus bijugatus* (Deflandre), CPC 30330 from 80DR/019–01; **P, Q,** *Rhabdosphaera pseudomorionum* Locker, P, CPC 30331, Q, CPC 30332, both from 80DR/019–01; **Ra, Rb,** *Sphenolithus radians* Deflandre, CPC 30333 from 80DR/019–01; **S,** *Chiasmolithus grandis* (Bramlette & Riedel), CPC 30334 from 80DR/019–01; **T–V,** *Nannotetrina fulgens* (Stradner), T [*Nannotetrina alata* (Martini) of some authors] CPC 30335, U, CPC 30336, V, CPC 30337, all from 80DR/019–01.
All specimens ×2000.

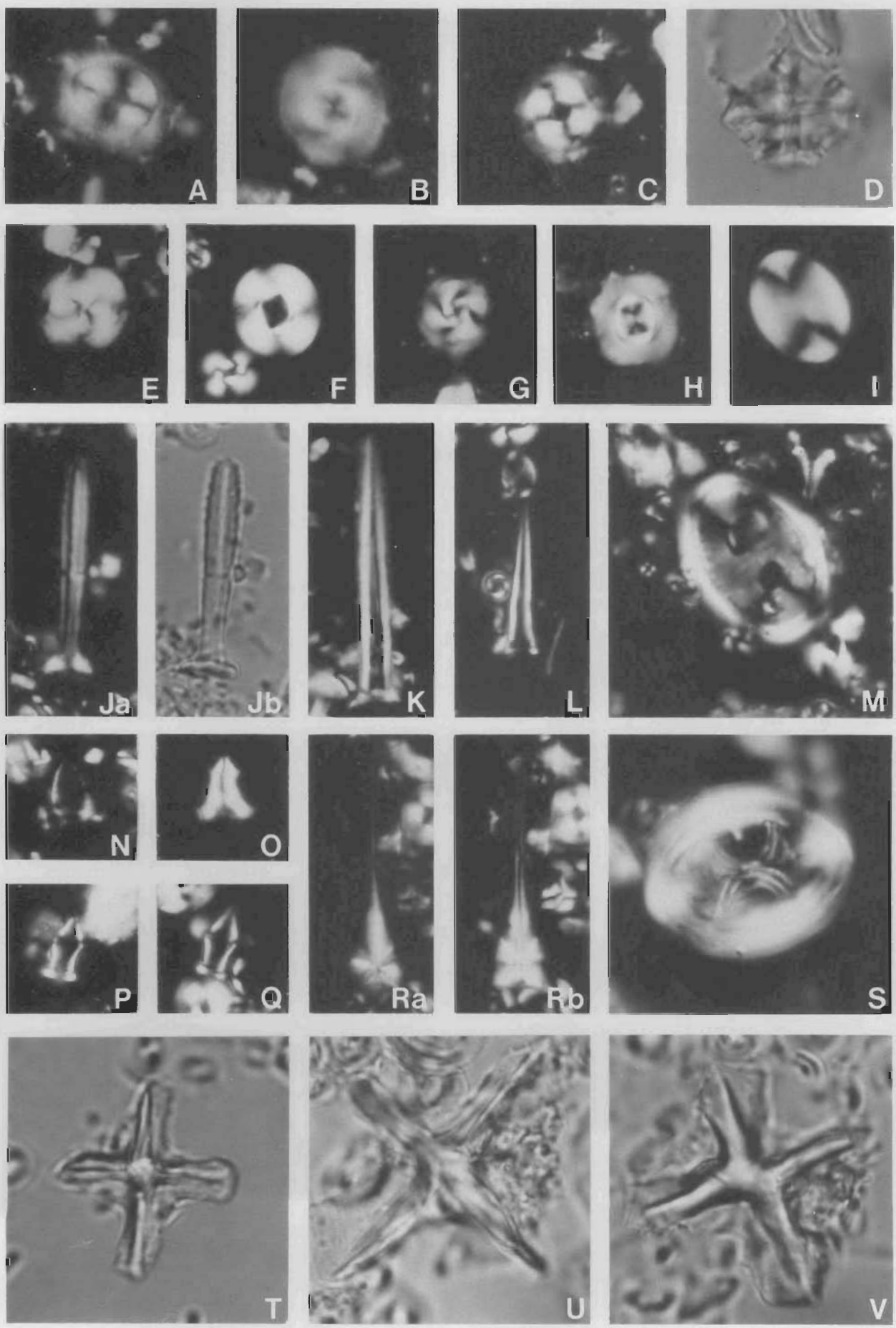
A
B
C
D
E
F
G
H
I
Ja
Jb
K
L
M
N
O
P
Q
Ra
Rb
S
T
U
V

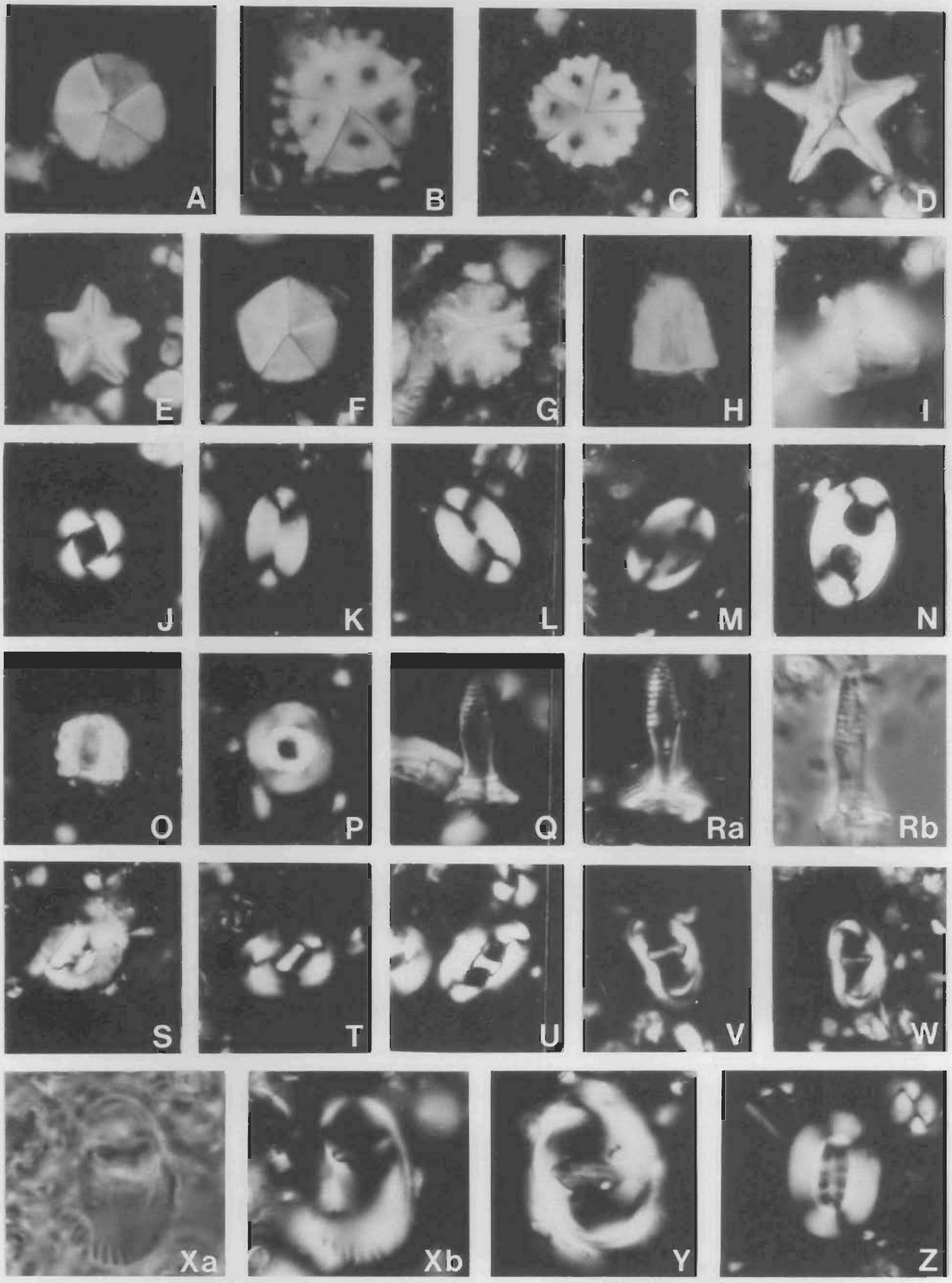

Figure 10. Optical microscopic micrographs of Eocene nannofossil taxa from the Fremantle Canyon, South Perth Basin.
A, *Braarudosphaera discula* Bramlette & Riedel, CPC 30338 from 80DR/003–06; **B,** *Pemma papillatum* Martini, CPC 30339 from 80DR/009–01; **C,** *Pemma basquensis* (Martini), CPC 30340 from 80DR/009–01; **D,** *Micrantholithus entaster* Bramlette & Sullivan, CPC 30341 from 80DR/020–05; **E,** *Micrantholithus flos* Deflandre, CPC 30342 from 80DR/003–06; **F,** *Micrantholithus crenulatus* Bramlette & Sullivan, CPC 30343 from 80DR/003–06; **G, H,** *Micrantholithus altus* Bybell & Gartner, G, CPC 30344, H, CPC 30345 both from 80DR/009–01; **I,** *Braarudosphaera orthia* Bybell & Gartner, CPC 30346 from 80DR/020- 05; **J,** *Reticulofenestra dictyoda* (Deflandre), CPC 30347 from 80DR/019–01; **K,** *Pontosphaera plana* (Bramlette & Sullivan), CPC 30348 from 80DR/019–01; **L,** *Pontosphaera ocellata*

the canyon succession (samples 80DR/009–1, 80DR/013–1 and 80DR/008–2) helps confirm the wide geographic evidence of that reworking episode.

Late Eocene (Challenger Formation)

Sample 80DR/014–11, a grey, fairly well-cemented calcilutite dredged from the northern wall of the Fremantle Canyon (Fig. 2), yielded a poorly-preserved Late Eocene nannofossil assemblage (Checklist 2). The Late Eocene age is based on the co-occurrence of the index species *Chiasmolithus oamaruensis* and *Cyclicargolithus reticulatus*. Signs of dissolution abound (but not in all preparations examined from the sample), and some reworking from Paleocene source(s) was detected. Neither *Neococcolithes dubius* nor the index species *Isthmolithus recurvus* was encountered; the stratigraphic ranges of these two species are usually exclusive. The assemblage can be assigned to either the biostratigraphic DI:**Chiasmolithus oamaruensis*/**Isthmolithus recurvus* or to the broader DI: **Chiasmolithus oamaruensis*/+*Cyclicargolithus reticulatus*.

The former assignment, being pre-*I. recurvus*, assumes that the absence of *Neococcolithes dubius* is due to preservational factors. On the other hand, the absence of *I. recurvus* may signify an exclusion due to ecological factors such as warm surface waters. The presence of *Sphenolithus pseudoradians*, without the association of other warm-water species such as *Discoaster barbadiensis* in the assemblage from 80DR/014–11, is somewhat tenuous evidence for warming. Specimens of *Discoaster saipanensis* exceed in number those of *Chiasmolithus oamaruensis* in this assemblage, which favours a possible warming.

In constrast to its absence from this assemblage, the cold-water *Isthmolithus recurvus* was encountered frequently in a younger (latest Eocene to Early Oligocene) assemblage from the same dredge haul (sample 80DR/014–4; see below). This seems to be in general agreement with the considerable cooling which occurred near the end of the Eocene (see, e.g., Kennett & von der Borch, 1985, and references therein).

The presence of *Lanternithus minutus*, *Pontosphaera plana* and *Zygrhablithus bijugatus* suggests that deposition was probably on the shelf or upper slope (outer neritic to upper bathyal environments). These taxa are prone to dissolution, and they were not found in all preparations examined from sample 80DR/014–11. Post-depositional alterations, including dissolution, apparently did not occur uniformally throughout this sample. Some reworking from Paleocene source(s) is indicated by the presence of *Chiasmolithus bidens*, *C. consuetus*, *Coccolithus robustus*, *Toweius pertusus* and *Zygodiscus herlynii*.

Remarks. The foraminiferal assemblage from sample 80DR/014–11 is almost identical to Quilty's Challenger No. 1 lower sample at 567–597 m (Apthorpe *in* Marshall & others, 1989). Quilty (1978) labelled his assemblage as 'Late Eocene, P15/16', but Apthorpe correlated the similar assemblage from sample 80DR/014–11 with the Middle Eocene zone P14 equivalent, on the presence of *Acarinina primitiva* and *A. pseudotopilensis*. These two species could be either reworked or misidentified, however, considering the younger nannofossil evidence of *Chiasmolithus oamaruensis* in the sample. In southern Australia, older levels with foraminiferal assemblages from near the base of the nannofossil species *Chiasmolithus oamaruensis* (where *Chiasmolithus grandis* and *C. oamaruensis* co-occur) are distinctly higher than the highest occurrence of the foraminiferid *Acarinina primitiva* (see Shafik, 1983).

The nannofossil assemblage from sample 80DR/014–11 can be correlated with the foraminiferal zonal interval P15/P16 (Fig. 7). This correlation indicates that the sample came from the Challenger Formation (or from the combined Porpoise Bay/Challenger Formation; see discussion below). In the light of the argument presented above for a possible warming, based on the nannofossil assemblage from the same sample, it must be noted that Quilty (1978) has pointed out that the faunas and lithology of the type section of the Challenger Formation are consistent with warm-water deposition.

Latest Eocene–Early Oligocene (Challenger Formation)

Sample 80DR/014–4, a white, moderately-cemented, chalky calcilutite dredged from the northern wall of the canyon (Fig. 2), yielded a moderately to poorly-preserved nannofossil assemblage (Checklist 2). Discoasters are relatively rare, and most are heavily calcified. The assemblage is dominated by *Reticulofenestra scissura* and *R. umbilicus*. The holococcolith taxa *Zygrablithus bijugatus* and *Lanternithus minutus* are fairly common. The key species *Isthmolithus recurvus* is frequent but all specimens encountered were heavily calcified. The absence of the rosette-shaped discoasters (*Discoaster barbadiensis* and *D. saipanensis*) and the index species *Cyclicargolithus reticulatus*, in the presence of other key species such as *Reticulofenestra hampdenensis*, *Isthmolithus recurvus* and *Coccolithus formosus*, suggests an Early Oligocene age. However, as discoasters are rare in this sample, the absence of *Discoaster barbadiensis* and *D. saipanensis* may be considered as an unreliable criterion. The assemblage is, therefore, assigned to the (broad) biostratigraphic DI: +*Cyclicargolithus reticulatus*/+*Reticulofenestra hampdenensis*, which spans the latest Eocene and earliest Oligocene (see Fig. 7). Unfortunately, the foraminiferal evidence from the same sample is not very helpful for narrowing down this age assignment. According to Apthorpe (*in* Marshall & others, 1989), the assemblage is dominated by *Globigerina ampliapertura* and *Turborotalia increbescens* which normally are found not only in Late Eocene but also in younger assemblages. Furthermore, the associated presence of very rare *Acarinina primitiva* and *A. pseudotopilensis*, which are known to disappear earlier in the Eocene, complicated the matter. (These two species of *Acarinina* in sample 80DR/014–4 are considered here either to be reworked or misidentified, based on their association with the Late Eocene–Early Oligocene nannofossil key species *Isthmolithus recurvus*. The presence of the same foraminiferids in the Upper Eocene assemblage from sample 80DR/014–11 has been treated above as a result of reworking, but their misidentification cannot be ruled out.)

The depositional environment is similar to that deduced for the Upper Eocene sample 80DR/014–11, based on the similar occurrence of *Lanternithus minutus* and *Zygrhablithus bijugatus*. However, surface waters were probably colder during the deposition of 80/DR014–4, as suggested by the

(Bramlette & Sullivan), CPC 30349 from 80DR/020–05; **M**, *Pontosphaera panarium* (Bramlette & Sullivan), CPC 30350 from 80DR/020–05; **N**, *Transversopontis pulcher* (Deflandre), CPC 30351 from 80DR/019–01; **O**, *Daktylethra punctulata* Gartner, CPC 30352 from 80DR/009–01; **P**, *Toweius?* sp. cf. *T. crassus* (Bramlette & Sullivan), CPC 30353 from 80DR/020–05; **Q**, **Ra**, **Rb**, *Rhabdosphaera galdius*, Q, CPC 30354, R, CPC 30355, both from 80DR/019–01; **S**, *Helicosphaera compacta* Bramlette & Wilcoxon, CPC 30356 from 80DR/009–01; **T**, *Helicosphaera lophota* Bramlette & Sullivan, CPC 30357 from 80DR/019–01; **U**, *Helicosphaera seminulum* Bramlette & Sullivan, CPC 30358 from 80DR/019–01; **V**, **W**, *Lophodolithus reniformis* Bramlette & Sullivan, V, CPC 30359, W, CPC30360, both from 80DR/003–03; **Xa**, **Xb**, *Lophodolithus rotundus* Bukry & Percival, CPC 30361 from 80DR/019–01; **Y**, *Lophodolithus mochlophorus* Deflandre, CPC 30362 from 80DR/020–05; **Z**, *Ellipsolithus lajollaensis* Bukry & Percival, CPC 30363 from 80DR/019–01.
All specimens ×2000.

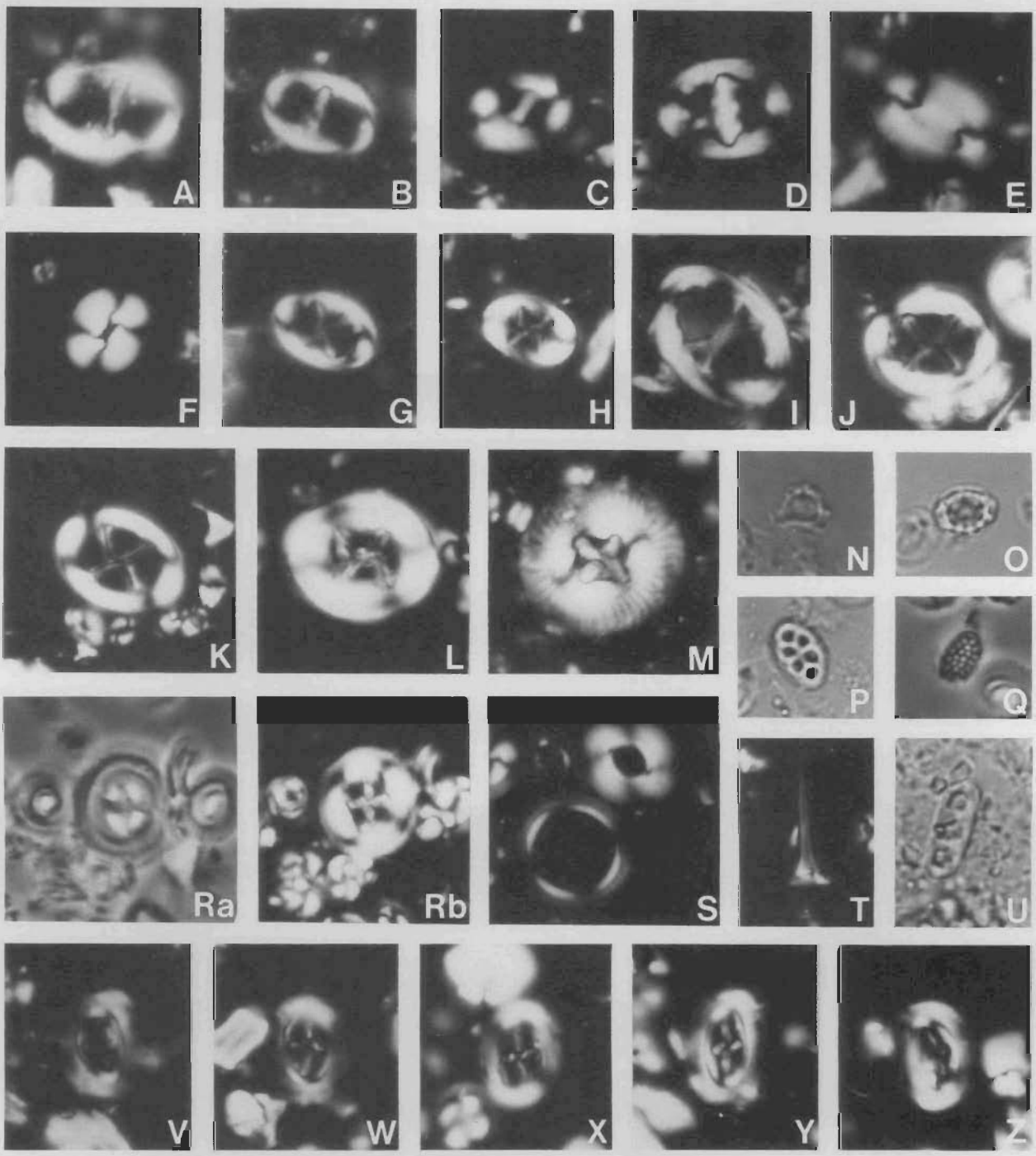

Figure 11. Optical microscopic micrographs of Eocene nannofossil taxa from the Fremantle Canyon, South Perth Basin.
A, *Lophodolithus mochlophorus* Deflandre, CPC 30364 from 80DR/003–06; **B,** *Lophodolithus nascens* Bramlette & Sullivan, CPC 30365 from 80DR/003–06; **C,** *Helicosphaera seminulum* Bramlette & Sullivan, CPC 30366 from 80DR/019–01; **D,** *Zygodiscus adamas* Bramlette & Sullivan, CPC 30367 from 80DR/003–03; **E,** *Ellipsolithus macellus* (Bramlette & Sullivan), CPC 30368 from 80DR/020–05; **F,** *Reticulofenestra* sp. cf. *R. dictyoda* (Deflandre), CPC 30369 from 80DR/019–01; **G,** *Neochiastozygus concinnus* (Martini), CPC 30370 from 80DR/003–06; **H,** *Neochiastozygus distentus* (Bramlette & Sullivan), CPC 30371 from 80DR/003–06; **I,** *Neochiastozygus junctus* (Bramlette & Sullivan), CPC 30372 from 80DR/020–05; **J, K,** *Chiasmolithus expansus* (Bramlette & Sullivan) Gartner, J, CPC 30373, K, CPC 30374, both from 80DR/019–01; **L,** *Chiasmolithus solitus* (Bramlette & Sullivan) Locker, CPC 30375 from 80DR/019–01; **M,** *Chiasmolithus californicus* (Sullivan), CPC 30376 from 80DR/020–05; **N, O,** *Orthozygus aureus* (Stradner), N, CPC 30377, O, CPC 30378, both from 80DR/019–01; **P,** *Holodiscolithus solidus* (Deflandre), CPC 30379 from 80DR/019–01; **Q,** *Holodiscolithus macroporus* (Deflandre), CPC 30380 from 80DR/019–01; **Ra, Rb,** *Birkelundia staurion* (Bramlette & Sullivan), CPC 30381 from 80DR/019–01; **S,** (upper specimen) *Reticulofenestra dictyoda* (Deflandre) CPC 30382A, (lower specimen) *Calcidiscus protoannulus* (Gartner) CPC 30382B from 80DR/019–01; **T,** *Rhabdosphaera* sp., CPC 30383 from 80DR/019–01; **U,** *Isthmolithus recurvus* Deflandre, CPC 30384 from 80DR/014–04; **V–Z,** *Campylosphaera* sp., V, CPC 30385 from 80DR/003–06, W, CPC 30386 from 80DR/003–03, X, CPC 30387 from 80DR/003–03, Y, CPC 30388 from 80DR/020–05, Z, CPC 30389 from 80DR/020–05.
All specimens ×2000.

notable absence of rosette-shaped discoasters. Thus, a comparison between the assemblages from 80DR/014–11 and 80DR/014–4 supports the possibility that the presence of *Isthmolithus recurvus* in the assemblage from 80DR/014–4 may be related to the chilling event which occurred near the end of the Eocene.

Discussion. Based on results given by Quilty (1978), Cockbain & Hocking (1989) described the Porpoise Bay Formation as Middle Eocene and the Challenger Formation as Late Eocene. This is not entirely correct (see Fig. 3). The discussion presented earlier shows that the type section of the Challenger Formation ranges from the Middle Eocene into Oligocene. Also, as discussed below, the type section of the Porpoise Bay Formation is likely to range into the Upper Eocene, with the implication that the two formations partly overlap. Quilty (1978, p. 115) raised the possibility that the Middle Eocene sediments in Rottnest Island Bore (type section of the Porpoise Formation) were 'formed during the early part of the transgression that led to the deposition of the Late Eocene sediments in Challenger No. 1' (type section of the Challenger Formation).

Both Quilty (1978) and Shafik (1978) studied the lower parts of the type section of Porpoise Bay Formation, but not its upper parts. A total of more than 100 m of sediment in the upper part of the type section of the Porpoise Bay Formation in the Rottnest Island Bore has not been studied, and the calcareous microfossil content is unknown. It is possible that this 100 m of the type Porpoise Bay Formation overlaps with the lower part of the Challenger Formation (as the latter extends into the Middle Eocene; discussed above), especially if this top 100 m of the type Porpoise Bay Formation includes an Upper Eocene interval, which is not unlikely. The nannofossil data in the present study suggest that a continuous sequence through (at least) the entire Eocene is likely in the canyon succession (see Fig. 7); only *minor* disconformities are expected within the Eocene sequence. It is thus possible that the Porpoise Bay and Challenger Formations merge into one unit in the canyon succession.

In Figure 7, the Middle/Upper Eocene boundary is *arbitrarily* used as the demarcation between equivalents of the Porpoise Bay and Challenger Formations. The similar lithologies of the canyon samples are consistent with the conclusion that the two formations merge into one unit along the walls of the canyon. Sample 80DR/014–4 is likely to have come from within the upper part of this combined (Porpoise Bay and Challenger Formations) unit.

Mid Oligocene nannofossils from the Fremantle Canyon (no known onshore equivalent)

Sample 80DR/022–4, a whitish soft calcilutite with abundant siliceous spicules dredged from the base of the southern wall of the Fremantle Canyon (Fig. 2), yielded a rich, moderately well-preserved nannofossil assemblage datable as mid Oligocene; some signs of partial dissolution are evident and discoasters are overgrown with secondary calcite. Some reworking from Eocene source(s) is apparent. The assemblage includes *Chiasmolithus altus*, (reworked) *C. eograndis, Coccolithus eopelagicus, Cyclicargolithus abisectus, C. floridanus*, (reworked) *Coccolithus formosus*, heavily calcified *Discoaster deflandrei* 'group', *Helicosphaera euphratis, H. recta*, (reworked) *Reticulofenestra hampdenensis, R. scissura, Scapholithus* sp., *Sphenolithus distentus, S. predistentus, S.* sp. aff. *S. ciperoensis, S. moriformis, Zygrhablithus bijugatus bijugatus* and *Z. bijugatus crassus*. A few specimens of severely etched *Pontosphaera plana* were also noted.

The association of the key species (illustrated in Fig. 12) *Chiasmolithus altus, Cyclicargolithus abisectus, Helicosphaera recta, Reticulofenestra scissura, Sphenolithus distentus*, and *S.* sp. aff. *S. ciperoensis* suggests a late Early Oligocene age. According to data in Martini (1971), and in the light of revised correlation by Berggren & others (1985), some elements in this association suggest correlation with the foraminiferal zone P21a. Deposition was probably on the upper continental slope (upper bathyal environment) as evinced by the rare occurrence of *Pontosphaera plana*; the presence of *Zygrhablithus bijugatus* also tends to support this conclusion. However, both *Pontosphaera plana* and *Zygrhablithus bijugatus* could be allochthonous, like some of the associated species (such as *Coccolithus formosus*), being reworked from an Eocene source(s).

Discussion

Previous biostratigraphic studies on the Tertiary sequences of the Perth Basin (e.g. Quilty, 1974a,b) suggest a significant biostratigraphic gap in the marine record, between the 'Upper Eocene' Challenger Formation and the Lower to Middle Miocene Stark Bay Formation; marine sediments of Oligocene age are apparently missing. Quilty (1977) indicated that the Oligocene period corresponds to the lowest Tertiary sea level reached along the Australian western margin. Moreover, seismic sections in the offshore area west of Perth suggested to Quilty & others (in press) that the Oligocene was a period of erosion. Accordingly, the late Early Oligocene nannofossil assemblage from sample 80DR/022–4 is a significant finding. It is regarded as being from an unnamed new unit.

Oligocene sediments containing calcareous microplanktic remains have never been recorded previously in the Perth Basin, or from nearby oceanic sections (discussed later), and very few such sediments are known from the Carnarvon Basin to the north. This suggests doubts about the wisdom of considering a new Oligocene unit, particularly with only one canyon sample (80DR/022–4) containing nannofossils of definite Oligocene age. Furthermore, planktic foraminiferids in the same sample have been interpreted as Middle Eocene in age (Apthorpe *in* Marshall & others, 1989). However, the presence of the nannofossil index species *Sphenolithus distentus* is compelling evidence for a mid Oligocene age. The associated Middle Eocene foraminiferids and their coeval nannofossils (those in the same 80DR/022–4 sample) are interpreted here as being reworked from the same source(s). The Middle Eocene section on the Naturaliste Plateau at DSDP site 264 is thought to be this source.

The truncated nature of the Eocene section at site 264 is likely to be a result of erosion; what is preserved from this section is rich with calcareous microplanktic remains (nannofossils and foraminiferids). The Eocene at site 264 is immediately overlain by Upper Miocene. It is tempting, therefore, to suggest that the Eocene section on the Naturaliste Plateau is the source for the Middle Eocene nannofossils and foraminiferids found (reworked) in the mid Oligocene assemblage in the Fremantle Canyon succession. Large scale erosion was postulated for the mid Oligocene in the Australian sector of the Southwest Pacific region (see Kennett & others, 1972; Kennett & others, 1975). It seems that during the (mid) Oligocene the Naturaliste Plateau was a site for erosion and not sedimentation; no Oligocene sediments have yet been recorded on the Naturaliste Plateau.

In the earlier discussion on the planktic foraminiferids of the Challenger Formation, the presence of both *Globorotalia opima opima* and *Subbotina angiporoides* was taken as an indication that the uppermost part of that formation is (Early) Oligocene in age; in Figure 3, the top of the type section of the

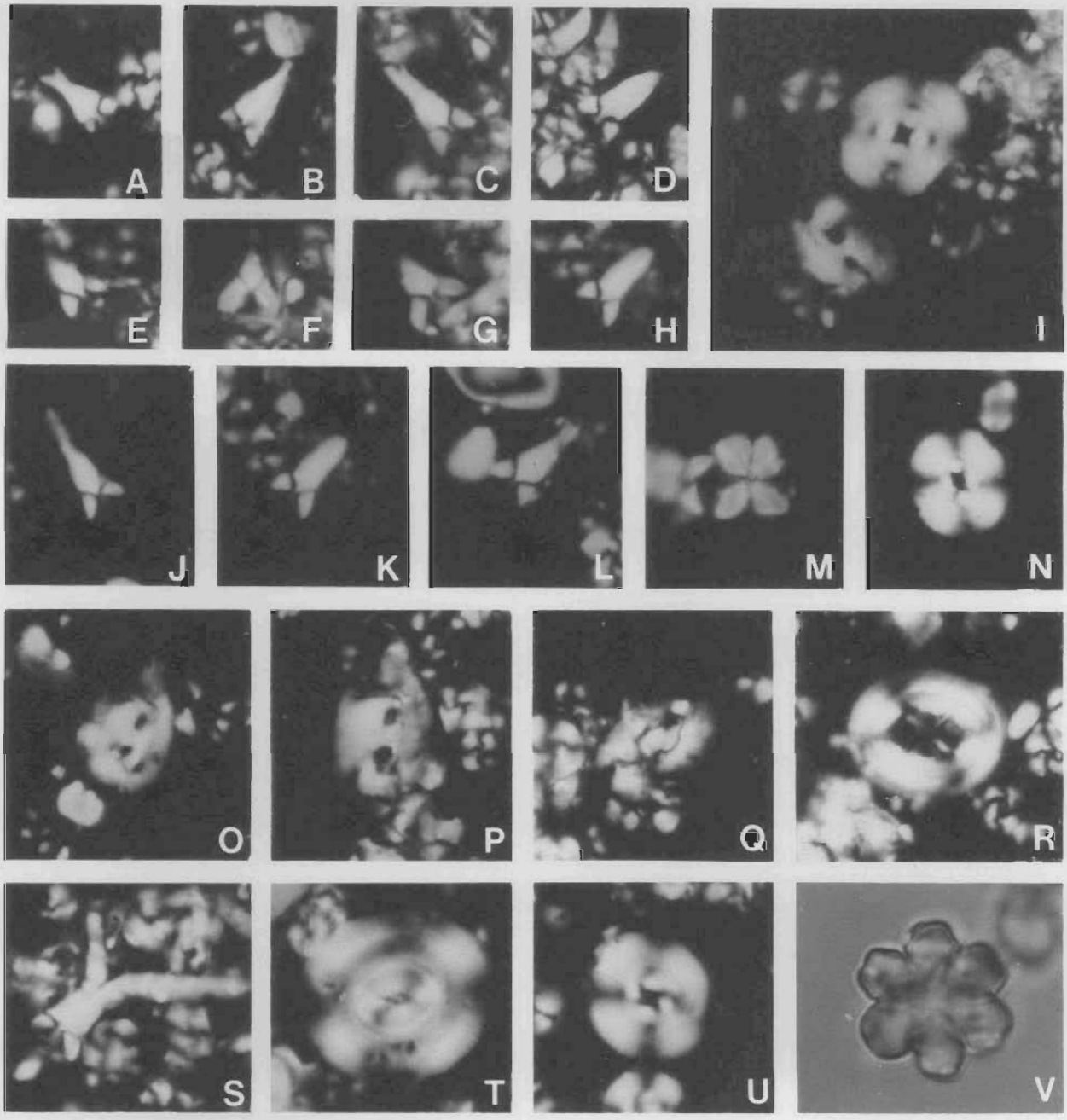

Figure 12. Optical microscopic micrographs of Oligocene nannofossil taxa from sample 80DR/022–04 from the Fremantle Canyon, South Perth Basin.

A–D, S, *Sphenolithus predistentus* Bramlette & Wilcoxon, A, CPC 30390, B, CPC 30391, C, CPC 30392, D, CPC 30393, S, CPC 30394; **E–H, J–L,** *Sphenolithus distentus* (Martini), E, CPC 30395, F, CPC 30396, G, CPC 30397, H, CPC 30398, J, CPC 30399, K, CPC30400, L, CPC 30401; **I,** (top specimen) *Cyclicargolithus abisectus* (Müller) CPC 30402A, (bottom specimen) *Helicosphaera recta* Haq CPC 30402B; **M,** *Sphenolithus moriformis* (Brönnimann & Stradner), CPC 30403; **N,** *Cyclicargolithus floridanus* (Roth & Hay), CPC 30404; **O, P,** *Helicosphaera recta* Haq, O, CPC 30405, P, CPC 30406; **Q,** *Helicosphaera euphratis* Haq, CPC 30407; **R,** *Chiasmolithus altus* Bukry & Percival, CPC 30408; **T,** *Reticulofenestra scissura* Hay, Mohler & Wade, CPC 30409; **U,** *Cyclicargolithus abisectus* (Muller), CPC 30410; **V,** *Discoaster deflandrei* Bramlette & Riedel, CPC 30411.
All specimens ×2000.

Challenger Formation is shown at a mid point within the Early Oligocene. Be this as it may, I cannot judge whether the type section of the Challenger Formation extends to the level of the mid Oligocene nannofossil assemblage recorded here, without studying the nannofossils of that formation. At this stage, I prefer to consider that the nannofossil assemblage containing *Sphenolithus distentus* (sample 80DR/022–4) is from a unit previously unreported (see Fig. 3). As indicated earlier, the type section of the Challenger Formation in the Challenger No. 1 well is inappropriate because initially it was not sampled adequately.

Early to Middle Miocene nannofossils from the Fremantle Canyon (Stark Bay Formation)

Three samples recovered from station 80DR/007, high along the southeastern wall of the Fremantle Canyon (Fig. 2), yielded poorly preserved nannofossil assemblages. The worst of these is from sample 80DR/007–1, where only a very few species could be identified. These are *Calcidiscus leptoporus, Cyclicargolithus abisectus* and *Sphenolithus moriformis*, which may collectively suggest an Early Miocene age.

Sample 80DR/007–3, a weakly-cemented calcilutite, yielded *Braarudosphaera bigelowii, B. discula, Calcidiscus leptoporus, Coronocyclus nitescens, Cyclicargolithus abisectus, C. floridanus*, heavily calcified *Discoaster* spp. (mainly members of the *D. deflandrei* 'group'), *Helicosphaera euphratis, H. kamptneri, Micrantholithus* sp., *Rhabdosphaera procera* and *Sphenolithus moriformis*. Severely etched specimens of *Pontosphaera* were also noted.

The association of *Calcidiscus leptoporus, Helicosphaera kamptneri, H. euphratis, Cyclicargolithus abisectus* and *C. floridanus* in the assemblage from 80DR/007–3 suggests an Early Miocene age. The abundant occurrence of pentaliths in this assemblage suggests shallow-water deposition on the continental shelf.

Rare nannofossils were found in preparations from the calcilutite of sample 80DR/007–2, but these include the key species *Sphenolithus heteromorphus*, whose lowest occurrence indicates a position late in the Early Miocene and a correlation within either the foraminiferal zone N6 (see Martini, 1971) or N7 (see base of the nannofossil zone CN3 relative to the N zonation in Berggren & others, 1985). The highest occurrence of *S. heteromorphus* has been placed within the foraminiferal zone N10 (data in Martini, 1971 and Berggren & others, 1986). Other nannofossils identified in 80DR/007–2 are *Braarudosphaera bigelowii, Calcidiscus leptoporus* and *Cyclicargolithus floridanus*. Deposition was on the continental shelf (probably in a nearshore environment), as shown by the presence of *Braarudosphaera bigelowii*.

Discussion

Quilty (1974a) introduced the Lower to Middle Miocene Stark Bay Formation based on material from several offshore wells west of Perth. The type section of this formation is in Gage Roads No. 2 (Fig. 1). It consists of 215 m of white bryozoan and echinodermal calcarenite, becoming brown dolomite and chert in places, especially in the lower parts. It unconformably overlies either Cretaceous sediments or the Kings Park Formation (Quilty, 1974a). Diagnostic foraminiferal species are abundant in places, mostly indicating zones N8 and N9. Based on *Globorotalia barisanensis* and *Globigerina woodi woodi* at the bottom of the formation in one section (Gage Roads No. 1; Fig. 1), zone N7 was suspected (Quilty, 1974b).

As indicated above, the nannofossil assemblage of sample 80DR/007–2 falls within the foraminiferal zonal interval N7–N10, which brackets the biostratigraphic range of the Stark Bay Formation in Gage Roads No. 1 and 2 (N7–N9). The other two (Lower) Miocene samples are probably older than sample 80DR/007–2, but lithologically similar to the Stark Bay Formation. Thus samples studied from dredge station 80DR/007 are thought to have come from the Stark Bay Formation. It is likely that this formation is a transgressive unit, having an older base in the canyon succession than in its type section (Gage Roads No. 2, Fig. 1).

Cretaceous and Tertiary sediments from nearby DSDP sites

Oceanic Cretaceous and Tertiary sediments were recovered from several Deep Sea Drilling Project sites in the Perth Abyssal Plain and on the Naturaliste Plateau, off the southwestern corner of Australia. The nannofossil data for the discussion below are derived from Thierstein (1974) for site 258, Proto-Decima (1974) for site 259, Bukry (1974, 1975) for sites 259 and 264, Hayes & others (1975) for site 264 and Shafik (1985) for site 264.

The Tertiary sections at these DSDP sites are discontinuous. At site 258, the entire Palaeogene is apparently missing, and a Santonian–Upper Miocene unconformity has been recorded. At site 259, the entire nannofossil-bearing Tertiary is represented by an Upper Paleocene–Lower Eocene section sandwiched between sediments free of nannofossils. At site 264, at least three disconformities have been recorded within the Tertiary, (a) at the base of the Tertiary (basal Tertiary being missing), (b) between the Paleocene and Eocene (Upper Paleocene and Lower Eocene are missing), and (c) between the Middle Eocene and Upper Miocene.

Cretaceous

No Maastrichtian sediments with calcareous planktic remains were recovered from the DSDP sites under discussion. The Cretaceous at site 258 is represented by a thick Albian to Santonian sequence directly underlying Upper Miocene sediments. The youngest Cretaceous nannofossils at site 259 are Albian. These Albian fossils came from a section separated from a nannofossil-bearing Paleocene above by sediments lacking nannofossils, seemingly as a result of dissolution. The youngest Cretaceous recorded from the Naturaliste Plateau is Early Campanian at site 264, based on the occurrence of *Broinsonia parca* and *Eiffellithus eximius* in core 264–11.

A widespread Late Maastrichtian transgression has been documented in onshore sediments along the Australian western margin in the Carnarvon and Perth Basins (Shafik, 1990a) and also in the offshore Fremantle Canyon (this study). This could be traced in the Great Australian Bight Basin as a marine ingression (Shafik, 1990b). It is based on occurrences of rich, moderately to well preserved nannofossils such as those recovered from the Breton Marl equivalent in the Fremantle Canyon succession. Obviously, evidence for this Late Maastrichtian transgression is lacking in the oceanic sections of the Perth Abyssal Plain and the Naturaliste Plateau. In these sections there is instead evidence for carbonate dissolution and/or disconformity. This contrast in the Upper Maastrichtian settings along both margins of Australia and in the nearby oceanic sections is probably a shelf/basin fractionation.

Paleocene

The assemblages representing the Paleocene at DSDP site 259 include the index species *Discoaster multiradiatus, D. nobilis, Fasciculithus tympaniformis, Chiasmolithus bidens* and *Placozygus sigmoides*. They suggest a Late Paleocene age, and a correlation with a level within the upper part of the Kings Park Formation, both onshore and offshore. However, the Paleocene assemblages recorded from DSDP site 264 are older than the base of the Kings Park Formation *sensu strictu*, and can be placed, in the canyon succession, between this base and the youngest Lower Paleocene level sampled at station 80DR/020 (see Fig. 4). No Paleocene sediments were recorded from DSDP site 258.

The occurrence of Upper Paleocene (and Lower Eocene, see below) marine sediments in the nearby Perth Abyssal Plain (site 259) supports the conclusion that, during the Late Paleocene–Early Eocene, there was a significant sea level rise indicated by the *onshore* Kings Park Formation which also represents the culmination of the Paleocene transgression over the Perth Basin.

Eocene

The Eocene section at DSDP site 259 spans the biostratigraphic interval from the highest occurrence of *Fasciculithus* spp. to

the lowest occurrence of *Discoaster lodoensis*, and may be correlated with the lower part of the unnamed (mainly) Lower Eocene unit of the Fremantle Canyon. The Eocene section at DSDP site 264 is more substantial, spanning the biostratigraphic interval between the lowest occurrences of *Discoaster sublodoensis* and *Cyclicargolithus reticulatus*. It may be correlated with the upper part of the unnamed (mainly) Lower Eocene unit and the lower part of the combined Porpoise Bay and Challenger Formations of the Fremantle Canyon. No Eocene sediments were reported from DSDP site 258.

At DSDP site 264, the Eocene section is overlain by Upper Miocene sediments. Assemblages from immediately below this disconformity contain the key species *Cyclicargolithus reticulatus* but no reworked Cretaceous nannofossils. They are thought to be stratigraphically from immediately below the assemblages with *C. reticulatus* and reworked nannofossils, recorded from the Fremantle Canyon succession and elsewhere on the Australian western and southern margins (see Shafik, 1985, fig. 5). In other words, levels equivalent to these widespread Middle Eocene sediments with reworked Cretaceous nannofossils were either eroded from the Eocene section on the Naturaliste Plateau or not deposited in the first place. The erosion option accords with the possibility that during the mid Oligocene the Naturaliste Plateau was the provenance for the displaced Middle Eocene nannofossils and foraminiferids found in the Oligocene of the Fremantle Canyon succession at station 80DR/022.

Oligocene

No Oligocene nannofossil-bearing sediments were reported from DSDP sites 258, 259 and 264. This increases the significance of the late Early Oligocene nannofossil assemblage recorded here from the Fremantle Canyon at station 80DR/022.

The proposed mid Oligocene erosion of the Naturaliste Plateau (resulting in deposition of Middle Eocene components within Oligocene sediments at the Fremantle Canyon) may be connected with the Oligocene unconformity recorded widely in the Southwest Pacific region at several DSDP sites.

Miocene

Calcareous nannofossils found in the Upper Miocene sediments recovered from the Naturaliste Plateau at DSDP site 258 and 264 are distinctly younger than the calcareous planktic remains of the (mainly) Middle Miocene Stark Bay Formation. At site 258, the Upper Miocene directly overlies Santonian sediments, and at site 264 the Upper Miocene rests directly on Middle Eocene sediments. No Miocene nannofossil-bearing sediments were recorded from the Perth Abyssal Plain at site 259. Recovery here between the Pleistocene (core 1) and the Eocene (core 4) was very poor, and sediments obtained lacked nannofossils.

Summary and conclusions

Material from the Fremantle Canyon and the continental slope to its north has yielded several calcareous nannofossil assemblages which were fitted within a scheme of Late Maastrichtian–Early Miocene biostratigraphic events. Most of the assemblages could be correlated with the low-latitude foraminiferal P and N zones, and were used to elucidate the lithostratigraphic succession of the canyon. In addition to the five previously-known rock units forming the Maastrichtian–Miocene succession of the Perth Basin, two (or possibly three) new units were discovered in the Fremantle Canyon succession. The recovered nannofossil assemblages also helped confirm two important physical events known to have occurred during the Late Maastrichtian and Middle Eocene in several western and southern marginal basins of Australia. The age of the type section of the Challenger Formation, given previously as Late Eocene (Quilty, 1978; Cockbain & Hocking, 1989), was revised to Middle Eocene through to (Early) Oligocene, based on reinterpretation of its planktic foraminiferids as originally listed by Quilty (1978). The Maastrichtian–Tertiary section in the Fremantle Canyon, particularly the Paleocene–Eocene part, is more complete than contemporaneous sections in the Perth Abyssal Plain at DSDP site 259, and on the Naturaliste Plateau at DSDP sites 258 and 264. For most of the Maastrichtian–Tertiary section of the canyon, deposition occurred in outer shelf and upper slope palaeoenvironments.

A widespread Late Maastrichtian transgression occurred over the Carnarvon and Perth Basins (Shafik, 1990a) and over the Great Australian Bight Basin (as marine ingression; Shafik, 1990b). Evidence for this comes from the Fremantle Canyon succession, where an equivalent of the Upper Maastrichtian Breton Marl, known previously from land-based sections in the Perth Basin (Shafik, 1990a), was indicated. The nannofossil evidence from the canyon material, suggesting that surface waters were cool to cold during the Late Maastrichtian, matches the evidence from the onshore Perth Basin material. At the nearby DSDP sites 258, 259 and 264, sediments of Maastrichtian age are either missing or represented by barren intervals. This contrast in the Maastrichtian setting between sections along the Australian western margin and in the nearby oceanic sites is probably a result of shelf/basin fractionation.

The evidence from the Fremantle Canyon points to a hiatus at the Cretaceous/Tertiary boundary, because the uppermost Maastrichtian and lowermost Paleocene appear to be missing. Onshore, the hiatus between the Cretaceous and Tertiary is more substantial, with the absence of the entire Lower Paleocene sequence.

A Lower Paleocene sequence, previously unknown in the Perth Basin, was reported in the Fremantle Canyon. Available data are not enough to decide whether this sequence is a discrete unit(s) or a part of the younger Kings Park Formation. A consequence of the preferred latter option is that the lower boundary of the Kings Park Formation becomes older offshore, suggesting that the formation is transgressive. The transgressive nature of the Kings Park Formation is also indicated by other (younger) Paleocene assemblages in the canyon. Evidently, the Kings Park Formation occurs widely along the walls of the canyon, but mainly as calcilutites. Thus, the terrigenous components of the onshore Kings Park Formation, thought to have been provided (to the Perth metropolitan area) by a river system (Shafik, 1978), did not reach the depositional sites presently occupied by the Fremantle Canyon. The lithology and age of the Kings Park Formation in the Perth metropolitan area and in the Fremantle Canyon suggest that the onshore Kings Park Formation represents a rapid rise in sea level and culmination of the Paleocene transgression over the Perth Basin; the bathymetry of the shelf area west of Perth supports this conclusion. The Lower Paleocene sequence in the canyon has no counterparts in the nearby DSDP sections in the Perth Abyssal Plain and Naturaliste Plateau (sites 259, 258 and 264), but assemblages similar to those from the upper part of the Kings Park Formation are known from the Perth Abyssal Plain at site 259.

An Early to early Middle Eocene nannofossil biostratigraphic sequence of events, previously unknown in the Perth Basin, has been constructed on the basis of assemblages dredged from the Fremantle Canyon. It suggests a new unnamed rock unit in the Perth Basin, apparently consisting of a succession of calcilutites and calcarenites. Evidently, this (mainly) Lower

Eocene unit is widespread in the Fremantle Canyon, and also occurs on the continental slope to its north. Because the lithology of the new (mainly) Lower Eocene unit and that of the offshore equivalent of the Kings Park Formation are similar, the nannofossil genus *Fasciculithus* is suggested as a good working criterion for differentiating these two rock units. *Fasciculithus* is present in the Kings Park Formation equivalent but is absent from the younger unit; it is also absent from the newly reported Lower Paleocene sediments in the canyon.

In the Fremantle Canyon succession, the Middle Eocene equivalent of the Porpoise Bay Formation, being calcarenites and calcilutites, is difficult to distinguish lithologically from the similar Upper Eocene to Lower Oligocene carbonates correlatable with the Challenger Formation. This, together with the nannofossil data presented, suggests that the Porpoise Bay and Challenger Formations merge along the walls of the canyon. The Eocene section on the Naturaliste Plateau (DSDP site 264) corresponds to the upper part of the new unnamed (mainly) Lower Eocene unit and the lower part of the combined Porpoise Bay and Challenger Formations in the Fremantle Canyon succession.

Evidence of a reworking episode during the Middle Eocene of a Cretaceous source or sources was recorded in the Fremantle Canyon succession (at a Middle Eocene level within the unit comprising the Porpoise Bay and Challenger Formations). It agrees with Shafik's (1985) similar findings at contemporaneous levels in several sections in the Perth, Carnarvon, Eucla and Otway Basins; such evidence is missing from the Eocene section of DSDP site 264 on the Naturaliste Plateau.

The presence of the key species *Isthmolithus recurvus* in the uppermost Eocene–lowermost Oligocene sediments of the Fremantle Canyon and its absence from the Upper Eocene sediments in the same section confirm a previously-known climatic scenario: chilling of the ocean near the end of the Eocene after generally warm surface-water conditions during the Late Eocene.

An unnamed mid (upper Lower) Oligocene unit was discovered from the Fremantle Canyon succession, based on a nannofossil assemblage containing the index species *Sphenolithus distentus*, and indicating a correlation with the foraminiferal zone P21a. Apparently, this unit has no counterpart elsewhere in the Perth Basin or at the nearby DSDP sites 258, 259 and 264. It fits between the Lower–Middle Miocene Stark Bay Formation and the combined (mainly Eocene) Porpoise Bay–Challenger Formation in the canyon succession, still leaving a large biostratigraphic gap between them. This mid Oligocene unit contains evidence of reworking of Middle Eocene marine sediments which were probably on the Naturaliste Plateau. The already known mid Oligocene erosional event in the Southwest Pacific region, which has been recorded by Kennett and co-workers (see, e.g., Kennett & others, 1972) in several DSDP sites in the Australian sector, was apparently felt on the Naturaliste Plateau.

The key nannofossil species *Sphenolithus heteromorphus*, found in a calcilutite sample, was used to suggest that the Stark Bay Formation was sampled. Two slightly older Miocene levels were recorded in the Fremantle Canyon succession. The base of the Stark Bay Formation apparently becomes older in a westerly direction.

Acknowledgements

I thank N.F. Exon and J.F. Marshall for their constructive criticism of the manuscript. Figures were drawn by Brian Pashley (BMR), and photographs were printed by G. Sparksman (BMR). The manuscript benefited from criticism by two anonymous reviewers.

List of calcareous nannofossils mentioned in this paper

Palaeogene species

Biantholithus sparsus Bramlette & Martini, 1964
Birkelundia staurion (Bramlette & Sullivan) Perch-Nielsen, 1971
Blackites creber (Deflandre) Sherwood, 1974
Blackites spinulus (Levin) Roth, 1970
Braarudosphaera bigelowii (Gran & Braarud) Deflandre, 1947
Braarudosphaera discula Bramlette & Riedel, 1954
Braarudosphaera orthia Bybell & Gartner, 1972
Calcidiscus leptoporus (Murray & Blackman) Loeblich & Tappan, 1978
Calcidiscus protoannulus (Gartner) Loeblich & Tappan, 1978
Campylosphaera dela (Bramlette & Sullivan) Hay & Mohler, 1967
Campylosphaera eodela Bukry & Percival, 1971
Chiasmolithus altus Bukry & Percival, 1971
Chiasmolithus bidens (Bramlette & Sullivan) Hay & Mohler, 1967
Chiasmolithus californicus (Sullivan) Hay & Mohler, 1967
Chiasmolithus consuetus (Bramlette & Sullivan) Hay & Mohler, 1967
Chiasmolithus danicus (Brotzen) van Heck & Perch-Nielsen, 1987
Chiasmolithus edentulus van Heck & Prins, 1987
Chiasmolithus edwardsii (Romein) van Heck & Prins, 1987
Chiasmolithus eograndis Perch-Nielsen, 1971
Chiasmolithus expansus (Bramlette & Sullivan) Gartner, 1970
Chiasmolithus gigas (Bramlette & Sullivan) Radomski, 1968
Chiasmolithus grandis (Bramlette & Riedel) Radomski, 1968
Chiasmolithus inconspicuus van Heck & Prins, 1987
Chiasmolithus oamaruensis (Deflandre) Hay, Mohler & Wade, 1966
Chiasmolithus solitus (Bramlette & Sullivan) Locker, 1968
Chiasmolithus titus Gartner, 1970
Chiphragmalithus acanthodes Bramlette & Sullivan, 1961
Clathrolithus ellipticus Deflandre *in* Deflandre & Fert, 1954
Clausicoccus cribellum (Bramlette & Sullivan) Prins, 1979
Coccolithus eopelagicus (Bramlette & Riedel) Bramlette & Sullivan, 1961
Coccolithus formosus (Kamptner) Wise, 1973
Coccolithus robustus (Bramlette & Sullivan) Shafik, n. comb. (basionym: *Cyclolithus? robustus* Bramlette & Sullivan, 1961, p. 141, pl. 2, figs 7a–c)
Coronocyclus nitescens (Kamptner) Bramlette & Wilcoxon, 1967
Cruciplacolithus asymmetricus van Heck & Prins, 1987
Cruciplacolithus frequens (Perch-Nielsen) Romein, 1979
Cruciplacolithus latipons Romein, 1979
Cruciplacolithus primus Perch-Nielsen, 1977
Cruciplacolithus tenuis (Stradner) Hay & Mohler *in* Hay & others, 1967
Cyclagelosphaera alta Perch-Nielsen, 1979
Cyclagelosphaera reinhardtii (Perch-Nielsen) Romein, 1979
Cyclicargolithus abisectus (Müller) Wise, 1973
Cyclicargolithus floridanus (Roth & Hay) Bukry, 1971
Cyclicargolithus gammation (Bramlette & Sullivan) Shafik, 1990b
Cyclicargolithus luminis (Sullivan) Bukry, 1971
Cyclicargolithus reticulatus (Gartner & Smith) Bukry, 1971
Daktylethra punctulata Gartner *in* Gartner & Bukry, 1969
Discoaster barbadiensis Tan Sin Hok, 1929
Discoaster binodosus Martini, 1958
Discoaster deflandrei Bramlette & Riedel, 1964
Discoaster diastypus Bramlette & Sullivan, 1961
Discoaster distinctus Martini, 1958
Discoaster falcatus Bramlette & Sullivan, 1961
Discoaster lenticularis Bramlette & Sullivan, 1961
Discoaster lodoensis Bramlette & Riedel, 1954
Discoaster mediosus Bramlette & Sullivan, 1961
Discoaster mohleri Bukry & Percival, 1971
Discoaster multiradiatus Bramlette & Riedel, 1954
A form transitional between *D. multiradiatus* and *D. barbadiensis*
Discoaster nobilis Martini, 1961
Discoaster robustus Haq, 1969
Discoaster saipanensis Bramlette & Riedel, 1954
Discoaster septemradiatus (Klumpp) Martini, 1958
Discoaster sublodoensis Bramlette & Sullivan, 1961

Discoaster tanii nodifer Bramlette & Riedel, 1954
Discoaster tanii tanii Bramlette & Riedel, 1954
Discoaster wemmelensis Achuthan & Stradner, 1969
Discoasteroides kuepperi Bramlette & Sullivan, 1961
Ellipsolithus distichus (Bramlette & Sullivan) Sullivan, 1964
Ellipsolithus lajollaensis Bukry & Percival, 1971
Ellipsolithus macellus (Bramlette & Sullivan) Sullivan, 1964
Ericsonia subpertusa Hay & Mohler, 1967
Fasciculithus alanii, Perch-Nielsen, 1971
Fasciculithus bobii, Perch-Nielsen, 1971
Fasciculithus involutus Bramlette & Sullivan, 1961
Fasciculithus lillianiae Perch-Nielsen, 1971
Fasciculithus tonii Perch-Nielsen, 1971
Fasciculithus tympaniformis Hay & Mohler *in* Hay & others, 1967
Fasciculithus ulii Perch-Nielsen, 1971
Helicosphaera compacta Bramlette & Wilcoxon, 1967
Helicosphaera dinesenii Perch-Nielsen, 1971
Helicosphaera euphratis Haq, 1966
Helicosphaera kamptneri Hay & Mohler *in* Hay & others, 1967
Helicosphaera lophata Bramlette & Sullivan, 1961
Helicosphaera recta Haq, 1966
Helicosphaera reticulata Bramlette & Wilcoxon, 1967
Helicosphaera seminulum Bramlette & Sullivan, 1961
Heliolithus cantabriae Perch-Nielsen, 1971
Heliolithus kleinpellii Sullivan, 1964
Heliolithus riedelii Bramlette & Sullivan, 1961
Holodiscolithus macroporus (Deflandre) Roth, 1970
Holodiscolithus solidus (Deflandre) Roth, 1970
Isthmolithus recurvus Deflandre *in* Deflandre & Fert, 1954
Lithostromation opersum (Deflandre) Bybell, 1975
Lanternithus minutus Stradner, 1962
Lophodolithus mochlophorus Deflandre *in* Deflandre & Fert, 1954
Lophodolithus nascens Bramlette & Sullivan, 1961
Lophodolithus reniformis Bramlette & Sullivan, 1961
Lophodolithus rotundus Bukry & Percival, 1971
Markalius astroporus (Stradner) Hay, Mohler & Wade, 1967
Markalius inversus (Deflandre) Bramlette & Martini, 1964
Micrantholithus altus Bybell & Gartner,1972
Micrantholithus attenuatus Bramlette & Sullivan, 1961
Micrantholithus crenulatus Bramlette & Sullivan, 1961
Micrantholithus entaster Bramlette & Sullivan, 1961
Micrantholithus flos Deflandre *in* Deflandre & Fert, 1954
Micrantholithus procerus Bukry & Percival, 1971
Micrantholithus vesper Deflandre *in* Deflandre & Fert, 1954
Nannotetrina cristata (Martini) Perch-Nielsen, 1971
Nannotetrina fulgens (Stradner) Achuthan & Stradner, 1969
Neochiastozygus chiastus (Bramlette & Sullivan) Perch-Nielsen, 1971
Neochiastozygus concinnus (Martini) Perch-Nielsen, 1971
Neochiastozygus denticulatus (Perch-Nielsen) Perch-Nielsen, 1971
Neochiastozygus distentus (Bramlette & Sullivan) Perch-Nielsen, 1971
Neochiastozygus junctus (Bramlette & Sullivan) Perch-Nielsen, 1971
Neochiastozygus saepes Perch-Nielsen, 1971
Neococcolithes dubius (Deflandre) Black, 1967
Neococcolithes protenus (Bramlette & Sullivan) Black, 1967
Orthozygus aureus (Stradner) Bramlette & Wilcoxon, 1967
Pedinocyclus larvalis (Bukry & Bramlette) Loeblich & Tappan, 1973
Pemma basquensis (Martini) Baldi-Beke, 1971
Pemma papillatum Martini, 1959
Pemma rotundum Klumpp, 1953
Placozygus sigmoides (Bramlette & Sullivan) Romein, 1979
Pontosphaera multipora (Kamptner) Roth, 1970
Pontosphaera ocellata (Bramlette & Sullivan) Perch-Nielsen, 1984
Pontosphaera panarium (Deflandre) Shafik, n. comb. (basionym: *Discolithus panarium* Deflandre *in* Deflandre & Fert, 1954, p. 141, text-figs 39, 40)
Pontosphaera pectinata (Bramlette & Sullivan) Sherwood, 1974
Pontosphaera plana (Bramlette & Sullivan) Haq, 1971
Prinsius bisulcus (Stradner) Hay & Mohler, 1967
Reticulofenestra dictyoda (Deflandre) Stradner *in* Stradner & Edwards, 1968
Reticulofenestra hampdenensis Edwards, 1973
Reticulofenestra samodurovii (Hay, Mohler & Wade) Roth, 1970
Reticulofenestra scissura Hay, Mohler & Wade, 1966
Reticulofenestra scrippsae (Bukry & Percival) Shafik, 1981
Reticulofenestra umbilicus (Levin) Martini & Ritzkowski, 1968
Rhabdolithus gladius Locker, 1967
Rhabdosphaera inflata Bramlette & Sullivan, 1961
Rhabdosphaera perlongus Deflandre *in* Grassé, 1952
Rhabdosphaera procera Martini, 1969
Rhabdosphaera pseudomorionum Locker, 1968
Rhabdosphaera solus Perch-Nielsen, 1971
Scapholithus fossilis Deflandre *in* Deflandre & Fert, 1954
Scapholithus rhombiformis Hay & Mohler, 1967
Semiholollithus kerabyi Perch-Nielsen, 1971
Sphenolithus anarrhopus Bukry & Percival, 1971
Sphenolithus ciperoensis Bramlette & Wilcoxon, 1967
Sphenolithus conicus Bukry, 1971
Sphenolithus distentus (Martini) Bramlette & Wilcoxon, 1967
Sphenolithus heteromorphus Deflandre, 1953
Sphenolithus moriformis (Brönnimann & Stradner) Bramlette & Wilcoxon, 1967
Sphenolithus predistentus Bramlette & Wilcoxon, 1967
Sphenolithus primus Perch-Nielsen, 1971
Sphenolithus pseudoradians Bramlette & Wilcoxon, 1967
Sphenolithus radians Deflandre in Grassé, 1952
Striatococcolithus pacificanus Bukry, 1971
Thoracosphaera operculata Bramlette & Martini, 1964
Toweius? crassus (Bramlette & Sullivan) Perch-Nielsen, 1984
Toweius eminens (Bramlette & Sullivan) Perch-Nielsen, 1971
Toweius pertusus (Sullivan) Romein, 1979
Toweius tovae Perch-Nielsen, 1971
Transversopontis fimbriatus (Bramlette & Sullivan) Locker, 1968
Transversopontis pulcher (Deflandre) Perch-Nielsen, 1967
Transversopontis pulcheroides (Sullivan) Baldi-Beke, 1971
Tribrachiatus bramlettei (Brönnimann & Stradner) Proto Decima & others, 1975
Tribrachiatus contortus (Stradner) Bukry, 1972
Tribrachiatus orthostylus Shamarai, 1963
Zygodiscus adamas Bramlette & Sullivan, 1961
Zygodiscus herlynii Sullivan, 1964
Zygrhablithus bijugatus bijugatus (Deflandre) Deflandre, 1959
Zygrhablithus bijugatus crassus Locker, 1967

Cretaceous species

Actinozygus regularis (Górka) Gartner, 1968
Acuturris scotus Wind & Wise *in* Wise & Wind, 1977
Ahmuellerella octoradiata (Górka) Reinhardt, 1967
Arkhangelskiella cymbiformis Vekshina, 1959
Arkhangelskiella orthocancellata (Bukry) Shafik, 1990a
Arkhangelskiella specillata Vekshina, 1959
Biscutum melaniae (Górka) Reinhardt, 1969
Broinsonia bukryi Shafik, 1990a
Calculites obscurus (Deflandre) Prins & Sissingh *in* Sissingh, 1977
Chiastozygus litterarius (Górka) Manivit, 1971
Corollithion exiguum Stradner, 1961
Cretarhabdus surirellus (Deflandre & Fert) Reinhardt, 1970
Cribrosphaerella daniae Perch-Nielsen, 1973
Cribrosphaerella ehrenbergii (Arkhangelsky) Deflandre *in* Deflandre & Fert, 1954
Eiffellithus eximius (Stover) Perch-Nielsen, 1968
Eiffellithus turriseiffeli (Deflandre) Reinhardt, 1965
Gartnergo obliquum (Stradner) Reinhardt, 1970
Haqius circumradiatus (Stover) Roth, 1978
Heterorhabdus sinuosus Nöel, 1970
Kampterius magnificus Deflandre, 1959
Lithraphidites carniolensis Deflandre, 1963
Lithraphidites quadratus Bramlette & Martini, 1964
Manivitella pemmatoidea (Deflandre *in* Manivit) Thierstein, 1971
Micula prinsii Perch-Nielsen, 1979
Micula staurophora (Gardet) Stradner, 1963
Nephrolithus corystus Wind, 1983
Nephrolithus frequens Górka, 1957
Placozygus fibuliformis (Reinhardt) Hoffmann, 1970
Prediscosphaera bukryi Perch-Nielsen, 1973
Prediscosphaera cretacea (Arkhangelsky) Gartner, 1968
Prediscosphaera majungae Perch-Nielsen, 1973
Prediscosphaera spinosa (Bramlette & Martini) Gartner, 1968
Prediscosphaera stoveri (Perch-Nielsen) Shafik & Stradner, 1971
Quadrum gothicum (Deflandre) Prins & Perch-Nielsen *in* Manivit & others, 1977
Reinhardtites biperforatus (Gartner) Shafik, 1979
Reinhardtites levis Prins & Sissingh *in* Sissingh, 1977
Rhagodiscus angustus (Stradner) Reinhardt, 1971
Rhagodiscus reniformis Perch-Nielsen, 1973
Tetrapodorhabdus decorus (Deflandre) Wind & Wise, 1983

Tranolithus orionatus (Reinhardt) Reinhardt, 1966
Vekshinella elliptica Gartner, 1968
Watznauria barnesae (Black) Perch-Nielsen, 1968
Zygodiscus bicrescenticus (Stover) Wind & Wise *in* Wise & Wind, 1977
Zygodiscus deflandrei Bukry, 1969

References

Berggren, W.A., Kent, D.V. & Flynn, J.J., 1985 — Jurassic to Paleogene: Part 2. Paleogene geochronology and chronostratigraphy. *In* Snelling, N.J. (editor), The chronology of the geological record. *The Geological Society, Memoir*, 10, 141–195.

Blow, W.H., 1969 — Late Middle Eocene to Recent planktonic foraminiferal biostratigraphy. *In* Brönnimann, P. & Renz. H.H. (editors), *Proceedings of the First International Conference on Planktonic Microfossils*, I, 199–421.

Blow, W.H., 1979 — The Cainozoic Globigerinida. *E.J. Brill, Leiden*, vols 1–3, pp. 1–1413.

Bolli, H.M. & Saunders, J.B., 1985 — Oligocene to Holocene low latitude planktic foraminifera. *In* Bolli, H. M. & others, Plankton stratigraphy. *Cambridge University Press, Cambridge*, 155–262.

Bukry, D., 1973 — Low-latitude coccolith biostratigraphic zonation. *In* Edgar, N.T., Saunders, J.B. & others, Initial Reports of the Deep Sea Drilling Project, 15. *U.S. Government Printing Office, Washington*, 653–711.

Bukry, D., 1974 — Coccolith stratigraphy, offshore Western Australia, Deep Sea Drilling Project Leg 27. *In* Veevers, J.J., Heirtzler, J.R. & others, Initial Reports of the Deep Sea Drilling Project, 27. *U.S. Government Printing Office, Washington*, 623–630.

Bukry, D., 1975 — Coccoliths and silicoflagellate stratigraphy near Antarctica, Deep Sea Drilling Project, Leg 28. *In* Hayes, D.E., Frakes, L.A. & others, Initial Reports of the Deep Sea Drilling Project, 28. *U.S. Government Printing Office, Washington*, 709–723.

Cockbain, A.E., 1973 — Kings Park Formation in Claremont Asylum No. 2 Bore. *Geological Survey of Western Australia, Palaeontological Report* 52/1873 (unpublished).

Cockbain, A.E. & Hocking, R.M., 1989 — Revised stratigraphic nomenclature in Western Australian Phanerozoic basins. *Geological Survey of Western Australia, Record*, 1989/15.

Coleman, P.J., 1952 — Foraminiferal investigations in the Perth Basin, Western Australia. *Journal of the Royal Society of Western Australia*, 36(1), 31–43.

Hayes, D.E. & others, 1975 — Site 264. *In* Hayes, D.E., Frakes, L.A. & others, Initial Reports of the Deep Sea Drilling Project, 28. *U.S. Government Printing Office, Washington*, 19–48.

Jenkins, D.G., 1985 — Southern mid-latitude Paleocene to Holocene planktic foraminifera. *In* Bolli, H. M. & others, Plankton stratigraphy. *Cambridge University Press, Cambridge*, 263–282.

Johnstone, M.H., Lowry, D.C. & Quilty, P.G., 1973 — The geology of southwestern Australia — a review. *Journal of the Royal Society of Western Australia*, 56, 5–15.

Kennett, J.P., Burns, R.E., Andrews, J.E., Churkin, M., Davies, T.A., Dumitrica, P., Edwards, A.R., Galehouse, J.S., Packham, G.H. & van der Lingen, G.J., 1972 — Australian–Antarctic continental drift, palaeocirculation changes and Oligocene deep-sea erosion. *Nature (Physical Science)*, 239(91), 51–55.

Kennett, J.P., Houtz, R.E., Andrews, P.B., Edwards, A.R., Gostin, V.A., Hajos, M., Hampton, M.A., Jenkins, D.G., Margolis, S.V., Ovenshine, A.T. & Perch-Nielsen, K., 1975 — Cenozoic paleoceanography in the southwest Pacific Ocean, Antarctic glaciation and development of the circum-Antarctic current. *In* Kennett, J.P., Houtz, R.E. & others, Initial Reports of the Deep Sea Drilling Project, 29. *U.S. Government Printing Office, Washington*, 1155–1169.

Kennett, J.P. & von der Borch, C.C., 1985 — Southwest Pacific Cenozoic paleoceanography. *In* Kennett, J.P., von der Borch, C.C. & others, Initial Reports of the Deep Sea Drilling Project, 90. *U.S. Government Printing Office, Washington*, 1493–1517.

Marshall, J.F., Ramsay, D.C., Lavering, I., Swift, M.G., Shafik, S., Graham, T.G., West, B.G., Boreham, C.J., Summons, R.E., Apthorpe, M. & Evans, P.R., 1989 — Hydrocarbon prospectivity of the offshore South Perth Basin. *Bureau of Mineral Resources, Australia, Record* 1989/23.

Martini, E., 1971 — Standard Tertiary and Quaternary calcareous nannoplankton zonation. *In* Farinacci, A. (editor), Proceedings of the Second Planktonic Conference, Roma 1970. *Edizioni Tecnoscienza*, 1, 739–785.

McGowran, B., 1964 — Foraminiferal evidence for the Paleocene age of the King's Park Shale (Perth Basin, Western Australia). *Journal of the Royal Society of Western Australia*, 47, 9–74.

McGowran, B., 1968 — Late Cretaceous and Early Tertiary correlations in the Indo-Pacific region. *Memoirs of the Geological Society of India*, 2, 335–360.

McGowran, B., 1978 — Stratigraphic record of Early Tertiary oceanic and continental events in the Indian Ocean region. *Marine Geology*, 26, 1–39.

McWhae, J.R.H., Playford, P.E., Lindner, A.W., Glenister, B.F. & Balme, B.E., 1958 — The stratigraphy of Western Australia. *Journal of the Geological Society of Australia*, 4(2), 1–161.

Perch-Nielsen, K., 1979 — Calcareous nannofossils from the Cretaceous between the North Sea and the Mediterranean. *Aspekte der Kreide Europas. IUGS Series A*, 6, 223–272.

Playford, P.E., Cockbain, A.E. & Low, G.H., 1976 — Geology of the Perth Basin, Western Australia. *Geological Survey of Western Australia, Bulletin*, 124 pp.

Playford, P.E., Cope, R.N., Cockbain, A.E., Low, G.H. & Lowry, D.C., 1975 – Phanerozoic. *In* Geology of Western Australia. *Geological Survey of Western Australia, Memoir*, 2, 223–433.

Proto-Decima, F., 1974 — Leg 27 calcareous nannoplankton. *In* Veevers, J.J., Heirtzler, J.R. & others, Initial Reports of the Deep Sea Drilling Project, 27. *U.S. Government Printing Office, Washington*, 589–621.

Quilty, P.G., 1974a — Cainozoic stratigraphy in the Perth area. *Journal of the Royal Society of Western Australia*, 57, 16–31.

Quilty, P.G., 1974b — Tertiary stratigraphy of Western Australia. *Journal of the Geological Society of Australia*, 21, 301–318.

Quilty, P.G., 1977 — Western Australian Cenozoic sedimentaion cycles. *Geology*, 5, 336–340.

Quilty, P.G., 1978 — The Late Cretaceous–Tertiary section in Challenger No. 1 (Perth Basin) — details and implications. *In* Belford, D.J. & Scheibnerova, V. (compilers), The Crespin Volume: Essays in honour of Irene Crespin. *Bureau of Mineral Resources, Australia, Bulletin* 192, 109–124.

Quilty, P.G., Lowry, D.C., Moore, A.M.G. & Thomas, B.M., in press — The Fremantle Canyon, Western Australia — a description and geological history. *Marine Geology*.

Roth, P.H., 1973 — Calcareous nannofossils — Leg 17, Deep Sea Drilling Project. *In* Winterer, L.E., Ewing, J.L. & others, Initial Reports of the Deep Sea Drilling Project, 17. *U.S. Government Printing Office, Washington*, 695–795.

Shafik, S., 1978 — Paleocene and Eocene nannofossils from the Kings Park Formation, Perth Basin, Western Australia. *In* Belford, D.J. & Scheibnerova, V. (compilers), The Crespin Volume: Essays in honour of Irene Crespin. *Bureau of Mineral Resources, Australia, Bulletin* 192, 165–171.

Shafik, S., 1983 — Calcareous nannofossil biostratigraphy: an assessment of foraminiferal and sedimentation events in the Eocene of the Otway Basin, southeastern Australia. *BMR Journal of Australian Geology & Geophysics*, 8, 1–17.

Shafik, S., 1985 — Cretaceous coccoliths in the middle Eocene of the western and southern margins of Australia: evidence of a significant reworking episode. *BMR Journal of Australian Geology & Geophysics*, 9, 353–359.

Shafik, S., 1990a — Late Cretaceous nannofossil biostratigraphy and biogeography of the Australian western margin. *Bureau of Mineral Resources, Australia, Report* 295.

Shafik, S., 1990b — Maastrichtian and Early Tertiary record of the Great Australian Bight Basin and its onshore equivalents on the Australian southern margin: a nannofossil study. *BMR Journal of Australian Geology & Geophysics*, 11, 473–497.

Shafik, S. & Chaproniere, G.C.H., 1978 — Nannofossil and planktic foraminiferal biostratigraphy around the Oligocene–Miocene boundary in parts of the Indo-Pacific region. *BMR Journal of Australian Geology & Geophysics*, 3, 135–151.

Stainforth, R.M., Lamb, J.L., Luterbacher, H., Beard, J.H. & Jeffords, R.M., 1975 — Cenozoic planktonic foraminiferal zonation and characteristics of index forms. *The University of Kansas Paleontological Contributions, Article* 62, 1–425.

Thierstein, H.R., 1974 — Calcareous nannoplankton — Leg 26, Deep Sea Drilling Project. *In* Davies, T.A., Luyendyk, B.P. & others, Initial Reports of the Deep Sea Drilling Project, 26. *U.S. Government Printing Office, Washington*, 619–667.

Toumarkine, M. & Luterbacher, H., 1985 — Paleocene and Eocene planktic foraminifera. *In* Bolli, H. M. & others, Plankton stratigraphy. *Cambridge University Press, Cambridge*, 87–154,

Checklist 1. Distribution of Maastrichtian and Paleocene calcareous nannofossils in Fremantle dredge samples, South Perth Basin.

	80DR/020–11	80DR/020–10	80DR/020–09	80DR/014–05	80DR/014–10	80DR/020–08	80DR/014–08	80DR/004–02	80DR/022–03	80DR/016–03	80DR/016–02	80DR/014–03	80DR/005–09	80DR/005–08	80DR/014–13	80DR/014–12	80DR/017–03	80DR/021–05	80DR/020–06
Actinozygus regularis		+		+		+													
Ahmuellerella octoradiata			+																
Arkhangelskiella cymbiformis	+	+	+	+	+														
Arkhangelskiella specillata		+	+																
Biscutum melaniae			+																
Calculites obscurus					+														
Corollithion exiguum				+															
Cretarhabdus surrirellus		+					+												
Cribrosphaerella daniae	+	+	+	+															
Cribrosphaerella ehrenbergii	+	+	+	+	+														
Eiffellithus eximius					+								+						
Eifellithus turriseiffeli	+	+	+	+	+														
Gartnerago obliquum							+												
Haqius circumradiatus						+													
Heterorhabdus sinuosus	+	+	+																
Kamptnerius magnificus	+	+																	
Lapideacassis spp.		+		+	+	+													
Lithraphidites carniolensis			+																
Lithraphidites quadratus	+	+																	
Manivitella pemmatoidea				+															
Micula staurophora	+	+	+	+			+												
Nephrolithus corystus	+																		
Nephrolithus frequens	+	+	+	+	+														
Placozygus fibuliformis	+	+	+	+															
Prediscosphaera bukryi-stoveri	+		+																
Prediscosphaera cretacea	+	+		+	+														
Prediscosphaera majungae	+	+			+														
Prediscosphaera spinosa		+			+														
Quadrum gothicum	+																		
Reinhardtites levis				+															
Rhagodiscus augustus	+	+																	
Rhagodiscus reniformis		+	+																
Tetrapodorhabdus decorus	+	+	+																
Vekshinella elliptica	+																		
Watznaueria barnesae	+	+	+					+					+	+					
Thoracosphaera operculata				+	+	+	+								+	+			
Biantholithus sparsus				+	+														
Braarudosphaera bigelowii								+		+	+	+	+	+	+	+	+		+
Braarudosphaera discula											+	+	+	+		+			
Campylosphaera eodela																		+	+
Chiasmolithus bidens								+	+	+	+	+	+	+		+	+	+	+
Chiasmolithus californicus																		+	+
Chiasmolithus consuetus							+					+	+	+	+	+		+	+
Chiasmolithus danicus					+		+												
Chiasmolithus edentulus							+												
Chiasmolithus edwardsii													+						
Chiasmolithus inconspicuus					+														
Coccolithus eopelagicus										+									+
Coccolithus robustus				+	+	+	+	+	+	+	+	+	+	+	+	+			
Cruciplacolithus asymmetricus				+	+		+				+	+		+	+				
Cruciplacolithus platipons				+			+								+				
Cruciplacolithus primus				+	+														
Cruciplacolithus tenuis					+	+	+	+			+	+	+						
Cyclagelosphaera alta				+															
Cyclagelosphaera reinhardtii					+														
Discoaster diastypus																			?
Discoaster lenticularis													+	+				+	
Discoaster mediosus																			+
Discoaster mohleri									+	+	+	+	+	+	+		+	+	
Discoaster multiradiatus																	+	+	+
Discoaster nobilis															+	+	+	+	
Ellipsolithus distichus								+				+	+	+	+	+	+	+	+
Ellipsolithus macellus											+								
Ericsonia subpertusa				+	+														
Fasciculithus alanii														+					
Fasciculithus bobii														+					
Fasciculithus involutus									+	+	+	+	+	+		+		+	+
Fasciculithus lillianiae														+					
Fasciculithus spp.							+	+	+	+	+	+		+	+	+	+	+	
Fasciculithus tonii														+					

Checklist 1 (cont'd).

	80DR/020–11	80DR/020–10	80DR/020–09	80DR/014–05	80DR/014–10	80DR/020–08	80DR/014–08	80DR/004–02	80DR/022–03	80DR/016–03	80DR/016–02	80DR/014–03	80DR/005–09	80DR/005–08	80DR/014–13	80DR/014–12	80DR/017–03	80DR/021–05	80DR/020–06
Fasciculithus tympaniformis									+	+				+		+			
Fasciculithus ulii							+												
Heliolithus cantabriae							+							+					
Heliolithus kleinpellii								+	+	+	+			+					
Heliolithus riedelii											?				?		?	+	+
Lophodolithus nascens																			+
Markalius astroporus				+	+	+	+			+		+					+		
Micrantholithus attenuatus										+			+						
Micrantholithus crenulatus														+		+			
Micrantholithus entaster								+				+		+			+		
Micrantholithus vesper														+					
Neochiastozygus chiastus					+	+	+	+				+	+	+				+	+
Neochiastozygus denticulatus					+														
Neochiastozygus junctus					+								+	+			+	+	
Placozygus sigmoides		+		+	+	+	+		+				+	+					
Pontosphaera plana																	+	+	+
Prinsius bisulcus						+			+					+		+			
Scapholithus fossilis																		+	
Scapholithus rhombiformis														+					
Scapholithus sp.											+		+						+
Semihololithus kerabyi													+	+	+	+			
Sphenolithus primus							+												
Sphenolithus anarrhopus										?					+				
Toweius eminens									+	+	+		+	+	+	+	+	+	+
Toweius pertusus							+	+	+	+	+	+	+	+	+	+	+		
Toweius tovae													+			?		+	
Toweius? magnicrassus																			+
Transversopontis pulcher																			+
Zygodiscus adamas														+					
Zygodiscus herlynii								+			+	+	+	+	+	+	+	+	
Zygrhablithus bijugatus																	+	+	+

Checklist 2. Distribution of Eocene and older calcareous nannofossils in Fremantle dredge samples, South Perth Basin.

	80DR/018–01	80DR/014–14	80DR/020–07	80DR/020–05	80DR/017–01	80DR/003–06	80DR/003–09	80DR/003–01	80DR/003–02	80DR/003–03	80DR/003–07	80DR/003–08	80DR/022–01	80DR/021–11	80DR/023–01C	80DR/019–04	80DR/019–01	80DR/019–03	80DR/018–02	80DR/009–01	80DR/013–01	80DR/008–02	80DR/014–11	80DR/014–04
Birkelundia staurion																	+							
Blackites creber														+										
Blackites spinulus																	+		+					
Braarudosphaera bigelowii	+	+	+	+	+	+	+		+	+	+	+	+	+	+					+	+	+		
Braarudosphaera discula	+		+		+	+			+	+	+	+	+											
Braarudosphaera orthia				+																				
Calcidiscus protoannulus		+	+	+	+	+		+		+	+	+	+	+	+	+	+		+	+				
Campylosphaera dela	+			+		+			+	+	+	+	+	+	+		+							
Campylosphaera eodela		+	+	+	+										+									
Campylosphaera sp. 1				+		+				+														
Chiamolithus bidens		+	+	+			+																+	
Chiasmolithus californicus		+		+		+					+	+												
Chiasmolithus consuetus	+	+	+	+	+	+																	+	
Chiasmolithus eogranids	+	+	+	+	+			+	+		+				+				+					
Chiasmolithus expansus						+											+			+				
Chiasmolithus grandis		+	+	+	+	+			+	+		+	+	+	+	+	+	+		+	+			
Chiasmolithus oamaruensis																							+	+
Chiasmolithus solitus	+		+	+			+		+		+	+	+	+	+	+	+	+	+	+	+	+		
Chiasmolithus titus	+			+	+	+			+	+		+	+	+								+		
Chiphragmalithus acanthodes																		+						
Clathrolithus ellipticus			+		+																			
Clausicoccus cribellum	+		+								+			+	+	+	+			+	+	+		
Coccolithus eopelagicus			+		+		+			+			+	+	+			+	+	+	+	+	+	+
Coccolithus formosus	+	+		+					+	+	+	+	+	+	+	+	+	+	+	+	+	+	+	+
Coccolithus robustus				+			+																+	
Cruciplacolithus latipons	+			+		+																		
Cruciplacolithus sp. 1		+	+	+		+																		
Cruciplacolithus tenuis														+										
Cyclicargolithus floridanus														+	+	+	+	+	+	+				
Cyclicargolithus gammation							+		+	+	+		+	+	+									
Cyclicargolithus luminis	+																+							
Cyclicargolithus reticulatus																				+	+	+	+	
Cyclicargolithus sp. 1 *(eogammtion)*														+		+								
Daktylethra punctulata																	+			+	+	+		
Discoaster barbadiensis	+	+	+	+	+	+	+	+	+	+	+	+	+	+	+	+		+		+	+	+		
Discoaster binodosus				+	+																			
Discoaster deflandrei											+	+				+	+		+			+		+
Discoaster diastypus		+	?				+																	
Discoaster distinctus																	+							
Discoaster falcatus		+		?																				
Discoaster lodoensis									+	+	+	+	+	+	+									
Discoaster mediosus						+																		
Discoaster mobleri							+																	
Discoaster multiradiatus	+		+	+																				
Discoaster multiradiatus/ D. barbadiensis		+			+	+				+			+	+										
Discoaster robustus													+											
Discoaster saipanensis															+		+	+	+			+	+	
Discoaster septemradiatus			+																					
Discoaster sp. 1			+	+																				
Discoaster sublodoensis										+	+	+	+	+	+	+								
Discoaster tanii																							+	+
Discoaster tanii nodifer												?			+				+	+	+		+	+
Discoaster wemmelensis														+					+					
Discoasteroides kuepperi										+	+		+	+	+									
Ellipsolithus distichus	+	+		+																				
Ellipsolithus lajollaensis																	+							
Ellipsolithus macellus	+	+	+	+	+	+		+																
Fasciculithus involutus																							+	
Helicosphaera compacta																?				+	+			
Helicosphaera dinesenii																				+				
Helicosphaera lophata															+		+		+	+				
Helicosphaera reticulata																					+			
Helicosphaera seminulum										+	+	+	+	+	+	+	+	+						+
Holodiscolithus macroporus					+												+		+	+	+			
Holodiscolithus solidus			+		+												+		+	+	+			
Isthmolithus recurvus																								+
Lanternithus minutus																+	+			+	+	+	+	+
Lapideacassis sp.						+																		
Lithostromation opersum						+																		
Lophodolithus mochlophorus				+		+				+	+	+			+									
Lophodolithus nascens	+		+	+	+	+				+	+	+												
Lophodolithus reniformis					+				+	+	+	+			+									
Lophodolithus rotundus																	+							
Markalius astroporus			+	+		+				+												+		
Markalius inversus	+				+							+	+	+		+							+	
Micrantholithus altus																				+				
Micrantholithus attenuatus						+				+	+									+				

Checklist 2 (cont'd).

	80DR/018–01	80DR/014–14	80DR/020–07	80DR/020–05	80DR/017–01	80DR/003–06	80DR/003–09	80DR/003–01	80DR/003–02	80DR/003–03	80DR/003–07	80DR/003–08	80DR/022–01	80DR/021–11	80DR/023–01C	80DR/019–04	80DR/019–01	80DR/019–03	80DR/018–02	80DR/009–01	80DR/013–01	80DR/008–02	80DR/014–11	80DR/014–04
Micrantholithus crenulatus				+		+			+				+	+										
Micrantholithus entaster	+	+		+	+	+			+			+	+											
Micrantholithus flos						+																		
Micrantholithus procerus																				+	+	+		
Micrantholithus vesper						+																		
Nannifula sp. 1						+																		
Nannotetrina cristata																	+							
Nannotetrina fulgens																	+							
Neochiastozygus chiastus				+	+	+																		
Neochiastozygus concinnus						+																		
Neochiastozygus distentus						+																		
Neochiastozygus junctus				+																				
Neococcolithes dubius		+	+	+	+						+	+	+	+	+	+	+	+	+			+		
Neococcolithes protenus				+		+			?	+	?	?												
Orthozygus aureus																	+		+					
Pedinocyclus larvalis																				+				
Pemma basquensis																				+				
Pemma papillatum																				+	+			
Pemma rotundum																		+	+	+	+	+		
Placozygus sigmoides	+					+																		
Pontosphaera multipora																+	+		+	+		+		
Pontosphaera ocellata	+		+	+									+		+		+	+						
Pontosphaera panarium				+			+										+							
Pontosphaera pectinata	+																							
Pontosphaera plana	+	+	+	+	+	+			+	+		+	+				+	+	+	+	+	+	+	
Reticulofenestra dictyoda										+	+	+	+	+	+	+	+	+	+					
Reticulofenestra hampdenensis																				+	+	+	+	+
Reticulofenestra samodurovii														+		+	+	+	+			+		
Reticulofenestra scissura																						+	+	+
Reticulofenestra scrippsae																							+	
Reticulofenestra sp. *(praescrippsae)*														+	+									
Reticulofenestra umbilicus																		+		+	+	+	+	+
Rhabdosphaera gladius			+							+					+	+	+			+				
Rhabdosphaera sp.																	+	+						
Rhabdosphaera inflata																+								
Rhabdosphaera perlongus	+	+		+	+			+	+			+	+				+							
Rhabdosphaera pseudomorionum																	+							
Rhabdosphaera solus										+														
Rhabdosphaera pseudomorionum																	+							
Scapholithus fossilis										+		+												
Sphenolithus anarrhopus			+																					
Sphenolithus moriformis			+	+	+	+											+	+			+	+	+	+
Sphenolithus pseudoradians																							+	
Sphenolithus radians	+				+	+	+		+	+	+	+	+	+		+	+	+		+				
Striatococcolithus pacificanus										+		+												
Toweius eminens				+																				
Toweius pertusus	+	+	+	+	+	+	+	+	+	+	+	+	+		+								+	
Toweius? crassus	+	+	+	+	+	+	+	+	+	+	+	+	+		+									
Transversopontis fimbriatus										+							+							
Transversopontis pulcher	+	+	+	+	+	+	+	+	+	+	+	+	+	+	+		+	+	+			?		
Transversopontis pulcheroides										+			+						+					
Tribrachiatus orthostylus				+	+	+				+	+	+	+											
Zygodiscus adamas				+						+														
Zygodiscus herlynii	+	+	+	+		+	+	+				+							+			+		
Zygrhablithus bijugatus bijugatus	+	+	+	+	+	+			+						+	+	+				+		+	+
Zygrhablithus bijugatus crassus		+			+	+	+		+	+	+	+	+	+	+	+		+			+	+		
Arkhangelskiella orthocancellata			+																					
Arkhangelskiella specillata																	+					+		
Broinsonia bukryi		+																						
Chiastozygus litterarius				+																+	+	+		
Eiffellithus eximius						+							+							+	+			
Eiffellithus turriseiffeli				+		+																		
Gartnergo obliquum																				+	+			
Kamptérius magnificus																				+				
Micula staurophora																				+				
Prediscosphaera cretacea																						+		
Reinhardtites biperforatus																				+	+	+		
Tranolithus orionatus			+		+																+			
Vekshinella elliptica					+																+			
Watznaria barnesae	+	+	+																	+	+	+		
Zygodiscus bicrescenticus			+																		+	+		
Zygodiscus deflandrei	+		+																	+	+			

BMR Journal of Australian Geology & Geophysics, 12, 93–118

Revised Late Cambrian (pre-Payntonian–Datsonian) conodont biostratigraphy at Black Mountain, Georgina Basin, western Queensland, Australia

Robert S. Nicoll[1] & John H. Shergold[1]

Examination of new Late Cambrian samples from the upper part of the Chatsworth Limestone and lower part of the Ninmaroo Formation from Black Mountain, Georgina Basin, western Queensland (representing the pre-Payntonian, Payntonian and Datsonian Stages) has delineated five conodont assemblages in an interval that had previously not been subdivided using conodonts. Examination of the conodont fauna unambiguously confirms that the entire Payntonian Stage is of Cambrian age, as earlier indicated by the trilobite fauna, and provides three conodont assemblages that may subsequently form the basis for a conodont zonation. The Datsonian Stage, defined by the FAD of the *Cordylodus proavus* conodont assemblage and previously considered to equate with the Early Tremadoc (= Early Ordovician) of Europe, is now considered to represent the terminal Cambrian stage in northern Australia. The base of the Ordovician, equated with the base of Tremadoc correlatives, lies close to the Datsonian/Warendian boundary on the Black Mountain section. Two new conodont genera, *Eodentatus* and *Hispidodontus*, are established, along with four new species, *E. bicuspatus*, *H. resimus*, *H. appressus* and *H. discretus*. All are found in the Payntonian Stage in the upper part of the Chatsworth Limestone or the lower part of the Ninmaroo Formation.

Introduction

The 1020 m thick section of carbonate rocks at Black Mountain, 62 km north of Boulia (Fig. 1) in western Queensland, has been the intermittent focus for Cambrian–Ordovician research in Australia since 1936, when F.W. Whitehouse recognised ellesmeroceratid cephalopods in the Ninmaroo Formation and assigned them a 'Lower Ozarkian (Lower Tremadocian)' age (Whitehouse, 1936, p. 69). Considerable impetus was given to biostratigraphical studies in the Burke River Structural Belt by the report of Jones (1961) which identified for the first time the occurrence of Late Cambrian conodonts in the Chatsworth Limestone at neighbouring Mt Ninmaroo. These conodonts, and others from both the Chatsworth Limestone and overlying Ninmaroo Formation at Black Mountain, Mt Ninmaroo and Mt Datson, were then described (Druce & Jones, 1968, 1971), and a biostratigraphical zonation based on conodonts was established in the Ninmaroo Formation. Concurrently, Shergold (1975) collected and described the trilobite faunas from the same sections that had been trough sampled by Druce & Jones (1971), and recognised a succession of assemblage-zones, particularly in the Chatsworth Limestone.

Jones, Shergold & Druce (1971) integrated the conodont and preliminary trilobite biostratigraphies. In their work, three stages were recognised in the Cambrian–Ordovician boundary interval: Payntonian of latest Cambrian age, Datsonian and Warendian of earliest Ordovician age. The Cambrian–Ordovician boundary was considered to coincide with the first appearance datum (FAD) of conodonts belonging to the *Cordylodus proavus* Assemblage-Zone that defines the base of the Datsonian Stage at Black Mountain. This event was located 567 m above the base of the measured section at Black Mountain, 147 m above the base of the Unbunmaroo Member of the Ninmaroo Formation. In 1971, the basal Ninmaroo Formation provided few age-diagnostic fossils, apart from an occurrence of saukiid trilobites assigned to what was considered to be the terminal Cambrian (late Payntonian) *Mictosaukia perplexa* Assemblage-Zone (Shergold, 1975, horizon K145), some 40 m above the base of the formation. Below this, the richly fossiliferous upper Chatsworth Limestone was assigned to the *Neoagnostus quasibilobus/Shergoldia nomas* Assemblage-Zone, of early Payntonian age.

In 1971, detailed biostratigraphical knowledge of the Cambrian–Ordovician boundary interval which could be readily applied in northern Australia was essentially derived from three sources:

1. North American cratonic sections from which a conodont biostratigraphy was emerging (e.g. Miller 1969), based on pioneering conodont studies of Furnish (1938), Müller (1959) and Ethington & Clark (1965);
2. Mexico, where sections at Nochixtlán, Oaxaca Province, had recently been described by Robison and Pantoja-Alor (1968); and
3. the Sino-Korean Platform, where trilobite-bearing sequences had been established since the 1920s (e.g. Sun, 1924; Kobayashi, 1931, 1933, 1934, 1935 *inter alia*; Endo, 1931; Resser & Endo, 1937), and were being embellished (Kobayashi, 1960a,b, 1962, 1966a,b, 1967, 1969).

While some correlation was also possible with the shelly faunas of the Baltic Platform in Sweden and the Leningrad region (Pander, 1856; Lindström, 1955; Tjernvik, 1956, 1958; Viira, 1966; Sergeeva, 1966), it was not possible to easily correlate the Black Mountain succession with the Acado-Baltic Tremadocian graptolite sequences. This last correlation was essential for the correlation of the trilobite–conodont faunas of Black Mountain with the graptolite sequences of southeastern Australia in Victoria. As such, it was only very indirectly possible to make a correlation between the early Ordovician (Tremadoc) of North Wales and the Datsonian/Warendian Stages of Black Mountain.

The biostratigraphic succession established by Jones & others (1971) was perturbed by Miller who, in 1976, collected samples around the Chatsworth/Ninmaroo boundary during a field excursion associated with the 25th International Geological Congress. Miller (SW Missouri State University, written communication, 1977; see also Druce, Shergold & Radke, 1982; Miller, 1984) reported the occurrence of elements of the *Cordylodus proavus* Assemblage-Zone from levels 1 m below and 18 m above the base of the Ninmaroo Formation. Elements identified included '*Oneotodus nakamurai*' and *Hirsutodontus hirsutus*, and a second species of *Hirsutodontus* (aff. *H. simplex*) was identified higher in the Ninmaroo Formation at levels 67, 76 and 81 m above its base. These determinations suggested considerable overlap of the trilobite and conodont zonation at Black Mountain with the base of the early Ordovician Datsonian *Cordylodus proavus* Assemblage-Zone predating the late Payntonian *Mictosaukia perplexa* Assemblage-Zone, as indicated by Druce (1978a) and shown by Druce & others (1982, fig. 4).

This has led to the current inclusion of 'late Cambrian' trilobites of the Australo-Sinian saukiid-tsinaniid biofacies

[1] Onshore Sedimentary & Petroleum Geology Program, Bureau of Mineral Resources, Geology & Geophysics, GPO Box 378, Canberra ACT 2601

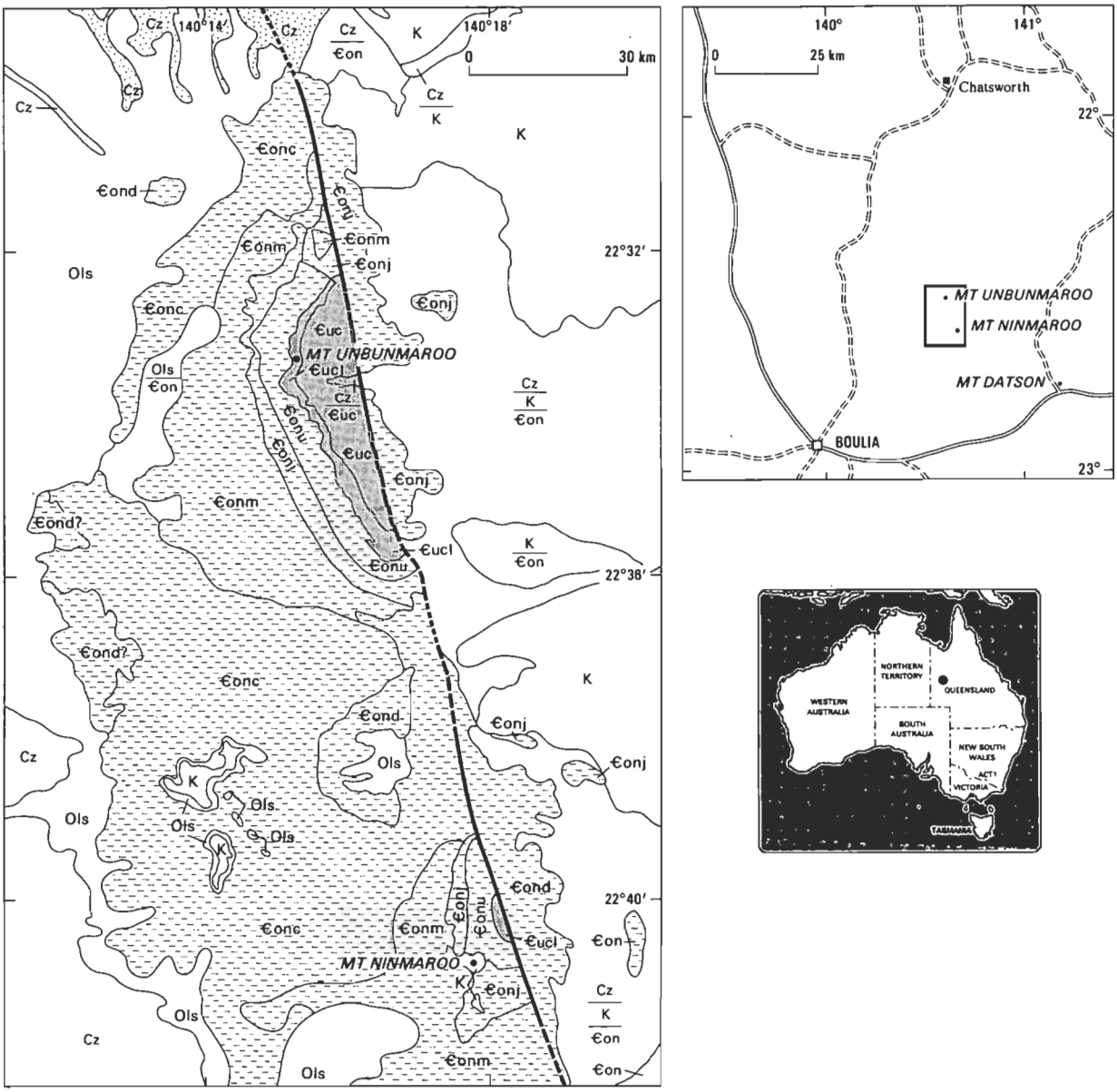

			Cz	*Alluvium, sand, black and brown soil, clay*
CRETACEOUS			K	*Sandstone, ferruginous sandstone, conglomerate, siltstone, claystone*
ORDOVICIAN TO TERTIARY		Digby Peaks Breccia	OTb	*Silcrete, silicified ferruginized chert, breccia*
		Swift Formation	Ols	*Sandstone, siltstone, coquinite (all silicified in part), chert*
	NINMAROO FORMATION		€on	*Limestone*
		Datson Member	€ond	*Thin bedded limestone or dolomite with interbedded chert*
EARLY ORDOVICIAN		Corrie Member	€onc	*Limestone (pelmatozoan, peloid, clast and ooid grainstone) dolomitic sandstone, calcareous siltstone*
		Mort Member	€onm	*Limestone (intraclast, ooid and peloid grainstone calcareous siltstone)*
		Jiggamore Member	€onj	*Thin to thick bedded limestone (peloid and intraclast grainstone, micrite, two-toned limestone), calcareous siltstone*
		Unbunmaroo Member	€onu	*Medium to thick bedded limestone (intraclast and peloid grainstone, mudstone, stromatolitic boundstone), dolomite, calcareous siltstone*
LATE CAMBRIAN	CHATSWORTH LST	Lily Creek Member	€ucl	*Calcareous cross stratified sandstone, sandy limestone, calcareous siltstone*
			€uc	*Thin bedded light to medium grey limestone (peloid grainstone), limestone, calcareous siltstone*

20/F54-10/1

Figure 1. Locality map, showing geology of the Black Mountain (Unbunmaroo) and Ninmaroo inliers.

(Shergold, 1988) in the early Ordovician, as interpreted and defined in Australia (Jones & others, 1971). This situation is manifestly unsatisfactory, since it has led to the stratigraphic condensation of the Payntonian Stage, and transfer of the former 'late Payntonian' *Mictosaukia perplexa* Assemblage-Zone to the early Datsonian Stage. Over the past decade, however, it has become increasingly apparent that the correlation of the base of the Ordovician (= basal Tremadoc) in North Wales was made at an erroneously low level in northern Australia (see discussion below). Accordingly, the apparent overlap of trilobites of latest Cambrian aspect with conodonts previously considered early Ordovician becomes a local biostratigraphic dilemma: the subject of this paper.

Nevertheless, there is a resurgence of international opinion which argues for a stratigraphic horizon for the base of the Ordovician which can be recognised globally. The first appearance of the *Cordylodus proavus* Assemblage-Zone is such a horizon. Hence, a resolution of the Australian biostratigraphy at the late Payntonian/early Datsonian level is a valuable contribution to international debate on the Cambrian–Ordovician boundary datum. Furthermore, it will assist in the quest for a unified Australian biochronological scale (see also discussions in Webby & others, 1981; Shergold & others, 1985; Shergold, 1989; Webby & Nicoll, 1989).

During August 1989, the Black Mountain sections were recollected for magnetostratigraphic analysis by R.L. Ripperdan and J.L. Kirschvink (California Institute of Technology), as part of a wider project to investigate the palaeomagnetism of the Cambrian–Ordovician boundary interval. The sections had been originally collected by Druce & Jones (1971) and Shergold (1975), lithostratigraphically analysed by Radke (1980, 1981, 1982) and stratigraphically re-evaluated by Druce & others (1982). The position of the samples is shown on Figure 2. Orientated block samples from irregular 5 to 10 m intervals were collected from the base to the 750 m level of the Black Mountain section, about 330 m above the base of the Ninmaroo Formation and just below the first occurrence of *Cordylodus lindstromi*. The samples were taken to the Bureau of Mineral Resources in Canberra for coring and measurement, and the opportunity was taken to acid etch the residual material, with quite unanticipated results. Samples from the interval reported weighed an average of 570 g, produced over 1100 conodonts and yielded conodonts from a sample as small as 180 g.

Many of the samples recovered fauna from stratigraphic intervals that had been sampled by Druce & Jones (1971) and which had produced almost no conodonts. The fine sieve used in the earlier study appears to have been about a 125μ mesh size, while that used in the present study was a 75μ mesh size. This meant that the smaller conodont elements from samples of the early study would have been lost in the processing stage. In many of the samples from the present study, 80–90 per cent of the elements would have passed through a 125μ mesh sieve.

Conversely, samples from low in the Chatsworth Limestone recovered no elements of *Westergaardodina*, a form which had been consistently present, though not abundant, in the earlier collection. We believe the absence of some elements of the fauna reported by Druce & Jones (1971) may be related to the types of lithologies collected for the magnetostratigraphic study. The trough samples of Druce & Jones (1971) were collected over a 6 m interval and favoured bioclastic carbonates. The samples of Ripperdan & Kirschvink tended to be from the interbedded muddy or silty carbonates.

As a result of these new samples, it is now possible to give a more substantial account of the conodont biostratigraphy during the late Payntonian/Datsonian interval, and to clarify and refine the relationships of these stages at Black Mountains. The interpretations accruing are of international significance and form the substance of this paper.

Status of the international Cambrian–Ordovician Boundary deliberations

A review of the historical development of concepts pertinent to definitions of the Cambrian–Ordovician boundary before 1972 was published by Henningsmoen (1973). This became a basis for subsequent deliberations by the Cambrian–Ordovician Boundary Working Group that was founded within the International Union of Geological Sciences (IUGS) International Commission on Stratigraphy (ICS), during the Symposium on the Ordovician System held in Birmingham, England, in 1974.

Within this Working Group there has been a general acceptance of the coincident base of the Ordovician System and Tremadoc Series, a traditional Scandinavian boundary promoted by Moberg (1900) and still used there (Henningsmoen, 1957, 1973; Bruton, Erdtmann & Koch, 1982). This is defined by the well known FAD of quadriradiate nematophorid and other planktic graptolites (Cooper, Erdtmann & Fortey, 1990).

It has also been widely accepted that there is a hiatus in the faunal record between the Tremadoc and the underlying Olenid Series in the type area of the Tremadoc in North Wales, and that in a wider Acado-Baltic geographical context, older rocks belonging to the *Boeckaspis hirsuta* trilobite zone, predating the nematophorid expansion event, have been included within the Tremadoc Series (Henningsmoen, 1973; Bruton & others, 1982; Landing, 1988).

Inevitably, there have been difficulties in correlating this geographically localised, conodont impoverished, graptolite-olenid trilobite biofacies outside the traditional Acado-Baltic Province (but see Shergold, 1988). As noted above, in Australia the base of the Tremadoc Series has been correlated to the FAD of *Cordylodus proavus*, which defines the base of the Datsonian Stage. This implies a coincidence of this conodont zone with the incoming of species of *Rhabdinopora* (Jones & others, 1971; Druce, 1978a,b). In Canada, the FAD of the same conodont defines the base of the Ordovician at the base of the Ibexian Series (Hintze *in* Ross & Bergström, 1982) in the opinion of Ludvigsen & Westrop (1985).

Contemporaneously, in North American cratonic sections, the base of the Ordovician was placed at the base of the Canadian Series, lying within the base of the *Cordylodus proavus* Zone, within the *Hirsutodontus hirsutus* Subzone on the conodont biostratigraphic scale, and at the base of the *Missisquoia* Zone, *M. depressa* Subzone, on the trilobite scale (Miller, 1978, 1980, 1984, 1987, 1988). The base of the Tremadoc Series in these schemes is correlated with the incoming of the trilobite *Missisquoia* and postdates the FAD of *Cordylodus proavus* which in turn lies within the top of the Trempealeauan *Saukia* Zone, *Eurekia apopsis* Subzone, on the trilobite biostratigraphic scale.

The base of the Tremadoc has been pushed considerably higher during the last 10 years as a result of research on extracratonic sections, notably in western Newfoundland. Here, Fortey & Skevington (1980) and Fortey & others (1982) have demonstrated that the base of the Tremadoc cannot be correlated with the base of the *Missisquoia* trilobite zone, but is younger, lying within the *M. typicalis* Zone or that of *Symphysurina* which succeeds it. Landing (1988) currently places the base of the Tremadoc within the lower part of Miller's (1978, 1988) conodont Fauna B, within the *Symphysurina bulbosa* Subzone

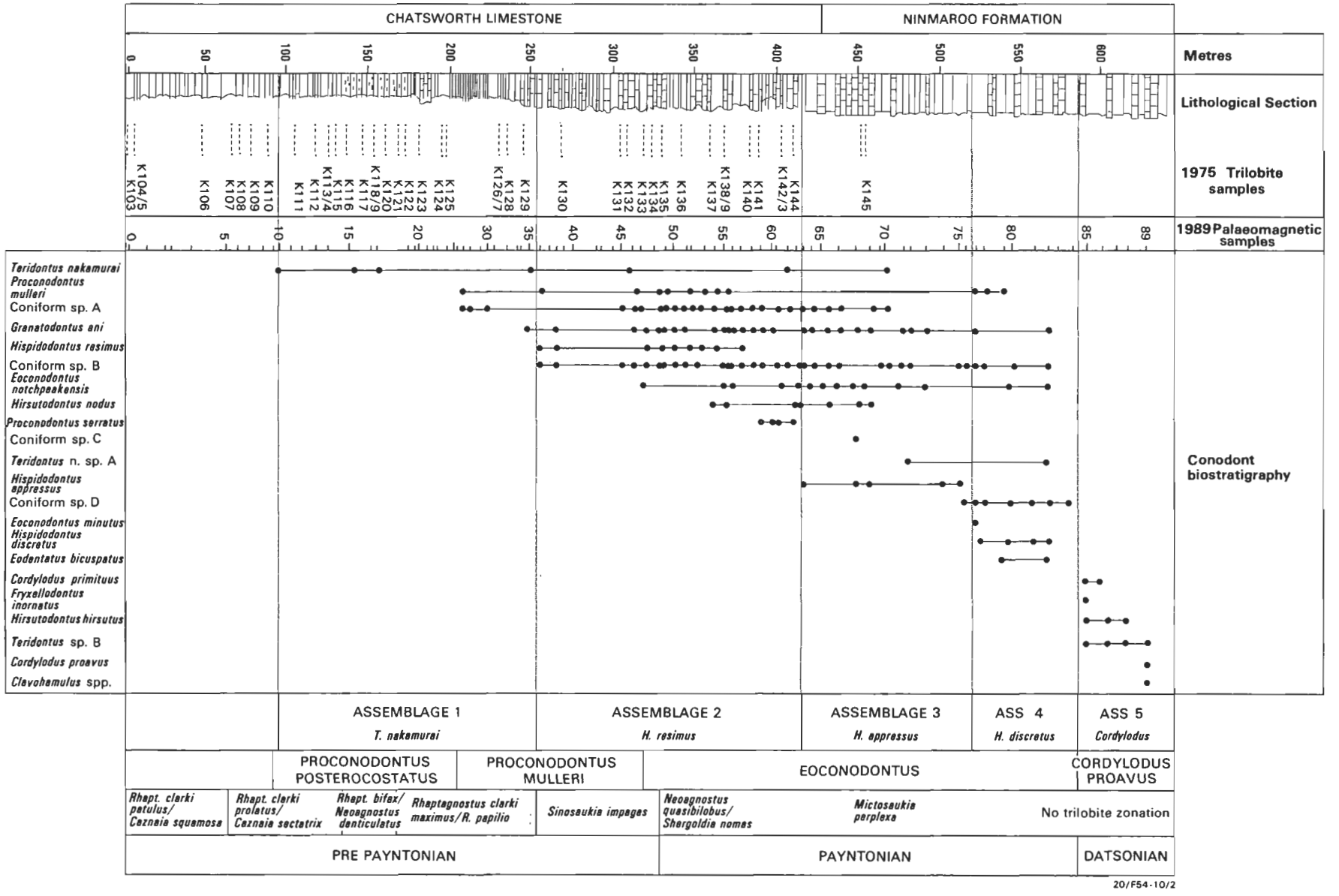

Figure 2. Conodont range chart and biostratigraphic subdivisions.

of the *Symphysurina* Zone (according to the correlations of Miller, 1988). In Australian terms, following the biostratigraphic revisions of Nicoll (1990), it lies within the *Cordylodus lindstromi* Zone. This, in turn, is due to recognition that *C. prion sensu* (Druce & Jones, 1971) is an element of *C. lindstromi* (Nicoll, 1990). It means that the base of the Tremadoc lies very close to the base of the Warendian Stage, because the latter was defined by Druce & Jones (1971) on the incoming of the *Cordylodus caseyi* Subzone assemblage. Eventually, when ranges of individual multielement species are further refined, it may be possible to unify the *C. lindstromi* Zone with both the *C. prion* and *C. caseyi* Subzones, and redefine the base of the Warendian Stage at the base of the combined zone. This could have considerable ramification for the status of the Lancefieldian Stage in the Victorian graptolite succession (Cooper, 1979; Cooper & Stewart, 1979; Cas & VandenBerg, 1988; VandenBerg, 1981).

Conodont fauna

The conodont fauna recovered from the late pre-Payntonian and Payntonian of the Georgina Basin is essentially the same as that reported from China (Chen & Gong, 1986). Major elements of the fauna found in both areas include *Teridontus nakamurai, Granatodontus ani*, the various species of *Proconodontus, Eoconodontus notchpeakensis* and *Hirsutodontus nodus*. Most elements of this fauna have also been reported from North America (Miller, 1969, 1980).

Distinctive elements of the fauna are limited to the three species of *Hispidodontus* and to *Eodentatus bicuspatus*. These species have not been reported from outside the Georgina Basin in pre-Datsonian rocks. The record of *Hispidodontus (Clavohamulus triangularis)* from the Lena River area of Siberia (Abaimova, 1975) appears to be associated with *Cordylodus proavus* and is thus of Datsonian age. This Siberian occurrence extends the distribution and range of *Hispidodontus* beyond Australia and the Payntonian.

The pre-*Cordylodus* fauna considered in this study is extremely important to the understanding of several aspects of the origins and trends in the organisation, composition and morphology of the apparatus structure of the conodont animal. Among these are the first species with multiple denticulation, and the development of extensive white matter in the cusps and secondary denticles.

Multiple denticulation takes two forms, the development of nodes or short spiny denticles scattered on the surface of the element (*Hispidodontus, Hirsutodontus, Granatodontus, Ancidontus*) and the development of secondary denticles on a linear process (*Eodentatus, Cordylodus, Iapetognathus*). Nodes are developed on a variety of paraconodonts and euconodonts, and there appears to be a gradual progression from the development of simple scattered low nodes to the more structured spiny denticles with white matter. Examples of this would be *Hispidodontus resimus* → *H. appressus* → *H. discretus* or *Teridontus nakamurai* → *Hirsutodontus nodus* → *H. hirsutus* → *H. simplex*.

The gradual development of nodes contrasts with the apparent abruptness of denticle development. *Eodentatus bicuspatus* (n. gen., n. sp.), the first conodont to develop multiple denticulation, appears in our samples abruptly and without obvious ancestral forms. *Cordylodus primitivus*, the second species to develop denticles, is part of a well documented lineage (Miller, 1980, 1984) but there is no suggestion of incipient denticulation in the *Cordylodus* precursor *Eoconodontus*. *Iapetognathus*, the third denticulate lineage, lacks a recognised ancestral species.

Contrary to views expressed 10 years ago (see Miller, 1980, for example), multimembrate apparatus structures are the norm for most, if not all, species of Ordovician and Cambrian conodonts. Nicoll (1990) has discussed some aspects of this status of multimembrate apparatus structure. Here we will only note that we can observe multimembrate apparatuses in all of the taxa dealt with in this study that were present in reasonable numbers. The recognition of 4 element types for *Hispidodontus resimus* and 5 element types for *H. discretus*, based on a study of 20 and 101 elements respectively, is a reflection of how an understanding of the morphology of discrete elements can enhance our interpretation of associated elements of morphologically diverse taxa.

Conodont biostratigraphy

The Black Mountain section was measured initially by Brown (1961), and then by Druce & Jones (1971), Shergold (1975) and Radke (1981) during investigations on conodonts, trilobites and carbonate petrology respectively (Fig. 2). The section of the Chatsworth Limestone in Shergold (1975) is used as the base for our section diagram. The key to correlation of the original trough samples of Druce & Jones with the section collected for trilobites by Shergold is given in Shergold (1975), and this permits the correlation of the palaeomagnetic samples of Ripperdan and Kirschvink.

Five successive conodont assemblages occur within an apparently continuous 600 m sequence of carbonates, that extends from the pre-Payntonian through the Payntonian into the basal Datsonian.

Assemblage 1, characterised by *Teridontus nakamurai*, also contains *Proconodontus muelleri, Granatodontus ani*, and coniform species A. Druce & Jones (1971) also recorded several species of *Furnishina, Oneotodus, Problematoconites* and *Westergaardodina* from the same interval (their trough samples 10–42). Assemblage 1 spans a stratigraphic interval between 95 m and 250 m within the lower Chatsworth Limestone at Black Mountain. The assemblage is considered a correlative of the *Proconodontus posterocostatus* and part of the *P. muelleri* Subzones of the *Proconodontus* Zone in North America (e.g. Miller, 1988). The range of Assemblage 1 conodonts more or less coincides with the *Rhaptagnostus clarki prolatus/Caznaia sectatrix, R. bifax/Neoagnostus denticulatus* and *R. clarki maximus/R. papilio* trilobite Assemblage-Zones described by Shergold (1975) from his collected horizons K107 and K129 respectively.

Assemblage 2 contains all the taxa occurring in Assemblage 1, as well as *Hispidodontus resimus, Eoconodontus notchpeakensis, Hirsutodontus nodus, Proconodontus serratus*, and coniform species B. It extends stratigraphically between 250 m and 415 m on the measured section. This interval yielded only five other conodont species to Druce & Jones (1971) from their samples 62, 64, 71 and 74: *Proconodontus muelleri, Teridontus nakamurai*, two species assigned to *Furnishina*, and '*Oneotodus tenuis*'. On the North American conodont biochronological scale, Assemblage 2 ranges from early in the *P. muelleri* Subzone of the *Proconodontus* Zone into the early *Eoconodontus* (=*Cambrooistodus*) Zone. On the Australian trilobite biochronological scale, it ranges through the *Sinosaukia impages* and *Neoagnostus quasibilobus/Shergoldia nomas* Assemblage-Zones, i.e. across the pre-Payntonian/Payntonian boundary, as defined by Shergold (1975), embracing collecting horizons K130–K144. The conodonts suggest that the *Sinosaukia impages* A–Z more properly represents an initial Payntonian biostratigraphic unit, a choice not available at the time of original definition (Jones & others, 1971) of the Payntonian Stage.

Assemblage 3 ranges across the Chatsworth Limestone/Ninmaroo Formation (Unbunmaroo Member) contact, between 415 m and 520 m on the measured section. This is the most specifically diverse assemblage recognised in this study. It contains 12 taxa: *Teridontus nakamurai*, *T.* n. sp. A, coniform species A, B, C and D, *Proconodontus muelleri*, *Granatodontus ani*, *Eoconodontus notchpeakensis*, *E. minutus*, *Hirsutodontus nodus*, and *Hispidodontus appressus*. Druce & Jones (1971) recorded only *T. nakamurai* from this stratigraphic interval which extends through the middle part of the *Eoconodontus (Cambrooistodus)* Zone by correlation with North America. It corresponds with the *Mictosaukia perplexa* trilobite assemblage. Although this trilobite assemblage is poorly defined (horizon K145 only) at Black Mountain, the horizon is better represented in the sections at Mt Datson and Mt Ninmaroo (Shergold, 1975). The specimens, recovered by Miller in 1976, and determined as *Hirsutodontus hirsutus* and '*Oneotodus*' *nakamurai*, occur early in the time span of Assemblage 3, immediately below the Chatsworth/Ninmaroo contact.

Assemblage 4, ranging between 520 m and 567 m in the lower Ninmaroo Formation (Unbunmaroo Member), has not previously been recognised as a biostratigraphic unit. Druce & Jones (1971) obtained no material from this interval, which is also barren of trilobites (Shergold, 1975). The assemblage contains 7 taxa: *Proconodontus muelleri*, *Granatodontus ani*, *Eoconodontus notchpeakensis*, coniform species B and D, *Hispidodontus discretus* and *Eodentatus bicuspatus*. This assemblage correlates with the late *Eoconodontus* Zone of North America. It contains the last species of the *Hispidodontus* lineage known at Black Mountain.

Assemblage 5 consists of the faunal elements of the early *Cordylodus proavus* Zone, and was recognised and described by Druce & Jones (1971). This assemblage first appears at about 584 m on the measured section at Black Mountain on the basis of present sampling: Druce & Jones (1971) found it in their trough sample 94, but Druce & others (1982) considered that this event occurred at 567 m. Originally only *Cordylodus proavus* was recognised, but here we also record *C. primitivus*, *Teridontus* sp. B, *Hirsutodontus hirsutus* and *Fryxellodontus inornatus*. At Black Mountain, the collecting has not been fine enough to resolve a distinct *H. hirsutus* Subzone, such as Miller has been able to recognise in Utah (Miller & others, 1982). There, it is a mere 4 m thick, and could easily fit into the Black Mountain section between 567 m and 584 m. The FAD of the *C. proavus* Zone has been used by Jones & others (1971) to define the base of the Datsonian Stage in northern Australia, and was originally correlated with the base of the European Tremadoc/base of the Ordovician System as indicated above.

Conclusions

1. Three Late Cambrian conodont assemblages predating the FAD of *Cordylodus proavus* can be defined on the basis of stratigraphically successive species of *Hispidodontus*, a new genus which has previously been confused with *Hirsutodontus*.

2. The last of these assemblages, characterised by *H. discretus*, has not previously been studied, even in the exhaustively studied carbonate platform sequences of North America. It presumably either represents an Australo-Sinian biofacies laterally equivalent to the latest *Eoconodontus* Zone (= *Cambrooistodus minutus* of Miller, 1988) of Utah/Texas/Oklahoma (Miller & others, 1982), or it is an assemblage not documented in those areas because of stratigraphic hiatus. If the latter, then the value of the FAD of *C. proavus* has to be questioned, in spite of its growing international utility in the definition of the Cambrian–Ordovician boundary.

3. Erroneous determinations of *Hirsutodontus hirsutus* at the Chatsworth Limestone/Ninmaroo Formation contact by Miller (SW Missouri State University, written communication, 1984) are corrected. The species which occurs is *Hispidodontus resimus*, which characterises Assemblage 3 in the Black Mountain section. This correction permits the reinstatement of the *Mictosaukia perplexa* trilobite assemblage and contemporaneous conodont assemblages as late Payntonian biofacies in the Burke River Structural Belt.

4. There is no evidence for the existence of a *Cordylodus proavus* assemblage significantly earlier than that originally documented by Druce & Jones (1971). The first occurrence of the *C. proavus* assemblage will be within 2 or 3 m of the level documented by Druce & Jones (1971). Hence, the original concepts of the Payntonian and Datsonian Stages can be maintained in the eastern Georgina Basin.

5. Latest Payntonian is represented by the *Mictosaukia perplexa* trilobite assemblage and conodont assemblages 3 and 4 as described here. The base of the Datsonian Stage remains at the FAD of *Cordylodus proavus*, or more properly *C. primitivus*, but its exact position on the measured section at Black Mountain requires more detailed resampling.

6. The rare trilobites, *Onychopyge* and leiostegiids, which are associated with the early Datsonian *Cordylodus proavus* Zone in the Burke River Structural Belt, strongly resemble those of south-central and eastern China, and provide independent support for the sequence of conodont assemblages in the Australo-Sinian sector of Gondwanaland.

7. These observations lead to the conclusion that in northern Australia and China the FAD of *C. proavus* is well within the Late Cambrian, as documented in Europe, central America (Mexico) and eastern maritime North America. The species *C. proavus* is, however, long-ranging, extending from the latest Cambrian to near the base of the Arenig.

8. It is now possible to revise earlier published Australian notions of the correlation of the FAD of *C. proavus* with the base of the Acado-Baltic Tremadoc, and thus the base of the Ordovician in the European sense. This, marked by the FAD of *Rhabdinopora* species of the *flabelliforme* complex, now correlates more convincingly with the incoming of conodonts of the *Cordylodus lindstromi* Assemblage-Zone.

9. The FAD of *C. proavus* in Australia is retained for the definition of the Datsonian Stage. The Datsonian Stage is now regarded as a pre-Tremadoc biochronological unit, pre-dating *C. lindstromi*, rather than being the Early Tremadoc correlative previously proposed.

Conodont systematics

Eodentatus gen. nov.

Type species. *Eodentatus bicuspatus* gen. et sp. nov.

Derivation of name. From *eos*, Gk. dawn, and *dentis* L., tooth, a reference to this very early example of ramiform conodont.

Diagnosis. Ramiform element with two denticles located on a single process. Anterior denticle located over shallow basal cavity tip that does not extend upward into the denticle. Base

hyaline, elongate and broadly, but shallowly, excavated. Denticles composed of solid white matter.

Remarks. Before this study, *Cordylodus* had been considered to contain the earliest multidenticulate conodont element, an element structured with denticles on a bar or blade-like process. The recovery of *Eodentatus bicuspatus* in this study extends downward the earliest occurrence of ramiform conodont elements.

There is no indication of a possible ancestral form of *E. bicuspatus* in the material we have studied, nor is there a clear indication of the multielement structure of its apparatus.

Eodentatus bicuspatus sp. nov.
Figure 3

Material studied. 4 elements.

Derivation of name. *Bicuspatus*, L., for the two cusps or denticles of the element.

Diagnosis. As for the genus above.

Description. Ramiform element with an elongated ovate base and two denticles. Both denticles are laterally compressed and composed of solid white matter which extends into the upper part of the hyaline matter of the base (Figs 3.2c, 3.3c). The base is hyaline and there is a thin band of hyaline material separating the white matter of the two denticles. The anterior and posterior margins of the element base are rounded. The anterior denticle, the smaller of the two, is directed forward at its base and is then recurved posteriorly. The larger posterior denticle is reclined and its tip extends beyond the posterior margin of the base. The basal attachment surface is large and is developed under the entire area of the base, but a shallow basal cavity tip extends upward a short distance into the lower part of the anterior denticle. The surface of the element is smooth and the denticles lack carinae, costae and keels. The element is bilaterally asymmetrical with the denticles in slightly different planes. Concentric growth laminae are well developed on the basal surface.

Remarks. Only four specimens have been recovered, so there is not enough morphological variation in this limited sample to establish if the apparatus is multimembrate.

The elements of *E. bicuspatus* are distinguished from all species of *Cordylodus* by the lack of a basal cavity extending deeply into the cusp, by the distinctive pattern of white matter extending down from the denticle into the basal part of the element, and by the broad and rounded posterior margin. The pattern of denticle development and white matter distribution is different from that found in *Iapetognathus*[1].

Hirsutodontus Miller, 1969

Type species. *Hirsutodontus hirsutus* Miller, 1969.

Diagnosis. A multimembrate coniform taxon with a narrow base, a cusp in which the upper part is formed by solid white matter, and which develops nodes or spines on part or all of the element. In some stratigraphically younger species these spines are composed of white matter. Size, shape and density of spine or node development is variable between species and even within elements of a single species. Spines may be developed either on the cusp or the base of the element. Members of the apparatus are differentiated by the cross-sectional shape of the element, and by the length ratio of base to cusp.

Remarks. *Hirsutodontus* is restricted to forms that have spine or node development on the base or the base and cusp of a coniform element. All species have the cusp, above the basal cavity tip, composed of solid white matter and the separation of hyaline-white matter is planar.

Hirsutodontus nodus (Zhang & Xiang, 1983)
Figures 4, 5.1

Synonymy

1983 *Teridontus nakamurai nodus* n. subsp. Zhang & Xiang *in* An & others, Pl. 6, figs 7, 8; text-fig. 14.19.

1986 *Dasytodus nodus* (Zhang & Xiang) Chen & Gong, p. 135, Pl. 28, fig.10; Pl. 31, fig. 9; text-fig. 42.

Material studied. 13 elements.

Diagnosis. Same as that of the genus, but with node development restricted to one or both of the lateral faces of the basal part of the element. Some elements have microstriations on the posterior margin of the element.

Description. Too few specimens were recovered in this study to attempt a rigorous description of the species, but the following observations are made. The elements of this species are robust coniform elements with a relatively short base and a moderately long cusp. The cusp above the basal cavity tip is round in cross-section and composed of white matter. The basal cavity extends only as far as the flexure point and terminates at the planar base of the white matter of the cusp. Ornamentation on the element surface consists of clusters of low, blister-like nodes on one or both of the lateral faces of the base. Unlike later species of the genus, the nodes are usually rounded at the tip and are not made of white matter. Two of the three elements photographed at magnifications of x200 were found to have microstriations on the posterior side of the element. The third element has a smooth surface. Elements of the apparatus can be differentiated by the cross-sectional shape of the base.

Remarks. Chen & Gong (1986) established the new genus *Dasytodus*, type species *D. transmutatus*, and assigned the earlier described subspecies *Teridontus nakamurai nodus* Zhang & Xiang (1983) to the new genus. Examination of the illustrated material and the new specimens from Queensland indicates to us that the two species should be assigned to different genera, on the basis of the morphology of the basal portion of the element. In *D. transmutatus* the base is thin, laterally compressed and relatively long in proportion to cusp length. In *H. nodus* the base is round to subround, thick, and short relative to cusp length. On this basis we assign the *nodus* material to *Hirsutodontus* and suggest retention of the *transmutatus* material in *Dasytodus*.

Hirsutodontus nodus appears to have evolved from *Teridontus nakamurai* by the development of nodes on the lateral surfaces of the elements. Like *T. nakamurai*, it has the tip of the basal cavity near the anterior margin of the element.

Some of the specimens considered by Miller (Druce & others, 1982) to be elements of *H. hirsutus*, from the top of the

[1] **Note added at proof stage**
An additional 13 kg of sample BMA 79 was collected by the authors in September, 1990, and yielded an additional 14 elements of *Eodentatus bicuspatus*. These elements do not resolve the apparatus structure of *E. bicuspatus*, but they confirm that a multielement structure exists. Both symmetrical and asymmetrical elements were recovered. Several of the elements have a very broad base, but others have a narrow base. All elements have the same general shape, with two denticles, and white matter distribution as described for the original four elements.

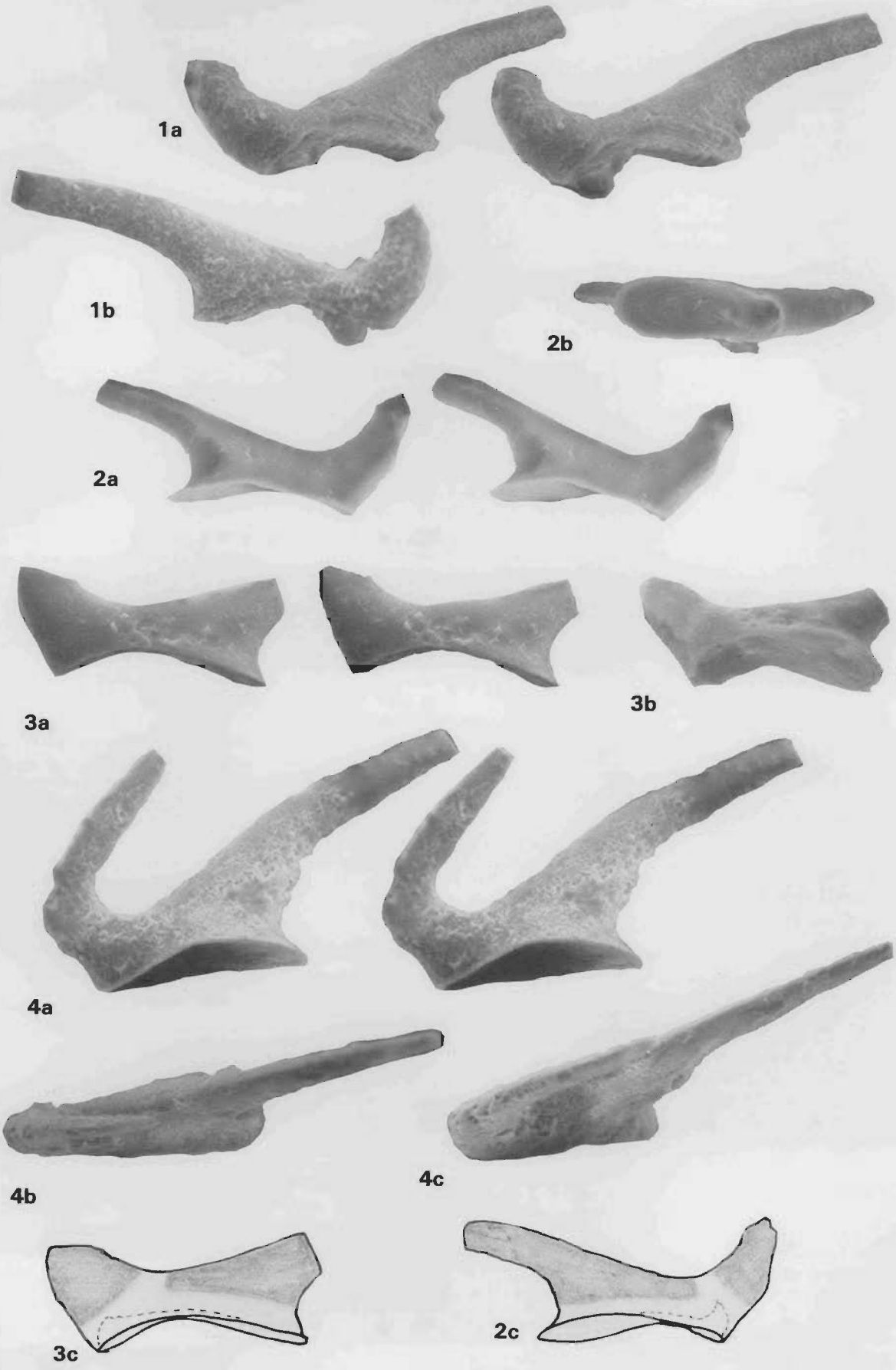
1a
1b
2b
2a
3a
3b
4a
4b
4c
3c
2c

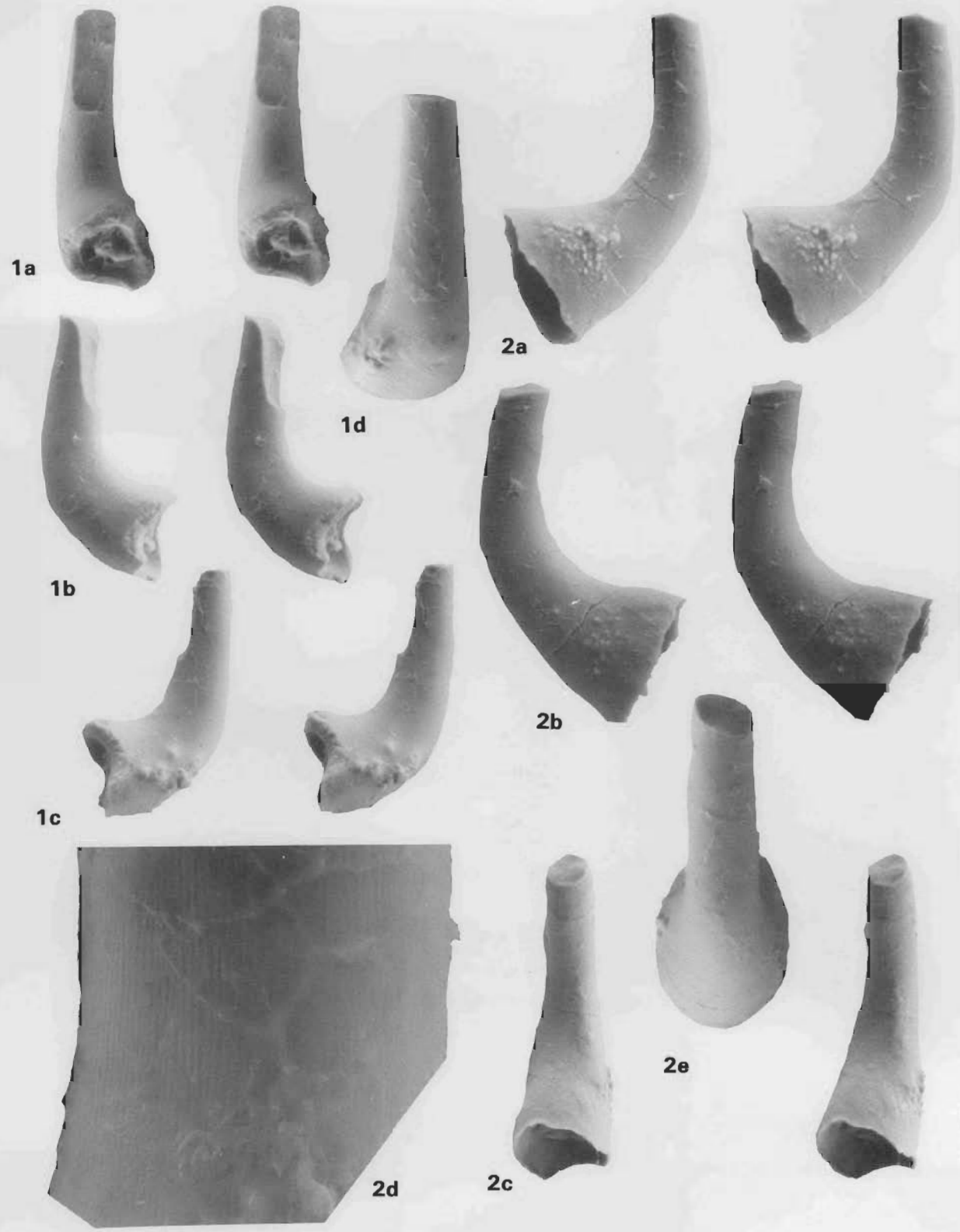

Figure 4. ***Hirsutodontus nodus*****, coniform element.**
All figures x200, except as noted.
1. Left element (CPC 29049)[JHS K-144]; **a,** stereo pair, posterior view; **b,** stereo pair, outer lateral view; **c,** stereo pair, inner lateral view; **d,** anterior view (x275). **2.** Left element (CPC 29050)[JHS K-144]; **a,** stereo pair, inner lateral view; **b,** stereo pair, outer lateral view; **c,** stereo pair, posterior view; **d,** enlargement of posterior surface of cusp showing microstriae, x1350; **e,** anterior view (x275).

Figure 3. ***Eodentatus bicuspatus*****, ramiform element.**
All figures x200. The number in parentheses is the Commonwealth Palaeontological Collection (CPC) number, and the number in square brackets indicates the sample from which the specimen was obtained.
1. (Paratype, CPC 29045)[BMA 79]; **a,** stereo pair, lateral view; **b,** lateral view. **2.** (Holotype, CPC 29046)[BMA 79]; **a,** stereo pair, lateral view; **b,** aboral view; **c,** sketch showing outline of basal cavity and white matter distribution. **3.** (Paratype, CPC 29047)[BMA 82]; **a,** stereo pair, lateral view; **b,** oblique base view; **c,** sketch showing outline of basal cavity and white matter distribution. **4.** (Paratype, CPC 29048)[BMA 79]; **a,** stereo pair, lateral view; **b,** oral view; **c,** oblique lateral view.

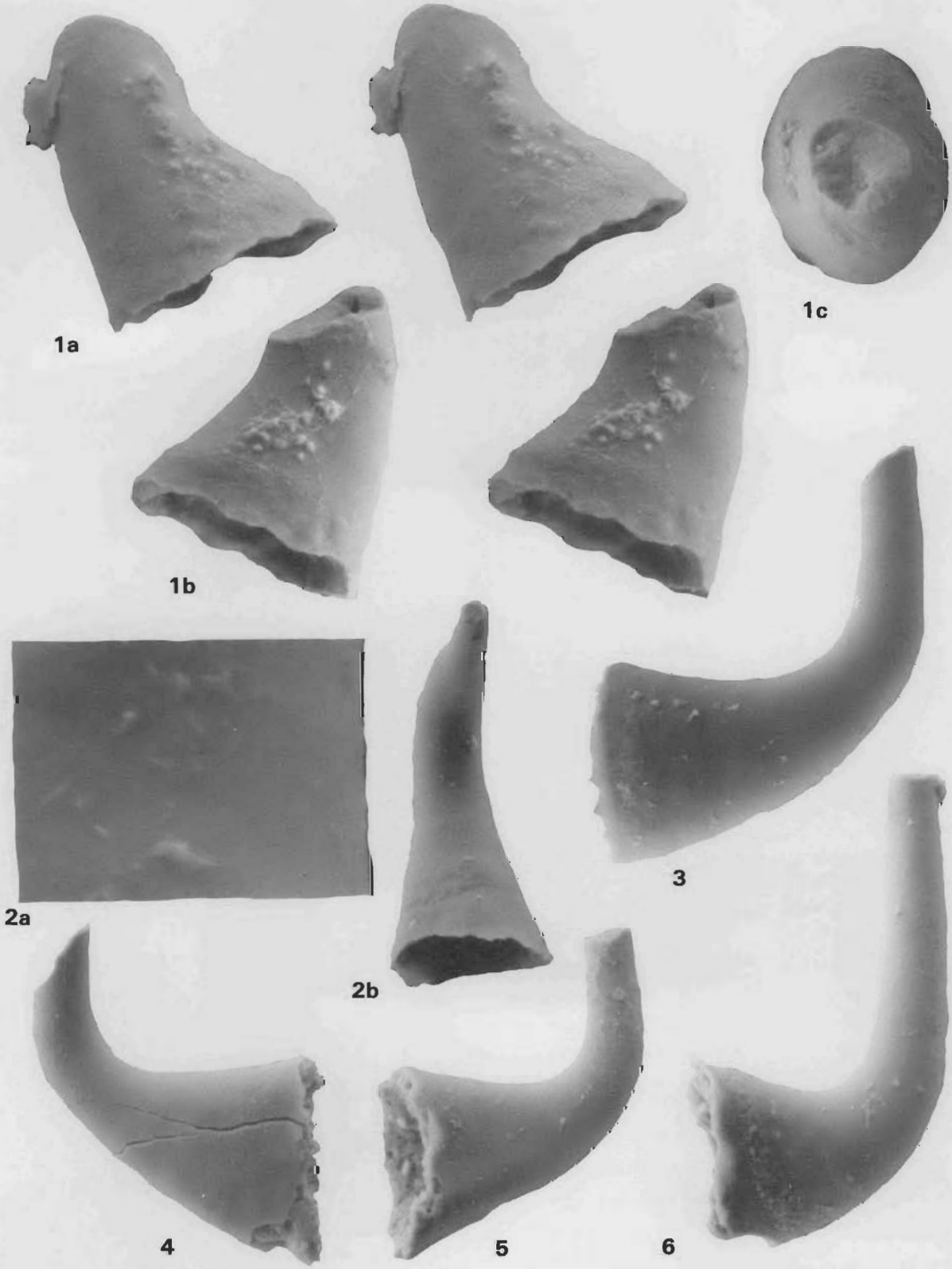

Figure 5. *Hirsutodontus nodus* and *Teridontus nakamurai*.
All figures x200, except as noted.
1. *Hirsutodontus nodus*, coniform element (CPC 29051)[JHS K-144]; right element; **a,** stereo pair, inner lateral view; **b,** stereo pair, outer lateral view; **c,** anterior view; note microstriae on posterior face in 1b and c. **2–6.** *Teridontus nakamurai*, coniform element. **2. Sa element** (CPC 29052)[BMA 15]; **a,** enlargement of posterior side of cusp showing non-microstriate surface, x950; **b,** oblique posterior view. **3.** (CPC 29053)[BMA 15]; outer lateral view. **4.** (CPC 29054)[BMA 15]; inner lateral view. **5.** (CPC 29055)[BMA 15]; outer lateral view. **6.** (CPC 29056)[BMA 15] outer lateral view.

Chatsworth Limestone and the Ninmaroo Formation, are possibly assignable to *H. nodus*.

Hispidodontus gen. nov.

Type species. *Hispidodontus discretus* gen. et sp. nov.

Derivation of name. *Hispidus*, L., bristly or prickly, and *odontos*, Gk., tooth.

Diagnosis. Multimembrate apparatus of at least five elements. Elements are modified coniform types with a broad shovel-shaped expansion of the anterior face and little or no growth of the posterior face. Shape of the individual elements is variable. The elements have a large basal plate and attachment area with a small basal pit located near the apex. In those elements with a prominent cusp the cavity extends into the large cusp denticle near the apex of the element. The oral surface is covered with short solid spines or denticles. On the distal edges of the outer surface the spines are discrete, but toward the apex the spines may be laterally appressed. Spine length and packing density are variable. Some elements have a distinct cusp. White matter may be present in the spines of some species.

Orientation. Examination of the elements of the three species assigned to this genus indicates that the elements should be oriented with the cusp (if developed) curving posteriorly, and the nodes or spines developed on the anterior face of the element. The basal attachment surface thus opens downward or posteriorly. This growth pattern indicates that the addition of phosphate takes place preferentially on the broad anterior face and almost no growth occurs on the posterior side of the element.

Apparatus structure and element designation. Five element types have been differentiated for the best preserved species found in this study. The elements are divided into S and P elements based on gross morphology. The S elements have splayed lateral edges, but the P elements have a more irregular outline. The Sa elements are anteriorly-posteriorly compressed. The rest of the S elements are separated on the basis of the increasing divergence of the lateral margins. The Sc element margins are nearly parallel and the Sd margins are the most divergent. Only one type of P element has thus far been differentiated, but with more material it would be expected that a second type of P element would be found. No M element was found; this confirms the suggestion by Nicoll (1990) that many coniform apparatuses lack an M element.

Remarks. *Hispidodontus* is similar to *Hirsutodontus* because both genera have spine development on the element surface. They may be distinguished easily because *Hirsutodontus* is a coniform element with a constricted basal diameter and *Hispidodontus* has an enlarged anterior face and basal attachment area. It is probable that the two genera were derived from different lineages and, despite the development of similar spine morphology, are not closely related. The oldest species assigned to *Hirsutodontus*, *H. nodus* (Zhang & Xiang, 1983), is a coniform element with a small diameter base and solid white matter in the upper part of the cusp. *Hirsutodontus* is probably derived from an early form of *Teridontus* Miller (1980) with the development of nodes, as the precursors of spines, on the lateral face of the base of the element. By contrast, *Hispidodontus* appears to be more closely related by morphology to forms like *Granatodontus ani*. Both *Hispidodontus* and *Hirsutodontus* are similar in that the larger (taller) nodes or spines of some species are formed by white matter.

Hispidodontus is a modified coniform element that has a very open or broad basal attachment area. Near the apex of this attachment area there may be a constriction that has a small basal pit which extends up into the cusp, if one is clearly defined, or into the tip of the element. The gross morphology of the genus is similar to that of the P elements of the genus *Pygodus*, but the structure of the apparatus in not similar to that genus.

Three species of the genus are differentiated in this study. They are distinguished on the basis of changes in oral surface ornamentation and cusp development (see below). There appears to be a gradual evolution of the features that distinguish these species, and we think that this indicates an essentially continuous record of the genus in our samples.

Hispidodontus appressus sp. nov.
Figures 6, 7, 16.3

Derivation of name. *Appressus*, L., close, referring to the closely spaced or touching spines.

Material studied. 23 elements.

Diagnosis. Multimembrate apparatus, two elements differentiated in the limited material studied, with enlarged attachment area and abundant closely spaced short spines on the oral surface. The small basal pit is at the apex of the element and, in most specimens, extends into a short, broad denticle. Development of an apical cusp is variable and in some specimens it may be lacking. Elements are differentiated by gross morphological features and element symmetry.

Description. Only the Sb and Sd elements have been recognised among the 23 elements so far recovered. The S elements of *H. appressus* have closely spaced short nodes or spines on a large anterior oral surface. The basal attachment area is large and narrows toward the element apex. The apex of most elements is marked by a short to squat conical cusp that is pointed and may have a number of nodes on the anterior surface. The posterior side of the element generally lacks nodes. The cusp may be lacking in some elements which have only a rounded apical surface that usually lacks nodes. There is a small basal pit under the cusp at the apex of the basal attachment area. The Sb element is subsymmetrical and the lateral margins make an angle of 45–60° with each other. The Sd element is asymmetrical with the cusp located off-centre. The element has boxed margins defining the edges of the apex of the attachment area.

Remarks. The three species of *Hispidodontus* differentiated are distinguished on the following features:

1. Both *H. appressus* and *H. resimus* have short, closely spaced nodes or spines on the oral surface. *H. discretus* has longer, widely spaced spines and the tips of some of the spines are composed of white matter.
2. *H. discretus* has a prominent cusp, *H. appressus* usually has a short, pointed stubby cusp, and in *H. resimus* the cusp, if developed, is short and blunt with one or more nodes on the oral surface.

The gross morphology of individual element types appears to be very similar in all three species. The Sa elements are laterally expanded and anteriorly-posteriorly compressed. The Sc element has the lateral flange margins of the base subparallel, the Sb element has the flange margins angled about 30–60° apart. The Sd element is similar to the Sb element in the angle of spread of the lateral margins, but instead of the flange margins narrowing to a rounded outline below the element apex, the last part of the margin is box-like with parallel lateral margins. Only one P element form is identified,

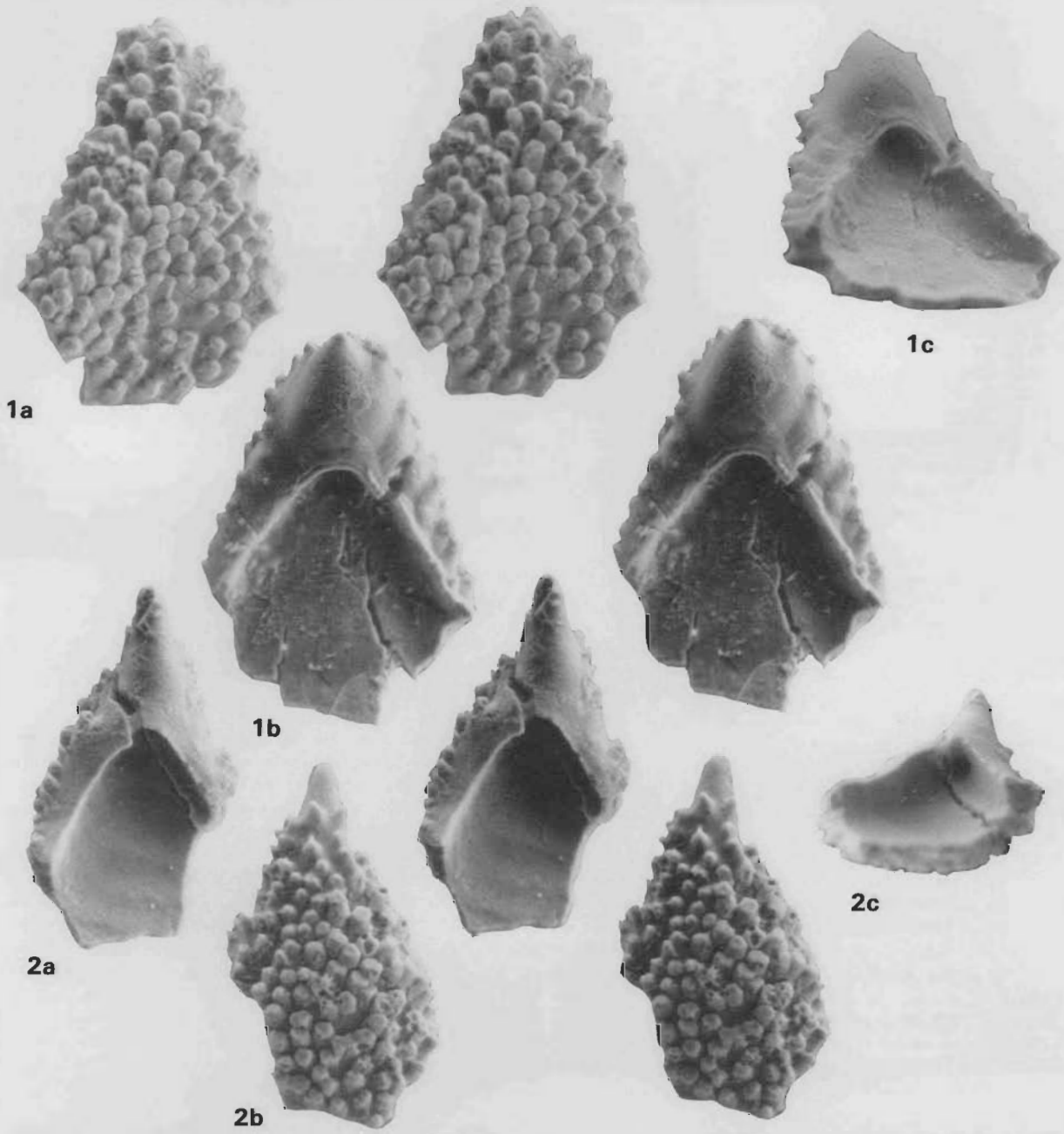

Figure 6. ***Hispidodontus appressus,*** **Sb element.**
All figures x200.
1. (Paratype, CPC 29057)[BMA 64]; **a,** stereo pair, anterior view; **b,** stereo pair, posterior view; **c,** view into basal pit. **2.** (Paratype, CPC 29058)[BMA 68]; **a,** stereo pair, posterior view; **b,** stereo pair, anterior view; **c,** view into basal pit.

and this element is subround in outline, rather than elongated like the S elements. Differentiation of these species from other genera is discussed above in remarks on the genus.

Abaimova (1975) described the species *Clavohamulus triangularis* based on three specimens. The illustrations are not sufficient to determine the nature of the species, but it was also illustrated with an SEM photo by Abaimova & Moskalenko (1984, Pl. 6, figs 2, 3) and this specimen is certainly an Sb element that is assignable to a species of *Hispidodontus*. Because the Sb elements of *H. resimus* and *H. appressus* are very similar, and are not necessarily species diagnostic, we are unable to determine if the Russian material is conspecific with either of these species. Additional Russian material of other elements of the species would have to be illustrated to determine the species relationship of the Australian and Russian material. However, the Russian material is associated with *Cordylodus proavus*, and must be considered slightly younger than the Australian material that occurs below the first occurrence of *Cordylodus*.

Hispidodontus discretus sp. nov.
Figures 8–13

Derivation of name. *Discretus*, L., separate, distinct, referring to the free standing nature of the spines.

Material studied. 101 elements.

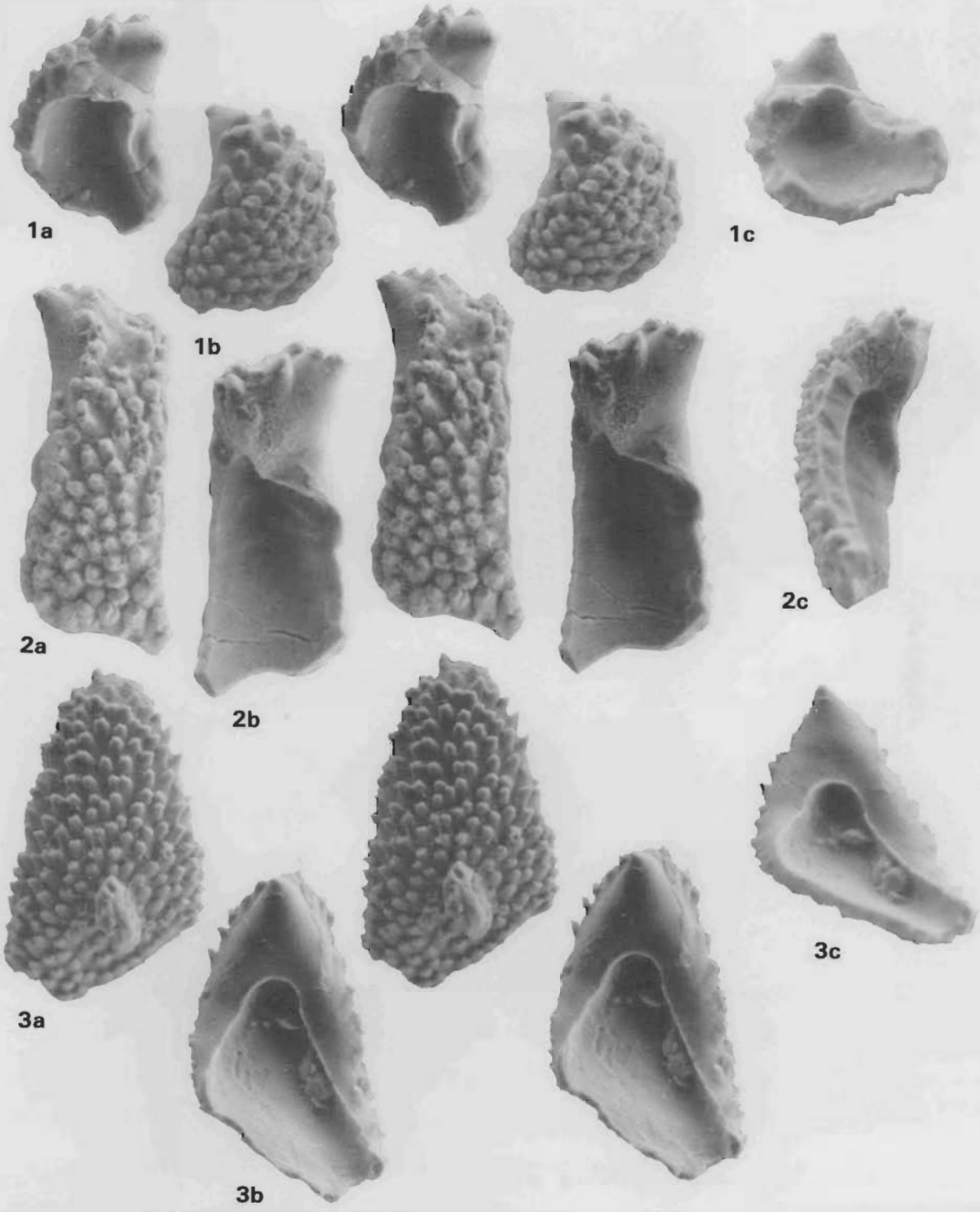

Figure 7. *Hispidodontus appressus*, Sb and Sd elements.
All figures x200.
1. Sd element (paratype, CPC 29059)[BMA 68]; left element; **a,** stereo pair, posterior view; **b,** stereo pair, anterior view; **c,** view into basal pit. **2. Sd element** (paratype, CPC 29060)[BMA 68]; left element; **a,** stereo pair, anterior view; **b,** stereo pair, posterior view; **c,** outer lateral view. **3. Sb element** (holotype, CPC 29061)[BMA 68]; **a,** stereo pair, anterior view; **b,** stereo pair, posterior view; **c,** view into basal pit.

Diagnosis. Multimembrate apparatus, five elements differentiated in the limited material studied, with enlarged attachment area and well developed discrete spines on the oral surface. The spines are of moderate length and the tips are composed of white matter. The small basal cavity extends into the cusp denticle and is near the apex of the element. Except for the spines the oral surface is smooth, lacking costae, keels or striae. Elements are differentiated by gross morphological features and element symmetry.

Description. All five elements of *H. discretus* recognised in this study have similar morphologic features on the oral and

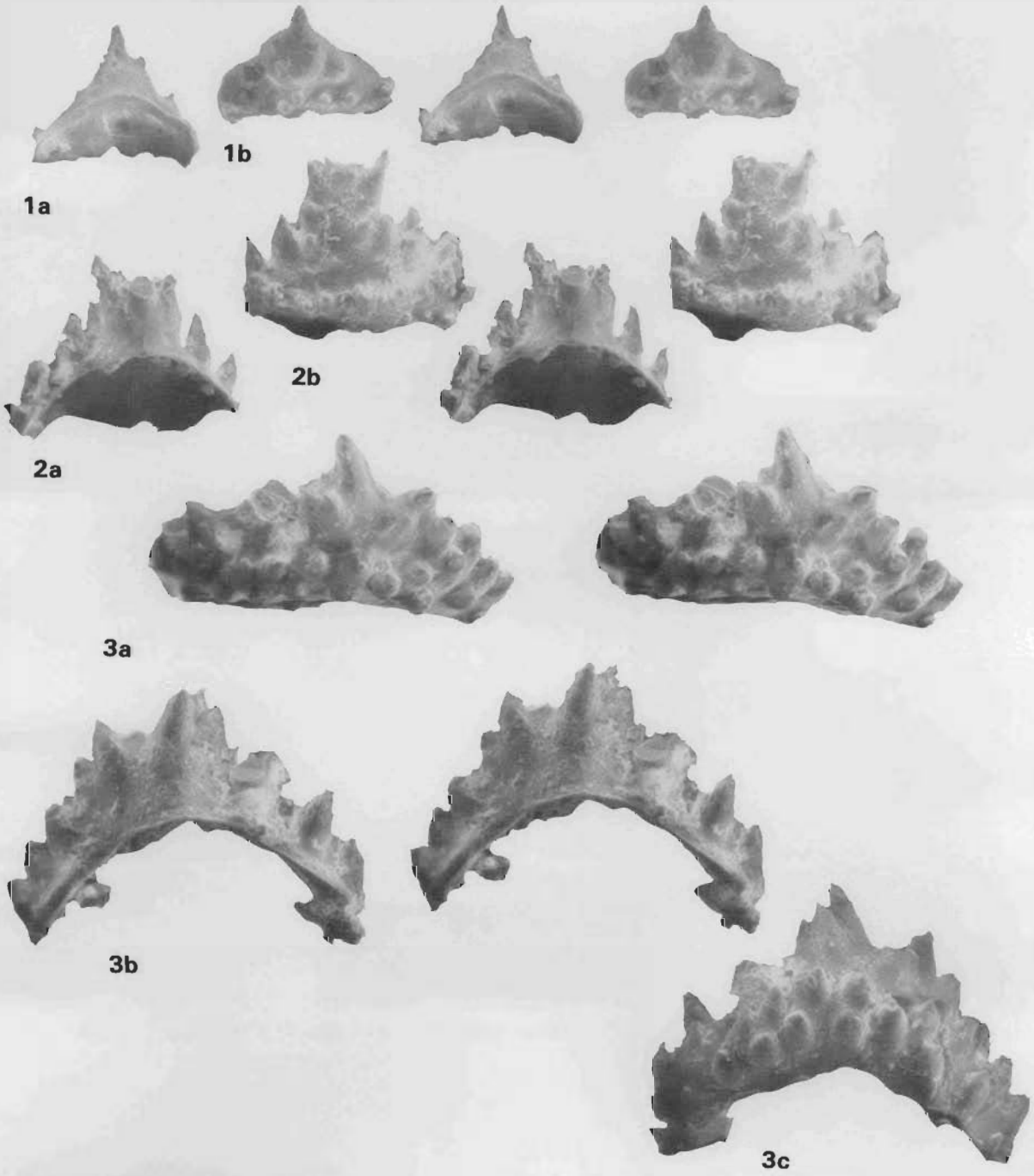

Figure 8. ***Hispidodontus discretus,*** **Sa element.**
All figures x200.
1. (Paratype, CPC 29063)[BMA 81] **a,** stereo pair, **2.** (Paratype, CPC 29064)[BMA 81]; **a,** stereo pair, oblique posterior view; **b,** stereo pair, anterior view. **3.** (Paratype, CPC 29065)[BMA 81]; **a,** stereo pair, oblique oral view; **b,** stereo pair, posterior view; **c,** anterior view.

aboral surfaces, and are differentiated on the basis of the element shape. The oral surface is covered with short to moderate length, discrete spines and the upper half to two-thirds of the spine is composed of white matter. Spines near the cusp appear to be randomly arranged, but those near the distal margin are arranged in rows of up to 10 or 12 spines parallel to the element margin.

The Sa element is anteriorly-posteriorly compressed with a single prominent cusp and up to 12 spines along the distal anterior margin. Two to three slightly irregular rows of spines can be observed on the larger elements.

The rest of the S elements are similar, differing mostly in the outline of the element. All are asymmetrical and have a slight degree of lateral curvature. The longest spine or denticle is located over the basal pit at the apex of the element. The spines are arranged in irregular arcuate rows that roughly parallel the distal anterior margin. All spines are discrete. The basal pit is in a slight depression, as the posterior lateral margins form a sort of flange round the posterior margin. There are no spines on the posterior side of the element.

The elements differ in the degree of lateral flare of the posterior lateral margins. The Sc element has roughly parallel lateral

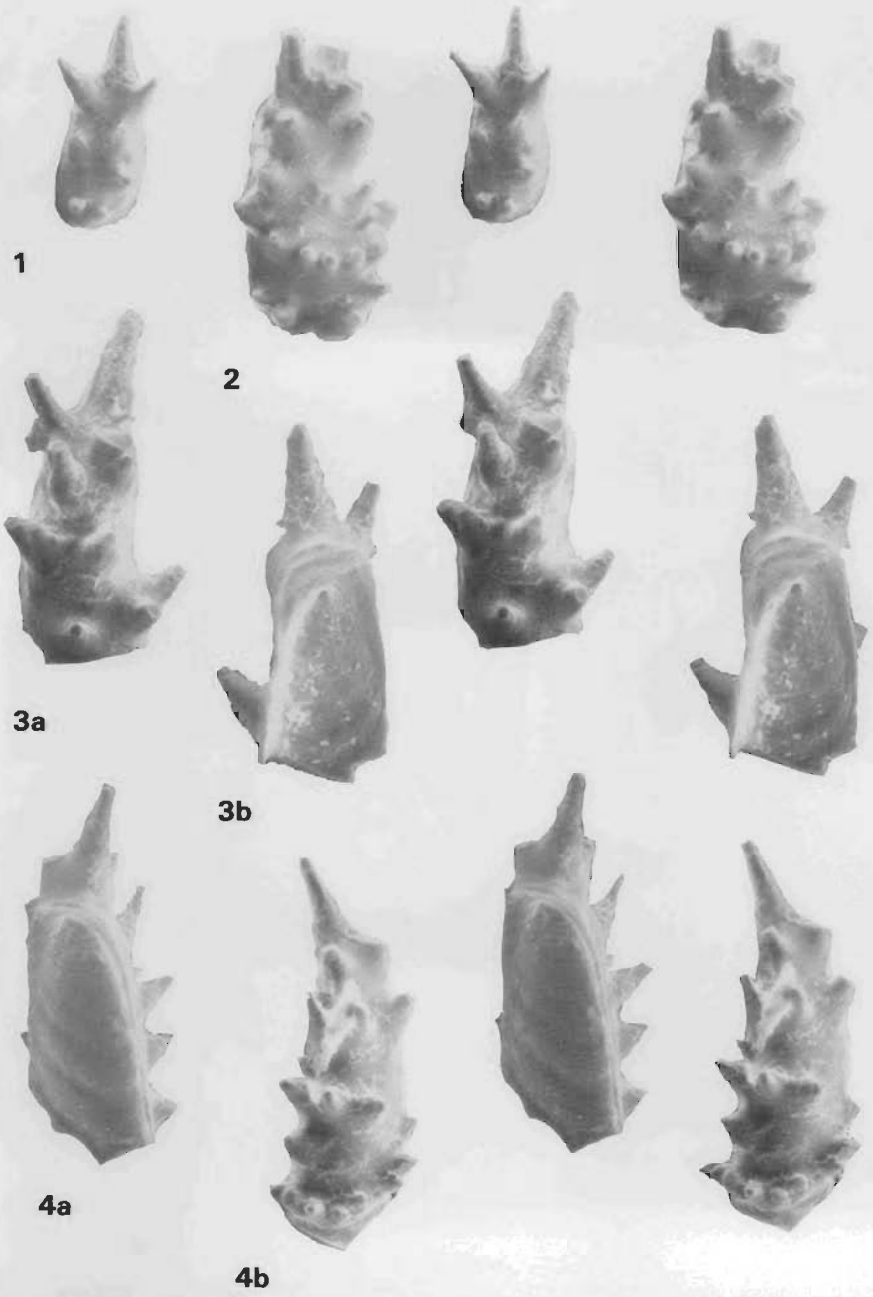

Figure 9. ***Hispidodontus discretus,*** **Sc element.**
All figures x200.
1. (Paratype, CPC 29066)[BMA 81] right element; stereo pair, anterior view. **2.** Left element (paratype, CPC 29067)[BMA 81]; stereo pair, anterior view. **3.** Left element (paratype, CPC 29068)[BMA 81]; **a,** stereo pair, anterior view; **b,** stereo pair, posterior view. **4.** Left element (paratype, CPC 29069)[BMA 81]; **a,** stereo pair, posterior view; **b,** stereo pair, anterior view.

margins and the distal anterior margin is rounded. The Sb element has an angle of 35–60° between the posterior lateral margins. The Sd element has a similar angle between the posterior lateral margins, but has a boxed area at the apex of the posterior lateral margins.

The P element differs from the S elements by lacking the laterally flared posterior lateral margins. The basal outline is irregular but almost round, with the basal pit located off-centre and toward the posterior margin. The pattern of denticles on the oral surface gives the element the appearance of having been laterally twisted.

Remarks. See remarks under *H. appressus*. *H. discretus* is the youngest of the three species of *Hispidodontus* recognised in this study, and has the largest and best developed spines.

Hispidodontus resimus sp. nov.
Figures 14, 15, 16.1–16.2

Derivation of name. *Resimus*, L., turned up, bent back, referring to the orientation of the apical protuberence.

Material studied. 20 elements.

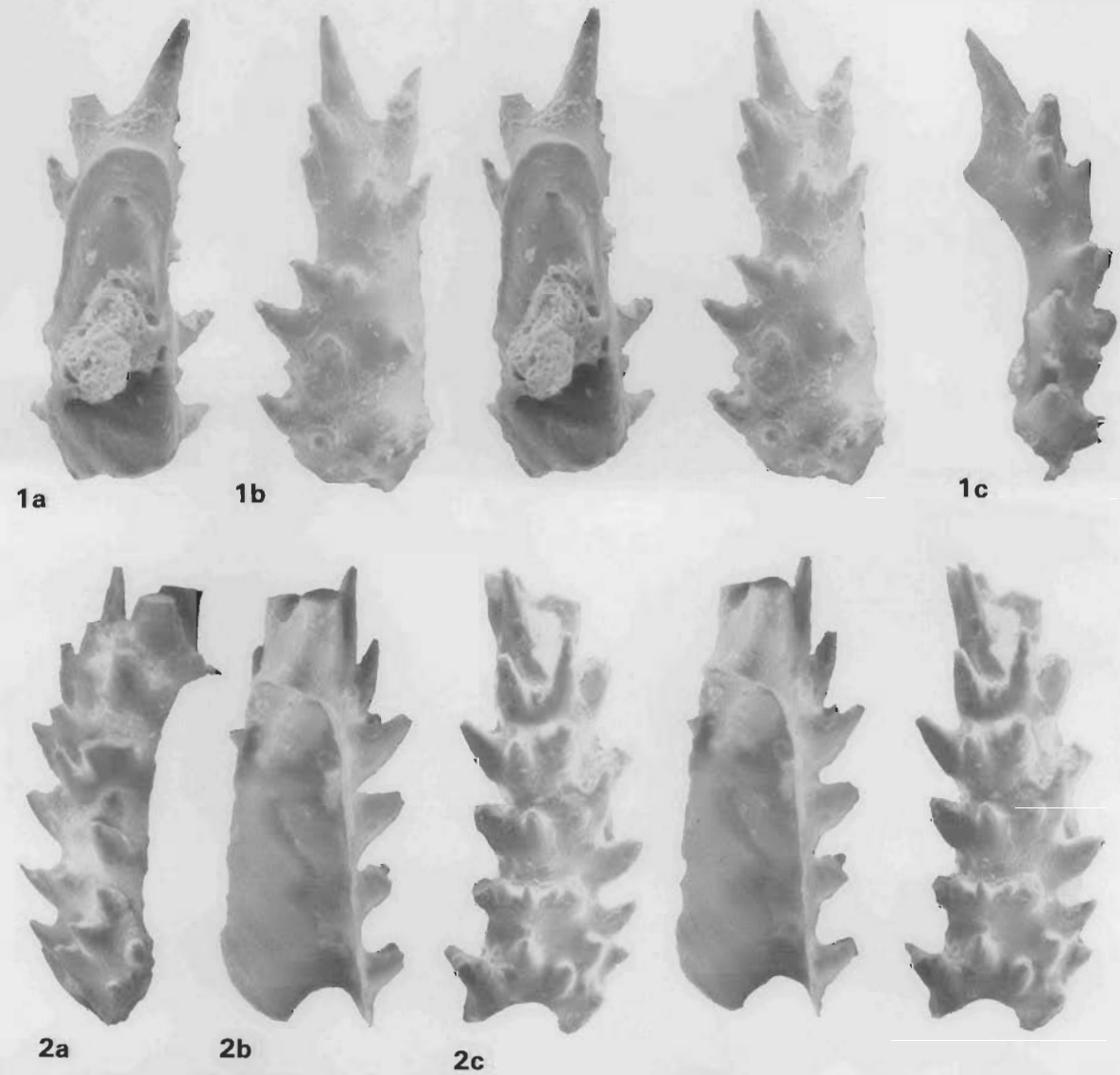

Figure 10. ***Hispidodontus discretus,*** **Sc element.**
All figures x200.
1. Right element (holotype, CPC 29070)[BMA 81]; **a,** stereo pair, posterior view; **b,** stereo pair, anterior view; **c,** inner lateral view. **2.** Right element (paratype, CPC 29071)[BMA 81] ; **a,** outer lateral view; **b,** stereo pair, posterior view; **c,** stereo pair, anterior view.

Diagnosis. Multimembrate apparatus with enlarged attachment area and abundant closely spaced short spines or nodes on the oral surface. The small basal pit is at the apex of the element. The apex is rounded in some elements, but other elements have a short, broad protuberance with several nodes on the upper and anterior surface. Elements are differentiated by gross morphological features and element symmetry.

Description. All four S elements (Sa, Sc, Sb & Sd) are differentiated in the limited material studied. They are modified coniform elements with an enlarged anterior face covered with short nodes or spines, and a very reduced posterior face that lacks nodes. The basal attachment area is enlarged and there is a small basal pit near the apex of the element. Some elements, usually the Sa and Sd elements, have a short blunt cusp at the apex of the element and this truncated cusp has several nodes on the upper and anterior surfaces.

The Sa element is symmetrical, with a short snubbed cusp that has several spines on its upper and anterior surface. The wide anterior face is covered with short, usually discrete, spines; in oral view, the anterior margins are curved posteriorly. The narrow posterior face lacks denticles on either the cusp or lateral wings.

The Sc and Sb elements are similar in shape with no cusp, but a broadly rounded apex. Both elements are slightly asymmetrical but differ in the angle of separation of the lateral posterior margins. In the Sc element the distal parts of the margins are essentially parallel, but in the Sb element the margins form an angle of divergence from the apex of about 40–60°.

The Sd element has a short cusp, similar to that found on the Sa element. It also is similar to the Sb element, except that the cusp is asymmetrically located and the lateral margins of the basal cavity near the apex are parallel to each other.

Remarks. No P elements were identified in the limited fauna examined, but based on their existence in the apparatus of *H. discretus*, it is anticipated that larger collections would establish the existence of two P elements.

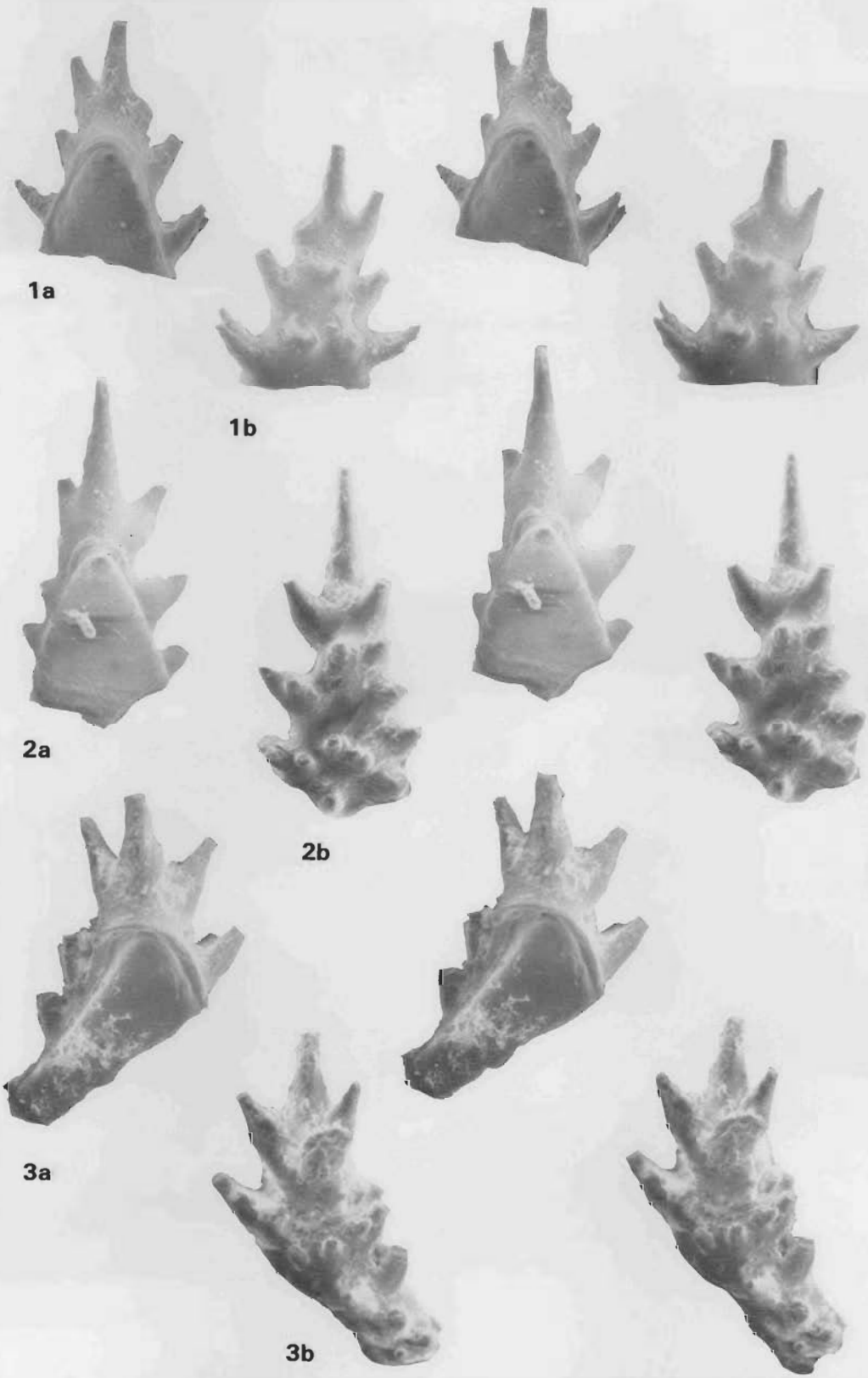

Figure 11. ***Hispidodontus discretus,*** **Sb and Sd elements.**
All figures x200.
1. Sb element (paratype, CPC 29072) [BMA 81]; **a,** stereo pair, posterior view; **b,** stereo pair, anterior view. **2. Sb element** (paratype, CPC 29073)[BMA 81]; **a,** stereo pair, posterior view; **b,** stereo pair, anterior view. **3. Sd element** (paratype, CPC 29074)[BMA 81]; **a,** stereo pair, posterior view; **b,** stereo pair, anterior view.

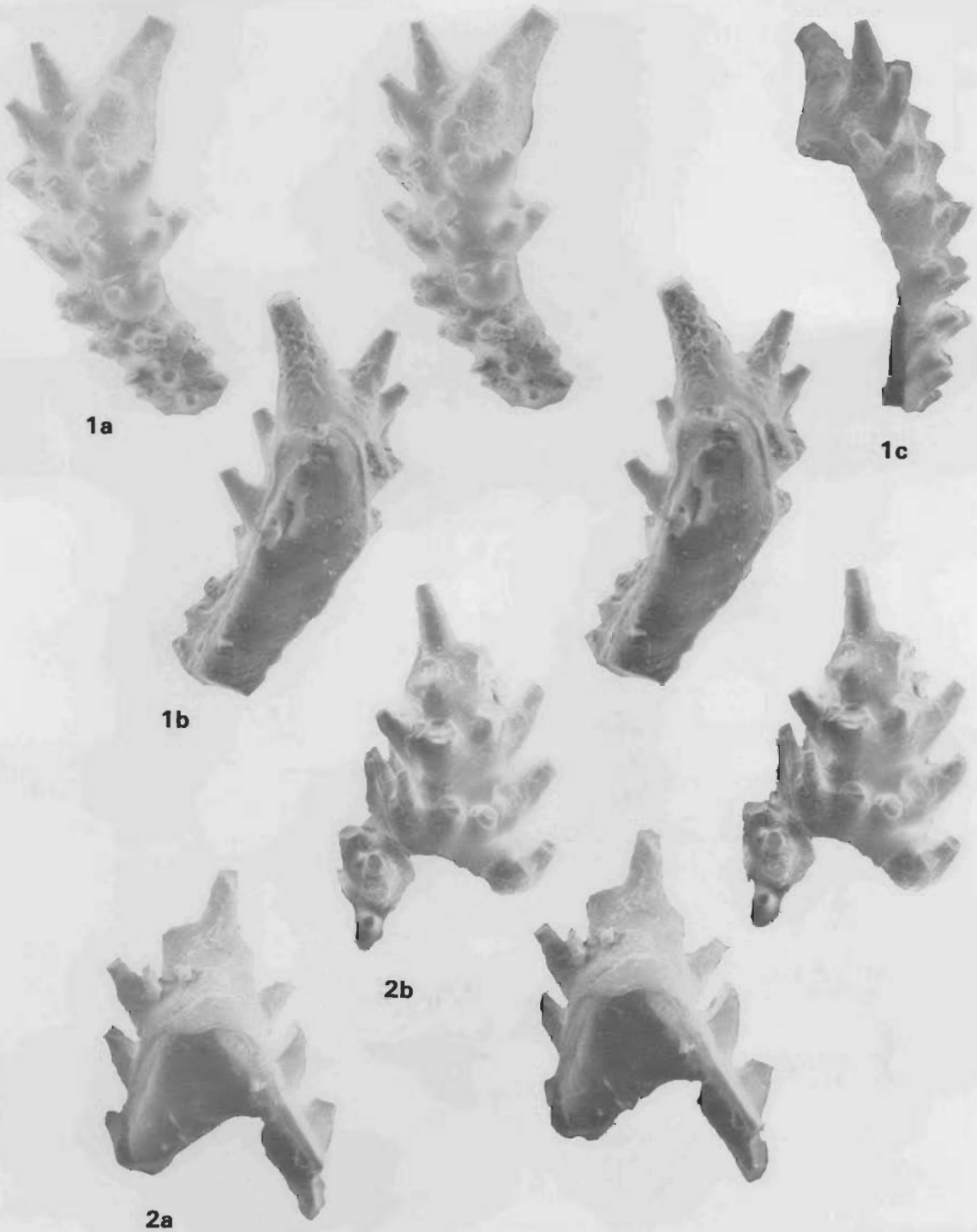

Figure 12. ***Hispidodontus discretus,*** **Sd element.**
All figures x200.
1. Left element (paratype, CPC 29075)[BMA 81]; **a,** stereo pair, anterior view; **b,** stereo pair, posterior view; **c,** lateral view. **2.** Right element (paratype, CPC 29076)[BMA 81]; **a,** stereo pair, posterior view; **b,** stereo pair, anterior view.

Teridontus Miller, 1980

Type species. *Oneotodus nakamurai* Nogami, 1967.

Emended diagnosis. Multimembrate coniform apparatus of six element types, lacking an M element. Elements lack keels, costae and carinae but may have smooth or striate surface texture. Elements of apparatus typified by a planar change from the hyaline base to the solid white matter of the cusp. Elements usually reclined, bent just above the tip of the basal cavity, and circular to laterally compressed in cross-section.

Remarks. Miller (1980), when he established the genus, did not include all of the element forms described by Nogami (1967) in the genus. Our observations include both the rounded and laterally compressed forms in the apparatus. Only coniform elements with a sharp, planar change from the

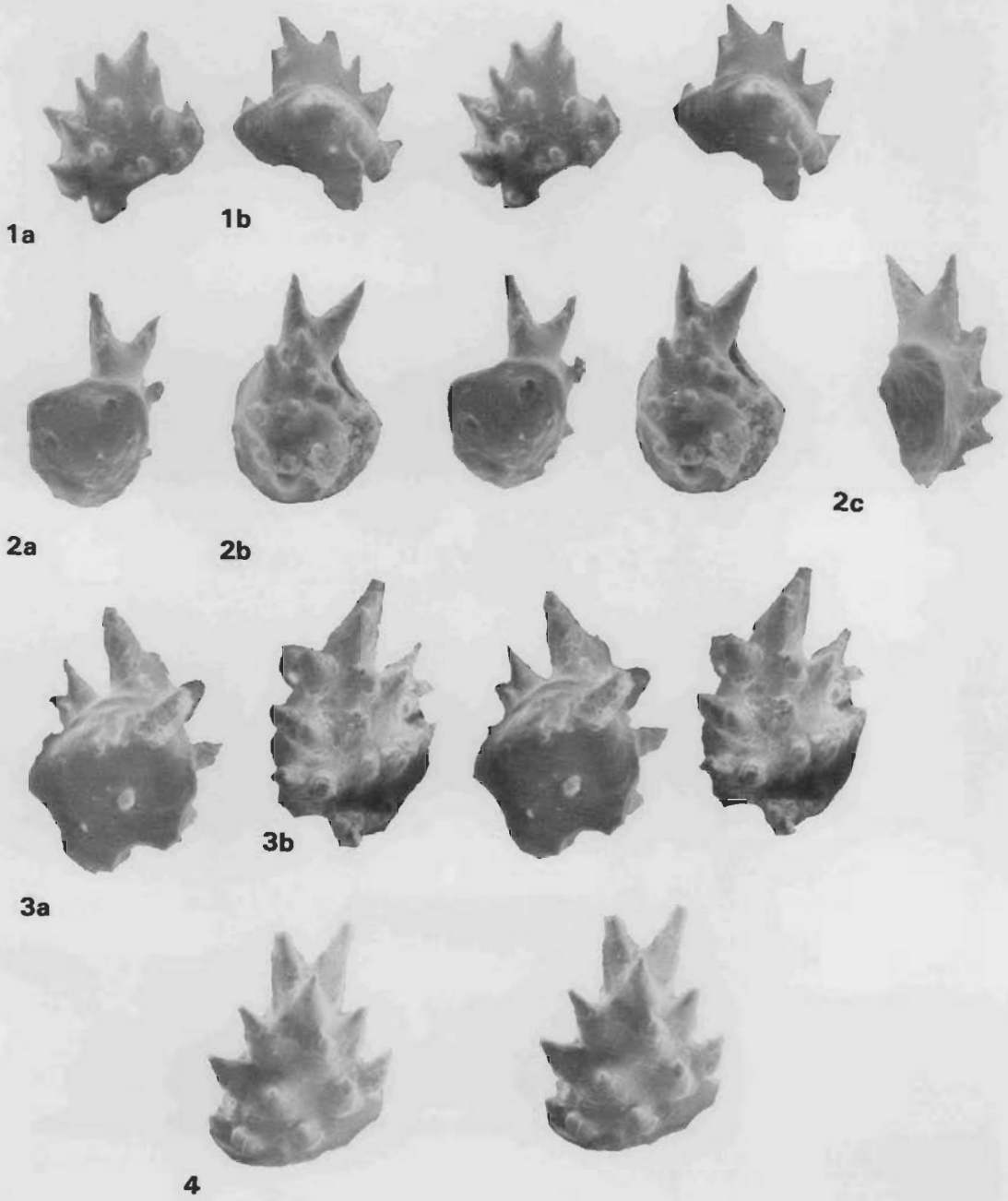

Figure 13. *Hispidodontus discretus*, P element.
All figures x200.
1. Left element (paratype, CPC 29077)[BMA 81]; **a**, stereo pair, anterior view; **b**, stereo pair, posterior view. **2.** Left element (paratype, CPC 29078)[BMA 81]; **a**, stereo pair, posterior view; **b**, stereo pair, anterior view; **c**, outer lateral view. **3.** Left element (paratype, CPC 29079)[BMA 81]; **a**, stereo pair, posterior view; **b**, stereo pair, anterior view. **4.** Left element (paratype, CPC 29080)[BMA 81]; stereo pair, anterior view.

hyaline base to the white matter of the cusp should be included in the genus. The white matter of the cusp is usually solid, and is neither confined to the growth axis nor diffuse.

Teridontus nakamurai (Nogami, 1967)
Figures 5.2–5.6

Synonymy.
1967 *Oneotodus nakamurai* Nogami, pp. 216–217, Pl. 1, figs 9–13, text-fig. 3 A–E (see remarks below).

Material studied. 36 elements.

Diagnosis. A multimembrate coniform apparatus with both S and P elements. All elements have a hyaline base and the tip of the cusp, that part above the tip of the basal cavity, is composed of dense white matter. Separation of white and hyaline material is abrupt and planar. Length of the basal cavity is variable, but in all cases the cavity extends to just above the bend of the cusp. The tip of the basal cavity terminates against white matter near the anterior margin. Element cross-section is variable, with some elements laterally compressed and others round to subround. A symmetrical Sa element can be identified. The cusp is round to subround in cross-section. The element surface is smooth, lacking surface ornamentation. At high magnification (x1000) no microstriation could be ob-

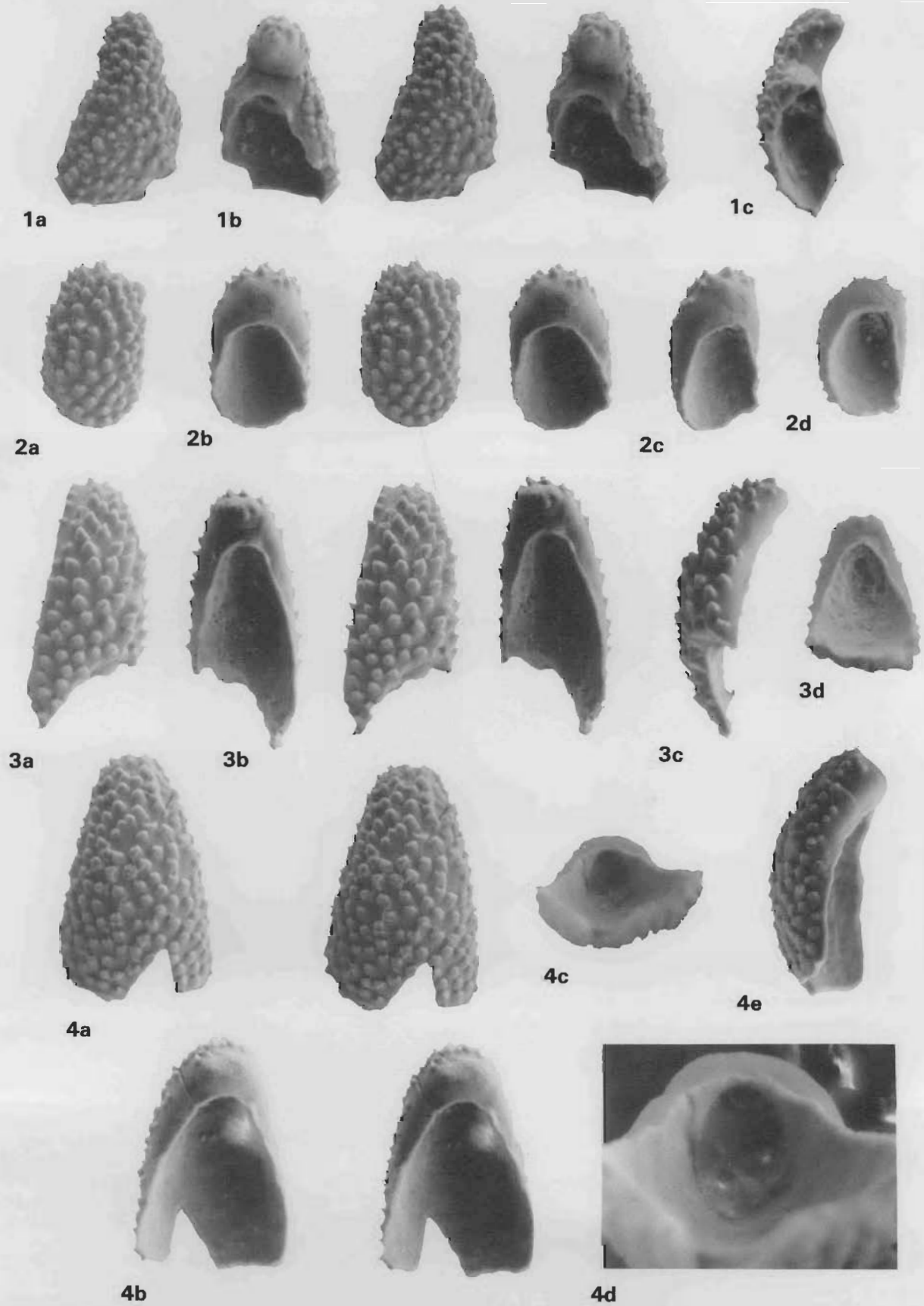

Figure 14. ***Hispidodontus resimus,*** **Sc, Sb and Sd elements.**
All figures x200, except as noted.
1. Sd element (paratype, CPC 29081)[BMA 50] right element; **a,** stereo pair, anterior view; **b,** stereo pair, posterior view; **c,** inner lateral view. **2. Sb element** (paratype, CPC 29082)[BMA 50] left element; **a,** stereo pair, anterior view; **b,** stereo pair, posterior view; **c,** oblique lateral view; **d,** view into basal cavity. **3. Sc element** (holotype, CPC 29083)[BMA 53] left element; **a,** stereo pair anterior view; **b,** stereo pair, posterior view; **c,** inner lateral view; **d,** view into basal cavity. **4. Sb element** (paratype, CPC 29084)[BMA 53] right element; **a,** stereo pair, anterior view; **b,** stereo pair, posterior view, **c,** view into basal cavity, **d,** enlargement of basal cavity opening (x430); **e,** outer lateral view.

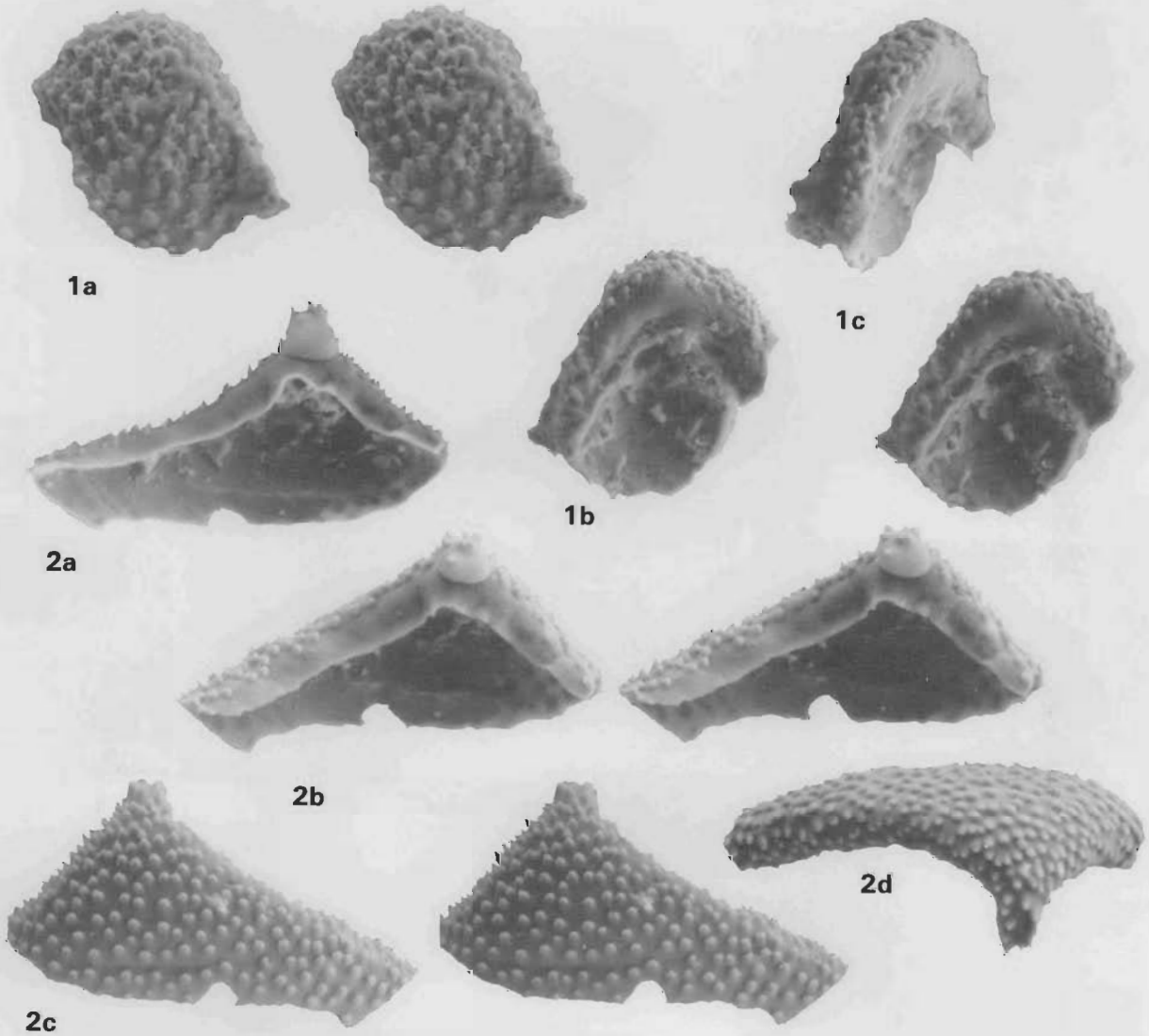

Figure 15. *Hispidodontus resimus*, S and Sa elements.
All figures x200.
1. S element (paratype, CPC 29085)[BMA 52] possible right element; **a,** stereo pair, anterior view; **b,** stereo pair, posterior view; **c,** outer lateral view. **2. Sa element** (paratype, CPC 29086)[BMA 54] symmetrical element; **a,** posterior view; **b,** stereo pair, oblique posterior view; **c,** stereo pair, anterior view; **d,** oral view.

served. Costae and keels are lacking. No M element appears to be associated with the apparatus.

Remarks. Miller (1980) established the new genus *Teridontus* and nominated *Oneotodus nakamurai* Nogami (1967) as the type species. Miller's (1980) description indicated that the species had microstriae on the surface of the base and cusp. However, examination of the material recovered from Black Mountain indicates that the surface of the elements is smooth, lacking striae, keels or costae. Nogami (1967) did not describe striae in his material. The material illustrated by Miller also differs from our specimens, and those illustrated by Nogami (1967). In Miller's material, the tip of the basal cavity of the striate forms is in the central part of the cusp, while the stratigraphically older specimens of our study, and those figured by Nogami (1967), have the cusp tip near the anterior margin. Miller also excluded some of the laterally compressed specimens of Nogami (1976, Pl. 1, figs 10, 11) and suggested that they belonged to *Eoconodontus notchpeakensis*. We have similar compressed elements in our collection and believe that they are part of the apparatus of *T. nakamurai*.

Our interpretation of *T. nakamurai* is thus of a multimembrate apparatus, as indicated by Nogami (1967, text-figs 3a–e), in which the distinction of element types is based primarily on variation in cross-sectional shape. The elements have a smooth surface, a basal cavity of moderate depth, and a cusp composed of white matter above the basal cavity. The tip of the basal cavity is near the anterior margin of the element. A planar surface at the tip of the basal cavity separates white and hyaline matter. We believe that careful examination of these coniform elements will exclude most of the elements previously assigned to *T. nakamurai* from stratigraphic levels above the *Eoconodontus* Zone.

Teridontus n. sp. A
Figures 17.1–17.5

Material studied. 6 elements.

Diagnosis. Multimembrate coniform apparatus of elements with coarse striae on the posterior and lateral margins and a

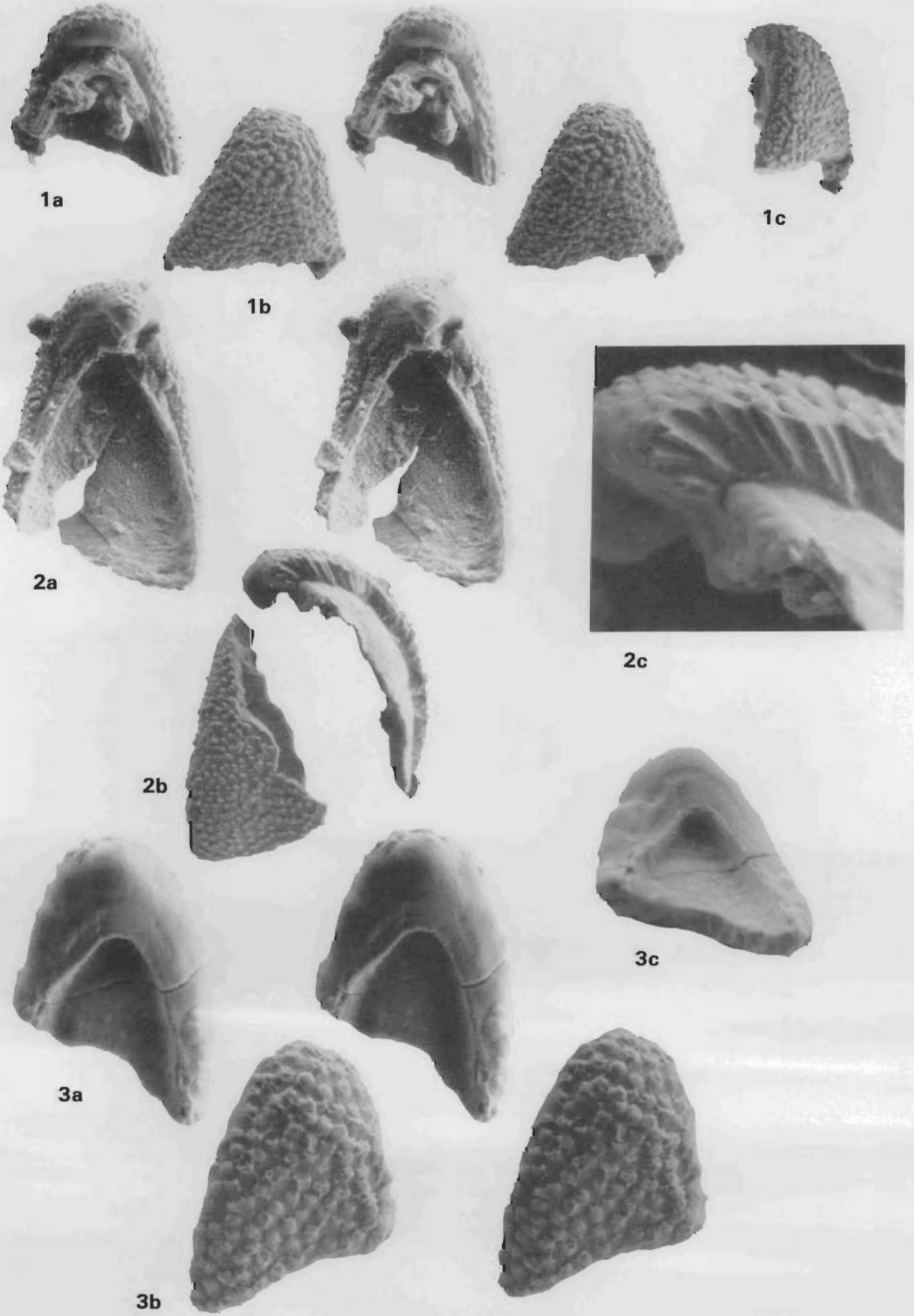

Figure 16. ***Hispidodontus resimus*** **and** ***Hispidodontus appressus*****, Sb elements.**
All figures x200, except as noted.
Hispidodontus resimus**. 1.** (Paratype, CPC 29087)[K-135]; **a,** stereo pair, posterior view; **b,** stereo pair, anterior view; **c,** lateral view. **2.** (paratype, CPC 29088)[K-135]; **a,** stereo pair, posterior view, repositioned broken fragments; **b,** anterior view, fragments not placed together; **c,** enlargement of lateral view showing structure of crown and basal plate (x760). **3.** ***Hispidodontus appressus*** (paratype, CPC 29062)[BMA 68]; **a,** stereo pair, posterior view; **b,** stereo pair, anterior view; **c,** view into basal cavity.

smooth anterior margin. All elements bent at the tip of the basal cavity. Basal cavity shallow; cusp composed of solid white matter. The base of the cusp white matter is planar and located at the tip of the basal cavity.

Description. Multimembrate coniform apparatus of elements with coarse striae on the posterior and lateral margins and a smooth anterior margin. The striae extend from the upper part of the cusp to near the base, but the basal margin has a smooth band extending around the element. Elements include a symmetrical element with an ovate cross-section, and asymmetrical elements with both round to laterally compressed basal cross-sections. Above the relatively shallow basal cavity, the cusp is composed of solid white matter. The white matter to hyaline matter transition is planar and located at the tip of the basal cavity.

Remarks. Too few elements were recovered to speculate about the apparatus structure of this species. It has been assigned to *Teridontus* on the basis of the elements lacking keels, carinae or costae, and the presence of solid white matter in the cusp that is separated from the hyaline material of the base by a planer surface.

Undescribed coniform taxa

As this is primarily a biostratigraphic paper, and because only a limited number of elements have been examined, we have not attempted to describe several of the coniform element apparatuses observed in samples examined. When more material becomes available we will treat these species in greater detail. However, because we make reference to these taxa in the range chart, the following observations will be made.

Coniform species A

Multimembrate coniform apparatus, entirely lacking white matter, even along the growth axis of the cusp. Cross-section round to laterally compressed.

Coniform species B

Multimembrate coniform apparatus, white matter found along the growth axis of the cusp only. Chen & Gong (1986) have applied the name *Teridontus gracilis* (Furnish) to similar material, but after examination of the type of *Distacodus*? *gracilis* Furnish, it is apparent that it represents a new species. Our material appears to be conspecific with that illustrated by Chen & Gong (1986, Pl. 39, figs 2, 10; Pl. 40, figs 10, 14; Pl. 47, figs 12, 15; text-figs 79–13, 14).

Coniform species C

Multimembrate coniform apparatus, similar to coniform species A in lacking white matter, but has an erect Sa element with an oval, flattened base.

Coniform species D

Multimembrate coniform apparatus, similar to coniform species A except for the presence of very diffuse white matter along the growth axis.

Teridontus ?species B

Multimembrate coniform apparatus, has white matter distribution similar to that of *T. nakamurai*, but has the tip of the basal cavity located centrally in the cusp. Element surface apparently smooth but not examined with scanning electron microscope.

Acknowledgements

The authors thank Clive Burrett (University of Tasmania) and Barry Cooper (South Australian Department of Mines and Energy) for their critical comments on the paper. The samples on which this study is based were collected for palaeomagnetic study by R.L. Ripperdan and J.L. Kirschvink (California Institute of Technology). New taxa described in this paper should be cited as Nicoll & Shergold. Photography was the work of Arthur T. Wilson (BMR).

References

Abaimova, G.P., 1975 — Early Ordovician conodonts from the middle reaches of the Lena River. *Siberian Scientific Research Institute of Geology, Geophysics and Mineral Resources (SMIIGGIMS), Transactions*, 207, 129 pp. [In Russian].

Abaimova, G.P. & Moskalenko, T.A., 1984 — Conodontophorida. *In* Kanugin, A.V., Obut, A.M. & Volkova, K.N. (editors), Ordovician of the Siberian Platform: Palaeontological Atlas. *USSR Academy of Sciences, Siberian Division, Institute of Geology and Geophysics, Transactions*, 590, 113–137. [In Russian].

An Taixiang, Zhang Fang, Xiang Weida, Zhang Youqin, Xu Wehao, Zhang Huijuan, Jiang Debiao, Yang Changsheng, Lin Liandi, Cui Zhantang & Yang Xinchang, 1983 — The conodonts of North China and adjacent regions. *Science Press, Beijing*, 223 pp. [In Chinese with English abstract].

Brown, G.A., 1961 — Stratigraphy, structure and sedimentary petrology of some Lower Palaeozoic limestones in the Boulia area, western Queensland. *M.Sc. thesis, University of Melbourne.*

Bruton, D.L., Erdtmann, B.-D. & Koch, L., 1982 — The Naersnes section, Oslo region, Norway: a candidate for the Cambrian–Ordovician boundary stratotype at the base of the Tremadoc Series. *In* Bassett, M.G. & Dean, W.T. (editors), The Cambrian–Ordovician Boundary: sections, fossil distributions and correlations. *National Museum of Wales, Geological Series*, 3, 61–69.

Cas, R.A.F. & Vandenberg, A.H.M., 1988 — Ordovician. *In* Douglas, J.G. & Ferguson, J.A. (editors), Geology of Victoria. *Geological Society of Australia, Victorian Division, Melbourne*, 63–102.

Chen Jun-yuan & Gong Wei-li, 1986 — Conodonts. *In* Chen Jun-yuan (editor) Aspects of the Cambrian–Ordovician Boundary in Dayangcha. *China Prospect Publishing House, Beijing*, 93–223.

Cooper, R.A., 1979 — Sequence and correlation of Tremadoc graptolite assemblages. *Alcheringa*, 3, 7–19.

Cooper, R.A., Erdtmann, B.-D. & Fortey, R.A., 1990 — Graptolites and the Cambrian–Ordovician boundary. *Contribution to IUGS Working Group on the Cambrian–Ordovician Boundary Circular*, 27.

Cooper, R.A. & Stewart, I., 1979 — The Tremadoc graptolite sequence of Lancefield, Victoria. *Palaeontology*, 22(4), 767–797, pl. 102–103.

Druce, E.C., 1978a — *Clavohamulus primitus* — a key North American conodont found in the Georgina Basin. *BMR Journal of Australian Geology & Geophysics*, 3, 351–355.

Druce, E.C., 1978b — Correlation of the Cambrian–Ordovician boundary in Australia. *In* Belford, D.J. & Scheibnerova, V. (editors), The Crespin volume: essays in honour of Irene Crespin. *Bureau of Mineral Resources, Australia, Bulletin* 192, 49–60.

Druce, E.C. & Jones, P.J., 1968 — Stratigraphical significance of conodonts in the Upper Cambrian and Lower Ordovician sequence of the Boulia region, western Queensland. *Australian Journal of Science*, 31(2), 88.

Druce, E.C. & Jones, P.J., 1971 — Cambro-Ordovician conodonts from the Burke River Structural Belt, Queensland. *Bureau of Mineral Resources, Australia, Bulletin* 110, 158 pp., 20 pl.

Druce, E.C., Shergold, J.H. & Radke, B.M., 1982 — A reassessment of the Cambrian–Ordovician boundary section at Black Mountain, western Queensland, Australia. *In* Bassett, M.G. & Dean, W.T. (editors), The Cambrian–Ordovician Boundary: sections, fossil distributions and correlations. *National Museum of Wales, Geological Series*, 3, 193–209.

Endo, R., 1931 — The Cambrian Period. *In* Iwanami Lecture Series, section on Geology, Palaeontology, Mineralogy and Petrology. *Iwanami Publishing Co., Tokyo*, 94 pp. [In Japanese].

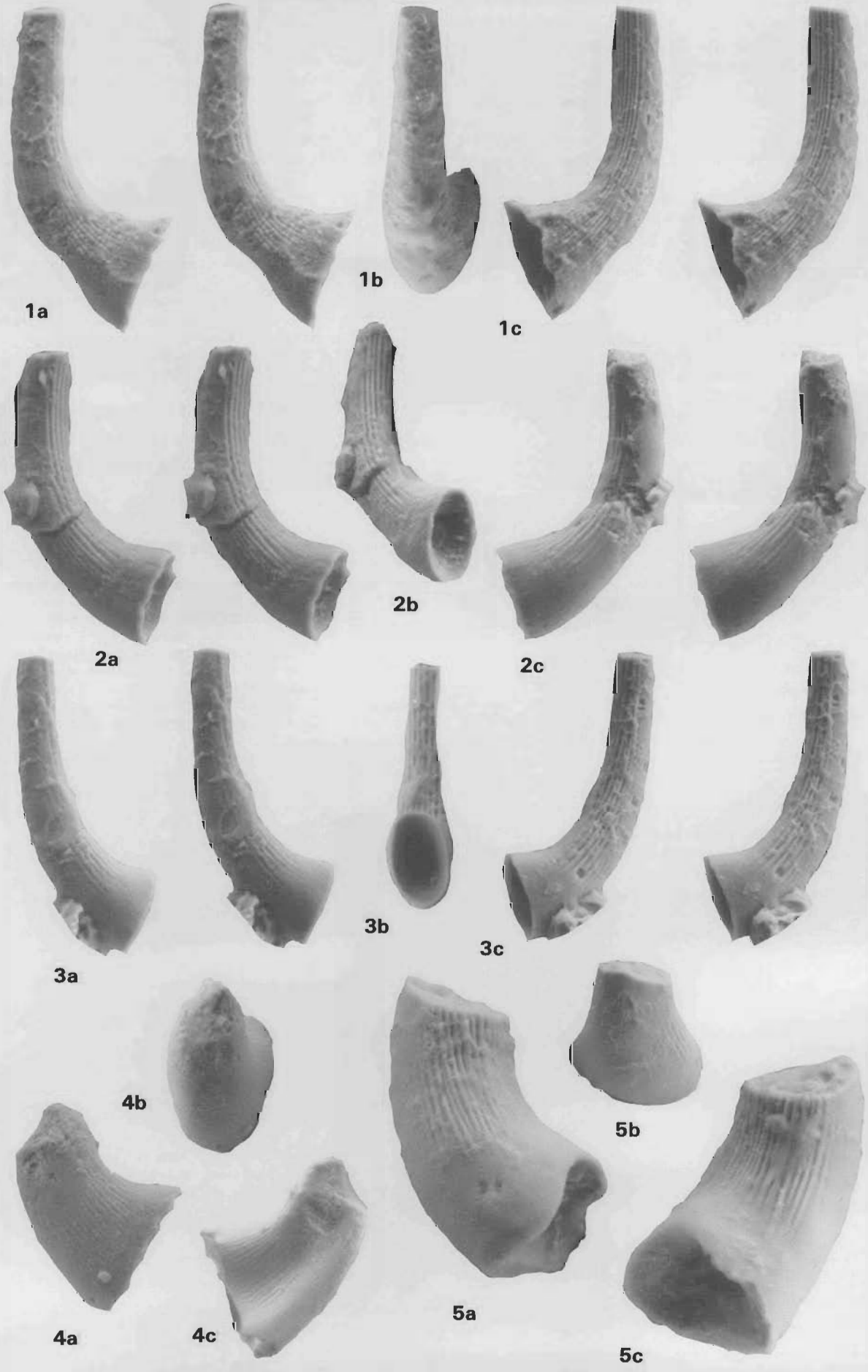
1a
1b
1c
2a
2b
2c
3a
3b
3c
4a
4b
4c
5a
5b
5c

Endo, R. & Resser, C.E., 1937 — The Sinian and Cambrian formations and fossils of southern Manchukuo. *Manchurian Science Museum, Bulletin* 1, 1–474, pl. 14–73.

Ethington, R.L. & Clark, D.L., 1965 — Lower Ordovician conodonts and other microfossils from the Columbia Ice Fields Section, Alberta, Canada. *Brigham Young University Geological Studies*, 12, 185–205.

Fortey, R.A., Landing, E. & Skevington, D., 1982 — Cambrian–Ordovician boundary sections in the Cow Head Group, western Newfoundland. *In* Bassett, M.G. & Dean, W.T. (editors), The Cambrian–Ordovician Boundary: sections, fossil distributions, and correlations. *National Museum of Wales, Geological Series*, 3, 95–129.

Fortey, R.A. & Skevington, D., 1980 — Correlation of Cambrian–Ordovician boundary between Europe and North America: new data from Western Newfoundland. *Canadian Journal of Earth Sciences*, 17(3), 382–388.

Furnish, W.M., 1938 — Conodonts from the Prairie du Chien (Lower Ordovician) Beds of the Upper Mississippi Valley. *Journal of Paleontology*, 12, 318–340.

Henningsmoen, G., 1957 — The trilobite family Olenidae with description of Norwegian material and remarks on the Olenid and Tremadocian Series. *Skrifter utgitt av Det Norske Videnskaps-Akademi i Oslo*, 1, 1–303.

Henningsmoen, G., 1973 — The Cambrian–Ordovician Boundary. *Lethaia*, 6, 423–439.

Hintze, L.F., 1982 — Ibexian Series (Lower Ordovician) type section, western Utah, USA. *In* Ross, R.J. & Bergström, S.A. (editors), The Ordovician System in the United States, correlation chart and explanatory notes. *International Union of Geological Sciences, Publication* 12, 7–10.

Jones, P.J., 1961 — Discovery of conodonts in the Upper Cambrian of Queensland. *Australian Journal of Science*, 24(2), 143.

Jones, P.J., Shergold, J.H. & Druce, E.C., 1971 — Late Cambrian and Early Ordovician Stages in western Queensland. *Journal of the Geological Society of Australia*, 18(1), 1–32.

Kobayashi, T., 1931 — Studies on the stratigraphy and palaeontology of the Cambro-Ordovician formation of Hua-lien-chai and Niu-hsin-tai, south Manchuria. *Japanese Journal of Geology and Geography*, 8(3), 131–190, pl. 16–22.

Kobayashi, T., 1933 — Upper Cambrian of the Wuhutsui Basin, Liaotung, with special reference to the limit of the Chaumitien (or Upper Cambrian), of eastern Asia, and its subdivision. *Japanese Journal of Geology and Geography*, 11(1–2), 55–155, pl. 9–15.

Kobayashi, T., 1934 — The Cambro-Ordovician formations and faunas of South Chosen. Palaeontology, pt. 2. Lower Ordovician faunas. *Journal of the Faculty of Science, Imperial University of Tokyo* [2], 3(9), 521–585, pl. 1–8.

Kobayashi, T., 1935 — The Cambro-Ordovician formations and faunas of South Chosen. Palaeontology, pt. 3. Cambrian families of South Chosen with special study on the Cambrian trilobite genera and families. *Journal of the Faculty of Science, Imperial University of Tokyo* [2], 4(2), 49–344, pl. 1–24.

Kobayashi, T., 1960a — The Cambro-Ordovician formations and faunas of South Korea, part 6. Palaeontology, 5. *Journal of the Faculty of Science, University of Tokyo* [2], 12(2), 217–275, pl. 12–14.

Kobayashi, T., 1960b — The Cambro-Ordovician formations and faunas of South Korea, pt. 7. Palaeontology 6. *Journal of the Faculty of Science, University of Tokyo* [2], 12(2), 329–420, pl. 19–21.

Kobayashi, T., 1962 — The Cambro-Ordovician formations and faunas of South Korea, pt. 9. Palaeontology, 8. The Machari fauna. *Journal of the Faculty of Science, University of Tokyo* [2], 14(1), 1–152, pl. 1–12.

Kobayashi, T., 1966a — The Cambro-Ordovician formations and faunas of South Korea, part 10. Stratigraphy of the Chosen Group in Korea and South Manchuria, and its relation to the Cambro-Ordovician formations of other areas. Section A, The Chosen Group of South Korea. *Journal of the Faculty of Science, University of Tokyo* [2], 16(1), 1–84.

Kobayashi, T., 1966b — The Cambro-Ordovician formations and faunas of South Korea, part 10. Stratigraphy of the Chosen Group in Korea and South Manchuria, and its relation to the Cambro-Ordovician formations of other areas. Section B, The Chosen Group of North Korea and northeast China. *Journal of the Faculty of Science, University of Tokyo* [2], 16(2), 209–311.

Kobayashi, T., 1967 — The Cambro-Ordovician formations and faunas of South Korea, part 10. Stratigraphy of the Chosen Group in Korea and South Manchuria, and its relation to the Cambro-Ordovician formations of other areas. Section C, The Cambrian of eastern Asia and other parts of the continent. *Journal of the Faculty of Science, University of Tokyo* [2], 16(3), 381–534.

Kobayashi, T., 1969 — The Cambro-Ordovician formations and faunas of South Korea, part 10. Stratigraphy of the Chosen Group in Korea and south Manchuria and its relation to the Cambro-Ordovician formations of other areas. Section D, The Ordovician of eastern Asia and other parts of the continent. *Journal of the Faculty of Science, University of Tokyo* [2], 17(2), 163–316.

Landing, E., 1988 — Cambrian–Ordovician Boundary in North America: revised Tremadocian correlations, unconformities and 'glacioeustacy'. *In* Landing, E. (editor), The Canadian paleontology and biostratigraphy seminar. *New York State Museum, Bulletin* 462, 48–58.

Lindström, M., 1955 — Conodonts from the lowermost Ordovician strata of south-central Sweden. *Geologiska Föreningens Förhandlingar*, 76, 517–603.

Ludvigsen, R. & Westrop, S.R., 1985 — Three new Upper Cambrian Stages for North America. *Geology*, 13, 139–143.

Miller, J.F., 1969 — Conodont fauna of the Notch Peak Limestone (Cambro-Ordovician), House Range, Utah. *Journal of Paleontology*, 43(2), 413–439, pl. 63–66.

Miller, J.F., 1978 — Upper Cambrian and lowest Ordovician conodont faunas of the House Range, Utah. *In* Miller, J.F. (editor), Upper Cambrian to Middle Ordovician conodont faunas of western Utah. *Southwest Missouri State University Geoscience Series*, 5, 1–33.

Miller, J.F., 1980 — Taxonomic revisions of some Upper Cambrian and Lower Ordovician conodonts with comments on their evolution. *The University of Kansas Paleontological Contributions, Paper* 99, 39 pp., 2 pl.

Miller, J.F., 1984 — Cambrian and earliest Ordovician conodont evolution, biofacies, and provincialism. *Geological Society of America, Special Paper* 196, 43–68.

Miller, J.F., 1987 — Upper Cambrian and basal Ordovician conodont faunas of the southwest flank of the Llano Uplift, Texas. *21st Annual Meeting, Geological Society of America, South-central Section*, 1–22.

Miller, J.F., 1988 — Conodonts as biostratigraphic tools for the redefinition and correlation of the Cambrian–Ordovician boundary. *Geological Magazine*, 125(4), 349–362.

Miller, J.F., Taylor, M.E., Stitt, J.H., Ethington, R.L., Hintze, L.F. & Taylor, J.F., 1982 — Potential Cambrian–Ordovician boundary stratotype sections in the western United States. *In* Bassett, M.G. & Dean, W.T. (editors), The Cambrian–Ordovician boundary: sections, fossil distributions, and correlations. *National Museum of Wales, Geological Series*, 3, 155–180.

Moberg, J.C., 1900 — Nya bildrag till utredning af frågen om gränsen mellan undersilur och kambrium. *Geologiska Föreningens Stockholm Förhandlingar*, 22, 523–540.

Müller, K.J., 1959 — Kambrische conodonten. *Zeitschrift der Deutsche Geologische Gesellschaft*, III, 435–485, pl. 11–15.

Nicoll, R.S., 1990 — The genus *Cordylodus* and a latest Cambrian–earliest Ordovician conodont biostratigraphy. *BMR Journal of Australian Geology & Geophysics*, 11(4), 529–558.

Nogami, Y., 1967 — Kambrische conodonten von China, Teil. 2 Conodonten aus den hoch oberkambrischen Yencho-Schichten. *Memoirs of the College of Science, University of Kyoto, Series B, Geology and Mineralogy*, 33(4), 211–218, 1 pl.

Figure 17. *Teridontus* n. sp. A, coniform element.

All figures x200.

1. Left element (CPC 29089)[BMA 82]; **a,** stereo pair, outer lateral view; **b,** anterior view; **c,** stereo pair, inner lateral view. **2.** Right element (CPC 29090)[BMA 82]; **a,** stereo pair, inner lateral view; **b,** oblique posterior view; **c,** stereo pair, outer lateral view. **3.** Left element (CPC 29091)[BMA 82]; **a,** stereo pair, outer lateral view; **b,** posterior view; **c,** stereo pair, inner lateral view. **4.** Left element (CPC 29092)[BMA 82]; **a,** outer lateral view; **b,** anterior view; **c,** inner lateral view. **5.** Right element (CPC 29093)[BMA 82]; **a,** inner lateral view; **b,** anterior view; **c,** outer lateral view.

Pander, C.H., 1856 — Monographie der fossilen Fische des Silurischen Systems der Russisch Baltischen Gouvernements. *Kaiserlichen Akademie der Wissenschlaften St Petersburg*, 91 pp.

Radke, B.M., 1980 — Epiric carbonate sedimentation of the Ninmaroo Formation (Upper Cambrian–Lower Ordovician), Georgina Basin. *BMR Journal of Australian Geology & Geophysics*, 5, 183–200.

Radke, B.M., 1981 — Lithostratigraphy of the Ninmaroo Formation (Upper Cambrian–Lower Ordovician), Georgina Basin, Queensland and Northern Territory. *Bureau of Mineral Resources, Australia, Report* 181, BMR Microform MF153.

Radke, B.M., 1982 — Late diagenetic history of the Ninmaroo Formation (Cambro-Ordovician), Georgina Basin, Queensland and Northern Territory. *BMR Journal of Australian Geology & Geophysics*, 7, 231–254.

Resser, C.E. & Endo, R., 1937: See Endo, R. & Resser, C.E., 1937.

Robison, R.A. & Pantoja-Alor, J., 1968 — Tremadocian trilobites from the Nochixtlán region, Oaxaca, Mexico. *Journal of Paleontology*, 42(3), 767–800, pl. 97–104.

Ross, R.J. & Bergström, S.A. (editors), 1982 — The Ordovician System in the United States, correlation chart and explanatory notes. *International Union of Geological Sciences, Publication* 12, 73 pp.

Sergeeva, S.P., 1966 — Biostratigraphical distribution of conodonts in the Tremadocian Stage (Ordovician) of the Leningrad region. *Doklady Akademii Nauk SSSR*, 1966, 167(3), 672–674. [In Russian].

Shergold, J.H., 1975 — Late Cambrian and Early Ordovician trilobites from the Burke River Structural Belt, western Queensland, Australia. *Bureau of Mineral Resources, Australia, Bulletin* 153 (2 vols), 251 pp., 58 pl.

Shergold, J.H., 1988 — Review of trilobite biofacies distributions at the Cambrian–Ordovician boundary. *Geological Magazine*, 125(4), 363–380.

Shergold, J.H. (compiler), 1989 — Australian Phanerozoic timescales: 1. Cambrian biostratigraphic chart and explanatory notes. *Bureau of Mineral Resources, Australia, Record* 1989/31.

Shergold, J.H., Jago, J.B., Cooper, R.A. & Laurie, J.R., 1985 — The Cambrian System in Australia, Antarctica and New Zealand. Correlation chart and explanatory notes. *International Union of Geological Sciences, Publication* 19, 85 pp.

Sun Yun-chu, 1924 — Contributions to the Cambrian faunas of North China. *Palaeontologia Sinica [B]*, 1(4), 1–109, pl. 1–5.

Tjernvik, T., 1956 — On the early Ordovician of Sweden. Stratigraphy and fauna. *Bulletin of the Geological Institutions, University of Uppsala*, 36, 107–284, pl. 1–11.

Tjernvik, T., 1958 — The Tremadocian beds at Flagabro in southeastern Scania (Sweden). *Geologiska Föreningens Förhandlingar*, 80(3), 259–276.

Vandenberg, A.H.M., 1981 — Victorian Stages and graptolite Zones. *In* Webby, B.D. (editor), The Ordovician System in Australia, New Zealand and Antarctica. *International Union of Geological Sciences, Publication* 6, 2–7.

Viira, V., 1966 — Distribution of conodonts in the Lower Ordovician sequence of Suhkrumagi (Tallinn). *Eesti NSV Teaduste Akadeemia Toimetised, XV Kide, 1966(1)*, 150–155. [In Russian].

Webby, B.D. (editor), 1981 — The Ordovician System in Australia, New Zealand and Antarctica. Correlation chart and explanatory notes. *International Union of Geological Sciences, Publication* 6, 64 pp.

Webby, B.D. & Nicoll, R.S. (compilers), 1989 — Australian Phanerozoic timescales: 2. Ordovician biostratigraphic chart and explanatory notes. *Bureau of Mineral Resources, Australia, Record* 1989/32.

Whitehouse, F.W., 1936 — The Cambrian faunas of north-eastern Australia: Part 1, stratigraphic outline; Part 2, Trilobita (Miomera). *Memoirs of the Queensland Museum*, 11(1), 59–112, pl. 8–10.

Zhang Huijuan & Xiang Weida, 1983 — See An Taixiang & others, 1983.

CONTENTS

9 780644 133814

B90/22163 Cat.No.90 21116